

**DEVELOPMENT OF ORGANOSILICON COMPOUNDS:
DERIVING SiC COATING, NANOMATERIALS AND
CERAMIC COMPOSITES**

By

JYOTI PRAKASH

CHEM01200904001

Bhabha Atomic Research Centre, Mumbai

*A thesis submitted to the
Board of Studies in Chemical Sciences
In partial fulfillment of requirements
For the Degree of*

DOCTOR OF PHILOSOPHY

of

HOMI BHABHA NATIONAL INSTITUTE



December, 2013

Homi Bhabha National Institute

Recommendations of the Viva Voce Committee

As members of the Viva Voce Committee, we certify that we have read the dissertation prepared by Shri Jyoti Prakash entitled “Development of Organosilicon compounds: deriving SiCcoating, nanomaterials and ceramic composites” and recommend that it may be accepted as fulfilling the thesis requirement for the award of Degree of Doctor of Philosophy.

Chairman –Prof. (Dr.) Vimal K. Jain

Date:18/7/2014

Guide / Convener –Prof. (Dr.) Sunil K. Ghosh

Date: 18/7/2014

Member 1 –Prof. (Dr.) Dr. A. K. Tyagi

Date: 18/7/2014

Member 2- Prof. (Dr.)S. K. Nayak

Date: 18/7/2014

Member 3 – Prof. (Dr.) S. K. Kannan

Date:18/7/2014

Final approval and acceptance of this thesis is contingent upon the candidate’s submission of the final copies of the thesis to HBNI.

I/We hereby certify that I/we have read this thesis prepared under my/our direction and recommend that it may be accepted as fulfilling the thesis requirement.

Date: 18/07/2014

Place: Mumbai

Guide

STATEMENT BY AUTHOR

This dissertation has been submitted in partial fulfillment of requirements for an advanced degree at Homi Bhabha National Institute (HBNI) and is deposited in the Library to be made available to borrowers under rules of the HBNI.

Brief quotations from this dissertation are allowable without special permission, provided that accurate acknowledgement of source is made. Requests for permission for extended quotation from or reproduction of this manuscript in whole or in part may be granted by the Competent Authority of HBNI when in his or her judgment the proposed use of the material is in the interests of scholarship. In all other instances, however, permission must be obtained from the author.

Jyoti Prakash

DECLARATION

I, hereby declare that the investigation presented in the thesis has been carried out by me. The work is original and has not been submitted earlier as a whole or in part for a degree / diploma at this or any other Institution / University.

Jyoti Prakash

List of Publications arising from the thesis

Journal

1. “Taguchi Method optimization of Parameters for growth of nano dimensional SiC wires by Chemical Vapor Deposition Technique”, Jyoti Prakash, Sunil Kumar Ghosh, D. Sathiyamoorthy, R. Venugopalan, B. Paul, *Current Nanoscience*, **2012**, 8, 161-169.
2. “Study of thermal degradation behavior of dense and nanostructured Silicon Carbide coated carbon fibers in oxidative environments”, Jyoti Prakash, R. Venugopalan, B. Paul, J. Bahadur, Sunil Kumar Ghosh, D. Sathiyamoorthy, *Corrosion Science*, **2013**, 67, 142-151.
3. “Study of properties of SiC layer in TRISO coated particles grown using different alkyl-silicon compounds”, Jyoti Prakash, Sunil Ghosh, Ramani Venugopalan, D. Sathiyamoorthy, *AIP Conf. Proc.*, **2013**, 1538, 26-29.
4. “A new approach to fabricate SiC nanowire embedded-dense SiC matrix/carbon fiber composite”, Jyoti Prakash, Kinshuk Dasgupta, B.M.Tripathi, J. Bahadur, Sunil Kumar Ghosh, J.K.Chakravartty, *Journal of Materials Science*, **2014**, 49, 6784–6792.
5. “Economical route synthesis of halogen-free organosilicon precursor and nanocrystalline silicon carbide thin film coating by low temperature fluidized bed CVD”, Jyoti Prakash, Sunil Kumar Ghosh, *Material Chemistry and Physics*, **2013**, Manuscript Number: MATCHEMPHYS-D-13-02450 (Under Review).
6. “A review on Production, Processing and application of one dimensional Silicon carbide nanostructures”, Jyoti Prakash, Ramani Venugopalan, B. M. Tripathi, Sunil K. Ghosh, J.K. Chakravartty, A. K. Tyagi, *Progress in Materials Science*, **2014** (Under Review).
7. “Role of SiC nanowire coating on oxidation behavior of carbon fiber: Kinetic and thermodynamic study”, Jyoti Prakash, K. Dasgupta, Sunil Kumar Ghosh, J. K. Chakravartty, *Surface and Coatings technology*, **2014**, Manuscript Number: SURFCOAT-D-14-01448 (Under Review).

Chapters in books

1. “Catalyst-free chemical vapor deposition for synthesis of SiC nanowires with controlled morphology”, Jyoti Prakash, Sunil Kumar Ghosh, Dakshinamoorthy Sathiyamoorthy, chapter 9 in Book "Silicon based Nanomaterials", Chief Edi. : Zhiming M. Wang, Springer **2013**.

2. “Low temperature coating deriving from Metal-Organic precursors: An economical and environmentally benign approach” Jyoti Prakash, B. M. Tripathi, Sunil Kumar Ghosh, book chapter in Book titled “Intelligent coating for corrosion control, First edition”, Edited by: Atul Tiwari, J.W.Rawlins and L.H.Hirara, Elsevier **2014**.

Conferences

1. “The growth of SiC coatings by pyrolysis of Different Alkyl Silicon Compounds”. Jyoti Prakash, Sunil Ghosh, Ramani Venugopalan, D. Sathiyamoorthy, Proceedings of 3rd International symposium on Materials Chemistry, held on 7th -11th Dec **2010** at BARC, Mumbai.
2. “Microstructural analysis of silicon carbide coating on the carbon fibre”, Jyoti Prakash, Sunil Ghosh, Ramani Venugopalan, D Sathiyamoorthy, Proceedings of International conference on Electron Nano scopy, held on 6th -8th july **2011** at Hyderabad.
3. “Study of oxidation resistive property of dense Silicon Carbide coated carbon fiber” Jyoti Prakash, Sunil Ghosh, D. Sathiyamoorthy, Proceedings of 17th National symposium and workshop on thermal analysis held on 9-11 March **2012** at Mumbai.
4. “Synthesis of Silicon carbide coated carbon composite using sol gel method and study of its oxidation property” Jyoti Prakash, Ramani Venugopalan, Sunil Kumar Ghosh, Dakshinamoorthy Sathiyamoorthy, Proceedings of National Conference On CARBON MATERIALS 2012 (CCM12) held on 1st - 3rd November **2012** at Mumbai.
5. “Sol Gel route synthesis of high surface area porous silicon carbide” Jyoti Prakash, Ramani Venugopalan, Sunil Kumar Ghosh, Dakshinamoorthy Sathiyamoorthy, Proceedings of International symposium on Materials Chemistry held on 11th -15th Dec **2012** at BARC, Mumbai.

Jyoti Prakash

***DEDICATED TO MY
PARENTS.....***

Shri Lal Chand Gupta

&

Smt. Jamwanti

ACKNOWLEDGEMENT

It gives me immense pleasure to acknowledge all the people who have helped me in completing this thesis. I express my deep sense of gratitude to my guide Dr. Sunil K. Ghosh. This work would not have been completed without his invaluable guidance and encouragement.

I also would like to thank Dr. D. Sathiyamoorthy for his invaluable guidance support to carry out my research work. I am grateful from the deep of my heart to Dr. J.K. Chakravartty, Director, Materials group for permitting me to continue my PhD and support in finishing the work. I would like to thank my thesis committee members: Profs. V.K.Jain, A.K. Tyagi, S.K.Nayak, S. Kannan, for their valuable suggestions and constructive criticism.

I am thankful to Dr. K. Dasgupta and Dr. Ramani Venugopalan for their encouragement and valuable suggestions. I would like to thank my colleagues Brij Kumar, Sandeep Sharma, Amit Verma, Bhaskar Paul, B.M. Tripathi, Ravikanth, P.K. Mollick, P.T. Rao, R.D. Bedse, Jitendra Bahadur, Jitendra Sonebar, TSRC Murthy, Sanjay Singh and others, for their diversified help and fruitful scientific discussions throughout the course of my PhD research work. My special thank goes to my childhood friends Vindeshwari Gupta, Sanjay Singh and Vijay Mishra for their moral support.

Finally, I would like to thank my family. My Parents have loved me, supported me and encouraged me throughout the course of my life. My brother Shiv Prakash and sisters Archana, Arpana and Aditi Gupta encouraged me throughout my life. I would like to thank my wife, Sunita Gupta, and my lovely son Snehil Prakash for their companionship to excel in my life.

Jyoti Prakash

CONTENTS

| | |
|---|-----------|
| SYNOPSIS | 1 |
| LIST OF FIGURES | 12 |
| LIST OF TABLES | 21 |
| CHAPTER 1 | |
| 1. INTRODUCTION | 25 |
| 1.1 History of Silicon Carbide | 25 |
| 1.2 Crystal structure of SiC | 27 |
| 1.3 Applications of SiC | 29 |
| 1.4 Research on advance SiC coating/composite development | 31 |
| 1.4.1 Coating techniques | 33 |
| 1.4.1.1 Chemical Vapor deposition: MOCVD variant techniques | 35 |
| 1.4.1.1.1 Laser induced chemical vapor deposition (LCVD) | 38 |
| 1.4.1.1.2 UV induced chemical vapor deposition (UVCVD) | 39 |
| 1.4.1.1.3 Plasma enhanced CVD (PECVD) | 40 |
| 1.4.1.1.4 Electron Beam Chemical Vapor Deposition (EBCVD) | 41 |
| 1.4.1.1.5 Fluidized Bed Chemical Vapor Deposition (FBCVD) | 42 |
| 1.4.1.1.6 Atomic Layer Deposition (ALD) | 43 |
| 1.4.2 Infiltration techniques | 44 |
| 1.4.3 Development of organosilicon precursors: literature survey | 45 |

| | |
|---|-----------|
| 1.4.4 Objectives and scope of the present thesis | 57 |
| CHAPTER 2 | |
| 2. SYNTHESIS OF ORGANOSILICON COMPOUNDS | 60 |
| 2.1 Organosilicon precursors | 62 |
| 2.1.1. 2,4,6-trimethyl-2,4,6-trisila-heptane Compound | 62 |
| 2.1.2. 2,4,6-trisilacyclohexane compound | 64 |
| 2.1.3. Mixture of organosilicon compounds (CVDP) | 68 |
| 2.2 Conclusion | 76 |
| 2.3 Experimental Section | 77 |
| 2.3.1. General Details | 77 |
| 2.3.2. General synthesis procedure for 2,4,6-trimethyl-2,4,6-trisila-heptane compound | 77 |
| 2.3.3. General synthesis procedure for 2,4,6-trisilacyclohexane compound | 79 |
| 2.3.4. General synthesis procedure for mixture of organosilicon compounds (CVDP) | 80 |
| CHAPTER 3 | |
| 3. COATING STUDY OF SILICON CARBIDE USING ORGANOSILICON COMPOUNDS | 83 |

| | |
|---|------------|
| 3.1 SiC layer coating using organosilicon precursors | 84 |
| 3.1.1. Silicon carbide thin film coating using synthesized organosilicon (CVDP) precursor | 84 |
| 3.1.1.1. Experimental methods and materials | 84 |
| 3.1.1.2. Results and discussion | 86 |
| 3.1.2. Silicon carbide thin film coating using Hexamethydisilane (HMDS) precursor | 90 |
| 3.1.2.1. Experimental methods and materials | 90 |
| 3.1.2.2. Results and discussion | 91 |
| 3.2 SiC layer coating studies on tri-isotropic (TRISO) Particles | 94 |
| 3.2.1. Experimental methods and materials | 95 |
| 3.2.2. Results and discussion | 96 |
| 3.3 Dense and nanowire morphology coating: Taguchi method study | 104 |
| 3.3.1 Brief Introduction of Taguchi Method | 104 |
| 3.3.2 Experimental methods and materials | 107 |
| 3.3.2.1 Parameter Selection for Taguchi Optimization | 107 |
| 3.3.2.2 Experimental Set up and synthesis of SiC wires | 108 |
| 3.3.3 Results and discussion | 110 |
| 3.3.3.1 Taguchi optimization calculations | 110 |
| 3.3.3.2 Morphological study by changing hydrogen to MTS ratio | 119 |
| 3.3.3.3 Growth Mechanism of SiC nanowires | 127 |
| 3.4 Conclusion | 130 |

CHAPTER 4

| | |
|---|------------|
| 4. STUDIES ON SOL GEL ROUTE PREPARATION OF | 134 |
| SiC AND SiC/CARBON COMPOSITE | |
| 4.1 Deriving silicon carbide carbon composite by sol-gel route using tetraethylorthosilicate as silicon source and phenol formaldehyde as carbon source | 138 |
| 4.1.1 Experimental methods and materials | 138 |
| 4.1.2 Result and Discussion | 142 |
| 4.1.2.1 Morphology studies | 142 |
| 4.1.2.2 X-ray micro-tomography studies: SiC matrix distribution and Matrix-core interaction | 144 |
| 4.1.2.3 Phase analysis by XRD | 146 |
| 4.1.2.4 SAXS studies | 149 |
| 4.1.2.5 SiC nanowire growth mechanism | 153 |
| 4.2 Deriving silicon carbide- carbon composite by sol-gel route using Polymethylhydrosiloxane (PMHS), tetraethylorthosilicate (TEOS) as silicon source and glycerin as carbon source | 156 |
| 4.2.1 Experimental methods and materials | 156 |
| 4.2.2 Result and Discussion | 159 |
| 4.2.2.1 Morphology studies | 159 |
| 4.2.2.2 Phase analysis by XRD | 159 |
| 4.3 Conclusion | 162 |

CHAPTER 5

| | |
|--|------------|
| 5. STUDY OF THERMAL DEGRADATION BEHAVIOR AND KINETIC OF DIFFERENT COATED AND IMPREGNATED CARBON SAMPLES IN OXIDATIVE ENVIRONMENTS | 164 |
| 5.1. Study of thermal degradation behavior of dense and nanostructured Silicon Carbide coated carbon fibers in oxidative environments | 165 |
| 5.1.1 Materials and methods | 165 |
| 5.1.2 Results and discussion | 167 |
| 5.1.2.1 Morphology analysis of the SiC coating | 167 |
| 5.1.2.2 Oxidation study of bare carbon fibers and different SiC coated carbon fibers in presence of oxygen environment | 174 |
| 5.1.2.3 TG-DTG analysis of coated non coated carbon fibers in oxygen environment | 178 |
| 5.1.2.4 Oxidation study of bare carbon fibers and different SiC coated carbon fibers in presence of atmospheric environment | 182 |
| 5.1.2.5 Mechanism of oxidation of different SiC coated carbon fibers in different oxidative environment | 186 |
| 5.2. Kinetics model study for oxidation of carbon fiber and SiC nanowires coated carbon fibers | 189 |
| 5.2.1 Isothermal Oxidation properties of carbon fiber and SiC nanowire coated carbon fiber | 189 |
| 5.2.2 Kinetic Studies | 191 |

| | |
|---|------------|
| 5.2.3 Determination of most probable mechanism function and calculation of Activation energy, Pre-exponential factor for oxidation of carbon fiber | 197 |
| 5.2.4 Determination of most probable mechanism function and calculation of Activation energy, Pre-exponential factor for oxidation of SiC nanowire coated carbon fibers | 204 |
| 5.3. Oxidation study of bare carbon fabric and SiC impregnated carbon fabric in presence of atmospheric environment | 211 |
| 5.3.1 Materials and methods | 211 |
| 5.3.1.1 Kinetic Study | 211 |
| 5.3.1.2 Determination of the Most Probable Mechanism Function and Pre-exponential Factor | 213 |
| 5.3.2 Results and discussion | 214 |
| 5.3.2.1 Thermo gravimetric analysis and morphological studies | 214 |
| 5.3.2.2 Calculation of Activation Energy Values, Determination of the Most Probable Mechanism Function and Pre-exponential Factors | 220 |
| 5.4 Conclusion | 223 |
| CHAPTER 6 | |
| 6. SUMMARY AND FUTURE SCOPE OF WORK | 227 |
| 6.1 Summary | 227 |
| 6.2 Future scope of work | 236 |
| REFERENCE | 238 |

SYNOPSIS

Chapter 1: Introduction

This chapter deals with brief description about the different forms of silicon carbide and their applications along with an overview of different techniques used for their coating. The synthesis routes of various organosilicon compounds and their suitability as a precursor have also been discussed in the current chapter.

Ultra-pure performance SiC, Low resistivity performance SiC and other forms of SiC outlast conventional materials as they can withstand extremely hostile environments. The outstanding properties and performance of SiC include superior chemical and erosion resistance with phenomenal thermal properties. Owing to these properties, researchers are closely evaluating SiC-based materials such as in the form of composites either as SiC/SiC composite, SiC infiltrated carbon composite or coating of SiC on different substrates for various applications (1-4). Consequently, intense research over the past 30 years has been focused on the deriving SiC based materials from different sources such as silane plus hydrocarbon, both cyclic and acyclic organosilicon single compound precursors and organosilicon polymer. A lot of efforts are going on for economical synthesis of organosilicon compounds and to develop a process to derive SiC from such chemicals.

In past, many SiC coating have been produced by the CVD technique. However, most SiC coatings were grown at relatively high temperatures of 1300 °C- 1500 °C and at atmospheric pressure, using separate sources for silicon (SiH_4 , Si_2H_6 , and SiH_2Cl_2) and carbon (C_2H_2 , CH_4 , and C_3H_8) (5-7) or using single source compound, Methyltrichlorosilane (MTS, CH_3SiCl_3) (8). As a result, the coatings deposited contain higher levels of impurities with chlorine contents leading to a reduction in the properties of the coating (9). Moreover, the use of silane compounds

in traditional CVD requires safety precautions as these compounds are highly pyrophoric (10). Recent practice of using halogen free single source compounds in chemical vapor deposition is enjoying low deposition temperature, safe in handling and accurate stoichiometry (11-12). Since the single molecular precursor already has a Si-C bond in the precursor itself, it does not need further activation energy to make a Si-C bond in the film, resulting in deposition temperatures below 1000 °C. Efforts to obtain different morphological SiC materials from economically produced organosilicon precursors have been continued for low temperature growth with stoichiometric composition.

Chapter 2: Synthesis of Organosilicon compounds

This chapter describes two different aspects: (i) Proper selection of organosilicon compound for growth of SiC and, (ii) Synthetic process selection for bulk production.

Three potential SiC precursors 2,4,6-trimethyl-2,4,6-trisila-heptane, 2,4,6-trisilacyclohexane and mixture of organosilicon compounds (named as CVDP) were identified and their synthesis processes were developed.

The synthesis of 2,4,6-trimethyl-2,4,6-trisila-heptane involves two steps. In the first step chloromethyldimethylsilane is synthesized by reducing chloromethyldimethylchlorosilane using lithium aluminum hydride. In the second step Grignard reagent is formed by reacting stoichiometric amount of chloromethyldimethylsilane and magnesium at room temperature. This Grignard reagent was then reacted with dichloromethylsilane to give 2,4,6-trimethyl-2,4,6-trisila-heptane.

2,4,6-Trisilacyclohexane was synthesized in two step. In the first step 2,4,6-dichlorosilylcyclohexane (CH_2SiCl_2)₃ was synthesized by reaction of dichloromethane (CH_2Cl_2) with silicone (Si) and copper (Cu) metal powder in the form of pellets. In second step, reduction

of 2,4,6-(dichlorosila)cyclohexane was carried out using lithium aluminum hydride to yield 2,4,6-trisilacyclohexane. The final yield obtained of 2,4,6-trisilacyclohexane compound after reduction step was low. To improve its yield, the process was further modified. In the modified process silicon powder was fluidized in vertical furnace and efficient reaction of dichloromethane occurred with silicon in fluidized bed. The higher boiling mixture of organohalosilicon compounds were distilled out above 150 °C and further reduced with lithium aluminum hydride. The reduced mixture of organosilicon compounds contains 90% volatile part which can be used as CVD precursor (named as CVDP) and rest 10% contains polymeric viscous organosilicon liquid.

Chapter 3: Coating study of Silicon Carbide using Organosilicon compounds

3.1: SiC layer coating using organosilicon precursor

The current section of chapter deals with the coating studies carried out on graphite substrate using synthesized CVDP precursor and commercial available hexamethyldisilane precursor. The small graphite substrate was coated using chemical vapor deposition of CVDP precursor at 1000 °C. The small graphite and zircaloy substrate were coated using Hexamethyldisilane (HMDS) at 800-1000 °C. The morphology of coating and phase of the coating were characterized using SEM and XRD respectively. In both cases crystalline dense beta SiC deposition was obtained. Coating studies have revealed that the CVDP precursor is a potential precursor for low temperature deposition of SiC.

3.2: SiC layer coating studies on tri-isotropic (TRISO) Particles

The current section of chapter describes the deposition kinetics of SiC layers using MTS, HMDS and Tetramethylsilane (TMS) as precursors via spouted bed chemical vapor deposition on TRISO particles. The TRISO particles will be used as fuel for High Temperature Reactors. The

TRISO particles consist of three layers of pyrolytic carbon of different density and one layer of SiC. SiC coatings were deposited on simulated TRISO particles by spouted bed CVD at 1450 °C using MTS and at 1300 °C using HMDS and TMS precursors. The microstructure and mechanical properties of SiC coatings obtained from different precursors using spouted bed CVD process were studied. Dense and uniform coatings of SiC were obtained for MTS and HMDS in our spouted bed system however non uniform coating was obtained using TMS. More deposition of free carbon with SiC was occurred in case of HMDS as precursor may be due to non stoichiometric ratio of Si and C in HMDS. The mechanical properties were studied using micro indentation. SiC coatings using HMDS and MTS have shown almost similar hardness and fracture toughness. The hardness and fracture toughness values of coated SiC layers show that the coating has good strength. HMDS liquid precursor has a potential to replace corrosive and toxic Precursor MTS for SiC layer coating in TRISO particle.

3.3: Dense and nanowire morphology coating: Taguchi method study

SiC coating of different morphology using MTS and hydrogen by chemical vapor deposition under ambient pressure has been presented in the current section of the chapter. Taguchi method has been used to design experiments to get the optimum parameters for growing SiC wires of diameter in nanometer range. Results from XRD and SEM analyses showed the growth of β -SiC having dense and wire morphology. At higher temperature (1500 °C), the growth of SiC grains was observed rather than wires. The optimum deposition conditions for uniform diameter growth of SiC nano wires, smoothness of the surface and homogeneous growth of SiC on the surface have been obtained. The hydrogen to MTS flow rate ratio should be above 20 for the growth of SiC wires of nanometer diameter. The deposition temperature for the growth of crystalline SiC wires should be 1100-1300 °C. The total flow rate of carrier gas comprising of argon and

hydrogen for a particular H_2 /MTS flow rate ratio is critical for morphological outcome of SiC. The optimum deposition temperature i.e. 1300 °C was kept constant and further experiments were conducted by changing H_2 /MTS mole ratio to verify morphological outcome of SiC. A plausible mechanism has been suggested for the above observations using vapor-solid mechanism.

Chapter 4: Studies on sol gel route preparation of SiC and SiC/carbon composite

This chapter describes a novel and simple sol gel route for synthesis of SiC using organosilicon compounds. The current chapter further describes the development of fabrication process for SiC impregnated carbon fiber matrix composite using tetraethylorthosilicate (TEOS) as silicon source and phenol formaldehyde as carbon source. Two step sol gel process was used for generating SiC material. The experimental part involves dissolution of phenolic resin in ethanol and then mixing with tetraethylorthosilicate under stirring. Then, oxalic acid was added into the mixture under stirring. After addition final solution was sonicated for 2 h under stirring to enhance the hydrolysis of TEOS. The sonication step has drastically increased the hydrolysis rate and reduces the sol formation time. After sonication the solution was stirred at 80 °C for 10 h to form the carbonaceous silica sol. After rapid cooling in ice bath the sol tends to form gel, which was further heat treated to obtain SiC material. For preparation of SiC impregnated carbon composite during sol preparation the carbon fiber preform was dipped in this solution and the sol was cooled in ice bath for rapid gelation. The resulted impregnated carbon preform was further heat treated at 1500 °C to convert impregnated gel to SiC. Using current process SiC was impregnated in the carbon preform in dense and nanowire form. The analysis of scanning electron microscopy, energy dispersive spectroscopy, X-ray diffraction, X-ray tomography and TEM indicates that the SiC nanowires were distributed uniformly along with dense SiC in the carbon

fiber perform. The SiC nanowires located at the interface of advanced composites is very favorable to the interfacial bonding between composites matrix and carbon fibers, thereby increasing the strength of composites greatly. The feasibility of impregnating SiC in carbon matrix using Polymethylhydrosiloxane (PMHS) and Glycerine by sol gel method was also studied. The synthesis process includes the preparation of a carbonaceous silica gel and subsequent carbothermal reduction of gel. For the gel preparation, firstly PMHS was mixed with glycerine and ethanol under stirring. The resultant solution was further stirred for 24 h at room temperature after adding ethylenediamine to obtain xerogel. SiC was obtained by the carbothermal reduction of the carbonaceous silica xerogel 1500 °C in argon atmosphere. During sol formation the carbon preform was dipped in the sol and soaked for one hour for impregnation. Later on cooled down to get gel impregnated carbon perform, which was finally heat treated at 1500 °C. XRD and SEM analysis shows that the impregnated matrix was SiC having porous structure. A plausible mechanism for both sol gel process has been suggested for the above observations.

Chapter 5: Study of thermal degradation behavior and kinetic of different coated and impregnated carbon samples in oxidative environments

The current chapter describes thermal degradation behavior and kinetic of thermal decomposition of dense and nanowires morphology coated carbon samples and SiC impregnated carbon composites. The oxidation resistive properties of bare, dense SiC and nanostructured SiC coated carbon fibers were examined in different oxidative environments from room temperature to 1350 °C. The dense and nanostructured SiC coated carbon fibers have shown much improved oxidation resistive property in oxygen as well as in static air environment. In case of SiC nanowires coated carbon fiber the micropores present in between the SiC nanowires over carbon

fiber substrate serve as a channel for oxygen to penetrate into carbon fiber and lead to the oxidation of carbon fiber. In case of dense SiC coated carbon fiber the small microcracks formed in the coating due to the mismatch of coefficient of thermal expansion between the coating and carbon substrate act as the channel for oxygen diffusion and leads to the oxidation of carbon fiber. The SiO₂ layer formed over the SiC coating plays an important role in improving the anti oxidant property of the coating. Possible mechanism of oxidation behavior of dense and nanostructured SiC coated carbon fibers and role of SiO₂ have been discussed. The SiC impregnated carbon composite samples have shown much improved oxidation resistance property. The SiC carbon composites were characterized before and after oxidation using XRD, SEM and Small angle X-ray scattering. The possible mechanism of oxidation has been discussed. The oxidation kinetics model of different coated carbon samples were studied through the isothermal oxidation weight loss curve and nonisothermal thermo gravimetric (TG) and differential thermogravimetric (DTG) in oxygen as well as atmospheric condition. In the present work, the equations of Achar-Brindley-Sharp-Wendworth, Satava-Sestak, Coat-Redfern, Madhusudan Krishanan, Kissinger, Akahira & Sunose (KAS) and Ozawa were used to study the oxidation kinetics and to estimate most probable mechanism function of coated carbon fiber and SiC-carbon composites in non isothermal condition.

Chapter 6: Summary and future scope of work

Different organosilicon compounds have been synthesized and different commercial available precursors have been scrutinized. A mixture of organosilicon compound and commercial available precursor HMDS have been found to be a potential precursor of SiC in CVD process. Taguchi method study have proved that in case of coating from MTS for dense uniform coating high temperature (around 1400 °C) is desired and for uniform diameter growth of SiC nanowires,

smoothness of surface and homogeneous growth of SiC on the substrate, the hydrogen to MTS ratio must be high (for nano dimensional diameter growth H_2 /MTS ratio should be greater than 20), temperature of deposition should be 1100-1300 °C.

Precursor prepared by Sol gel route using PF Resin and TEOS has been used to impregnate carbon composites with SiC material which was composed of dense and 1D nanostructure SiC materials. Precursor prepared by Sol gel route using Glycerin, PMHS and TEOS resulted in porous SiC material.

The dense and nanostructured SiC coated carbon fibers have shown much improved oxidation property in oxygen as well as in static air environment. In nonisothermal condition the oxidation mechanism of nanostructured SiC coated carbon fibers in oxygen atmosphere was three- dimensional diffusion following ZLT mechanism. The kinetic parameters were: $E_a = 190 \text{ kJmol}^{-1}$ and $A = 3.77 \times 10^8 \text{ min}^{-1}$. The SiC impregnated carbon composites were prepared using sol gel method and these SiC carbon composites have shown much improved oxidation resistive property in static air environment. The activation energy for the oxidation of these composites was calculated using KAS and Ozawa method and found to be 85 and 100 kJmol^{-1} respectively.

Protective layer coated materials and ceramic composites have the potential to be use in harsh environment. In the present thesis, different organosilicon compounds as SiC precursor were synthesized, coating of different morphological SiC layer were carried out and SiC carbon composites were prepared. Further we have investigated their thermal degradation properties in oxidative environments. Dense SiC along with SiC wires coating over the carbon substrate is required to enhance its high temperature oxidation stability in oxygen environment with compatible CTE value. The SiC impregnated carbon composite has shown improved thermal oxidation properties but it has low density so to increase its density further a number of cycles of

impregnation/high pressure impregnations are required. It should be dense enough to obtain improved mechanical properties and thermal properties for application as structural material.

References

- (1) F.J. Buchanan, J.A. Little, Oxidation protection of carbon-carbon composites using chemical vapor deposition and glaze technology, *Corrosion Science* 35 (1993) 1243-1250.
- (2) N.S. Jacobson, D.M. Curry, Oxidation microstructure studies of reinforced carbon/carbon composite, *Carbon* 44 (2006) 1142-1150.
- (3) Y.H. Chu, Q.G. Fu, C.W. Cao, H.J. Li, K.Z. Li, Q. Lei, Microstructure and oxidation resistant property of C/C composites modified by SiC-MoSi₂-CrSi₂, *Surface Engineering* 27 (2011) 355-361.
- (4) Q.G. Fu, H.J. Li, Y.J. Wang, K.Z. Li, X.H. Shi, B₂O₃ modified SiC-MoSi₂ oxidation resistant coating for carbon/carbon composites by a two-step pack cementation, *Corrosion Science* 51 (2009) 2450-2454.
- (5) G.S. Fischman and W.T. Petuskey, Thermodynamic Analysis and Kinetic Implications of Chemical Vapor Deposition of SiC from Si-C-C1-H Gas Systems, *Journal of American Ceramics Society* 68 (1985) 185.
- (6) C.D. Stinspring and J.C. Wourmhoudt, Gas phase kinetics analysis and implications for silicon carbide chemical vapor deposition, *Journal of Crystal growth* 87 (1988) 481.
- (7) J.H. Koh and S.I. Woo, Computer Simulation Study on Atmospheric Pressure CVD Process for Amorphous Silicon Carbide, *Journal of Electrochemical Society* 137 (1990) 2215.
- (8) M.D. Allendorf and R.J. Kee, A Model of Silicon Carbide Chemical Vapor Deposition, *Journal of Electrochemical Society* 138 (1991) 841.

- (9) B.G. Mellor, Surface Coatings for Protection against Wear, Woodhead Publications, Cambridge, UK, 2006.
- (10) L. Tong, Y.J. Shi, A mechanistic study of gas-phase reactions with 1,1,3,3-tetramethyl-1,3-disilacyclobutane in the hot-wire chemical vapor deposition process, Thin Solid Films 517 (2009) 3461.
- (11) I. Golecki, F. Reidinger, Single-crystalline, epitaxial cubic SiC films grown on (100) Si at 750 °C by chemical vapor deposition, Applied Physics Letter 60 (1992) 1703.
- (12) S. Madapura, A. J. Steckl, M. Lobada, Heteroepitaxial Growth of SiC on Si(100) and (111) by Chemical Vapor Deposition Using Trimethylsilane, Journal of Electrochemical Society 146 (1999) 1197.

LIST OF FIGURES

CHAPTER 1

Fig. 1.1 The tetrahedral bonding of a carbon atom with the four neighboring silicon atoms

Fig. 1.2 The stacking sequence of double layer of the most common SiC polytypes

Fig. 1.3 The miller indices describing the hexagonal structure. The c-axis refers to the last index, whereas the first three describes the direction of the basal plane.

Fig. 1.4 Schematic representation of general chemical vapor deposition Process

Fig. 1.5 Schematic representation of Laser Induced Chemical Vapor Deposition (LICVD)

Fig. 1.6 Schematic representation of UV induced chemical vapor deposition (UVCVD)

Fig.1.7 Schematic representation of Plasma enhanced platinum CVD (PECVD)

Fig. 1.8 Schematic representation of Electron Beam Chemical Vapor Deposition (EBCVD)

Fig. 1.9 Schematic representation of Fluidized Bed Chemical Vapor Deposition (FBCVD)

Fig. 2.0 Schematic representation of Atomic Layer Deposition (ALD)

Fig. 2.1 The organic groups used for synthesis of organometallic precursor compounds.

CHAPTER 2

Fig. 2.1 Reaction scheme for synthesis of 2,4,6-trimethyl-2,4,6-trisila-heptane

Fig. 2.2 Reaction scheme for synthesis of different organosilicon compounds from tri-(dichlorosilylmethylene)

Fig. 2.3 XRD pattern of silicon –copper pellet before and after reaction.

Fig. 2.4 Schematic of reaction setup used for synthesis of 2,4,6-trisilacyclohexane compound.

Fig. 2.5 Schematic of fluidized bed system

Fig. 2.6 A schematic diagram of reaction setup for synthesis of mixture of organosilicon precursor.

Fig. 2.7 Actual reaction setup for synthesis of mixture of organosilicon precursor and schematic of fluidized bed zone.

Fig. 2.8 Reaction scheme for synthesis of mixture of organosilicon precursor.

Fig. 2.9 XRD pattern of the silicon powder used for the organosilicon precursor synthesis.

Fig. 2.10 The thermogravimetric weight loss curve of synthesized organosilicon precursor.

Fig. 2.11 The IR spectra of volatile organosilicon (named as CVDP) precursor.

CHAPTER 3

Fig. 3.1. The schematic of metalloorganic Fluidized bed CVD reactor used for SiC deposition.

Fig. 3.2 XRD pattern of the dense SiC coated zircaloy sheet using CVDP precursor.

Fig. 3.3 SEM image of the dense nanocrystalline SiC deposit on zircaloy substrate (a)(b)(c) surface morphology at different magnification (d) cross sectional view of SiC coating.

Fig. 3.4 EDX data of the elements in dense nanocrystalline SiC deposit on zircaloy substrate.

Fig. 3.5 SEM image of the dense SiC deposit on graphite substrate (a) surface morphology (b) cross sectional view of SiC coating.

Fig. 3.6 Schematic diagram of experimental setup for growing SiC coating.

Fig. 3.7 Schematic diagram of spouted bed furnace for coating on spherical microspheres.

Fig. 3.8 XRD pattern of the dense SiC coated zircaloy sheet using CVDP precursor.

Fig. 3.9 SEM image of the dense SiC deposit on graphite substrate (a) & (b) surface morphology of SiC coating using HMDS.

Fig. 3.10 The cross sectional microscopic images of the deposited SiC from HMDS at different magnification at zirconia microsphere.

Fig.3.11 Schematic of TRISO coated fuel particle

Fig. 3.12 XRD spectrum of SiC deposits using MTS and HMDS.

Fig.3.13 The cross sectional microscopic images of the deposited SiC from MTS at different magnification.

Fig. 3.14 X-ray tomography image of SiC coated spherical particle. (b) Murakami etched surface of SiC layer deposited from MTS.

Fig. 3.15 The cross sectional microscopic images of the deposited SiC from HMDS at different magnification.

Fig. 3.16 The cross sectional microscopic images of the deposited SiC from TMS at different magnification.

Fig. 3.17 EDX spectrum of SiC deposits using MTS and HMDS.

Fig. 3.18 SEM image of the SiC surface coated by MTS.

Fig. 3.19 SEM image of the SiC surface coated by HMDS.

Fig. 3.20 Schematic representation of lowest surface energy growth direction in fcc crystal.

Fig. 3.21 Schematic representation of higher surface energy growth direction in fcc crystal.

Fig. 3.22 XRD spectrum of the Different SiC deposits obtained through different experiments as presented in Table II.

Fig. 3.23 SEM images of the SiC deposits grown by experiments designed by Taguchi method.

Fig. 3.24 Graphical representation of the average effect of different factors on the deposition rate of SiC.

Fig.3.25 Graphical representation of the average effect of different factors on the growth diameter of SiC.

Fig. 3.26 SEM images of the SiC deposits grown by varying H₂/MTS ratio.

Fig. 3.27 Effect of H₂/MTS ratio on the growth morphology of SiC and deposition rate of SiC.

Fig. 3.28 Variation of deposition rate and morphology of SiC deposits with MTS flow rate at constant hydrogen to MTS ratio.

Fig. 3.29 Variation of deposition rate and morphology of SiC deposits with Total flow rate at constant hydrogen to MTS ratio.

Fig. 3.30 XRD spectrum of the SiC wires grown at $H_2/MTS = 70$ and $T = 1300$ °C. It shows the characteristic peaks of SiC and graphite.

Fig. 3.31 Raman spectrum of the SiC wires grown at $H_2/MTS = 70$ and $T = 1300$ °C. It shows the TO (796 cm^{-1}) and LO (972 cm^{-1}) mode of β -SiC.

Fig. 3.32 EDX spectrum of the SiC wires grown at $H_2/MTS = 70$ and $T = 1300$ °C. It shows the characteristic peaks of Si, C, O and corresponding table indicates the elemental concentration.

Fig. 3.33 TEM images of the SiC nanowires grown at $H_2/MTS = 70$ and $T = 1300$ °C.

Fig. 3.34 Schematic representation growth mechanism of SiC nanowires.

Fig. 3.35 The optimum deposition conditions for uniform diameter growth of SiC nano wires, smoothness of the surface and homogeneous growth of SiC.

CHAPTER 4

Fig. 4.1 The basic steps in sol-gel process using metal alkoxides.

Fig. 4.2 Flow sheet for preparation of SiC impregnated carbon composite by sol gel method.

Fig. 4.3 SEM images of (i) Bare carbon fabric (ii),(iii),(iv),(v) &(vi) Surface of the SiC impregnated carbon composite at different magnification.

Fig. 4.4 TEM images of (i) SiC nanowires (ii) middle portion of a SiC nanowire (iii) SAD pattern of a SiC nanowire.

Fig. 4.5 3D phase contrast images of (i) bare carbon fabric (ii) only carbon matrix (iii) only voids in carbon fabric (iv) SiC carbon composite (v) Only SiC (vi) only voids (vii) only carbon matrix in SiC carbon composite.

Fig. 4.6 2D X-ray tomography slices along XY and YZ directions of (i)&(ii) bare carbon fabric (iii)&(iv) SiC carbon composite.

Fig. 4.7 (i) XRD pattern of the SiC carbon composites after different heat treatment. (ii) XRD patterns of a series of representative samples heat treated at different temperature specially d_{002} peak (iii) variation in d_{002} values (iv) variation of L_c .

Fig. 4.8 (i) The SAXS profiles of the carbon fabric and SiC-carbon composites(ii),(iii) The pore size distribution as estimated by the SAXS data analysis for bare carbon fabric (iv) The nanowire radius distribution as estimated by the SAXS data analysis for SiC carbon composite heat treated at 1000 °C. (v) & (vi) The nanowire radius distribution as estimated by the SAXS data analysis for SiC carbon composite heat treated at 1500 °C.

Fig. 4.9 Networking of polymer silica and PF resin to form uniform carbonaceous silica xerosol.

Fig. 4.10 Flow sheet for preparation of SiC impregnated carbon composite by sol gel method using glycerin as carbon source and TEOS & PMHS as silicon source.

Fig. 4.11 SEM images of (i) Bare carbon fabric (ii),(iii),(iv) the microstructure of SiC impregnated carbon fabric prepared by first routes, and (v) (vi) &(vii) by second route at different magnification.

Fig. 4.12 XRD patterns of the SiC carbon composites after heat treatment prepared by first route (PMHS-TEOS-Glycerin) and second route (PMHS-Glycerin).

CHAPTER 5

Fig.5.1 SEM image of the dense SiC coated carbon fibers (a) lower and (b) higher magnification.

Fig. 5.2 EDX data of the elements in Dense SiC coated carbon fiber (a) before (b) after oxidation; SiC nanowires coated carbon fiber (c) before and (d) after oxidation in oxygen environment.

Fig. 5.3 Optical micrograph of the SiC nanowires coated carbon fibers.

Fig. 5.4 SEM images of (a) Bundle of SiC nanowires coated carbon fibers (b) One SiC nanowires coated carbon fiber (c) Surface of the SiC nanowires coating.

Fig. 5.5 (a) Scattering profiles for SiC nano wires coated and uncoated carbon fiber (b) The Fitted SANS profile of the SiC nanowires. The inset shows the nanowire radius distribution.

Fig. 5.6 Thermogravimetric analysis of (i) bare carbon fiber (ii) SiC nanowires coated carbon fiber (iii) Dense SiC coated carbon fiber in oxygen environment.

Fig. 5.7 SEM images of the Dense SiC coated carbon fibers after oxidation in oxygen environment (a) bunch of coated carbon fibers (b) surface of single coated carbon fiber.

Fig. 5.8 SEM images of the SiC nanowires coated carbon fiber after oxidation in oxygen environment.

Fig. 5.9 DTG curves of (i) bare carbon fiber (ii) SiC nanowires coated carbon fiber (iii) Dense SiC coated carbon fiber in oxygen environment.

Fig. 5.10 Thermogravimetric analysis of (i) bare carbon fiber (ii) SiC nanowires coated carbon fiber (iii) Dense SiC coated carbon fiber in atmospheric environment.

Fig. 5.11 SEM images of the Dense SiC coated carbon fibers after oxidation in atmospheric environment (a) surface of coated carbon fiber (b) Crack propagation through grain.

Fig. 5.12 SEM images of the SiC nanowires coated carbon fiber after oxidation in atmospheric environment (a) surface of a coated carbon fiber (b) & (c) microcracks, micropores and pits on the surface.

Fig. 5.13 The isothermal oxidation weight loss curve of bare carbon fiber and coated carbon fiber samples.

Fig. 5.14 Arrhenius curve of bare carbon fiber and coated carbon fiber samples.

Fig. 5.15 The nonisothermal TG curve of bare carbon fiber and coated carbon fiber samples.

Fig. 5.16 The DTG curve of (a) SiC nanowire coated carbon fiber samples (b) bare carbon fibers samples.

Fig. 5.17 Pictorial depiction of oxidation of SiC nanowires coated carbon fibers at different temperature region (For representation purpose only few SiC nanowires were shown over the surface of carbon fibers, actually they were densely grown over carbon fiber).

Fig. 5.18 Thermogravimetric analysis of bare carbon fabric and SiC carbon composites in atmospheric environment.

Fig. 5.19 The DTG curve of bare carbon fabric and SiC carbon composites in atmospheric environment.

Fig. 5.20 EDX data of the elements in SiC carbon composites before oxidation.

Fig. 5.21 The SEM micrograph of oxidized surfaces of composite at different stage of oxidation.

Fig. 5.22 EDX data of the elements in SiC carbon composites after oxidation at 1300 °C.

Fig. 5.23 (a) & (b) TG/DTG curve of oxidation of SiC carbon composite at different rates of 2.5, 5, 10 and 15 °C/min.

Fig. 5.24 KAS plot for the oxidation of SiC carbon composite.

Fig. 5.25 Ozawa plot for the oxidation of SiC carbon composite.

LIST OF TABLES

CHAPTER 1

Table 1.1 Commonly used SiC gaseous precursors and their applications.

CHAPTER 2

Table 2.1 Comparison of commercial available precursors

CHAPTER 3

Table 3.1 Concentration of different Elementals in different SiC coatings.

Table 3.2 Selection of parameters and their levels for Taguchi method.

Table 3.3 Design of L-9 orthogonal array for experiments.

Table 3.4 Experiments performed by varying H₂/MTS ratio at 1300 °C.

Table 3.5 Results from deposition, micro structural analysis of SiC and corresponding S/N ratio.

Table 3.6 Effect of different parameters on the deposition rate of SiC.

Table 3.7 Effect of different parameters on the growth diameter of SiC.

CHAPTER 4

Table 4.1 List of frequently used silicon and carbon precursors in sol-gel method and the various type of dried gel formation during drying and firing.

Table 4.2 Peak maximum 2θ (°) and width β (°) of the (022) XRD peaks under Gaussian approximation for SiC carbon composites heat treated at different temperature.

CHAPTER 5

Table 5.1 Elemental analysis of different SiC coated carbon fibers using EDX before and after oxidation.

Table 5.2 Thermal Oxidation behavior of carbon fiber and different SiC coated carbon fibers in different oxidation environment.

Table 5.3 Elemental analysis of different SiC coated carbon fibers using EDX before and after oxidation.

Table 5.4 Oxidation decomposition data of a , T and da/dT obtained from the TG–DTG curves for oxidation of carbon fiber.

Table 5.5 Oxidation decomposition data of a , T and da/dT obtained from the TG–DTG curves for oxidation of SiC nanowire coated carbon fiber.

Table 5.6 Kinetic model mechanism functions used for the kinetic analysis.

Table 5.7 Kinetic parameters (E_a , A , r and Standard Deviation) obtained from Achar-Brindly-Sharp Method for oxidation of carbon fiber.

Table 5.8 Kinetic parameters (E_a , A , r and Standard Deviation) obtained from Satava-Sestak Method for oxidation of carbon fiber.

Table 5.9 Kinetic parameters (E_a , A , r and Standard Deviation) obtained from Coats-Redfern Method for oxidation of carbon fiber.

Table 5.10 Kinetic parameters (E_a , A , r and Standard Deviation) obtained from Madhusudanan-Krishnan-Ninan Method for oxidation of carbon fiber.

Table 5.11 Kinetic parameters (E_a , A , r and Standard Deviation) obtained from Achar-Brindly-Sharp Method for oxidation of SiC nanowire coated carbon fiber.

Table 5.12 Kinetic parameters (E_a , A , r and Standard Deviation) obtained from Satava-Sestak Method for oxidation of SiC nanowire coated carbon fiber.

Table 5.13 Kinetic parameters (E_a , A , r and Standard Deviation) obtained from Coats-Redfern Method for oxidation of SiC nanowire coated carbon fiber.

Table 5.14 Kinetic parameters (E_a , A , r and Standard Deviation) obtained from Madhusudanan-Krishnan-Ninan Method for oxidation of SiC nanowire coated carbon fiber.

Table 5.15 Thermal Oxidation behaviors of carbon fabric and SiC impregnated carbon composite in atmospheric oxidation environment.

Table 5.16 Elemental analysis of SiC carbon composites before oxidation.

Table 5.17 Elemental analysis of SiC carbon composites after oxidation at 1300 °C.

Table 5.18 Activation Energy values and correlation coefficients (r^2) calculated using KAS and Ozawa method for oxidation of SiC carbon composite.

Table 5.19 Most probable mechanism function $g(\alpha)$, slopes, and correlation coefficients of linear regression (r^2) at 1000 and 1010 °C.

CHAPTER 1

INTRODUCTION

1. Introduction

1.1 History of Silicon Carbide

In the past, the Silicon Carbide (SiC) has never been attracted by Meteorologists, Chemists and scientists due to the almost total absence of SiC in natural form. It is known to occur and has been found in a meteorite (1905) by Morison. For this reason mineralogists call natural SiC for moissanite.

The first observation of SiC, was made in 1824, by Jöns Jacob Berzelius¹. At that time the properties of SiC were not understood. It was not until the invention of the electric smelting furnace by E. H. & A. H. Cowles² and its application to carbonaceous compounds by Acheson³ that the interest in SiC came into focus. The purpose of Achesons invention was to produce a material substituting diamond and other abrasive materials for cutting and polishing purposes. The crystalline products Acheson found after the process were characterized by hardness, refractability and infusibility. He called the product 'carborundum' and described it as silicide of carbon with the chemical formula SiC. The invention had a great impact and much material was produced using this process mainly for cutting and abrasive purposes. Shortly afterwards the electronic properties of SiC were investigated. The first Light Emitting Diode was made from SiC in 1907⁴. In 1955, a new concept of growing high quality crystals was presented. The research in SiC became more intensified after this and the first SiC conference was held in Boston 1958. The success and rapid growth of the Si technology was made, however, that the interest in SiC dropped. Research during this time (mid '60 to '70) was mainly carried out in the former Soviet Union. In the West, some research in SiC has been continued. In the year 1978, the discovery of comparable dimension and importance as the Acheson process, was presented by Tairov and Tsvetkov⁵. They discovered a way to produce substrates by a seeded sublimation

growth. Due to this discovery the SiC technology gained new momentum. The possibility to grow single crystal SiC on Si substrates was demonstrated by Matsunami et. al. ⁶ in 1981 was an important milestone not so much technologically but more as a further 'temperature increase' in the SiC field. Limitations of the Si technology and the III/V technology have further increased the interest in SiC and at present the field is growing rapidly much owing to the recent commercial availability of substrates.

In 1982, a composite of aluminum oxide and SiC whiskers was discovered at the Oak Ridge National Laboratories. This material proved to be exceptionally strong. Development of this laboratory-produced composite to a commercial product took only three years. In 1985, the first commercial cutting tools made from this alumina and SiC whisker-reinforced composite were introduced by the Advanced Composite Materials Corporation (ACMC) and Greenleaf Corporation.

In the recent context, the very good mechanical, physical and chemical properties of SiC have led to extensive research efforts on its manufacturing routes and potential applications. It possesses many favorable properties e.g. wide band gap, high thermal conductivity, high breakdown electric field strength, high saturated drift velocity, high thermal and chemical stability and high power applications. Although diamond has an even higher band gap, SiC-based devices are easier to manufacture due to the fact that it is more convenient to grow an insulating layer of silicon dioxide on the surface of a SiC wafer than on diamond.

1.2 Crystal structure of SiC

SiC is a wide band-gap semiconductor material, having different polytypes. All polytypes have a hexagonal frame with a carbon atom situated above the center of a triangle of Si atoms and underneath a Si atom belonging to the next layer (Fig. 1.1). The distance 'a' between

neighboring silicon or carbon atoms is approximately 3.08 Å for all polytypes⁷. The carbon atom is positioned at the center of mass of the tetragonal structure outlined by the four neighboring Si atoms so that the distance between the C atoms to each of the Si atoms

(marked as C-Si in the Fig. 1.1) is the same. Geometrical considerations give that this

distance, C-Si, is approximately equal to 1.89 Å. While the distance between two silicon planes is approximately 2.52 Å. The height of a unit cell 'c' varies between the different polytypes. The ratio c/a , thus, differs from polytype to polytype, but is always close to the ideal for a closed packed structure. This ratio is for instance approximately 1.641, 3.271 and 4.908 for the 2H-, 4H- and 6H-SiC polytypes, respectively. The difference between the polytypes is the stacking order between succeeding double layers of carbon and silicon atoms.

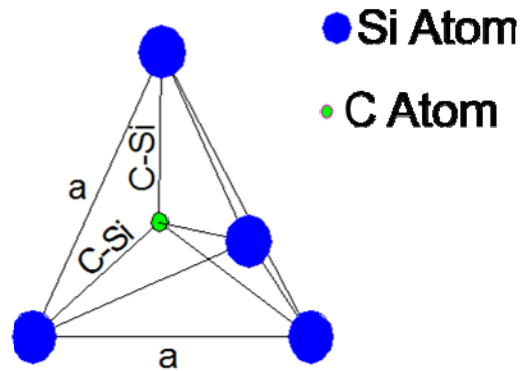


Fig. 1.1 The tetrahedral bonding of a carbon atom with the four neighboring silicon atoms

In the Fig. 1.2 the stacking sequence is shown for the three most common polytypes, 3C, 6H and 4H. If the first double layer is called the A position, the next layer that can be placed according to a closed packed structure will be placed on the B position or the C position. The different polytypes will be constructed by permutations of these three positions. For instance the 2H-SiC polytype have a stacking sequence ABAB... The number thus denotes the periodicity and the letter the resulting structure that in this case is hexagonal.

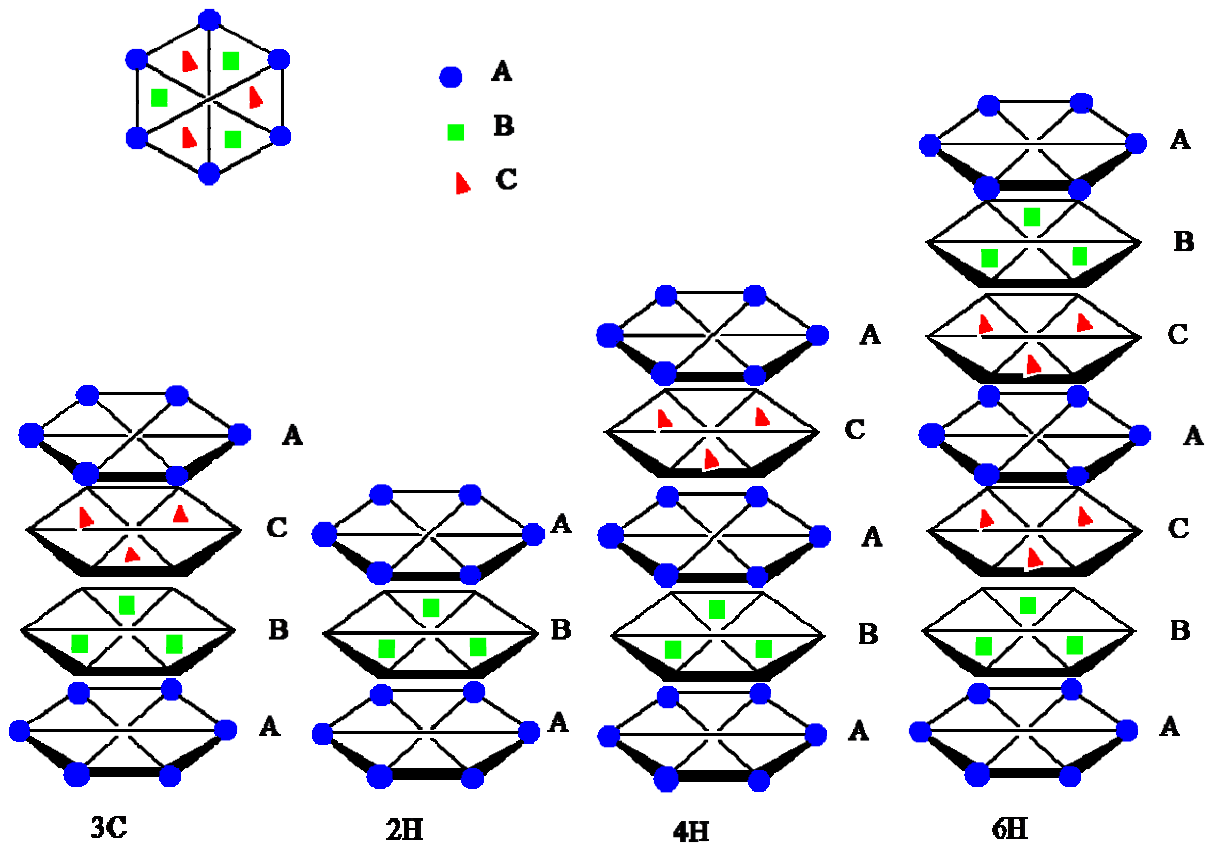


Fig. 1.2 The stacking sequence of double layer of the most common SiC polytypes

The 3C-SiC polytype is the only cubic polytype and it has a stacking sequence ABCABC... or ACBACB... A common crystalline defect is the so called Double Positioning Boundary (DPB), which is commonly seen in 3C-SiC grown on on-axis 6H-SiC substrates. The defect arises when islands of the two possible stacking sequences ABCABC and ACBACB meet. The growth of

3C-SiC on on-axis 6H-SiC substrates and the consequent evolution and control of the DPB defect has been studied in detail by Powell et. al.⁸⁻⁹.

There are four hexagonal Miller indices describing the directions in all SiC polytypes except for the 3C polytype where the normal cubic notation is used. The last hexagonal index refers to the c-direction, whereas the three first describes directions in the basal plane. The angle between two adjacent basal plane axes is 120° as shown in the Fig. 1.3. By definition, the sum of the first three indices must be zero.

1.3 Applications of SiC

The band gaps of Pure α -SiC (3.28 eV (4H) and 3.03 eV (6H)) make it to be used as an intrinsic semiconductor. SiC is also used for blue Light Emitting Diodes (LEDs), ultrafast Schotky diodes, Metal-Semiconductor Field Effect Transistors (MESFETs) and high temperature Insulated gate Bipolar Transistors (IGBTs) for high power switching. Due to its wide bandgap, SiC-based parts are capable of operating at high temperature (over 350°C), which together with good ‘thermal conductivity’ reduces problems associated with cooling of power parts. They also possess increased tolerance to radiation damage, making it a material desired for defense and aerospace applications. SiC is also used as an ultraviolet detector.

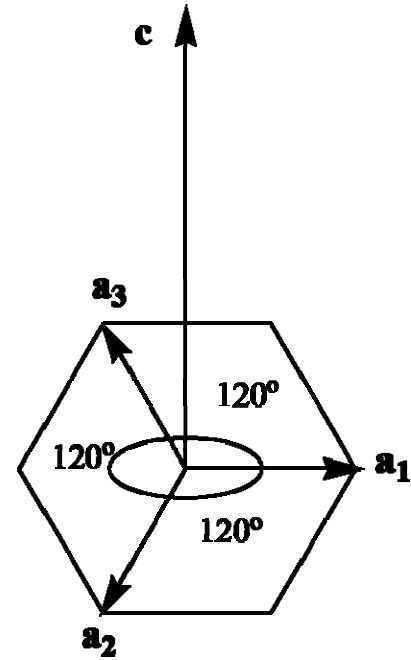


Fig. 1.3 The miller indices describing the hexagonal structure. The c-axis refers to the last index, whereas the first three describes the direction of the basal plane.

Silicon carbide's hardness and rigidity make it a desirable mirror material for astronomical work, although its properties also make manufacturing and designing such mirrors quite difficult.

SiC is a popular product in modern lapidary due to the durability and low cost of the material. It is also used in "super fine" grit sandpapers. Silicon-infiltrated carbon-carbon composite is used for high performance brake discs as it is able to withstand extreme temperatures. The silicon reacts with the graphite in the carbon-carbon composite to become SiC. These discs are used on some sports cars, including the Porsche Carrera GT and SiC is also used in a sintered form for Diesel Particulate Filters. It is used for producing ceramic membranes for industrial processes.

SiC dissolved in a basic oxygen furnace used for making steel acts as a fuel and provides energy, which increases the scrap to hot metal ratio. It can also be used to raise tap temperatures and adjust the carbon content.

Recently SiC has got great importance in nuclear industry. In triso-coated fuel particles for high temperatures gas cooled reactors (HTGR), one of the layers is SiC coating. The four layers of coating on spherical fuel particles are Porous Pyrolytic Carbon (PyC), dense PyC, SiC and another dense PyC. The function of these layers is to retain fission products within the particle. In particular the SiC layer acts as a diffusion barrier to metallic fission products and a miniature pressure vessel of the particle. The experimental results by Forthmann et al ¹⁰ and Bullock ¹¹ suggested that diffusion behavior of fission products in the SiC layer depend on microstructure of the layer. It is therefore important to clarify a relationship between deposition parameters, chemical composition and microstructure of the deposits.

SiC fibers and composites from graphite precursors also have shown its importance for fusion energy applications. A high purity β -SiC is ¹² projected to exhibit neutron stability in a fusion reactor environment because of its microstructure and physical dimension stability. A pure β -SiC fiber could therefore be expected to be an excellent candidate as reinforcement to produce β -SiC/ β -SiC composites. SiC has relatively high thermal conductivity, is stable in hydrogen and helium, has high temperature resistance, suffers little erosion and its decomposition products display little reactivity with other wall materials but the difficulty with monolithic SiC is its low thermal shock resistance, which leads to cracking and disintegration of the material by thermal fatigue.

1.4 Research on advance SiC coating/composite development

There is a lot of research going on to develop advance composites materials such as carbon/carbon composites by introducing compatible coating or by introducing second phase in the parent matrix, which can withstand extreme environment ¹³⁻¹⁷. The performance of composites in many cases, depend upon the development of suitable coatings to protect against environmental degradation. For example, carbon composite exhibits very poor oxidation resistance property so the applications of reinforced carbon composites have been limited to inert atmosphere to prevent the oxidation of carbon composite. To widen the application area of carbon composites, it is necessary to improve their oxidation resistance property. Hence, intensive efforts are underway to deposit a protective coating or impregnate with second phase ceramic material in parent matrix, which would prevent the oxidation of carbon for continuous use at elevated temperatures of 1000–1500 °C in an oxygen containing environment ¹⁸⁻¹⁹. In the last few years, ceramic coatings / ceramic composites have been receiving considerable attention

for a variety of reasons including economics (substitution of expensive alloys by cheaper alternatives, extension of service life of alloys), environment, material protection from wear, corrosion and erosion, and improvement and development of new material properties ²⁰⁻²⁸. Ceramic coatings/composites can be useful in a wide range of applications, such as thermal barriers for gas turbine blades and vanes, hot section parts of diesel engines, electrical insulation in electronic circuit substrates, nuclear technology and medical applications ²⁹⁻³². In case of coated materials, the performance of materials will enhance if the integrity of the coating can be maintained throughout the projected service life of the component. Among the several key issues that must be considered in selecting coating materials, some are as follow: (i) coating must possess the ability to resist reaction with aggressive environments, as well as low oxygen permeability to limit the transport of oxygen (ii) the coefficient of thermal expansion (CTE) of coating should be close to that of the substrate material in order to prevent delamination or cracking due to the stress caused by CTE mismatch (iii) coating must maintain a stable phase under thermal exposure because phase transformation typically accompanies a volumetric change, disrupting integrity of the coating and. (iv) coating must be chemically compatible with the substrate to avoid detrimental chemical interaction.

To avoid the formation of cracks in the ceramic coating due to above mentioned reasons reinforcement of a second phase such as whiskers ¹⁶, nanotubes ¹⁷ and nanowires ¹⁵ is required. Among these reinforced second phase, the SiC nanowire is more suitable for their smaller size, higher strength, and toughness. Better compatibility with ceramic coating and oxidation resistive property of SiC nanowires make it a potential candidate as reinforcement material with SiC coating on carbon substrate.

Following subsections will deal with the development of different coating techniques, infiltration techniques and organosilicon precursor in detail.

1.4.1 Coating techniques

There are a number of factors to be considered when developing a coating process for an application. These include capital investment, ease of manufacturing, coating performance and environmental issues. Though, a large number of coating techniques such as electrochemical plating³³, conversion coatings³⁴⁻³⁵, anodizing³⁴, polymer plating sol-gel coating or plasma polymerization^{27, 30, 36}, chemical vapor deposition (CVD)³⁷, physical vapor deposition (PVD)³⁷⁻³⁸ etc. are available for protecting materials. However the widespread use of materials in the industry is still deterred by the lack of appropriate protective coatings that can withstand harsh service conditions. Therefore, a great deal of research is going on to develop better, simpler and cheaper coating technologies using materials such as SiC to take advantages of its lower weight and excellent mechanical properties. CVD is the most frequently used technique to deposit thick SiC ceramic coating to protect engineering components against chemical diffusion, wear, friction, oxidation and corrosion³⁹. The cost of CVD for the protective coatings market is generally lower than the functional thin films for semiconductor industry as it involves coating a large volume of engineering components. Other competing deposition methods for protective coatings are plasma spraying⁴⁰ and PVD. The plasma spraying tends to produce a splat-like structure with a high degree of porosity, micro-cracks and surface roughness. In such a case, a thicker coating is required to provide adequate protection against wear and corrosion, and extensive grinding and polishing post deposition is required to obtain a smoother surface.

Moreover, the splat-like structure is mechanically not as robust as the equiaxed/ columnar structure deposited using the CVD and PVD techniques. The PVD method is a line-of-sight process. Therefore, in PVD process, use of multiple targets and a rotating substrate is often required to improve uniformity of coating on complex shape components. However, CVD does not have such limitations. In CVD process of ceramic coatings a high deposition temperature is usually required to ensure good adhesion of the thick coating on the substrate as compared to lower deposition temperatures in CVD of thin films. Good coating adhesion is essential for better thermal, chemical (corrosion, diffusion resistance) and/or mechanical (e.g. wear, abrasion resistance) properties. Therefore, this requirement limits the utilization of CVD as a coating for the substrate or engineering components which are susceptible to high temperatures. For example, the deposition of thick, hard and wear resistant coatings onto high speed cutting tool steels using thermally activated CVD is less suitable because tool steel has a low austenising temperature (450– 550 °C). The CVD deposition of protective coatings would require high temperatures (>800 °C), which is above the tempering temperature of most steels⁴¹. This leads to softening of the steel substrate and therefore, subsequent heat treatment is required for re-hardening which may cause deformation, change of substrate dimensions, and increase in the cost of production. However, there are other variants of CVD such as plasma enhanced CVD (PECVD) and metal-organic CVD (MOCVD) which can lower the deposition temperatures and produce high quality ceramic protective coatings without degrading the tool steel substrates, but their cost of production is still relatively high as compare to the other coating techniques. Many such limitations of CVD coating can be suitably addressed to a greater extent by replacing conventional inorganic precursors with metal-organic precursors in CVD coating. In addition, using metal-organic precursors in CVD is economical and environmentally benign. The present

section covers different variants of coating using metal-organic precursors as well as relatively cheaper synthesis routes for some of the metal-organic precursors which can be used for CVD coating.

1.4.1.1 Chemical Vapor deposition: MOCVD variant techniques

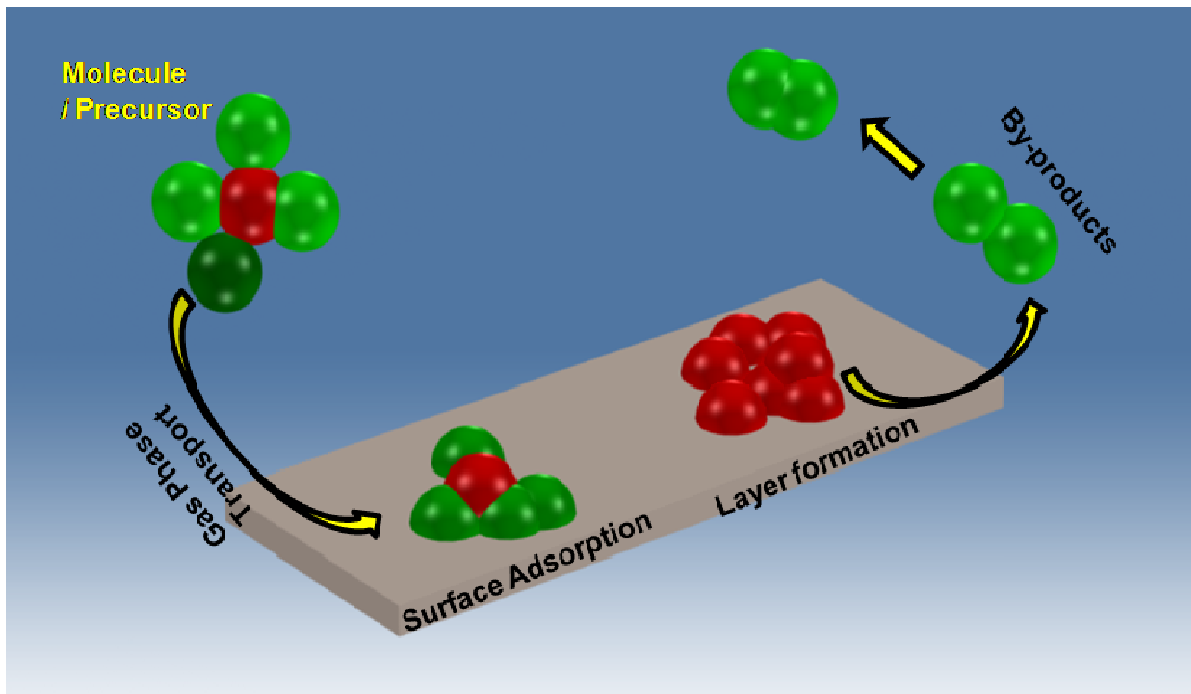


Fig. 1.4 Schematic representation of general chemical vapor deposition Process

CVD of films and coatings involve the chemical reactions of gaseous reactants on or near the vicinity of a heated substrate surface (Fig. 1.4). This atomistic deposition method can provide highly pure materials with structural control at atomic or nanometer scale level. Moreover, it can produce single layer, multilayer, composite, nanostructured, and functionally graded coating materials with well controlled dimension and unique structure at low processing temperatures. Furthermore, the unique feature of CVD over other deposition techniques such as the non-line-

of-sight-deposition capability has allowed coating of complex shape engineering components and the fabrication of nano-devices, carbon-carbon (C-C) composites, ceramic matrix composite (CMCs) and free standing shape components. The versatility of CVD had led to rapid growth and it has become one of the main processing methods for the deposition of thin films and coatings for a wide range of applications including semiconductors (e.g. Si, Ge, Si_{1-x}Ge_x, III-V, II-VI) for microelectronics, optoelectronics, energy conversion devices, dielectrics (e.g. SiO₂, AlN, Si₃N₄) for microelectronics, refractory ceramic materials (e.g. SiC, TiN, TiB₂, Al₂O₃, BN, MoSi₂, ZrO₂) used for hard coatings, protection against corrosion, oxidation or as diffusion barriers, metallic films (e.g. W, Mo, Al, Au, Cu, Pt) for microelectronics, protective coatings, fiber production (e.g. B and SiC monofilament fibers) and fiber coating.

The conventional CVD method, so called thermal activated CVD (TACVD)⁴², uses thermal energy to activate the chemical reactions. However, the CVD reactions can also be initiated using different energy sources. This has given rise to other variants of CVD methods such as plasma enhanced CVD (PECVD)⁴² and photo-assisted CVD (PACVD)⁴³ which use plasma and light respectively to activate the chemical reactions. Atomic Layer Epitaxy (ALE)⁴⁴ is a special mode of CVD where a 'monatomic layer' can be grown in sequence by sequential saturating surface reactions. Such CVD variants are useful for the controlled growth of epitaxial films, and the fabrication of tailored molecular structures. Flame assisted vapor deposition (FAVD)⁴⁵ uses a flame source to initiate the chemical reaction and/or heating the substrate. Electrochemical vapor deposition (EVD) is another variant of CVD that is tailored for the deposition of dense films onto porous substrates. Chemical vapor infiltration (CVI)⁴⁶ is a form of CVD that has been adapted for the deposition of a dense ceramic matrix during the fabrication of ceramic fiber reinforced ceramic matrix composites. Other CVD variants such as pulsed injection CVD⁴⁷ and

aerosol assisted CVD ⁴⁸ use special precursor generation and delivery systems unlike conventional CVD.

MOCVD ⁴⁹ is a variant of CVD, which has been classified according to the use of metal-organic compounds as precursors. Use of metal-organic precursors in MOCVD has several advantages like lower deposition temperature, safe operation and cost effectiveness. Metal-organic compounds also called as “metalorganics” contain metal atoms bonded to some organic fragments. The compounds having one or more direct metal–carbon covalent bonds are called “organometallics”. Metalorganics as well as organometallics both can be used as precursors in MOCVD. Use of organometallic precursors has led to the rename of the deposition process as organometallic CVD (OMCVD) to reflect more precisely the choice of precursors used. In conventional OMCVD, the precursor is vaporized at low temperature, under reduced pressure condition and subsequently, metal film is deposited on a substrate surface at higher temperature by adsorption and thermal decomposition of the precursor. The various parameters that control this deposition technique are as following: (1) convection of the gaseous reagents (2) diffusion of the reagents towards the substrate (3) adsorption of the reagents onto the substrate (4) chemical reaction of the adsorbed species producing nuclei and further reaction to give a metal film (5) desorption of the gaseous products of the reaction (6) diffusion of these products through the boundary layer and (7) gas evacuation of the system.

The choice of a CVD method among all those described shall be made according to the specifications of the deposit in terms of topology, purity, physical properties, process speed and cost.

1.4.1.1.1 Laser induced chemical vapor deposition (LCVD)

In this technique, decomposition of precursor is induced with a laser beam (Fig 1.5). LCVD⁵⁰⁻⁵¹ has the advantages of better control of the decomposition mechanism compared to the traditional method and is able to function on a substrate-limited surface. The process can be carried out with substrates that do not have high thermal conductivity and the deposit growth kinetics is often faster than

those observed with traditional OMCVD. In LCVD, it is also possible to work at higher precursor pressure than

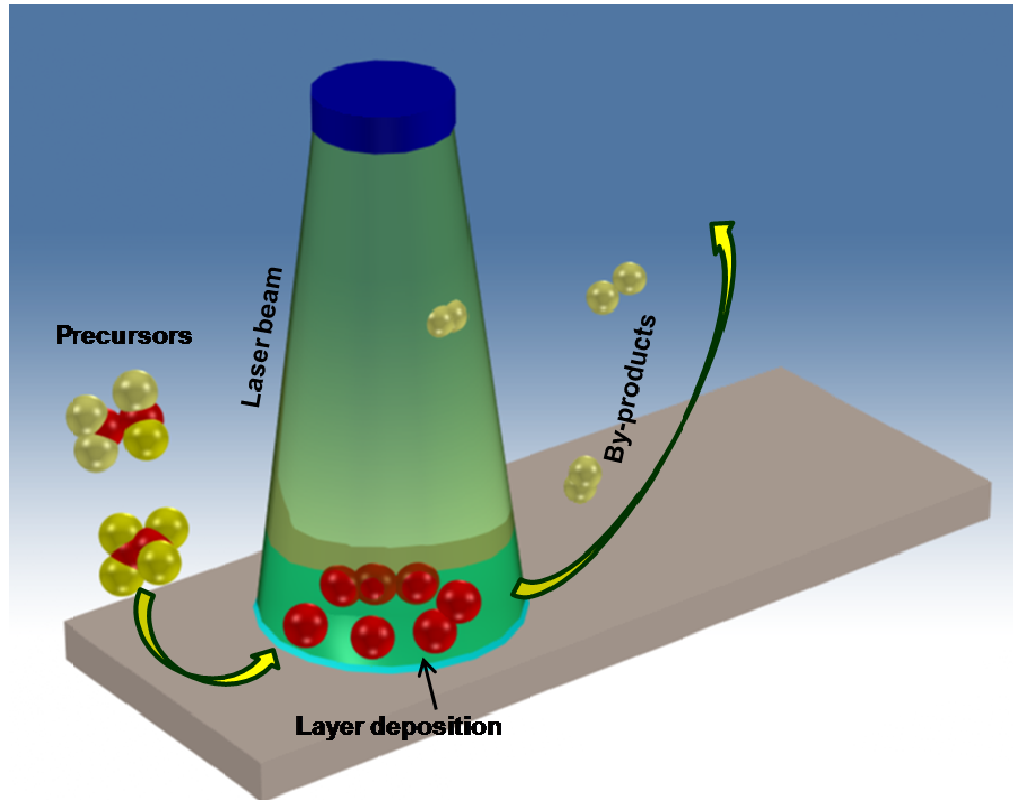


Fig. 1.5 Schematic representation of Laser Induced Chemical Vapor Deposition (LICVD)

growth kinetics here being limited by gas-phase decomposition. Partial pressure of precursor seems to be the critical factor, allowing an increase in deposition rate without loss in the overall deposit quality. To obtain a film with few impurities, the laser must de-coordinate all the precursor ligands; avoiding the incorporation of carbon and other elements into the film. The

growth rate depends on the wavelength of light used and on the laser power. Photolysis can occur in several stages with quantum yields depending on the laser wavelength.

1.4.1.1.2 UV induced chemical vapor deposition (UVCVD)

The OMCVD can also be carried out under the irradiation of a UV lamp, which can improve the process of

nucleation while

lowering the

operational

deposition

temperature (Fig

1.6). In this case

of deposition, two

methods are

described ⁵²⁻⁵³.

The first one

consists of

depositing the

precursor on the

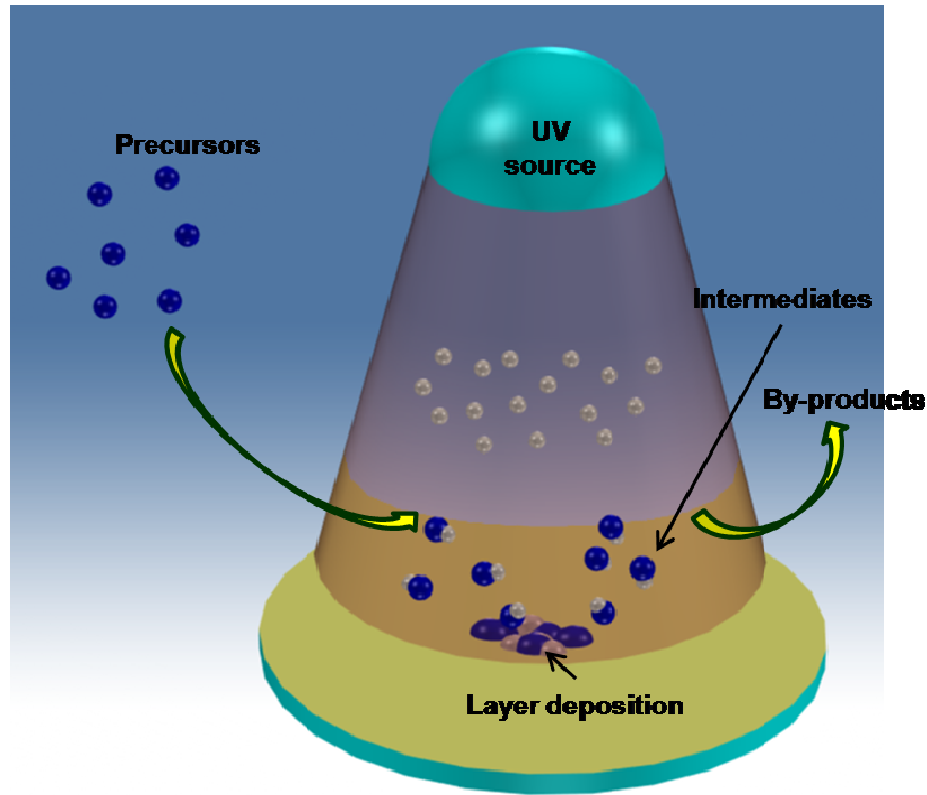


Fig. 1.6 Schematic representation of UV induced chemical vapor deposition (UVCVD)

substrate and then irradiation. In the second method, the metal is being deposited directly by adsorption followed by decomposition of the precursor by irradiation of the substrate. Without a lamp, decomposition of precursors is insignificant at room temperature and remains slow at higher temperature in absence of reactive gases.

1.4.1.1.3 Plasma enhanced CVD (PECVD)

PECVD ⁵⁴⁻⁵⁵

is also known as glow discharge chemical vapor deposition

(Fig. 1.7). It uses electron energy (plasma) as the activation method to enable

deposition to

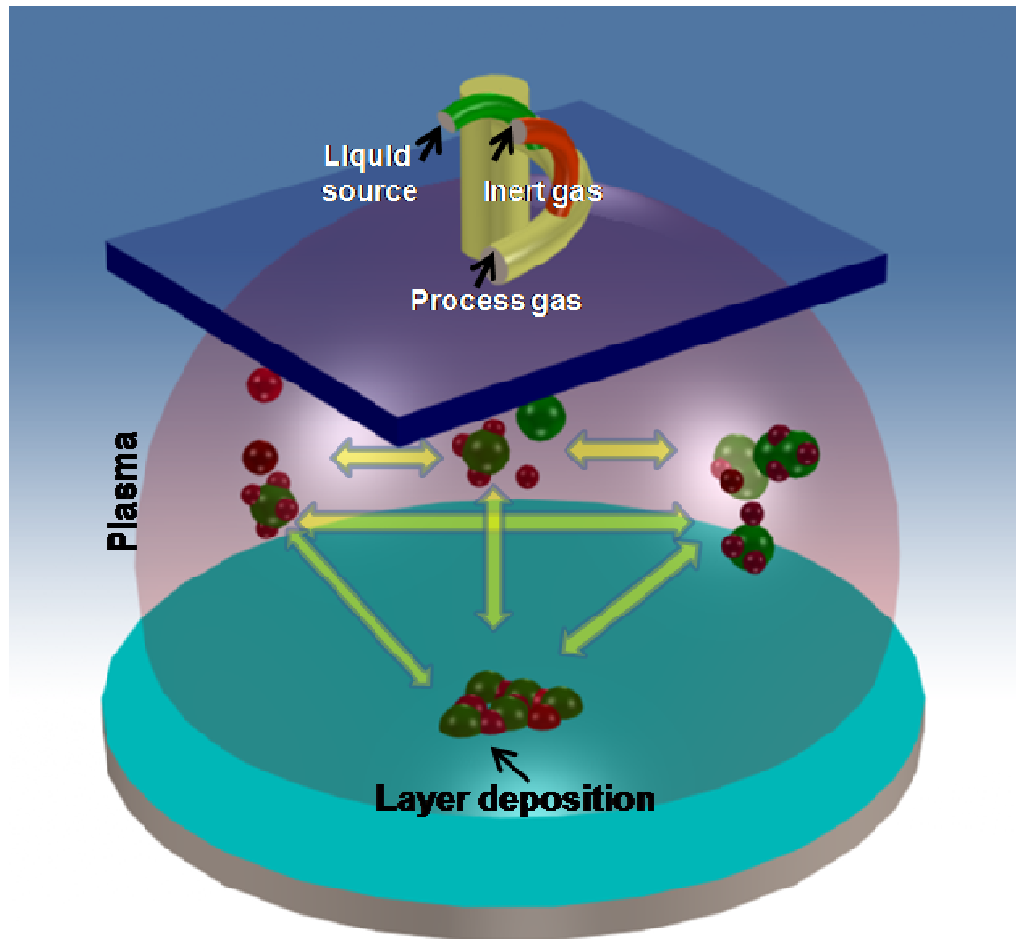


Fig.1.7 Schematic representation of Plasma enhanced platinum CVD (PECVD)

occur at a low temperature and at a reasonable rate. Supplying electrical power at a sufficiently high voltage to a gas at reduced pressures (<1.3 kPa), results in the breaking down of the gas and generates a glow discharge plasma consisting of electrons, ions and electronically excited species. The vapor reactants are ionized and dissociated by electron impact, and hence generating chemically active ions and radicals that undergo heterogeneous chemical reaction at or near the heated substrate surface and deposit thin film. The chemical reactions that occur during the glow discharges are complex and can be categorized into homogeneous gas phase

collisions and heterogeneous surface interactions. It is difficult to establish the relationship between the processing parameters and properties of the films because of the complexity of the PECVD reactions. Therefore, PECVD is limited to low temperature applications where it cannot be met by thermally activated CVD.

1.4.1.1.4 Electron Beam Chemical Vapor Deposition (EBCVD)

EBCVD⁵⁶⁻⁵⁷ is a technology that uses an electron beam to provide localized deposition for nano-scale structures or device fabrication (Fig. 1.8). In EBCVD, primary electrons from the beam impact a substrate, causing secondary electrons to be emitted. These secondary electrons

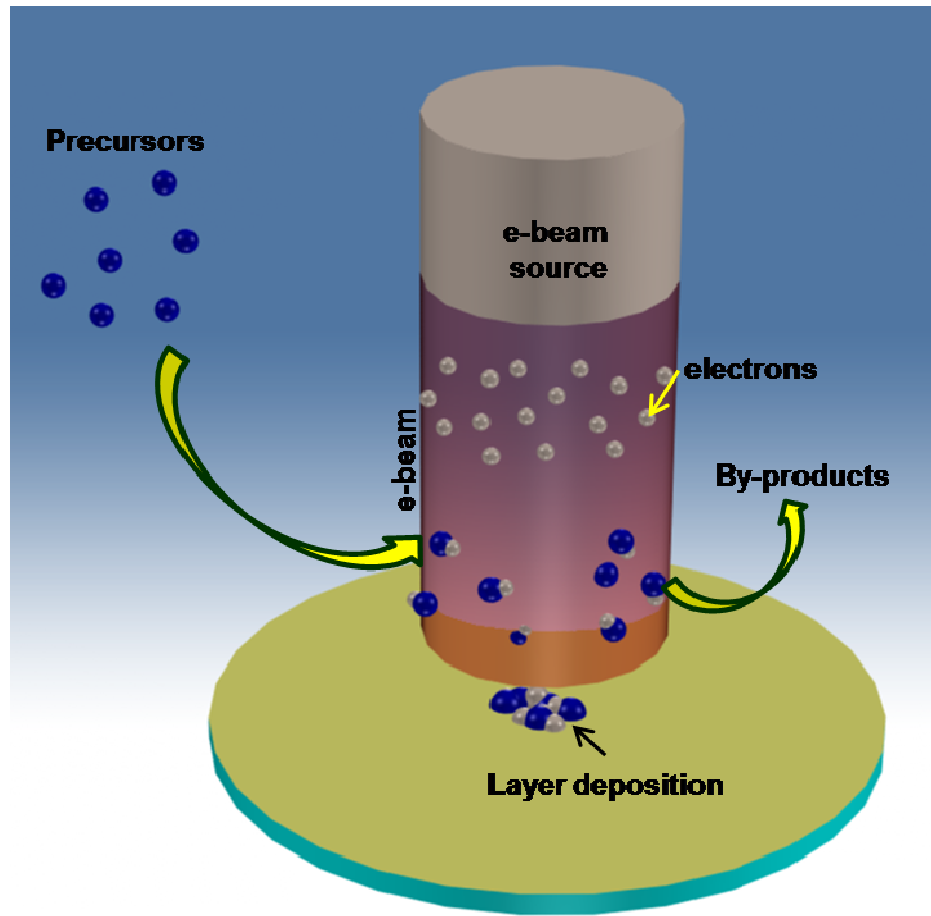


Fig. 1.8 Schematic representation of Electron Beam Chemical Vapor Deposition (EBCVD)

secondary electrons play a prominent role in dissociating adsorbed reagent molecules to form a deposit on the substrate and volatiles that are then evacuated from the chamber. The deposition process depends on many factors including the precursor and the electron beam properties. If the electron beam is

not moved relative to the substrate, a dot is grown. A fiber is grown if the growth time is increased. If the beam is moved, lines or other structures can be deposited as in rapid prototyping. A post-treatment, consisting of a heating step in the presence of

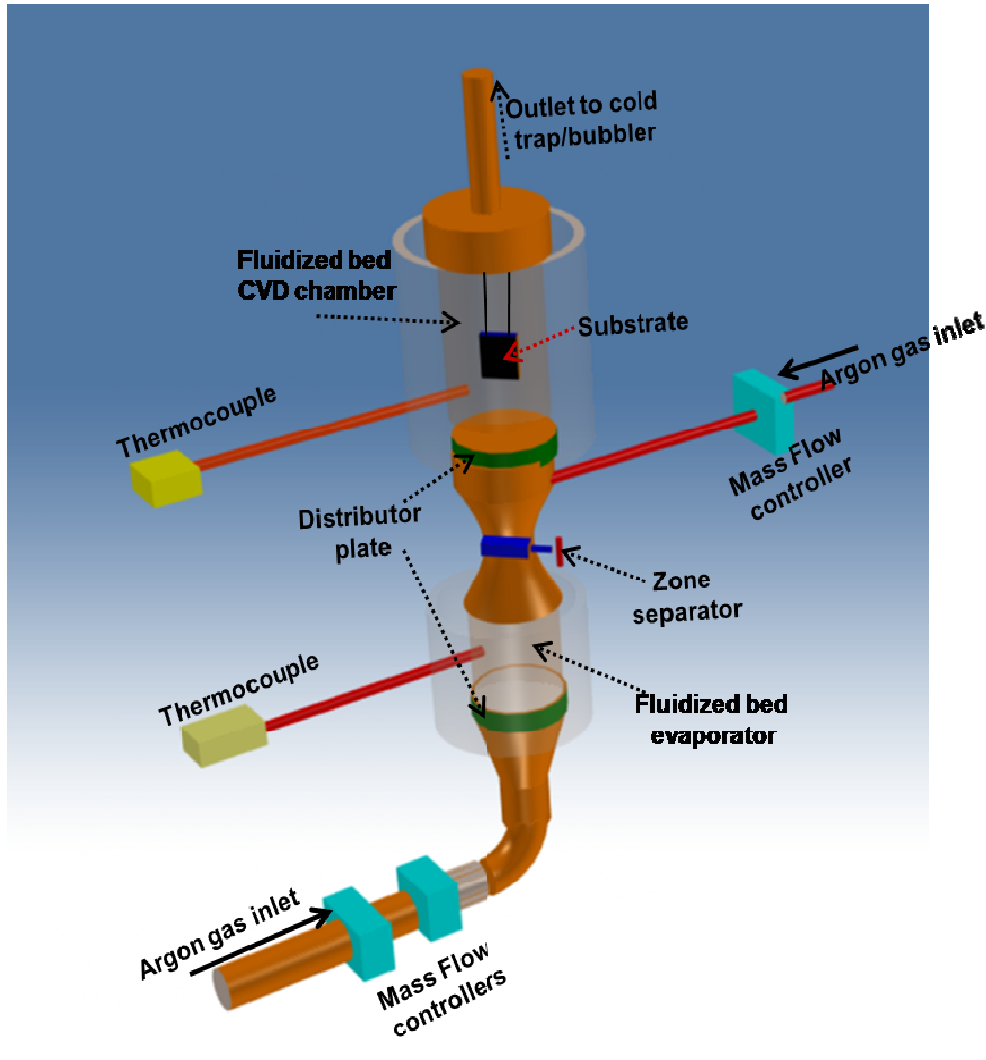


Fig. 1.9 Schematic representation of Fluidized Bed Chemical Vapor Deposition (FBCVD)

oxygen decreases the level of impurities. The deposit may then suffer from a volume reduction due to carbon impurity elimination.

1.4.1.1.5 Fluidized Bed Chemical Vapor Deposition (FBCVD)

FBCVD⁵⁸⁻⁵⁹ is one of the most efficient techniques to functionalize, to deposit on, or to coat each individual particle of a powder from gaseous species (Fig. 1.9). FBCVD combines two processes. One is the deposition itself, the other aims in suspending the particles in the

deposition zone, most often by flowing a gas upwards through the powder and in bringing heat to the powder. In contrast to CVD on flat surfaces which often operates in a surface kinetics limited regime, FBCVD is generally transport-limited. This is due to the extremely high available growth surface to heated volume ratios (S/V) in the deposition area. Consequently, gaseous precursors are very often totally consumed a few centimeters after their entrance into the fluidized bed reactor, but the high degree of gas solid mixing compensates for this discrepancy, and ensures isothermal conditions and uniform deposition.

1.4.1.1.6 Atomic Layer Deposition (ALD)

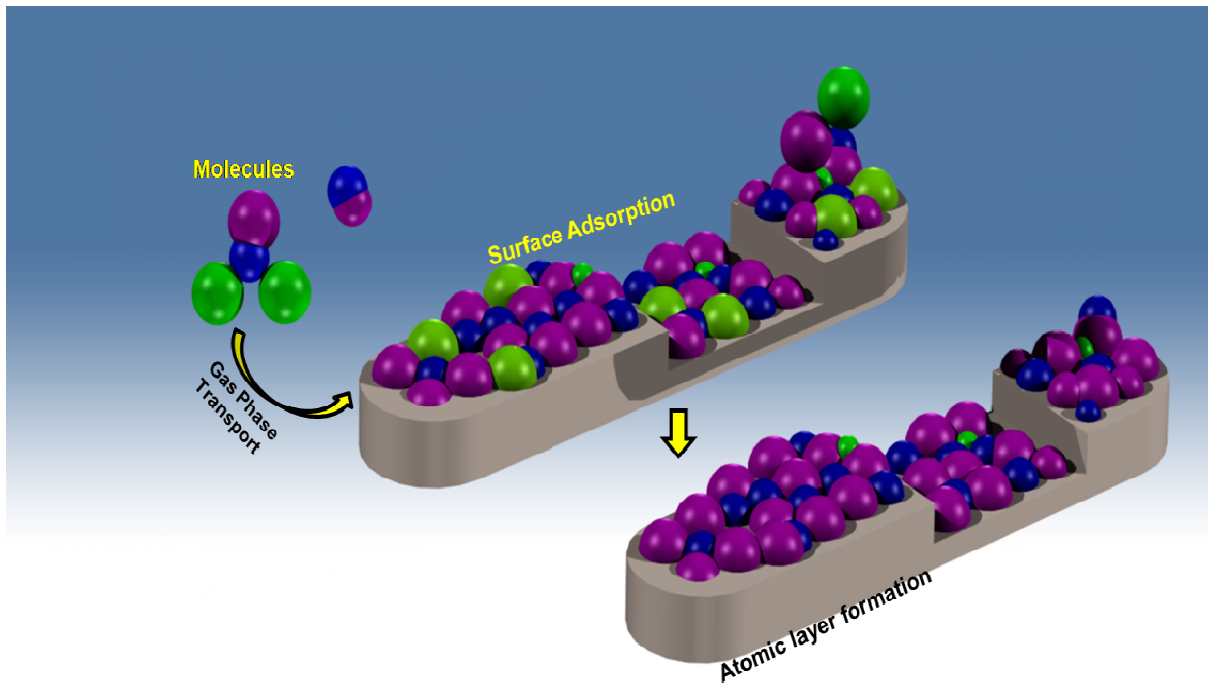


Fig. 2.0 Schematic representation of Atomic Layer Deposition (ALD)

ALE⁴⁴ can be considered as a special mode of CVD (Fig. 2.0). It is a surface deposition process that can be used for the controlled growth of epitaxial films, and the fabrication of tailored molecular structures on the surfaces of solid substrates. 'Monatomic layers' can be grown in

sequence which is a characteristic feature of ALE. Therefore, the desired coating thickness can be produced simply by counting the number of reaction sequences in the process. The surface reconstruction of the monolayer formed in the reaction sequence will influence the saturation mechanism and the saturation density of the precursor. The ALE reaction sequences are normally performed in an ‘effective overdosing’ condition to ensure a complete saturation of the surface reaction to form the monoatomic layer. Furthermore, such ‘effective overdosing’ condition also provides good conformal coverage that allows uniform coatings onto complex shaped substrates. The sequencing in ALE also eliminates the gas phase reactions, and enables a wider choice of reactants (e.g. halides, metalorganics, elemental metal, etc.). The ALE process has the potential to be scaled up for the deposition of high quality thin films with excellent uniformity and reproducibility onto large area substrate⁶⁰⁻⁶¹.

1.4.2 Infiltration techniques

In advance ceramic composites a second phase with different morphology such as whiskers, nanotubes and nanowires along with infiltrated ceramic matrix are required for better compatibility and improved mechanical and oxidation resistive properties^{14, 16, 31, 62-65}. Among these reinforced second phase, the SiC nanowire is more suitable to be used as the reinforcing material for their advantages of smaller size, higher strength, and toughness. SiC nanowires makes it a potential candidate as reinforcement material with SiC coating/ matrix for carbon composite because of its better compatibility with ceramic matrix and oxidation resistive property⁶⁶⁻⁶⁷. Infiltration of such second phase in original matrix may be achieved by two different impregnation routes namely gas phase impregnation⁶⁸⁻⁶⁹ and liquid impregnation⁷⁰⁻⁷³.

The most economical liquid impregnation method has gained importance for carbon/carbon composites. This process involves vacuum or pressure impregnation of porous solid with carbon yielding liquid precursor or SiC yielding liquid precursor, thereby the impregnant liquid has access to the inner fine pore. This can be used to make composites with complex structures.

CVI^{21, 74} is the most studied technique to prepare advance ceramic carbon composites due to its low processing temperature and ability of fabricating complex structural composites. There are several variants of CVI technique such as Isothermal Chemical Vapor Infiltration (ICVI)⁶⁹, Thermal gradient Chemical Vapor Infiltration Process⁶⁹, Differential pressure process⁶⁹, Forced flow-thermal gradient CVI (FCVI)⁶⁹ and Film boiling CVI⁶⁹. Composites with much higher densities can be prepared by a combination of liquid infiltration and CVI as the small pores resulting from multiple impregnations can be filled.

1.4.3 Development of organosilicon precursors: literature survey

SiC is most widely used material especially for corrosion resistance application. In past, many SiC coatings have been produced by the CVD technique, however, most SiC coatings deposited have been grown at relatively high temperatures of 1300 °C- 1380 °C and at atmospheric pressure using separate precursors for Si and C^{8, 75-77}. For instance, SiH₂ or Si₂H₆ have been used for Si and CH₄ or C₃H₈ have been used for C⁷⁸. Combination of methyltrichlorosilane (CH₃SiCl₃ or MTS) and hydrogen is the most popular single molecular precursor, partially because MTS contains the same number of silicon and carbon atoms⁷⁹. To achieve an optimal oxidation resistance, it is important that stoichiometric SiC is deposited. Although the C/Si molar ratio in MTS is one, deposition of silicon with SiC is encountered at temperature below 1000°C, whereas

carbon is deposited with SiC above 1600 °C. The mechanism of SiC deposition can be regarded as two independent subsystems, i.e. the deposition of carbon and the deposition of Si. Equal rates will result in stoichiometric SiC. Detailed knowledge of the kinetics in the gas phase and on the surface is, however, limited especially for chlorine containing SiC precursors like CH₃SiCl₃. The gas phase kinetic for the SiH₄-hydrocarbon system is relatively well understood⁸⁰⁻⁸¹ but more knowledge of the surface chemistry is needed. The use of MTS requires a source of hydrogen gas to combine with the chlorine atoms liberated during decomposition. The reaction forms hydrogen chloride as a by-product, which must be removed, thus requiring a scrubber as part of the equipment. Since the hydrogen chloride is corrosive, all equipment must be corrosion resistant. Table 1.1 shows examples of commonly used SiC gaseous precursors and their applications.

Table 1.1

Commonly used SiC gaseous precursors and their applications

| SiC Precursors | Condition of synthesis | | Application |
|-----------------------------------|------------------------|----------------|-----------------|
| | Temperature (°C) | Pressure (kPa) | |
| CH ₃ SiCl ₃ | 1323-1673 | n.r. | Coating |
| | 1200 | 1.7 | Coating |
| | 973-1073 | 10 to 35 | |
| | 973-1173 | 10 to100 | Composite (CVI) |

| | | | |
|--|-----------|-----------|------------|
| | 1052-1070 | 2 to 13.3 | |
| CH ₃ SiCl ₃ /CH ₄ | 1273-1523 | 4.6 | Coating |
| SiCl ₄ /CH ₄ | 1200-1400 | 100 | Coating |
| (CH ₃) ₂ SiCl ₂ | 1473-1600 | n.r | Coating |
| SiCl ₄ /carbon | 1300-1500 | 100 | Coating |
| SiH ₄ /C _x H _y | 1573-1723 | 100 | Electronic |

n.r. = not reported.

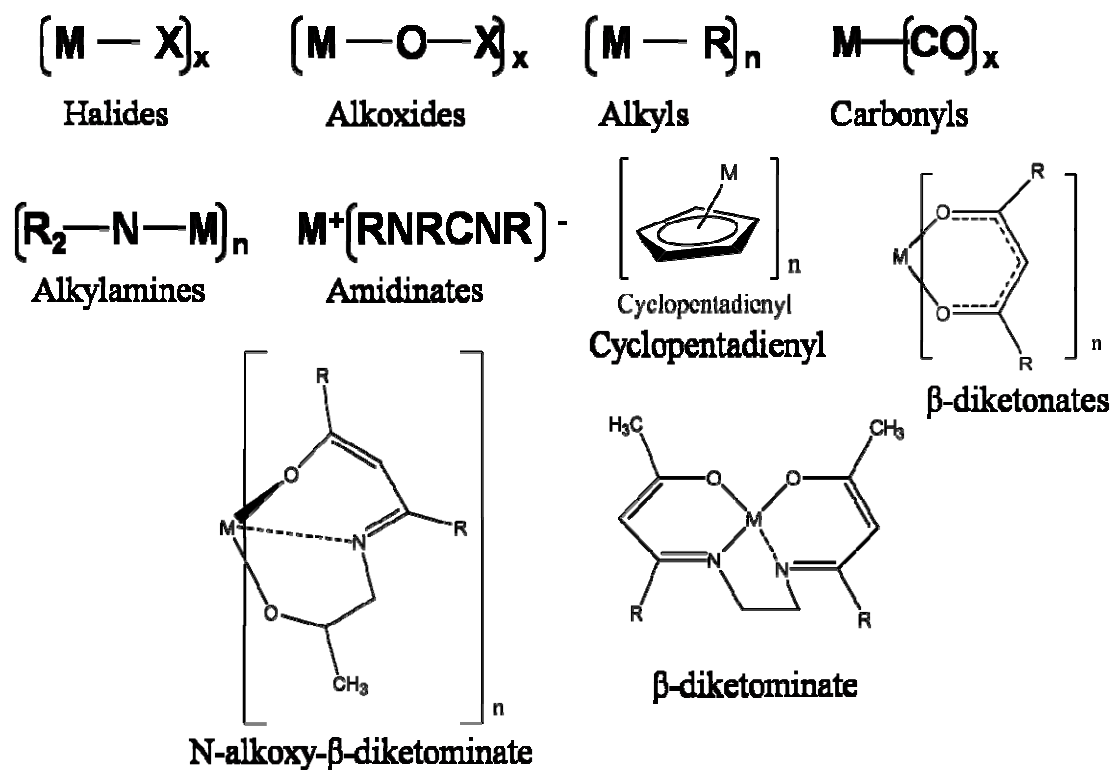


Fig. 2.1 The organic groups used for synthesis of organometallic precursor compounds.

Recent practice of using halogen free single source compounds in chemical vapor deposition is, in some cases, enjoying low deposition temperature and accurate stoichiometry.

Since the single molecular precursor already has a Si-C bond in the precursor itself, it does not need further activation energy to make a Si-C bond in the film, resulting in growth temperatures below 1000 °C. In chemical vapor deposition, the solid phase is formed on a surface from a gas phase via one or several chemical reactions. A key issue is the generation of the gas phase, whose composition must be stable during the deposition run. Hence, the choice of the precursors as well as of the delivery scheme is of utmost importance. Generally, organometallic precursors are preferred rather than halides since they are usually volatile at a much lower temperature (≤ 300 °C). The organic groups used for synthesis of organometallic precursor compounds broadly belong to β -diketonates, carbonyl & phosphine, cyclopentadienyl and olefin & allyl family (Fig. 2.1). Most commonly used precursors such as tetramethyl-heptanedionate compounds (tmhd: $C_{11}H_{19}O_2$), which are solid at room temperature belong to the β -diketonates family. These precursors can be dissolved in an appropriate solvent, like mono-glyme or octane. In case of organosilicon compounds the complexes with above mentioned ligands generally leads to co deposition of oxygen/oxides with the desired phase. To avoid this mostly aliphatic/cyclic organosilicon compounds are preferred as SiC precursor which has only carbon and silicon atoms.

Many research groups have thus performed growth of SiC either on different substrates using single precursor having carbon and silicon atoms. I.Golecki et. al.⁸² had grown single crystalline epitaxial cubic(100) films on (100) Si substrates at 750 °C by low pressure CVD, using methylsilane, CH_3SiH_3 and H_2 . They obtained the stichiometric SiC composition at low temperature because methylsilane can generate vapor which is stable at room temperature. The drawbacks of methylsilane are very low boiling point (-57 °C), pyrophoric and irritant gas and commercially available at high cost. A.J.Steckl et al.⁸³ have grown the cubic SiC on Si using the

precursor trimethylsilane and they have investigated the effect of temperature, flow rate of precursor on on-axis Si (100) and off-axis Si (111) substrates.

The use of trimethylsilane to form amorphous or polycrystalline SiC films is also known in the art. For instance, Kaplan et al.⁸⁴ have described the formation of SiC coatings on video disks using trimethylsilane in a glow discharge chemical vapor deposition process. Trimethylsilane gas is colorless, noncorrosive and nonpyrophoric precursor but excess carbon is deposited during SiC deposition. There are other organosilane type precursors available to obtain SiC film. K. Yasui et al.⁸⁵ have used dimethylsilane to get cubic SiC film while Y. Avigal et al.⁸⁶ have grown the SiC on the Si-SiC-C system using different precursors such as tetramethylsilane (b.p.=26-28 °C), diethylsilane (b.p.=56 °C), and tripropylsilane (b.p.=171 °C). The SiC has been grown in the range of 700-1400 °C regardless of the atmosphere but the films are contaminated with inclusions of silicon and free carbon. They found that pyrolysis of tetramethylsilane in H₂ produces less free carbon than in the presence of helium. It was also noticed that at lower temperature the CH₃ deposits more free carbon while at higher temperatures the C₃H₇ deposits more free carbon. Tetramethylsilane, diethylsilane and tripropylsilane are stable at room temperature. First two precursors have low vaporization temperature and tripropylsilane has high vaporization temperature. All three precursors are safe to handle but are costly.

S.H.Jeong et. al.⁸⁷ have prepared thin films of cubic SiC on Si(100) by high vacuum MOCVD using diethylmethylsilane [DEMS, (C₂H₅)₂(CH₃)SiH] (b.p.= 78 °C) at various temperatures. DEMS is stable at room temperature, nontoxic and no explosive. With a deposition temperature of 900 °C, relatively well oriented 3C-SiC layers were obtained. When the deposition temperature was increased from 700 to 900 °C, there was an improvement in crystallinity and grain size. However, above 900 °C crystallinity decreased with increasing temperature and

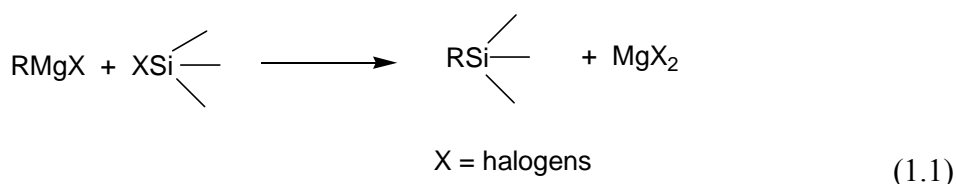
growth time due to a crystal shape change. These results show that the deposition temperature and time are important factors for influencing film crystallinity and carbon deposition.

J.H. Boo et. al.⁸⁸ have used a new precursor dimethylisopropylsilane $[(CH_3)_2CHSiH(CH_3)_2]$ (b.p.= 66-67 °C) to deposit cubic SiC films on Si (100) and Si (111) substrates at the temperature range of 750-970 °C using low pressure organometallic chemical vapor deposition (LP-OMCVD). They found that at low temperature amorphous SiC films and free carbon were deposited. They obtained cubic-type SiC films on uncarbonized Si (100) surfaces at 850 °C and a polycrystalline cubic SiC film on a carbonized Si (100) substrate at 960 °C. But they were not successful in obtaining epitaxial growth of cubic SiC on carbonized Si (100) using the same precursor.

The synthesis routes of these organosilane type precursors are described in literature. In general, in these methods first chlorine substituted silanes are taken that are product or byproduct of a technical process e.g. methylchlorosilane is a technical product which is obtained as a by-product of the direct synthesis.

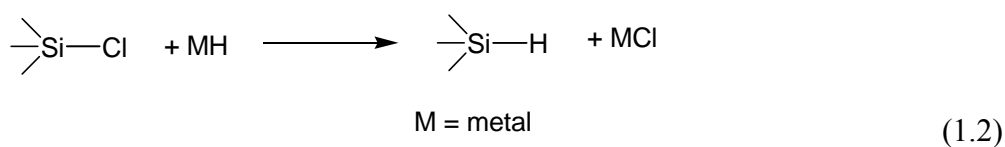
The organic groups can be introduced into these chlorinated silanes by the Grignard process (scheme-1.1) in which only the Si-Cl bond (but not the SiH bond) is involved. The Grignard reaction is of fundamental importance for the whole field of organosilicon chemistry⁸⁹. It utilizes organomagnesium compounds to transfer organic groups to silicon:

Scheme-1.1:



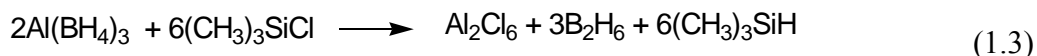
Conversely, the chlorine in chlorosilanes already containing organic substituents can be replaced by hydrogen (scheme-1.2). Reactions with metal hydrides, such as lithium tetrahydroaluminate ⁹⁰, lithium hydride ⁹¹, sodium hydride ⁹², and the reactive aluminum tetrahydroborate $\text{Al}(\text{BH}_4)_3$ ⁹³ are most suitable for the reaction, which proceeds in principle as follows:

Scheme-1.2:



The action of aluminum tetrahydroborate on trimethylchlorosilane can be represented schematically in scheme-1.3:

Scheme-1.3:



The reaction with sodium hydride dispersed in mineral oil or another inert high-boiling hydrocarbon requires temperatures of 175 to 350 °C ⁹². The addition of catalysts can lower the reaction temperature or increase the yield. Alkylborons, boric acid esters, and triethylaluminum are suitable catalysts ⁹⁴⁻⁹⁵. An interesting embodiment of the substitution reaction consists in passing the halogen compound through a eutectic melt of an alkali-metal halide containing lithium hydride. In this way, at 360 to 400 °C dimethyldichlorosilane yields dimethylsilane $(\text{CH}_3)_2\text{SiH}_2$ with 95% conversion and 89% yield ⁹⁶.

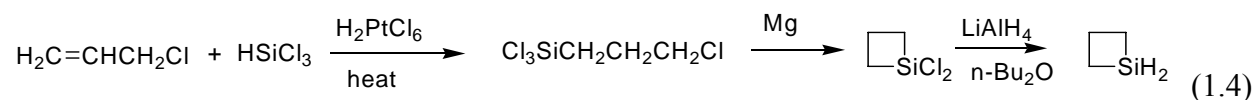
J. H. Boo et al.⁹⁷ have used a new single molecular precursor 1,3-disilabutane containing two silicons and carbon atoms. They have grown the cubic SiC films on Si (100) and Si (111) substrates in the temperature range 650-900 °C by LP-OMCVD using this precursor. Polycrystalline cubic SiC films were formed on Si(100) substrates at such a low temperature as 650 °C. The films obtained on carbonized Si (100) substrates at temperatures higher than 850 °C showed improved crystallinity in their X-ray diffraction patterns. On the other hand, highly oriented SiC films in the [111] direction were formed on carbonized Si(111) substrates at 900 °C. The precursor 1,3-disilabutane which contains silicon and carbon atoms at a ratio of 1:1 was obtained by reduction of 1,1,3,3-tetrachloro-1,3-disilabutane. The synthesis of 1,1,3,3-tetrachloro-1,3-disilabutane was reported by Jung⁹⁸ as follows.

The reaction of (chloromethyl)methyldichlorosilane with elemental silicon and hydrogen chloride using copper as a catalyst and cadmium as a cocatalyst leads to the attachment of a silicon atom to the organochlorosilane molecule, producing 1,1,3,3-tetrachloro-1,3-disilabutane. Reduction of this compound with metal hydrides (e.g., lithium aluminum hydride) in ether replaces the chlorine atoms with hydrogen atoms. The final compound is 1,3-disilabutane⁹⁹.

J. Steckl et al.⁸³ have grown the SiC films on different substrates using silacyclobutanes. In these precursors deposition of carbon occurs in SiC film, because of Si:C ratio is 1:3.

Silacyclobutane is synthesized according to scheme-1.4.

Scheme-1.4:

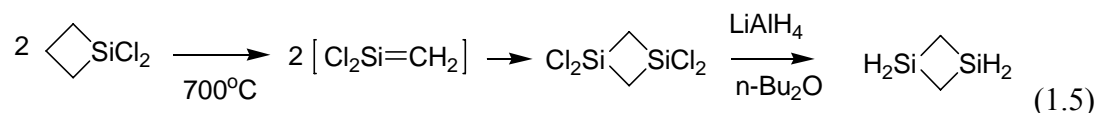


The 3-halopropyltrichlorosilanes are prepared by addition of trichlorosilane to an allylhalide with chloroplatinic acid as catalyst. The 1,1-dichloro-1-silacyclobutane¹⁰⁰⁻¹⁰¹ can be prepared from $\text{Cl}_3\text{SiCH}_2\text{CH}_2\text{CH}_2\text{Cl}$ using magnesium powder. This 1,1-dichloro-1-silacyclobutane is reduced using lithiumaluminumhydride in n-butyl ether at 0°C to get silacyclobutane, $(\text{CH}_2)_3\text{SiH}_2$.

Another precursor which is used because of same number of silicon and carbon atoms is 1,3-disilacyclobutane. D. J. Larkin et al.¹⁰² and A. K. Chaddha et al.²² have used this precursor to get stoichiometric SiC but this precursor needs relatively high temperature to grow SiC film and it has tedious synthesis route. It can be prepared by the LiAlH_4 reduction of 1,1,3,3-tetrachloro-1,3-disilacyclobutane. This 1,1,3,3-tetrachloro-1,3-disilacyclobutane is obtained by pyrolyzing 1,1-dichloro-1-silacyclobutane¹⁰³ at 700°C according to methods described by Nametkin et al.¹⁰⁴. This type of pyrolysis reaction is of considerable interest and it is postulated to go through the $[\text{Cl}_2\text{Si}=\text{CH}_2]$ intermediate.

The process is given in scheme-1.5:

Scheme-1.5:



The strained cyclic molecule i.e. 1,3-disilacyclobutane allows to grow β -SiC film at a temperature $>300^\circ\text{C}$ but lower than possible with a similar straight chain reagent. It is proposed that decomposition of the cyclic precursors directly produces intermediates that can

lead to deposition of stoichiometric SiC. The synthesis routes of cyclic compounds are complicated and tedious. Cyclic precursors are promising for both depositions of single crystal films at high temperature as well as for polycrystalline and single crystal films at low temperature.

Koji et. al.¹⁰⁵ have used the hexamethyldisilane (HDMS) (b.p.= 112-114 °C) to get cubic SiC films on Si and other substrates. At temperatures lower than 1100 °C, the growth rate is limited by thermal decomposition of HMDS molecules. At higher temperatures, the growth rate is limited by thermal diffusion of $(\text{CH}_3)_n\text{-Si-H}_{4-n}$ species through stagnant gas layers at the substrate surface. Temperature dependence of crystallinity of grown films reveals that the gas system is effective for low temperature epitaxy. With and without buffer layers, single-crystalline 3C-SiC containing twinings were grown on a Si (111) substrate at 1100 °C. In the case of Si (100) substrates, single crystals were grown only with a buffer layer. Even though growth temperatures were as low as 1100 °C crack lines were observed in a 5 μm thick layer grown on a Si (111) substrate. HDMS is stable at room temperature and gives codeposition of free carbon with SiC film.

An alternate of the single molecular precursors are the organometallic polymer precursors specially polysilanes and polycarbosilanes. These polymer compounds which, contains polysilanes and polycarbosilanes, must be volatile for CVD use. Generally the polymers of sufficiently high molecular weight, crosslinks before significant volatilization occurs. Such cross-linking before volatilization is highly undesirable for the application under consideration, where excessive silicon and carbon remain in polymer and do not come in vapor form. Presently, research is going on to get a polymer precursor, which gives stoichiometric SiC film and can be

used in CVD process but so far no precursor has been obtained in our knowledge which fulfills all criteria of an ideal precursor.

In the commercial available precursors for SiC, presently precursors are available with the name CVD 2000¹⁰⁶ and CVD 4000¹⁰⁶. CVD 2000 is a single molecular organometallic liquid precursor while CVD 4000 is single component liquid precursor having basic structure of $[\text{SiH}_2\text{-CH}_2]_n$. Their synthesis routes have not been disclosed and have high cost.

In the current section of chapter mostly precursors suitable for CVD/CVI technique were discussed. The other organosilicon precursors prepared and coated through sol-gel technique will be briefly described in current section. The sol-gel technique allows a good reproducibility of coating performances even though some problems have been evidenced due to complex shape substrate and thick film deposition. Moreover, in some case, coating cracking induced by the thermal treatment performed at the end of deposition, has been reported¹⁰⁷. Usually, a thermal treatment at a temperature around 600 °C provides a good chemical homogeneity and good corrosion resistant features to substrates. Nevertheless, some promising results, in terms of corrosion resistant, have also been obtained at lower temperature (400 °C)¹⁰⁸. Even using sol-gel technique infiltration of second phase with parent matrix can be achieved at lower temperature.

In general terms, the sol-gel process involves three stages: (i) a partial hydrolysis of the metallorganic compound in order to produce reactive monomers, (ii) a polycondensation of the reactive monomers which forms oligomers of colloidal size (sol) and (iii) and finally an additional hydrolysis which initiates and further promotes the polymerization and cross-linking of the precursor. The last step, gelation, will produce polymeric compounds of given morphology which upon pyrolysis yield oxide/nonoxide ceramics. The above reactions can be influenced by

controlling parameters such as pH, nature and composition of the solvent, temperature, reaction time, ratio of $[RO]/[H_2O]$ (RO is alkoxy group attached to metal) and the type of the R group¹⁰⁹⁻¹¹⁰. The nature of the starting metallorganic material undoubtedly constitutes an important parameter which influences all the steps of the sol-gel process. The most frequently used and studied precursors for silica and carbon are Tetraethylorthosilicate (TEOS)¹¹¹, Tetramethylorthosilicate (TMOS)¹¹² and activated carbon powder, isopropanol, carbon nanotubes respectively. These precursors have been shown to behave differently under similar conditions. This indicates the importance of the molecular structure in the process and the need for more research and studies of the structure/sol-gel relationship in which all the reaction parameters are involved. Silicon alkoxides are usually used as precursors and their hydrolysis rate can be controlled easily as compared to other faster hydrolyzed derivatives, such as $SiCl_4$ and $Si(OCOCH_3)_4$. Silicic acid and its acetate are also able to produce SiO_2 . The solvent will influence the physical characteristics of the final product, and in the case of methanol as the solvent, the porosity of the product will be lower than that produced from TEOS under similar conditions. Similarly, the bulk density increases with temperature and is higher when MeOH is used as solvent. In the acid-catalyzed system the hydrolysis rate usually decreases with an increase of C atoms in the straight-chain alkoxy group because of an inductive effect, whereas the rate is lowered with increased branching of the alkoxy group of the organosilicon alkoxides due to steric reasons. The polycondensation being a nucleophilic reaction will be influenced by the same factors up to the point at which cross-linking takes place. Other phenomena, such as diffusion and collisions between polymeric chains are increasingly involved and thus the kinetics depends on additional parameters. In general, the hydrolysis reaction is much faster than the condensation. Nevertheless, condensation starts as soon as an alkoxy group has been hydrolyzed

and thus the final results of the sol-gel of the silicon alkoxides will be influenced by a combination of the above mentioned factors. The gelation characteristics of gels produced from methoxy (TMOS), ethoxy (TEOS) and butoxy (TBOS) silicon alkoxides support the above theory. An increase of gelation time is observed when the same alkoxide is used in solvents of increasing molecular weight, e.g., MeOH, EtOH and PrOH. A similar increase is observed with increasing molecular weight of the alkoxide used ¹¹³. In this way sol-gel process has given a scope for deriving SiC from non corrosive, non toxic and commercially available precursors.

1.4.4 Objectives and scope of the present thesis

Owing to the development of different economical and environment friendly techniques for SiC coating/composite preparation, in the present thesis, following points have been studied.

- Different organosilicon compounds have been synthesized which are non toxic, non corrosive, easy in handling, having economical synthesis routes and requisite properties as a SiC precursor for chemical vapor deposition and sol-gel technique.
- The low temperature CVD process was developed using synthesized and commercial available SiC precursors, for SiC deposition. The coating studies were carried out on various substrates such as graphite, C/C composites, TRISO particles and Zircaloy sheet.
- Different morphological SiC were deposited using organosilicon compounds and Taguchi method was used to optimize the process parameters for different morphological SiC materials growth.
- Sol-gel route fabrication and oxidation resistance property study of SiC nanowire/carbon fiber/ SiC matrix composite were carried out. The dense and nanowire morphological SiC phases were impregnated simultaneously in carbon preform using current sol-gel process.

- The oxidation resistive properties and kinetics of oxidation of different morphological coated carbon samples and SiC impregnated samples were investigated in different oxidative environment.

CHAPTER 2

SYNTHESIS OF ORGANOSILICON COMPOUNDS

2. Synthesis of Organosilicon compounds

This chapter describes two different aspects: (i) Proper selection of organosilicon compound for growth of SiC and, (ii) Synthetic process development for bulk production of such organosilicon compounds.

There is a continued demand for the development of coating techniques, having environmentally safe chemicals which in turn should be easily and safely manufactured in bulk. In this view, a thorough literature survey has been carried out to obtain suitable SiC precursors. MTS is the most common and commercial precursor used for SiC deposition using CVD process. Since MTS is corrosive, toxic in nature and needs high temperature to deposit SiC, a lot of alternative precursors are proposed in the literature to replace it. The halogen free single molecular organometallic precursors such as dimethylsilane, $[(\text{CH}_3)_2\text{SiH}_2]$ ⁸⁵, trimethylsilane, $[(\text{CH}_3)_3\text{SiH}]$ ¹¹⁴, tetramethylsilane, $[(\text{CH}_3)_4\text{Si}]$ ⁸⁶, 1,3-disilabutane, $(\text{H}_3\text{SiCH}_2\text{SiH}_2\text{CH}_3)$ ¹¹⁵, 1,2-bis(silyl)ethane, $(\text{H}_3\text{SiCH}_2\text{CH}_2\text{SiH}_3)$ ⁸⁶, diethylsilane, $[(\text{C}_2\text{H}_5)_2\text{SiH}_2]$ ⁸⁶, tripropylsilane, $[(\text{C}_3\text{H}_7)_3\text{SiH}]$ ⁸⁶, silacyclobutane, $[\text{c-C}_3\text{H}_6\text{SiH}_2]$ ⁸³, 1,3-disilacyclobutane, $[\text{C}_2\text{H}_8\text{Si}_2]$ ⁸, and hexamethyldisilane, $[(\text{CH}_3)_6\text{Si}_2]$ ¹⁰⁵ were reported as alternates to MTS. Deposition of SiC has been reported using these precursors at relatively low temperature. The polymeric organometallic precursors such as polysilanes and polycarbosilanes have also been reported for SiC deposition¹¹⁶⁻¹¹⁷. To form SiC by CVD, the precursor composition must be cleanly and easily vaporizable. Many polymers are viscous oils or solids, which cannot be easily evaporated at very low pressure. Except CVD process, sol gel process is also one of the viable options for deposition of SiC using harmless precursors. Keeping all aspects in mind the potential precursors of SiC have been screened. The selection criteria of a suitable chemical precursor for SiC deposition were;

(a) Stability at room temperature,

- (b) Low vaporization temperature and high saturation vapor pressure for use in CVD process,
- (c) Undergo decomposition/chemical reaction at a temperature below the melting temperature and phase transformation of the substrate depending on the engineering applications,
- (d) Low toxicity, not explosive, not corrosive and not inflammable,
- (e) Cost-effective for SiC deposition.

On the basis of above criteria, 2,4,6-trimethyl-2,4,6-trisila-heptane (Trimethyltrisilaheptane), 2,4,6-trisilacyclohexane, mixture of organosilicon compounds (named as CVDP) and sol gel precursors comprising tetraethylortho silicate (as silicon source) and glycerine and phenol formaldehyde resin (as carbon source) have been selected as potential precursors for SiC. Three compounds, 2,4,6-trimethyl-2,4,6-trisila-heptane, 2,4,6-trisilacyclohexane and mixture of organosilicon compounds (CVDP) were identified as potential SiC precursor especially for CVD application. Synthesis of such precursors has been carried out. The detail synthesis processes for sol gel precursors has been discussed in Chapter 4.

2.1 Organosilicon precursors

2.1.1 2,4,6-Trimethyl-2,4,6-trisila-heptane

The synthetic sequence of 2,4,6-trimethyl-2,4,6-trisila-heptane is shown in Fig.2.1.

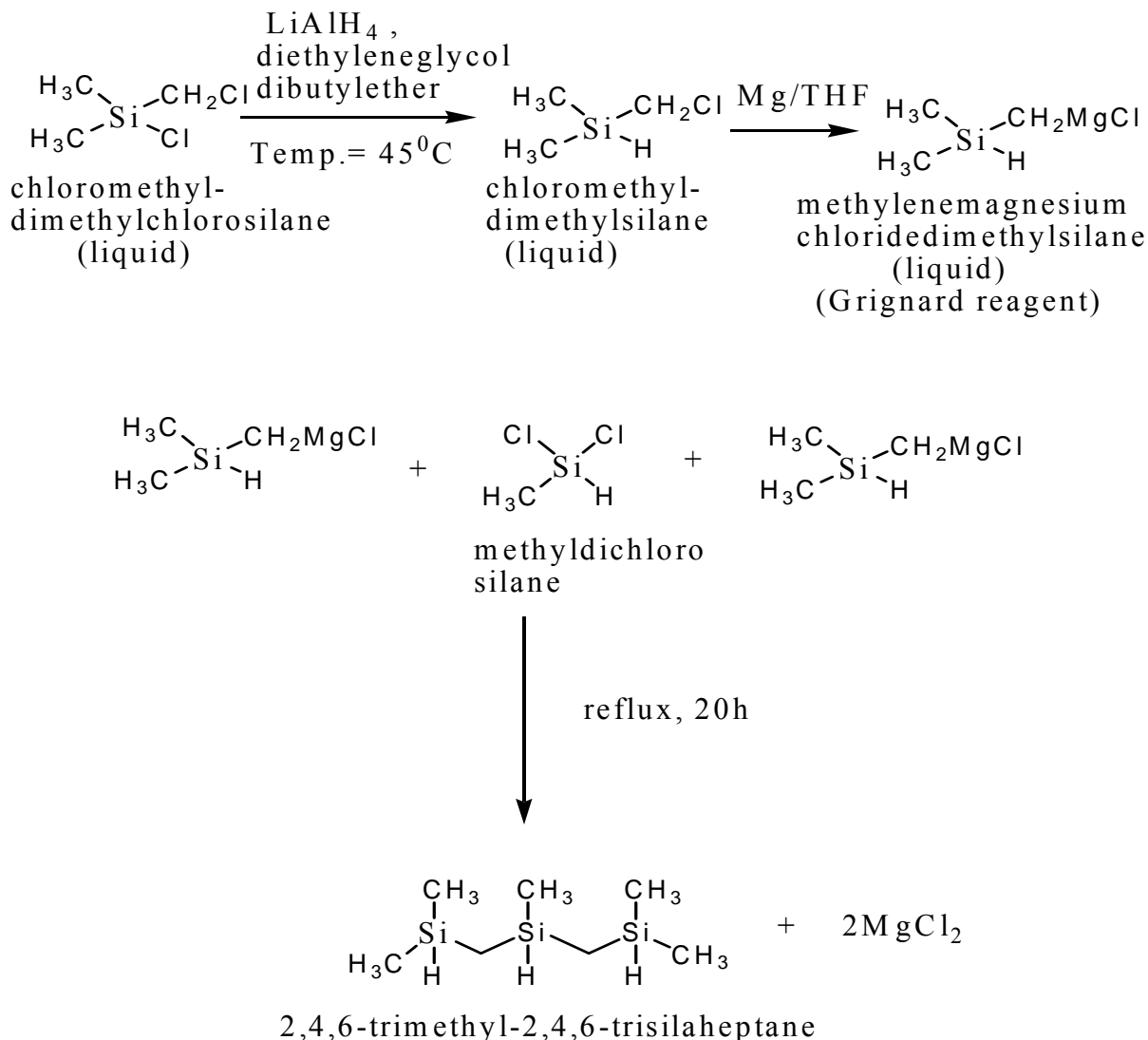


Fig. 2.1 Reaction scheme for synthesis of 2,4,6-trimethyl-2,4,6-trisila-heptane

Its synthesis involves two steps. In the first step, chloromethyldimethylsilane was synthesized by reducing chloromethyldimethylchlorosilane using lithium aluminum hydride. In the second step, Grignard reagent was prepared by reacting stoichiometric amount of chloromethyldimethylsilane and magnesium at room temperature. This Grignard reagent further reacted with

methyldichlorosilane and yielded 2,4,6-trimethyl-2,4,6-trisila-heptane. The structure of 2,4,6-trimethyl-2,4,6-trisila-heptane was confirmed from NMR data.

2,4,6-Trimethyl-2,4,6-trisila-heptane is a colorless liquid organosilane of low viscosity. It is soluble in common organic solvents such as hexane, toluene, THF, chloroform etc. It is insoluble in water and stable in air. The precursor synthesized is chlorine free and single compound SiC precursor. The main chain of compound comprises repeating Si-C units. The carbon to silicon ratio in the precursor compound is a relatively low 7:3. This compound contains no element other than Si, C and H. The chlorine free features provide a non-corrosive reaction environment and products. The composition is non-corrosive. The compound synthesized is chlorine free, single compound rather than a polymer, oligomers, mixture of compounds or reaction products. This compound can be conveniently used to form SiC coating by vapor deposition.

The final yield of 2,4,6-trimethyl-2,4,6-trisila-heptane was very poor. It was observed that in the first step the yield of chloromethyldimethylsilane was 20-30%. To improve its yield, a series of experiments were carried out by varying first step temperature from 40-80 °C and duration from 24-48 h. It was observed that about 40-45% yield was obtained when the first reaction was performed at 60°C for 36 h. In the second step Grignard reaction was performed to obtain desired compound 2,4,6-trimethyl-2,4,6-trisila-heptane. But after second step, improvement in yield of final product was not achieved. The overall yield obtained for the final compound i.e. 2,4,6-trimethyl-2,4,6-trisila-heptane was 5-10% starting from chloromethyldimethylchlorosilane. There was no significant increase in the yield of final product 2,4,6-trimethyl-2,4,6-trisila-heptane.

2.1.2 2,4,6-Trisilacyclohexane

The synthesis of 2,4,6-trisilacyclohexane was carried out in two steps. In first step, tri-(dichlorosilylmethylene) was synthesized and in the second step it was reduced to get the desired

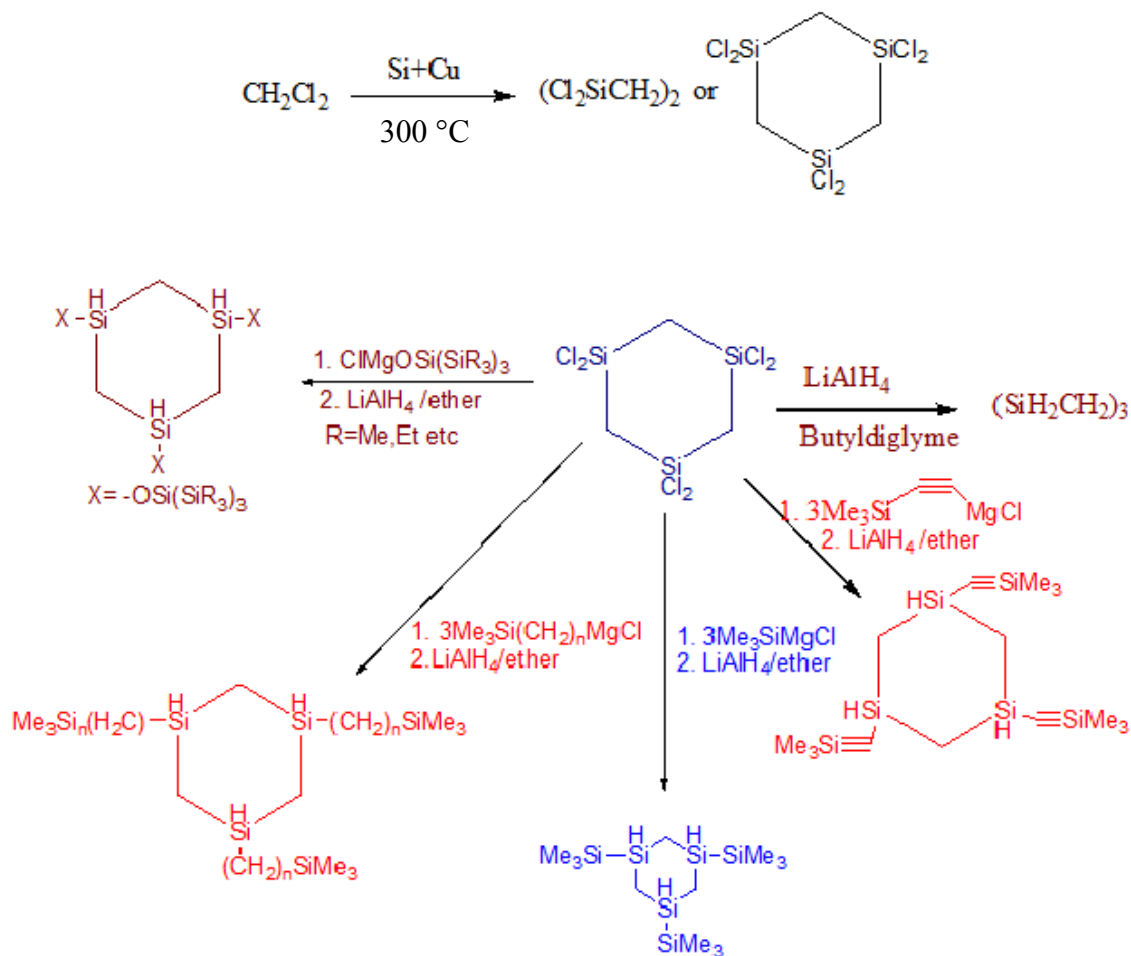


Fig. 2.2 Reaction scheme for synthesis of different organosilicon compounds from tri-(dichlorosilylmethylene)

compound. The compound tri-(dichlorosilylmethylene) synthesized in first step can be used as pre-precursors for different organosilicon compounds, which can be used as SiC precursor as shown in reaction scheme in Fig. 2.2. The compound tri-(dichlorosilylmethylene) is a potential pre-precursor for many SiC precursors e.g. reduction of tri-(dichlorosilylmethylene) using

lithium aluminum hydride leads to the 2,4,6-trisilacyclohexane compound. Further by substituting chlorine of this compound by different groups such as $-\text{SiR}_3$ (trialkylsilyl group) results in different types of organosilicon compounds, which can be possible precursor for SiC. Considering the cost and simplicity of synthesis route, the synthesis of 2,4,6-trisilacyclohexane compound was carried out. Silicon powder, copper powder and anhydrous methylene chloride (CH_2Cl_2) were used as the reagents. The direct synthesis procedure¹¹⁸ of organosilicon compounds by the reaction of methylene chloride with silicon-copper contact masses has been used in the current process.

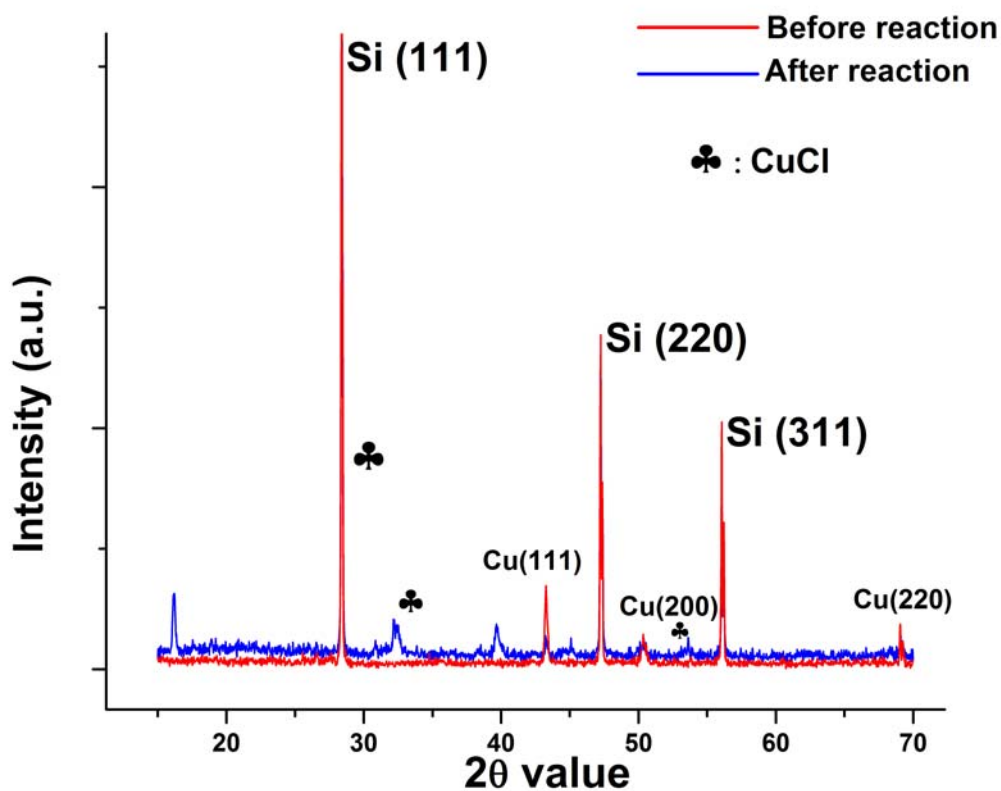


Fig. 2.3 XRD pattern of silicon –copper pellet before and after reaction.

In typical synthesis route, the charge of silicon and copper powders were mixed in 9:1 ratio and pressed and sintered to form the pellets. This mixture was fired in hydrogen atmosphere at 1100 °C for about 4 h to reduce any oxide layer present on silicon and copper powder. The XRD of reduced silicon and copper pellets (Fig. 2.3) show that there was no impurities and oxide phase of silicon or copper present in the silicon-copper mixed pellet. The reduced silicon copper pellets

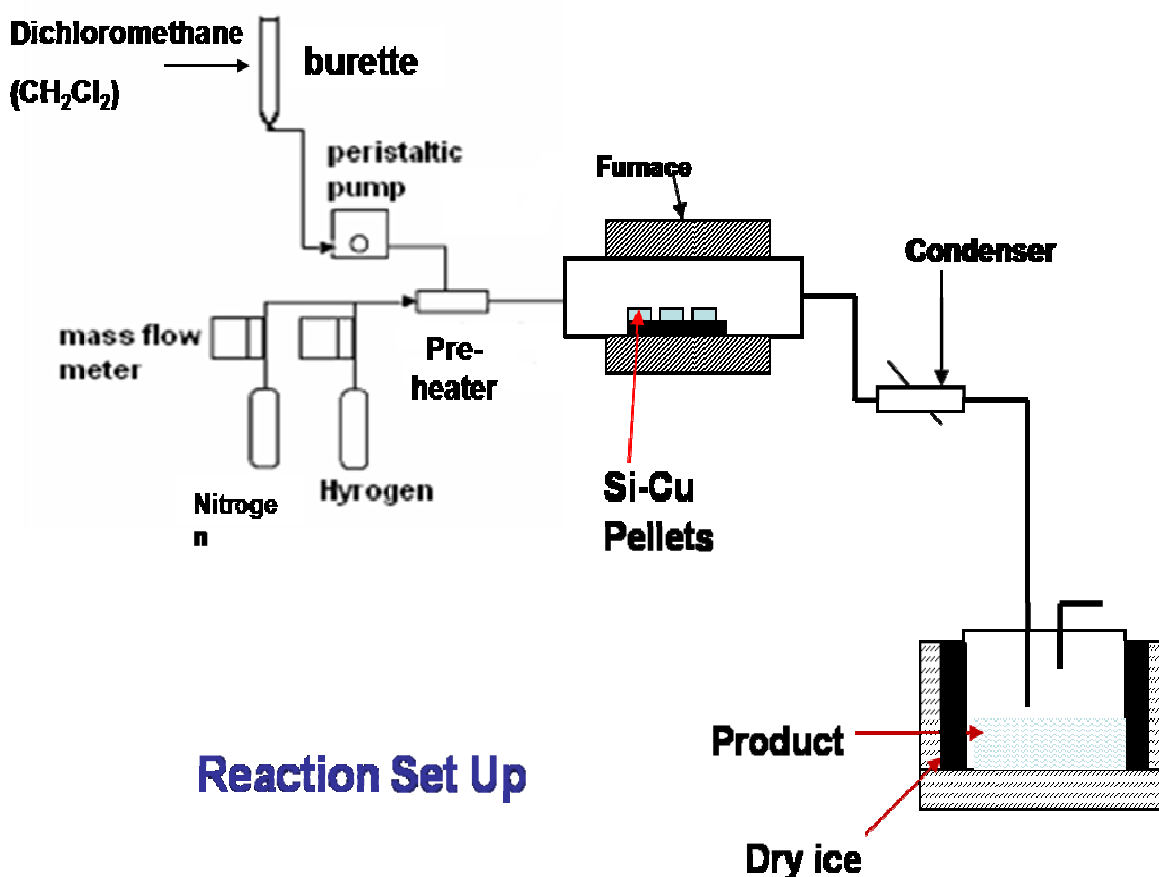


Fig. 2.4 Schematic of reaction setup used for synthesis of 2,4,6-trisilacyclohexane compound.

were reacted with methylene chloride at reaction temperature 300 °C. The Fig. 2.3 shows XRD pattern of silicon–copper pellet after reaction. It shows formation of some copper chloride phase in the pellets after reaction. The role of copper has been well studied in the literature in such kind of reaction. The main function of copper metal catalyst are, primarily to make the halogen of

alkyl halide readily available to react with and activate silicon and secondarily to make the organic group more available by transporting the free radicals and also prolonging their life in the form of copper alkyl.

The schematic of reaction setup used for synthesis is shown in Fig. 2.4. The condensate product collected contains small quantities of low boiling chlorosilanes. The unreacted methylene chloride was separated by fractional distillation at atmosphere pressure, leaving a fraction boiling above 155 °C. The latter fraction was vacuum (~10 mm) distilled at 90 °C to get the tri-(dichlorosilylmethylene). In the second step reduction of tri-(dichlorosilylmethylene) (1 eq.) was carried out using lithium aluminum hydride (4 eq.) to yield 2,4,6-trisilacyclohexane. The compound 2,4,6-trisilacyclohexane was distilled out at 140 °C at atmospheric pressure. ¹H and ¹³C NMR study of the synthesized compound confirms its structure. 2,4,6-trisilacyclohexane is a colorless liquid organosilane of low viscosity. It is soluble in common organic solvents such as hexane, toluene, THF, chloroform etc. It is insoluble in water.

Since the final yield of the compound 2,4,6-trisilacyclohexane was low, reaction parameters such as methylene chloride flow rate and reaction temperature were varied in the range 0.5 – 1 ml/min and 200-400 °C, respectively, keeping other parameters constant to observe their effect on the yield of 2,4,6-trisilacyclohexane. It was observed that with decrease in the methylene chloride flow rate from 1 to 0.5 ml/min, there was an increase in the conversion of methylene chloride to different organosilicon compounds. Finally, there was about 10% increase in the yield of the 2,4,6-trisilacyclohexane. It was observed that lower the temperature, more efficient was the incorporation of organic group in to the organosilicon products leading to increase in the yield of products. But the temperature has to be raised to one at which the

reaction has a convenient rate, as in the present case at reaction temperature 300 °C maximum yield of products was observed.

This compound can be a novel precursor to SiC due to its low boiling point 140 °C. The compound synthesized was chlorine free and single compound. The main chain of compound comprises repeating Si-C units in cyclic ring. The carbon to silicon ratio in the precursor compound is 1:1. This chlorine free precursor contains no element other than Si, C and H. The chlorine free features provide a non-corrosive reaction environment and products and 1:1 ratio of Si to C provides stoichiometric deposition of SiC. This compound can be used to form SiC coating by chemical vapor deposition.

2.1.3 Mixture of organosilicon compounds (CVDP):

As in the previous process the final yield of 2,4,6-trisilacyclohexane was low and to make this process more economical, it was modified. In the modified process rather than taking pellets of silicon and copper only powder of silicon was used as the reactant. The fluidized process was used to efficiently react silicon powder and dichloromethane vapor. The fluidized bed process effectively increases the contact area and duration between the solid and gaseous reactants. A fluidized bed is formed when a quantity of a solid particulate

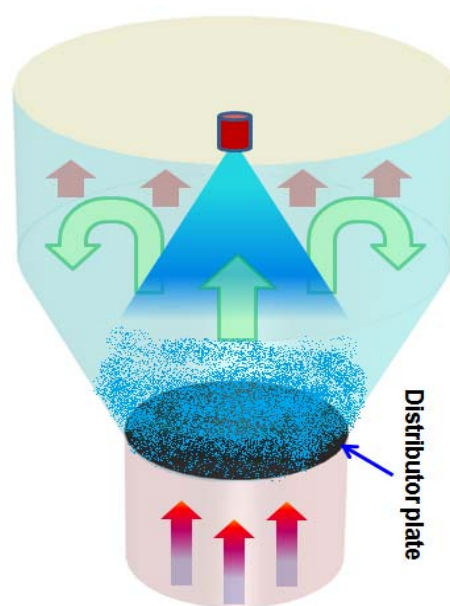


Fig. 2.5 Schematic of fluidized bed system

substance (usually present in a holding vessel) is placed under appropriate conditions to cause

the solid/fluid mixture to behave as a fluid (Fig. 2.5). This is usually achieved by the introduction of pressurized fluid through the particulate medium. This results in the fluidized medium having many properties and characteristics of normal fluids; such as the ability to free-flow under gravity, or to be pumped using fluid type technologies. The resulting phenomenon is called fluidization. Fluidized beds are used for several purposes, such as fluidized bed reactors (types of chemical reactors), fluid catalytic cracking, fluidized bed combustion, heat or mass transfer or interface modification, applying a coating onto solid items. In the Fig. 2.5 typical fluidized process is shown. The zoom area shows the fluidization region and how the particles movement occurs in this region.

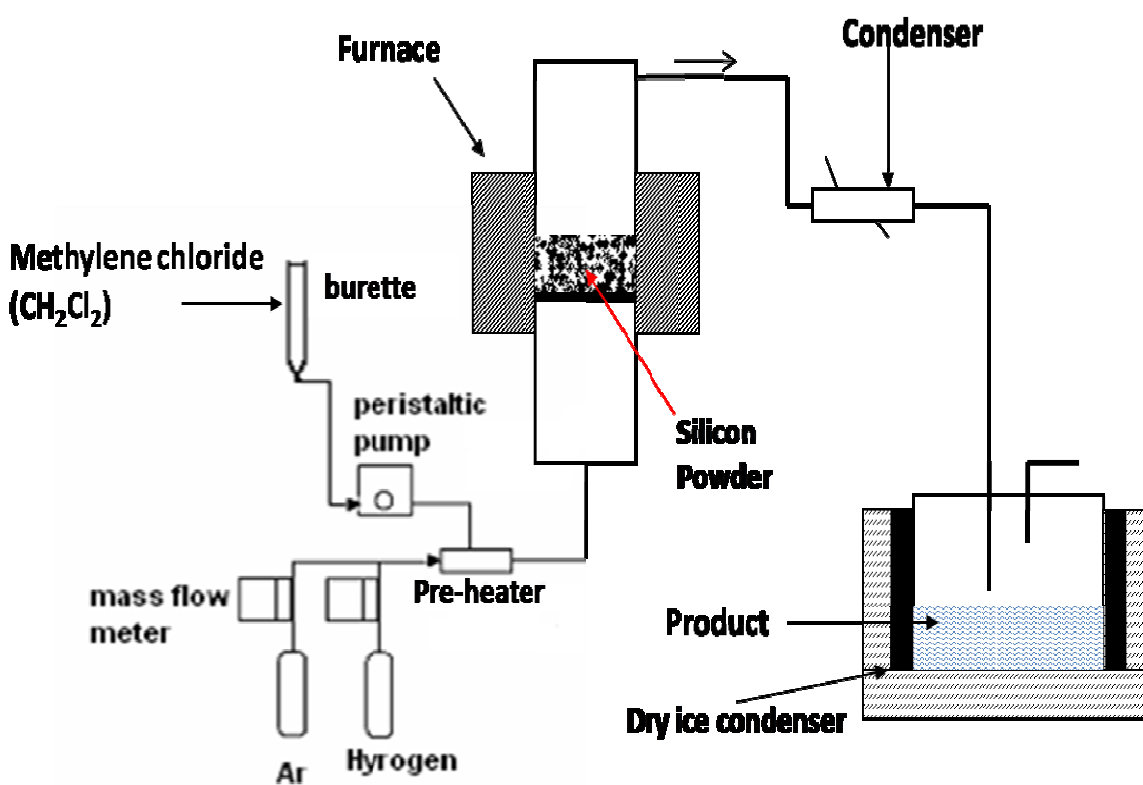


Fig. 2.6 A schematic diagram of reaction setup for synthesis of mixture of organosilicon precursor.

The schematic and actual reaction setup for modified process are shown in Figs. 2.6 & 2.7.

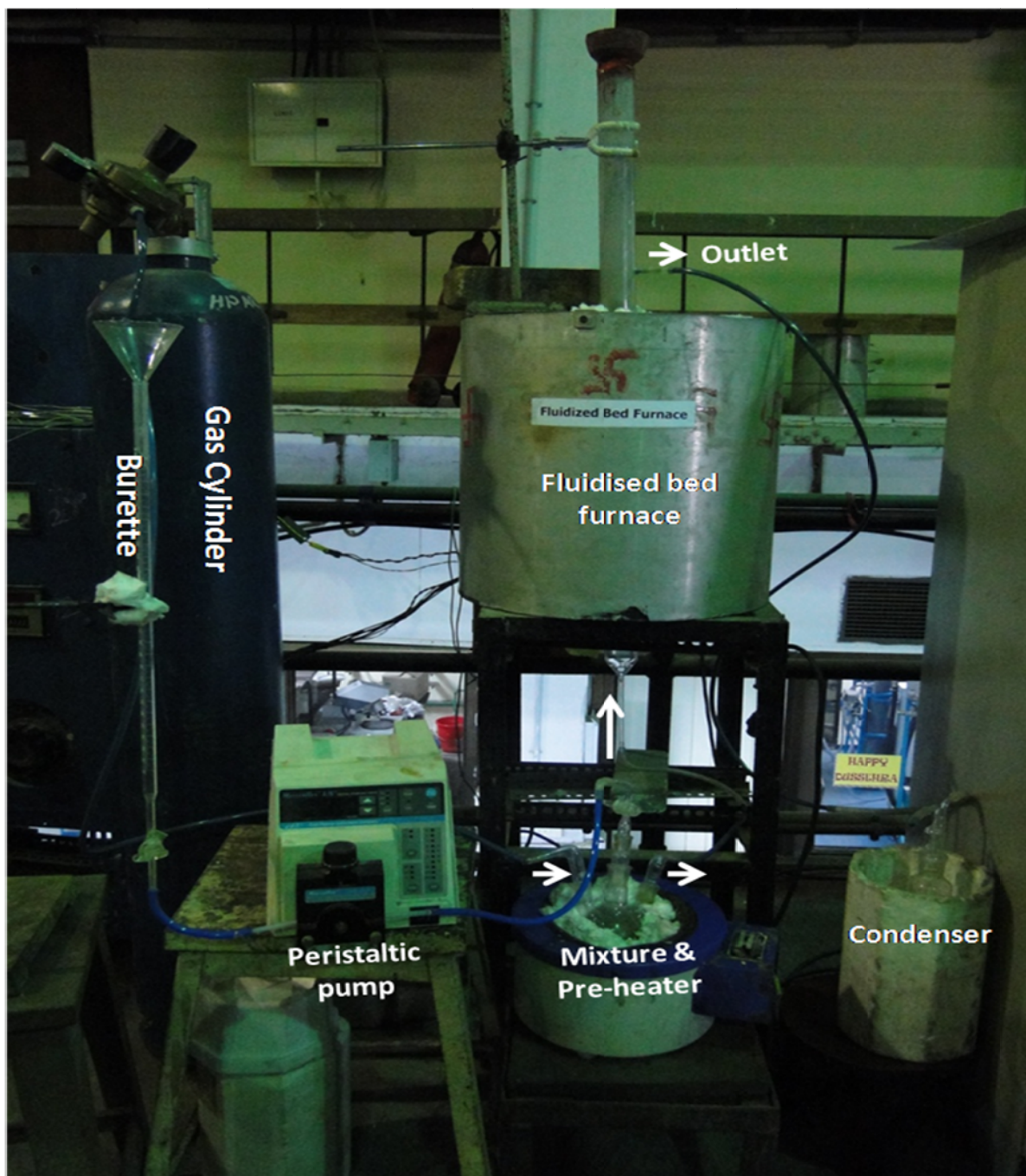


Fig. 2.7 Actual reaction setup for synthesis of mixture of organosilicon precursor and schematic of fluidized bed zone.

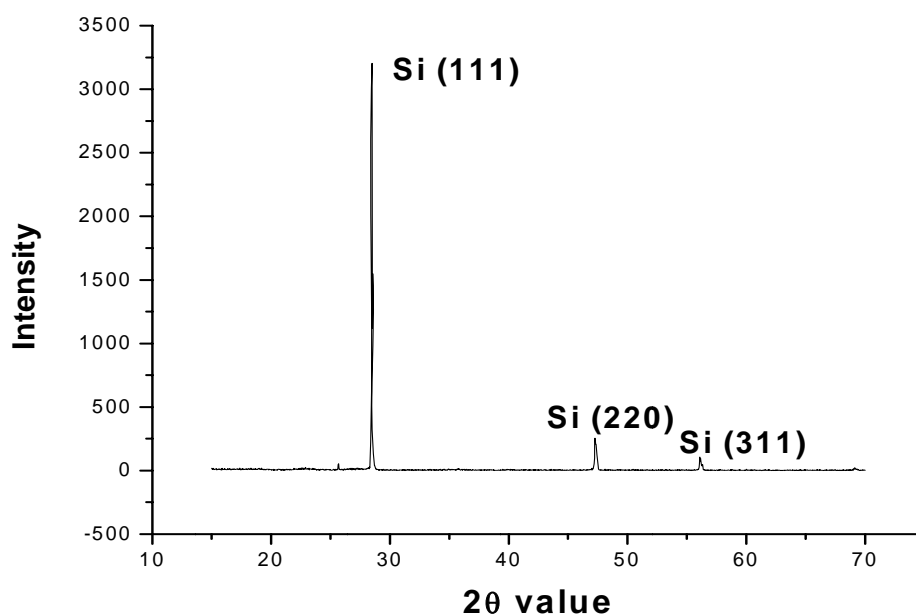


Fig. 2.9 XRD pattern of the silicon powder used for the organosilicon precursor synthesis.

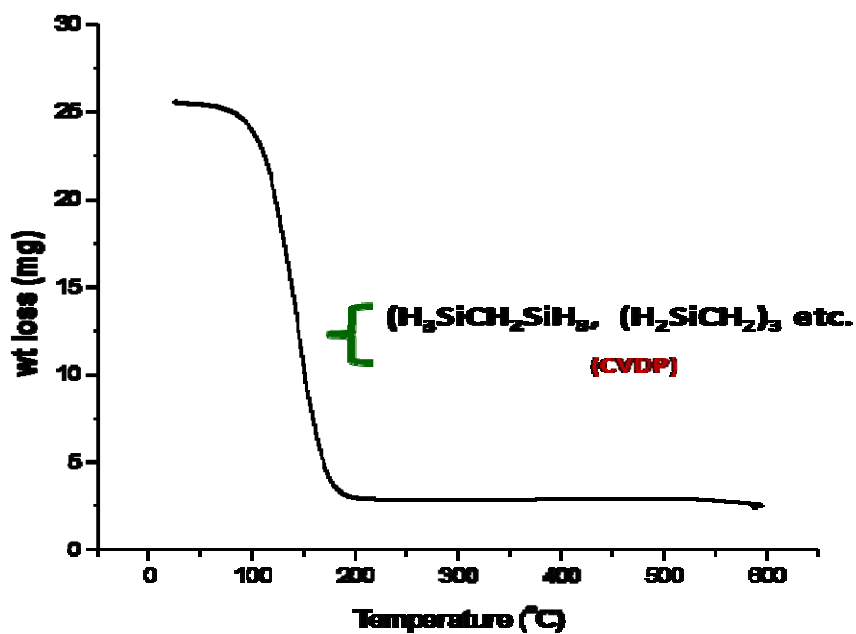


Fig. 2.10 The thermogravimetric weight loss curve of synthesized organosilicon precursor.

The process parameters such as temperature of reaction, dichloromethane flow rate, argon flow rate and reaction time have been optimized for bulk synthesis of CVDP precursor. It was observed that for process parameters, temperature of reaction: 400 °C, dichloromethane flow rate: 0.25 ml/min, argon flow rate: 500 sccm and reaction time: 3 h maximum yield of CVDP precursor was obtained.

The TG data of mixture of organosilicon compounds obtained after second stage reduction is shown in Fig. 2.10. It was observed that there was approximate 90-95% weight loss of the

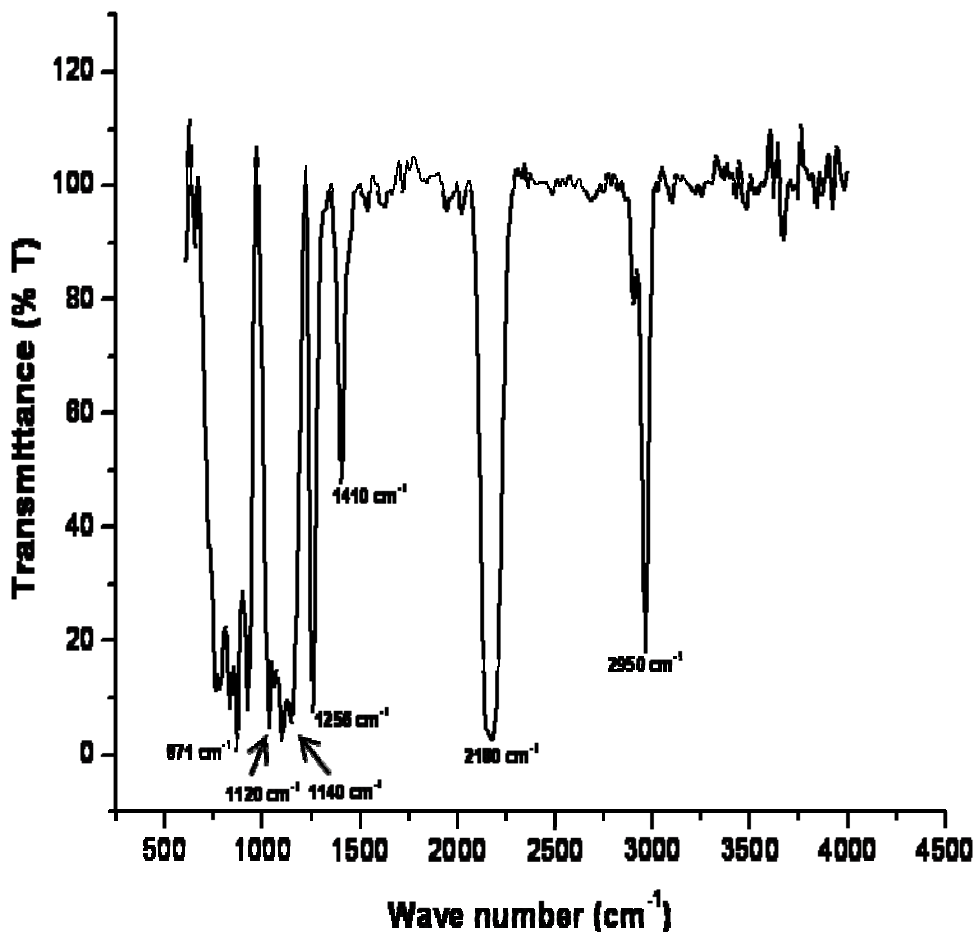


Fig. 2.11 The IR spectra of volatile organosilicon (named as CVDP) precursor.

mixture of organosilicon compounds upto 200 °C. The remaining approximate 5% liquid was colorless highly viscous liquid. The volatile part of mixture of organosilicon compounds was termed as CVDP precursor.

The IR spectra (Fig. 2.11) of CVDP precursor shows significant peaks at 1256 and 871 cm^{-1} : Si-CH₃ 1120 cm^{-1} and 1140 cm^{-1} (multiplet) ; Si-(CH₂)_n-Si 1410 cm^{-1} ; Si-C=C 2180 cm^{-1} ; Si-H 2950 cm^{-1} ; Si-C-H. The IR spectra has confirmed that the CVDP precursor was mixture of different organosilicon compounds such as H₃SiCH₂SiH₃, H₃SiCH₂SiCH₂SiH₃, (H₂SiCH₂)₃. The CVDP precursor was less viscous colorless liquid. This CVDP precursor was further used for SiC coating and has been discussed in Chapter 3.

A comparative study of commercial SiC precursors CVD 2000¹⁰⁶ and CVD 4000¹⁰⁶ with other conventionally used precursors and synthesized precursor CVDP was given in Table 2.1. It shows that CVDP is a potential precursor of SiC which can be economically produced.

Table 2.1

Comparison of commercial available precursors

| | CVD 2000 | CVD 4000 | MTS | Silane | Organometallic precursors developed in our lab |
|---------------------------------------|---|---|--|---|---|
| Precursors | Only CVD 2000 | Only CVD 4000 | MTS plus H ₂ (in exact ratios) | Silane Plus Methane (CH ₄) | mixture of organosilicon compounds (CVDP) |
| Precursors Hazards | Flammable (FP=51°C) Non corrosive and nontoxic | Flammable FP=9°C). Noncorrosive and nontoxic Air, moisture reactive at 140 °C | Corrosive, toxic, flammable (FP=3°C). Moist air and water reactive at 20 °C | Pyrophoric | Easy to handle; Non corrosive and nontoxic |
| % SiC in Precursor | 63% SiC (25% C, 12%H) | 91% SiC (9%H) | 27% SiC (71%Cl, 2%H) | Silane - 87% SiC (13% H ₂), Silane + Methane - 83% SiC (17% H ₂) | (CVDP) Approx. 80-83% SiC |
| By Products of the CVD Process | H ₂ and Methane (CH ₄) | H ₂ | HCl (highly corrosive) as well as H ₂ and silanes | H ₂ | H ₂ |
| Coating Composition Si:C | Varies with substrate temp., 1:1+5-15% carbon | 1:1± 0.5% | 1:1±1.2% plus Cl and trace metals | 1:1± 5-10% | 1:1± 5%, no trace metal deposition |
| Deposition Temperature | 800-900 °C | 600-900 °C | 1000-1400 °C | 1200-1500 °C | 700-1000 °C |

2.2 Conclusion

2,4,6-trimethyl-2,4,6-trisila-heptane, 2,4,6-trisilacyclohexane and mixture of organosilicon compounds (CVDP) were identified as potential SiC precursor especially for CVD application and their synthesis carried out. The yield of 2,4,6-trimethyl-2,4,6-trisila-heptane was very poor and could not be increased after variation in synthesis parameters. Considering the cost and simplicity of synthesis route, the synthesis of 2,4,6-trisilacyclohexane compound was carried out. Silicon powder, copper powder and anhydrous methylene chloride (CH_2Cl_2) were used as the reagents. The direct synthesis procedure of organosilicon compounds by the reaction of methylene chloride with silicon-copper contact masses has been used. Reaction parameters such as methylene chloride flow rate and reaction temperature were varied keeping other parameters constant to observe their effect on the yield of 2,4,6-trisilacyclohexane. It was observed that by varying these parameters, there was 10-15% increase in the yield of 2,4,6-trisilacyclohexane and the final yield can reach up to 20-25%. As in the previous process the final yield of 2,4,6-trisilacyclohexane was low and to make this process more economical, it was modified. In the modified process, mixture of compounds (CVDP) was synthesized with the same direct process which can be used as the SiC precursor rather than going for single molecule precursor. The CVDP precursor was synthesized by reacting methylene chloride with fluidizing silicon powder. The process parameter has been optimized for bulk synthesis of CVDP precursor. The comparative study of commercial SiC precursors and other conventionally used precursors with synthesized precursor CVDP has shown that CVDP is a potential precursor of SiC which can be economically produced.

2.3 Experimental Section

2.3.1 General Details

All reactions were performed in oven-dried (120 °C) or flame-dried glass apparatus under dry nitrogen (N₂) or argon (Ar) atmosphere.

Solvent purification: The solvents were dried and distilled from the indicated drying agents: THF from sodium/benzophenone; DMSO from CaH₂ and then stored over Ca metal. EtOH was dried over Mg and then stored over MS 4Å. All other alcohols were dried from CaH₂ and stored over molecular sieves.

Reagents: All the chemicals such as chloromethyldimethylchlorosilane, lithium aluminum hydride, magnesium, methyldichlorosilane, silicon powder, copper powder and methylene chloride were obtained either from Sigma Aldrich and Spectrochem (India).

NMR Study: ¹H NMR and ¹³C NMR spectra were recorded on a Bruker 200 MHz spectrometer. Spectra were referenced to residual chloroform (δ 7.26 ppm, ¹H; 77.00 ppm, ¹³C). Chemical shifts are reported in ppm (δ); multiplicities are indicated by s (singlet), d (doublet), t (triplet), q (quartet), quint (pentet), m (multiplet) and br (broad).

IR Study: IR spectra was recorded on a Nicolet Impact 410 FT IR spectrophotometer in NaCl cells or in KBr discs. Peaks are reported in cm⁻¹.

2.3.2 General synthesis procedure for 2,4,6-trimethyl-2,4,6-trisila-heptane compound

The detail steps involved in synthesis of **2,4,6-trimethyl-2,4,6-trisila-heptane** are as follows.

(i) Synthesis of Chloromethyldimethylsilane

A mixture of 20.0 ml of chloromethyldimethylchlorosilane and 40.0 ml of anhydrous butyl diglyme in a 500 ml flask was cooled by an ice water bath. Then 1.8 g of lithium aluminum hydride powder was added to the silane solution. The resultant mixture was stirred in the ice-water bath for 3 h and heated at 60 °C with stirring at this temperature for 36 h. After bringing it to room temperature, the reduced mixture was quenched with alkali solution. The organic layer was separated and dried over anhydrous sodium sulfate. Distillation in the temperature range of 80-82 °C at atmospheric pressure gave rise to the 8 ml of chloromethyldimethylsilane.

(ii) Synthesis of 2,4,6-trimethyl-2,4,6-trisila-heptane

A solution of 5 ml of chloromethyldimethylsilane in 30 ml of anhydrous tetrahydrofuran (THF) was added dropwise to 1.0 g of magnesium powder in a flask equipped with a stirrer and a condenser. The rate of addition was regulated to maintain reflux for the Grignard solution. To this Grignard reagent solution was then added dropwise 1.5 ml of methyldichlorosilane in the 15 ml THF. The resultant mixture was stirred overnight with gentle reflux. After cooled down to room temperature, the reaction was worked up by adding water. The organic phase was separated and dried over anhydrous sodium sulfate. Solvent THF was removed by atmospheric pressure distillation. Vacuum distillation at 85 °C yielded about 1 ml of 2,4,6-trimethyl-2,4,6-trisila-heptane.

The characterization of synthesized compound was carried out using ^1H and ^{13}C NMR. In ^1H NMR spectra a overlap peak of two multiplets was obtained at δ (ppm) value 3.97-3.99 (due to 2H and 1H, Si-H), a broad peak was obtained at δ (ppm) value -0.16 – 0.14 (the broad peak is overlap of (m,12H,Si-CH₃), (m,3H, Si-CH₃) and (m,4H, Si-CH₂-Si)). In ^{13}C NMR spectra three peaks were obtained at δ (ppm) values -2.0, -1.7 and -0.8 corresponding to terminal methyl -Si-CH₃, internal methyl -Si-CH₃, methylene group carbon Si-CH₂-Si.

2.3.3 General synthesis procedure for 2,4,6-trisilacyclohexane compound

In typical synthesis route, the charge of silicon and copper powders were mixed in 9:1 ratio and pressed & sintered to form the pellets of 10mm diameter and 5 mm height. The methylene chloride was dried over sodium and pellets were fired in hydrogen atmosphere at 1100 °C for about 4 h prior to reaction. A 50 mm inside diameter, 600 mm long quartz horizontal furnace, heated externally by a resistance type furnace was used to carry out synthesis. The experiments were carried out in single stage (20 gm scale of mixture of silicon-copper pellet). The fired silicon copper pellets were kept in the hot zone of the furnace at temperature 300 °C and a stream of argon containing dichloromethane was passed over it. The flow of liquid dichloromethane was controlled using peristaltic pump as shown in Fig. 2.4 and kept at 0.5 ml/min. The products from the furnace were condensed and collected. The condensate collected contains the small quantities of low boiling chlorosilanes. The methylene chloride was separated by fractional distillation at atmosphere pressure, leaving a fraction boiling above 155 °C. The latter fraction was vacuum distilled at 90 °C to get the tri-(dichlorosilylmethylene). In the second step reduction of tri-(dichlorosilylmethylene) (1 eq) was done using lithium aluminum hydride (4 eq) to yield 2,4,6-trisilacyclohexane as shown in Fig. 2.2. The reduction was carried out for about 14 h and later the reaction was worked up with water. The compound 2,4,6-trisilacyclohexane was distilled out at 140 °C at atmospheric pressure. It has been observed that for 100 ml of methylene chloride there was 5 ml yield of 2,4,6-trisilacyclohexane. The characterization of synthesized compound was carried out using ^1H and ^{13}C NMR. In ^1H NMR spectra a multiplets was obtained at δ (ppm) value 3.50-3.79 (due to 6H, Si-H), a broad peak was obtained at δ (ppm) value 1.31-1.42 (the broad peak was due to 6H,C-H). In ^{13}C NMR spectra one peak was obtained at δ (ppm) values – 23.4 corresponding to methylene group carbon Si-CH₂-Si.

2.3.4 General synthesis procedure for mixture of organosilicon compounds (CVDP)

Silicon powder (Sigma Aldrich make, 99% purity, 90-200 μm size) and anhydrous methylene chloride (CH_2Cl_2 , sigma Aldrich make) were used as the reagents. The methylene chloride was dried over sodium and silicon powder was charged in hydrogen atmosphere at 1100 $^\circ\text{C}$ for 2 h prior to reaction. A 50 mm inside diameter, 1000 mm long quartz fluidized bed reactor, heated externally by a resistance type furnace was used to carry out synthesis. A multihole distributor made up of silica (G3-silica porous plate) was used to achieve uniform fluidization and good gas distribution. The fluidizing gas argon was passed through silica gel column to remove moisture. The dry gas was then metered, passed over hot titanium sponge to remove any traces of oxygen. The minimum fluidization velocity of silicon powder was experimentally determined and the operating gas flow rate was fixed at 0.5 lpm, close to the minimum fluidization flow rate in order to achieve the plug flow condition in the fluidized bed. The fluidized process was used for efficient reaction between silicon powder and dichloromethane vapor. The fluidized bed process effectively increases the contact area and duration between the solid and gaseous reactants. The experiments were carried out in single stage (20 gm scale of silicon powder) at temperature 400 $^\circ\text{C}$. The methyl chloride was passed through peristaltic pump to the pre-heater zone and the argon gas swept away the vapors of methylene chloride to the silicon powder fluidizing hot zone at the rate of 0.25 ml/min. The products were collected in liquid nitrogen cooled condenser. The process variables such as reaction temperature, methylene chloride flow rate, argon flow rate and reaction time were optimized for maximum yield of the organohalosilane product. The organohalosilane compounds were later on reduced with lithium aluminum hydride to obtain the organosilicon compounds. The reduced mixture of organosilicon compounds was characterized by Infra red spectroscopy and thermogravimetric analysis. From this mixture of organosilicon

compounds, volatile fraction was separated at 200 °C and used for SiC coating. The volatile fraction of compounds used for SiC coating was named as CVDP precursor. It has been observed that for 100 ml of methylene chloride, the yield of CVD precursor was about 20-30 ml for 3 h of reaction.

CHAPTER 3

COATING STUDY OF SILICON CARBIDE USING ORGANOSILICON COMPOUNDS

3. Coating study of Silicon Carbide using Organosilicon compounds

The current chapter deals with the coating studies carried out on graphite, zircaloy substrates and tristructural isotropic (TRISO) particle using synthesized CVDP precursor and commercial available MTS, HMDS and TMS precursors.

It is desirable that SiC should have properties such as high thermal conductivity, high hardness and stiffness, mechanical strength at elevated temperature, low coefficient of thermal expansion, good dimensional stability under irradiation, small neutron capture cross sections, low density than other ceramics, and resistance to wear and abrasion so that it would be ideally suited for a vast number of applications. In nuclear industry, it is of interest to be used as a layer on TRISO fuels, Zircaloy, insulating material in nuclear fusion systems such as separators, insulating flow channel inserts, between tritium breeding and neutron multiplier materials composing Li–Pb blanket modules¹¹⁹⁻¹²⁴.

In past several SiC coating have been produced by the CVD technique, However, most of the deposits have been grown at relatively high temperatures (1300- 1380 °C) and at atmospheric pressure, using either separate precursors for Si and C¹²⁵⁻¹²⁶ or single source precursor such as MTS¹²⁷. The high temperature deposition results in the introduction of structural defects in the coating layers and difficulties while using the system¹²⁸. In a typical CVD process MTS decomposes and produces corrosive intermediate/byproducts such as HCl, SiHCl₃, SiCl₃, SiCl₄, and CH₄ as well as other silanes and hydrocarbons.¹²⁹⁻¹³⁰ The MTS-CVD gas phase products of chlorine results in deposition of chlorine in coating. The chlorine deposited in coating can migrate in coating and induce defects in layer. Even chlorine can diffuse to neighboring layer/matrix which is not desired specially in nuclear reactors. Therefore, it is worthy to employ

a source that is not pyrophoric, halogen free, decomposes at low temperatures and contains only silicon, hydrogen and carbon atoms. In the current chapter all such possibilities has been explored.

3.1 SiC layer coating using organosilicon precursor

The current section of chapter deals with the coating studies carried out on graphite / zircaloy substrate using synthesized CVDP precursor and commercially available HMDS precursor.

3.1.1 Silicon carbide thin film coating using synthesized organosilicon (CVDP) precursor

3.1.1.1 Experimental methods and materials

The metallorganic fluidized bed CVD (MOFBCVD) technique was used for the coating purpose. The Fluidized bed CVD reactor used in this study is illustrated in Fig. 3.1. The high-temperature fluidized bed reactor system consists of two zones. The first zone consists of a 50 mm (ID) × 600 mm (H) quartz tube and distributor plate (G3-silica porous plate) mounted inside a vertically oriented tube furnace at an upper temperature limit of 1000 °C. The coating on substrate was carried out in this zone by hanging substrate using carbon fibers in uniform temperature zone. The second zone consists of the quartz tube (ID: 50 mm × H: 200 mm) with distributor plate at the bottom to keep the precursor boat over it. In the present work, the advantages of fluidized bed technology such as temperature homogeneity, fast mass and heat transfer and better transport phenomena in gas-particle systems, higher rate of sublimation, to design, construct, and test a reliable liquid precursor delivery system for CVD reactors has been utilized. The fluidized bed evaporator is heated at the sublimation temperature and the fluidization gas is enriched with the

precursor vapors. SiC thin films were deposited using fluidized bed reactor as described above. In this process, the vapor of organosilicon compound CVDP was used as the source of SiC. The substrate material of zircaloy sheet (3 cm×3 cm) was hanged with carbon fiber through a

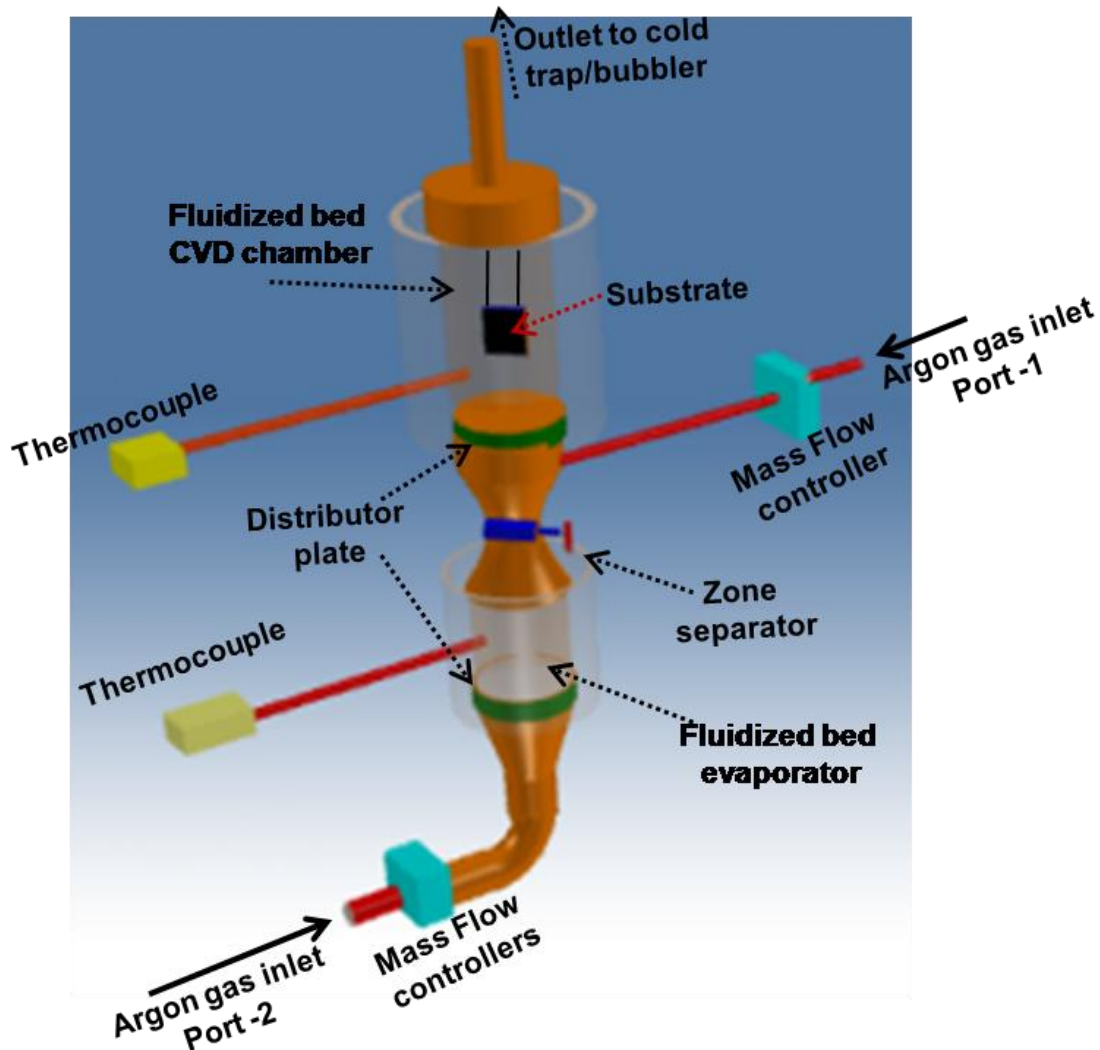


Fig. 3.1 The schematic of metalloorganic Fluidized bed CVD reactor used for SiC deposition.

detachable top in the fluidized bed reactor. The reactor was purged with argon gas through port 1 to maintain the coating system in an inert atmosphere. Prior to the deposition, the zircaloy sheet was heated at a temperature of 900 °C. After reaching the desired temperature for the CVD

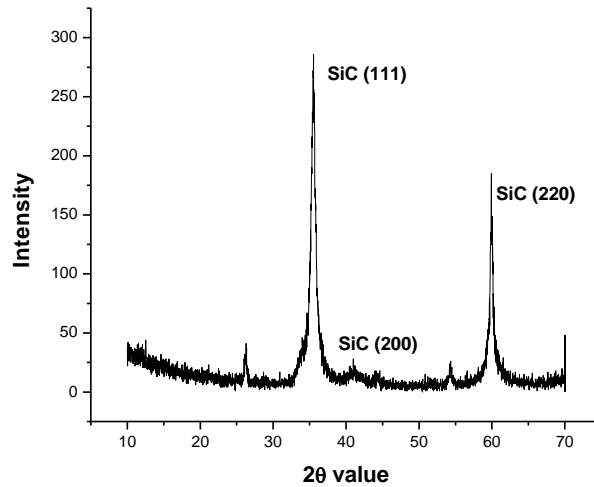
process, the temperature of the fluidized bed evaporator was kept at 200 °C. Precautions were taken to heat the fluidized bed evaporator chamber slowly to ensure that the pressure vaporized congruently and continuously. The argon gas flow was kept constant at 500 sccm through port 2. After having enough vapor pressure in fluidized bed evaporator zone, the zone separator valve was open and gas flow from port 1 was closed. The vapor of the precursor was transported to the high temperature deposition zone for 30 min, where the film growth onto the hot substrate was achieved. The fluidized bed evaporator chamber was then cooled to atmospheric temperature to avoid further transport of vapor into the deposition zone. Further experiments have been carried out to coat graphite substrate with SiC using CVDP precursor. The coated materials were unloaded when they completely cooled to room temperature. The phase of the deposited film was analyzed using X-ray diffraction (XRD)- Philips X pert pro XRD unit using Cu K_α radiation. The surface or cross-sectional morphology and elemental distribution was characterized using scanning electron microscopy (SEM)-Camscan MV2300CT/100, UK, equipped with energy dispersive spectroscopy (EDS).

3.1.1.2 Results and discussion

The coated zircaloy sheet and graphite substrate were collected and characterized. The zircaloy sheet was covered with a light gray color dense layer. To ensure the crystal structure and crystal type of as deposited materials, the SiC coated zircaloy sheet was analyzed by XRD at room temperature. The XRD pattern of the coating prepared on the surface of zircaloy substrate is shown in Fig. 3.2, from which the diffracting peaks of cubical β-SiC were detected. The XRD pattern showed the reflections from (111), (200) and (220) corresponding to β-SiC phase. β-SiC has zinc blend structure. The orientations and degrees of crystallinity in the SiC films have been analyzed by XRD. The deposited 10-12μm SiC film on zircaloy sheet was crystalline, with (111)

face growth having the most intense reflection at 2θ value of 35.5. The full width at half maximum (FWHM), measured from the various reflections (111), (200) and (220) of SiC coated zircaloy sheet surface were 0.69,

0.508 and 1.112 respectively. The average crystallite size was evaluated using Scherrer's equation and was found to be 22.5 nm. This values of the grain size suggested that the coating is composed of nanocrystalline SiC.



SEM micrographs of the coated carbon fiber at different magnifications are shown in Fig.

Fig. 3.2 XRD pattern of the dense SiC coated zircaloy sheet using CVDP precursor.

3.3. The SiC deposition on the zircaloy surface was homogeneous with dense grain deposition. The cross sectional SEM images show that the coating adhesion on the surface was strong, as no detachment of the coating was visible. The chemical compositions of the SiC coated zircaloy sheet surface have been characterized using EDX (Fig. 3.4). It was observed that Si and C were the major elements present in the coating while oxygen was present in small amount. The oxygen pick up may have come in the coating from environment during coating process. It can be avoided by creating proper vacuum in the chamber before coating.

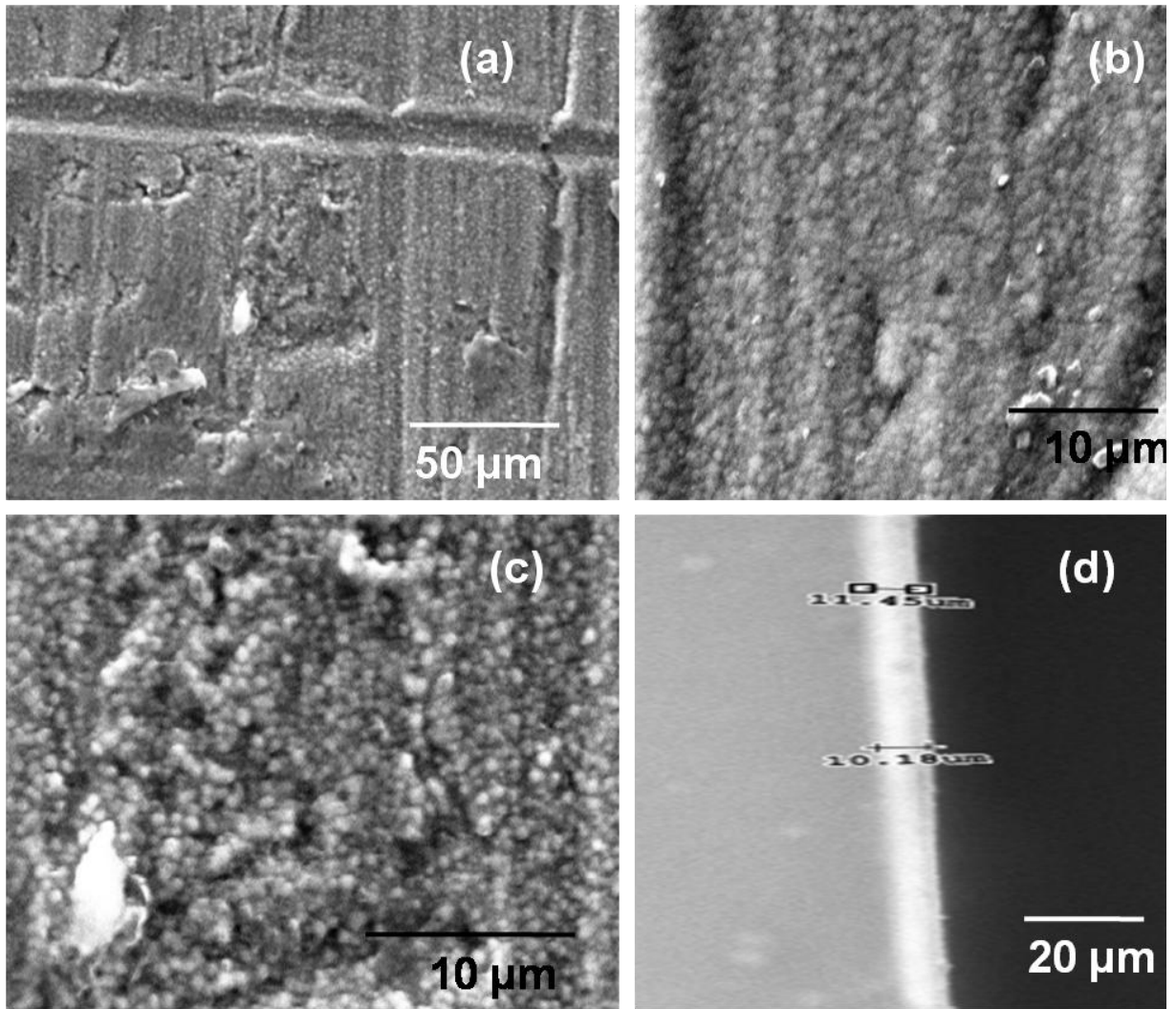


Fig. 3.3 SEM image of the dense nanocrystalline SiC deposit on zirconium substrate (a)(b)(c) surface morphology at different magnification (d) cross sectional view of SiC coating.

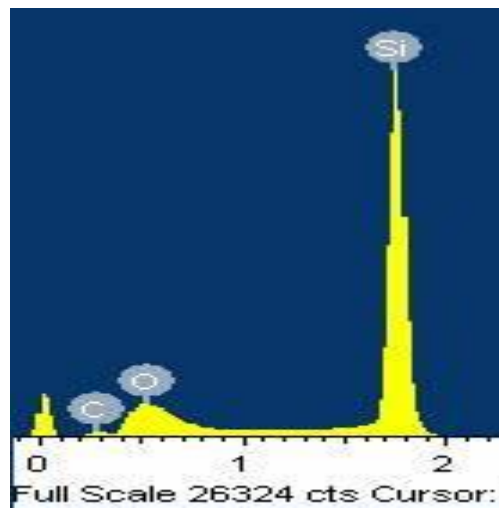
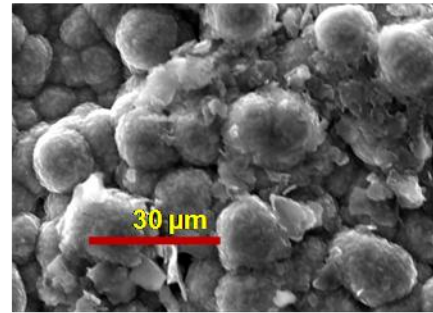


Fig. 3.4 EDX data of the elements in dense nanocrystalline SiC deposit on zirconium substrate.

The grayish color coated graphite substrate was characterized. The SEM images of SiC coated graphite substrate (Fig. 3.5) shows that there was dense layer deposition of SiC over the graphite substrates.

The XRD and SEM results revealed that the use of CVDP precursor yielded dense SiC films on zircaloy and graphite substrates. MTS is a well-known precursor for SiC coatings in the CVD process because of its 1:1 M ration of silicon to carbon. However, the three moles of

chlorine make the compound less useful in certain industrial applications. The presently developed CVDP precursor and fluidized bed coating process to deposit SiC coatings proves that there exists no chlorine etching problem, and the uniform coating of SiC can be achieved.



CVDP

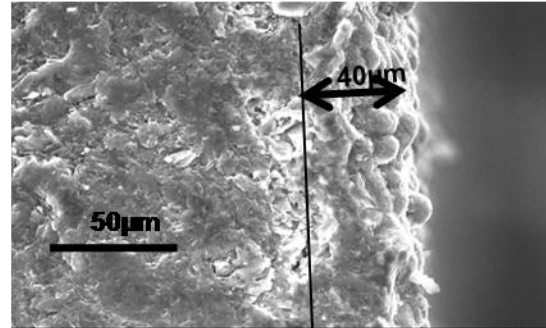


Fig. 3.5 SEM image of the dense SiC deposit on graphite substrate (a) surface morphology (b) cross sectional view of SiC coating.

3.1.2 Silicon carbide thin film coating using Hexamethydisilane (HMDS) precursor

3.1.2.1 Experimental methods and materials

The SiC layer was deposited on graphite (3.5 cm × 3.5 cm × 0.5 cm) block and Zirconia microspherical particles using CVD technique. The coating of graphite block was carried out in

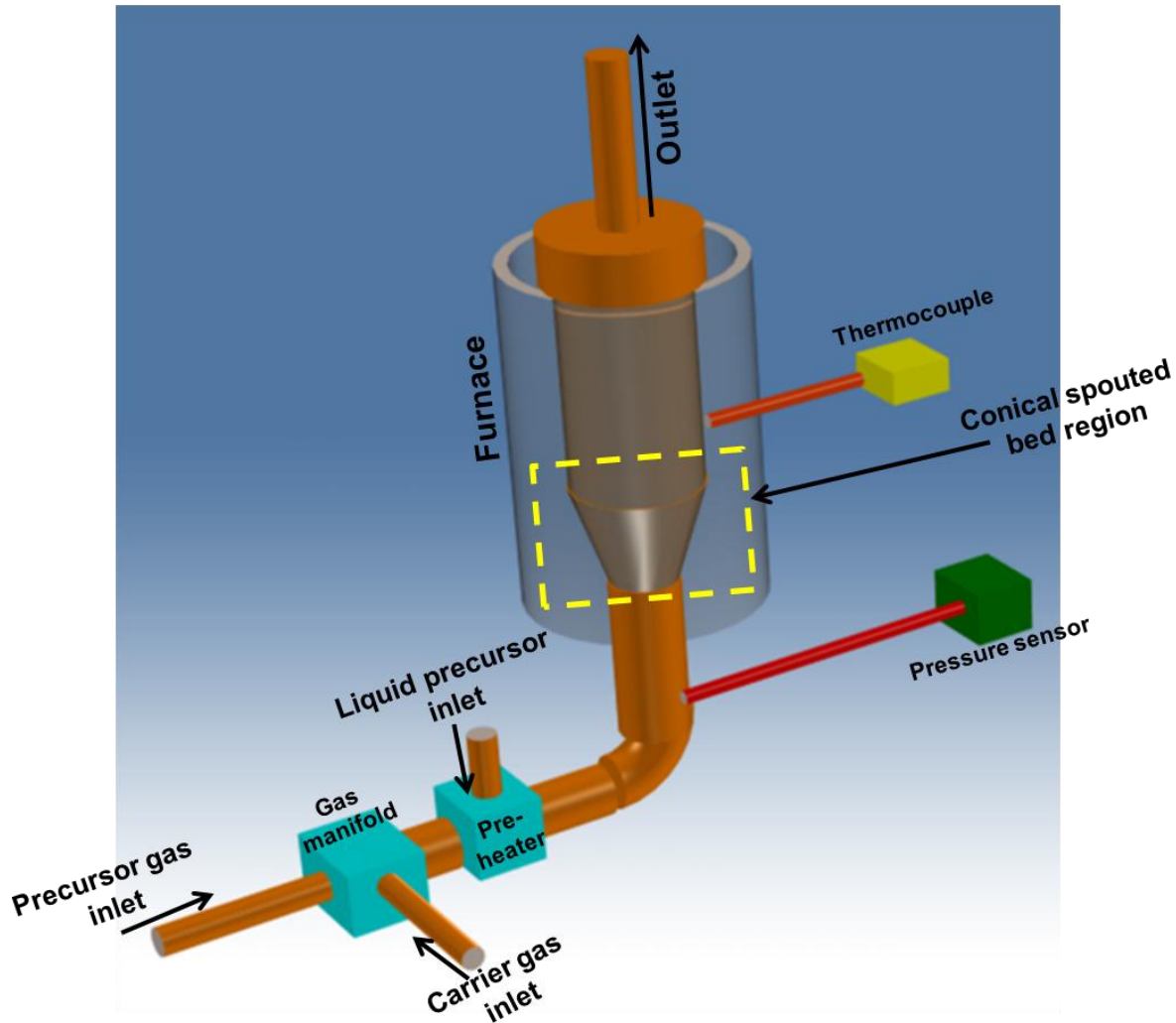


Fig. 3.6 Schematic diagram of spouted bed furnace for coating on spherical microspheres.

the set up as shown in Fig. 3.1. The graphite block was hanged with carbon fibers to place it in the hot zone. SiC coating has been carried out using HMDS as the source for SiC and argon as carrier gas. The deposition conditions used were as follows; deposition temperature: 1000 °C, Ar

flow rate: 500 sccm, coating time: 30 min. The coating on zirconia spherical particles was carried out in spouted bed reactor. A schematic of the spouted bed SiC coating apparatus used in the present experiment is shown in Fig. 3.6. SiC was deposited on a batch of 50 g of zirconia spherical particles with a diameter of $\sim 400 \mu\text{m}$. Argon and hydrogen were used as the carrier gas which sweeps away the SiC precursor from the preheating zone to the hot zone of the reactor. The deposition conditions used for HMDS were: deposition temperature: $1300 \text{ }^\circ\text{C}$, liquid flow rate: 1ml/min, Argon flow rate: 7 lpm, H_2 flow rate: 1.5 lpm, coating time: 30 min. The deposited layers of SiC have been characterized using SEM and XRD.

3.1.2.2 Results and discussion

To ensure the crystalline nature of as deposited materials, the SiC coated zirconia microsphere and graphite substrate have been analyzed by XRD at room temperature. The XRD pattern of the coating prepared on the surfaces is shown in Fig. 3.7, from which the diffracting peaks of cubical β -SiC have been detected for both the cases. The XRD pattern showed the reflections from (111), (200) and (220) corresponding to β -SiC phase. Beta SiC has zinc blend structure.

The SEM (Fig. 3.8) and Optical micrograph images (Fig. 3.9) of SiC coated graphite substrate and zirconia microsphere show that there was dense layer deposition of SiC over the graphite substrates and zirconia microsphere. The XRD and SEM results revealed that the use of HMDS

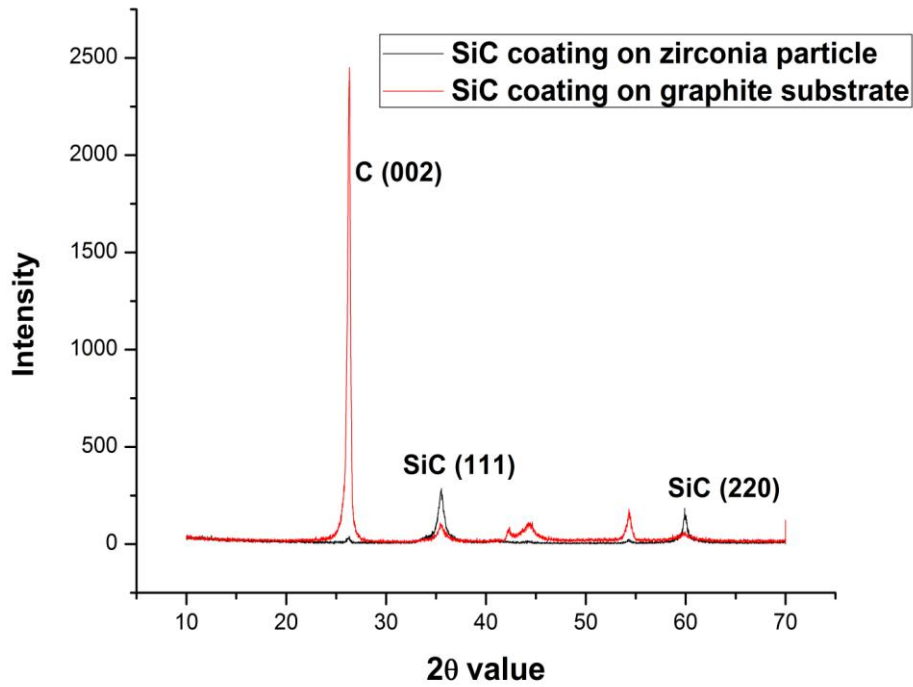


Fig. 3.7 XRD pattern of the dense SiC coated zircaloy sheet using CVDP precursor.

precursor yielded dense SiC coating on graphite substrates and zirconia microsphere at low deposition temperature.

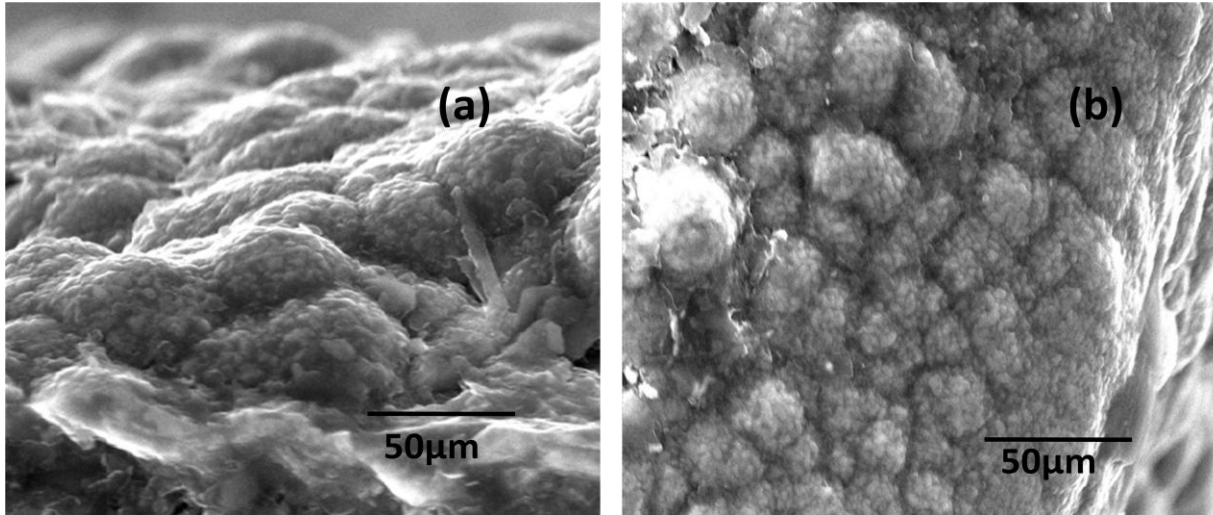


Fig. 3.8 SEM image of the dense SiC deposit on graphite substrate (a) & (b) surface morphology of SiC coating using HMDS.

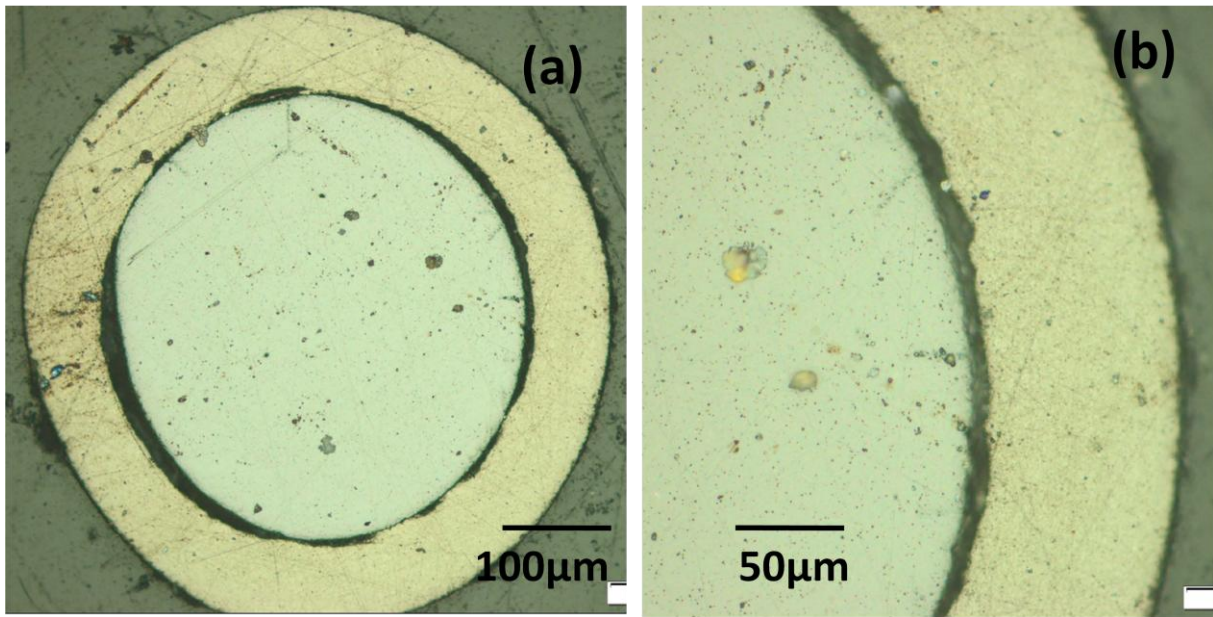


Fig. 3.9 The cross sectional microscopic images of the deposited SiC from HMDS at different magnification at zirconia microsphere.

3.2: SiC layer coating studies on tri-isotropic (TRISO) Particles

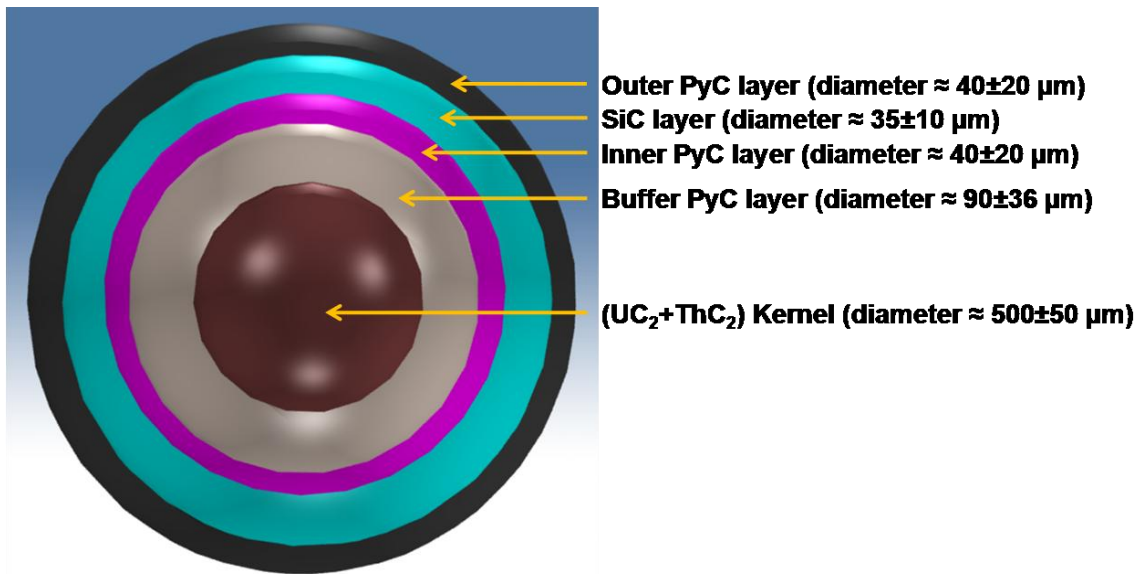


Fig.3.10 Schematic of TRISO coated fuel particle

TRISO coated particles are used as the fuel in High Temperature Reactors. A TRISO coated particle consists of a kernel, usually uranium oxide (UO_2) or mixed uranium oxide and uranium carbide (UCO) which is surrounded by four layers developed by chemical vapor deposition (CVD) (Fig. 3.10). The coated layers are: (i) buffer porous carbon layer, 90–100 μm thick; (ii) the inner pyrolytic carbon (IPyC) layer, 35–40 μm thick; (iii) the SiC layer with a thickness of $\sim 35 \mu\text{m}$; and (iv) the outer pyrolytic carbon (OPyC) layer, 35–40 μm thick. The different layers of the particle provide containment for fission products that can withstand the high operating temperatures ($>1100 \text{ }^\circ\text{C}$) environment. The SiC coating in the TRISO fuel particles is of interest to the nuclear industry due to its small neutron-capture cross-section and strong covalent/ionic Si-C bond, one which give long term resistance to irradiation and excellent mechanical properties. SiC coating is the most important component for structural integrity of TRISO fuel particles as it sustains most of the internal pressure produced by the fission gases produced

within the kernel. The SiC layer used for the formation of TRISO coated fuel particles is normally produced at high temperatures via fluidized bed chemical vapor deposition from MTS in a hydrogen environment. Conventionally the SiC layer in TRISO coated fuel particles is deposited from decomposition of MTS with hydrogen (H₂) at temperatures around 1200–1650 °C. Only the cubic polymorph of SiC (β -SiC) is desired for nuclear applications due to its dimensional stability under irradiation. The high temperature coating process is not desired for bulk production of coated radioactive TRISO coated particle. The drawbacks related to the use of MTS for SiC layer deposition are its toxicity, corrosive nature of MTS and the generation of gaseous corrosive reaction products. During CVD, corrosive gaseous products can attack the fuel kernel. The chlorine retained in the SiC layer can change to its radioisotope under irradiation and drift to the kernel. The mechanical properties of SiC can also degrade due to the presence of chlorine. Therefore an alternate precursor is required which is non-toxic, halogen free and contains both silicon and carbon atom as single molecule.

In the present work, the deposition of uniform SiC layers using different organosilicon precursors such as MTS and HMDS and TMS via spouted bed chemical vapor deposition have been studied.

3.2.1 Experimental methods and materials

The SiC coatings were grown on the pyrolytic carbon coated zirconia balls by the pyrolysis of MTS, HMDS and TMS in reducing hydrogen atmosphere in spouted bed using a graphite reactor. A schematic of the SiC coating apparatus used in the present experiment is shown in Fig. 3.6. SiC was deposited on a batch of 50 g of pyrolytic carbon coated zirconia spherical particles with a diameter of ~680 μ m. Argon and hydrogen were used as the carrier gas which sweeps

away the SiC precursor from the preheating zone to the hot zone of the reactor. Deposition conditions have been optimised for the SiC coating using MTS as precursor for the present spouted bed reactor and similar conditions were used to deposit SiC using HMDS & TMS as precursor except for the deposition temperature. The deposition conditions used for MTS precursor were deposition temperature: 1450 °C, MTS flow rate: 1 ml/min, Argon flow rate: 7 lpm, H₂ flow rate: 1.5 lpm, coating time: 50 min. The deposition conditions used for HMDS and TMS were: deposition temperature: 1300 °C, liquid flow rate: 1ml/min, Argon flow rate: 7 lpm, H₂ flow rate: 1.5 lpm, coating time: 30 min. The deposited layers of SiC were characterized using Optical Microscopy, XRD, SEM, EDX and microindentation.

3.2.2 Result and Discussion

Considering that the grain size in SiC is largely controlled by deposition temperature, (reducing

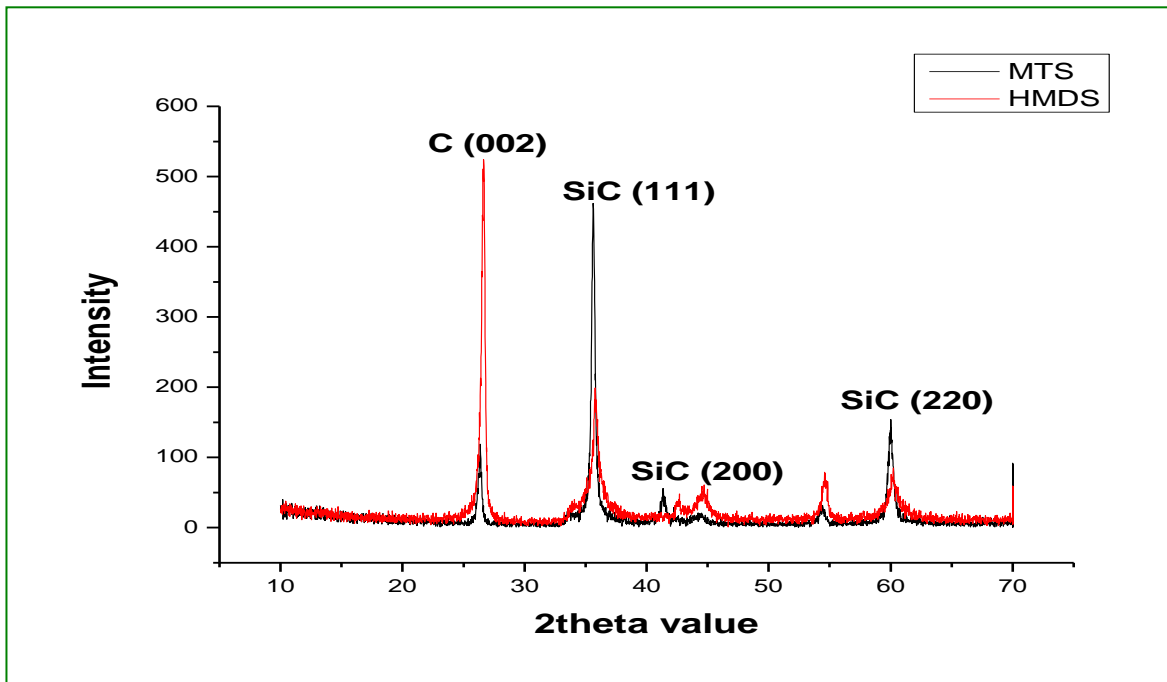


Fig. 3.11 XRD spectrum of SiC deposits using MTS and HMDS.

with lower deposition temperatures) our goal was to produce SiC coatings at temperatures below 1500 °C, so the deposition temperatures as 1450 °C for MTS and 1300 °C for HMDS were chosen. The XRD spectra (Fig. 3.11) confirmed that the β -SiC is the main phase grown in SiC layer using MTS and HMDS precursors. The XRD pattern showed the reflections from (111) and (220) corresponding to β -SiC phase. The cross sectional microscopic images (Fig. 3.12, 3.14 & 3.15) of the deposited SiC from MTS, HMDS and TMS showed the deposition of adherent layer of SiC in case of MTS and HMDS. Whereas in the case of coating deposited from TMS non uniform layer was obtained. To obtain the cross sectional surface of SiC coating, SiC coated particles were hot mounted in copper-loaded conductive resin. To reduce influence of the surface roughness, the CVD SiC coatings were first ground down to obtain a flat surface, where the micro-indentation could be carried out. The flat surface was further polished using increasingly finer diamond suspensions until 1/4 μm . The thickness of the coating after final polishing was estimated. It was observed that the SiC layer was of uniform thickness $\sim 60 \mu\text{m}$ in case of MTS precursor. The X-ray tomography images (Fig. 3.13(a)) further confirms the formation of uniform layer over the spherical particle. Murakami solution (i.e. NaOH and potassium ferricyanide) was used as etchant to see the SiC layer microstructure obtained from MTS. The presence of fine columnar grains in the radial direction was observed (Fig. 3.13 (b)). The width and length of grains were about 1 μm and about 2-3 μm respectively. It seems that etching is stronger in the first micron from the interface I-PyC/SiC. This phenomenon may occur due to the existence of very small grains of SiC. The SiC layer of thickness $\sim 30 \mu\text{m}$ has been obtained in case of HMDS precursor whereas non uniform layer of thickness $\sim 20 \mu\text{m}$ was obtained in case of SiC coating from TMS precursor.

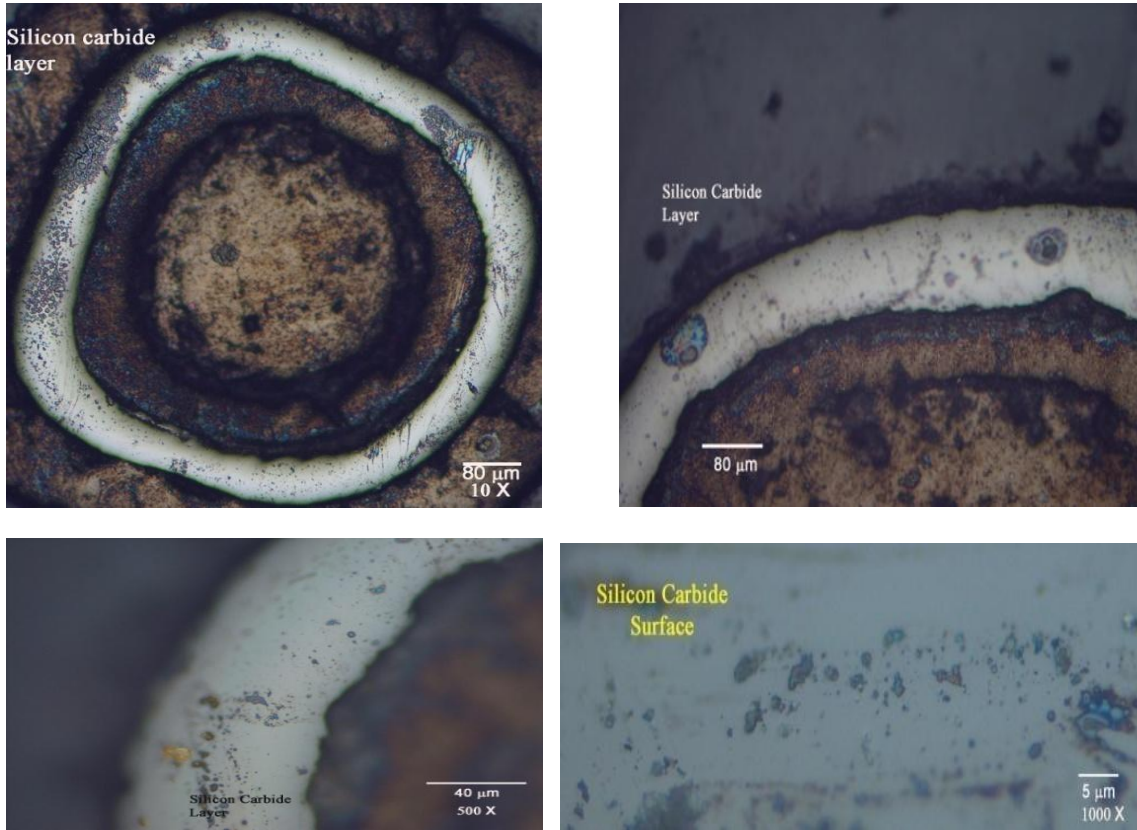


Fig.3.12 The cross sectional microscopic images of the deposited SiC from MTS at different magnification.

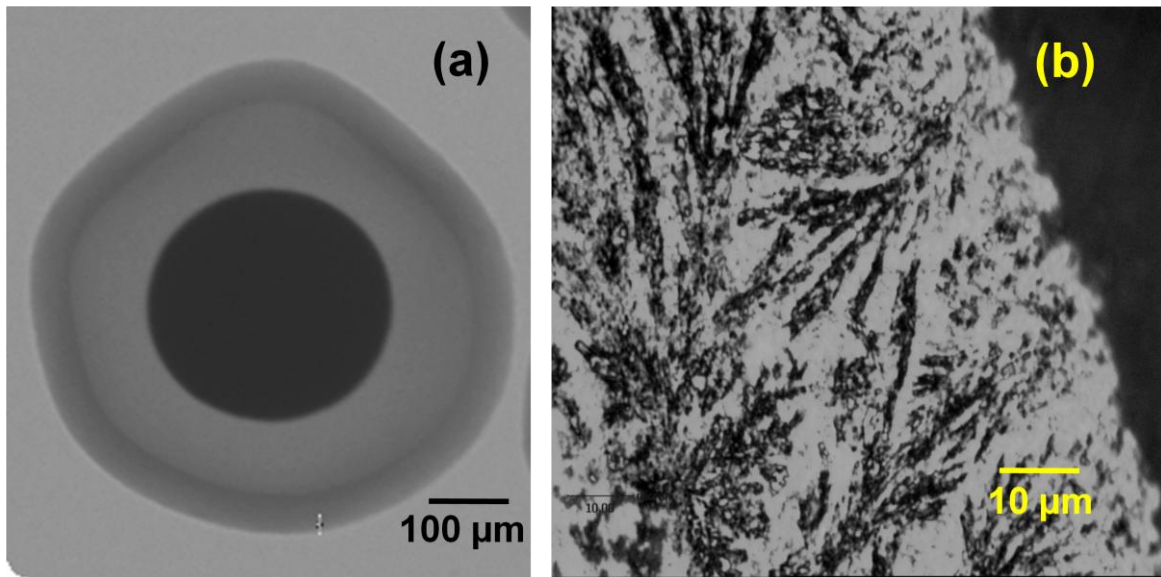


Fig. 3.13 (a) X-ray tomography image of SiC coated spherical particle. (b) Murakami etched surface of SiC layer deposited from MTS.

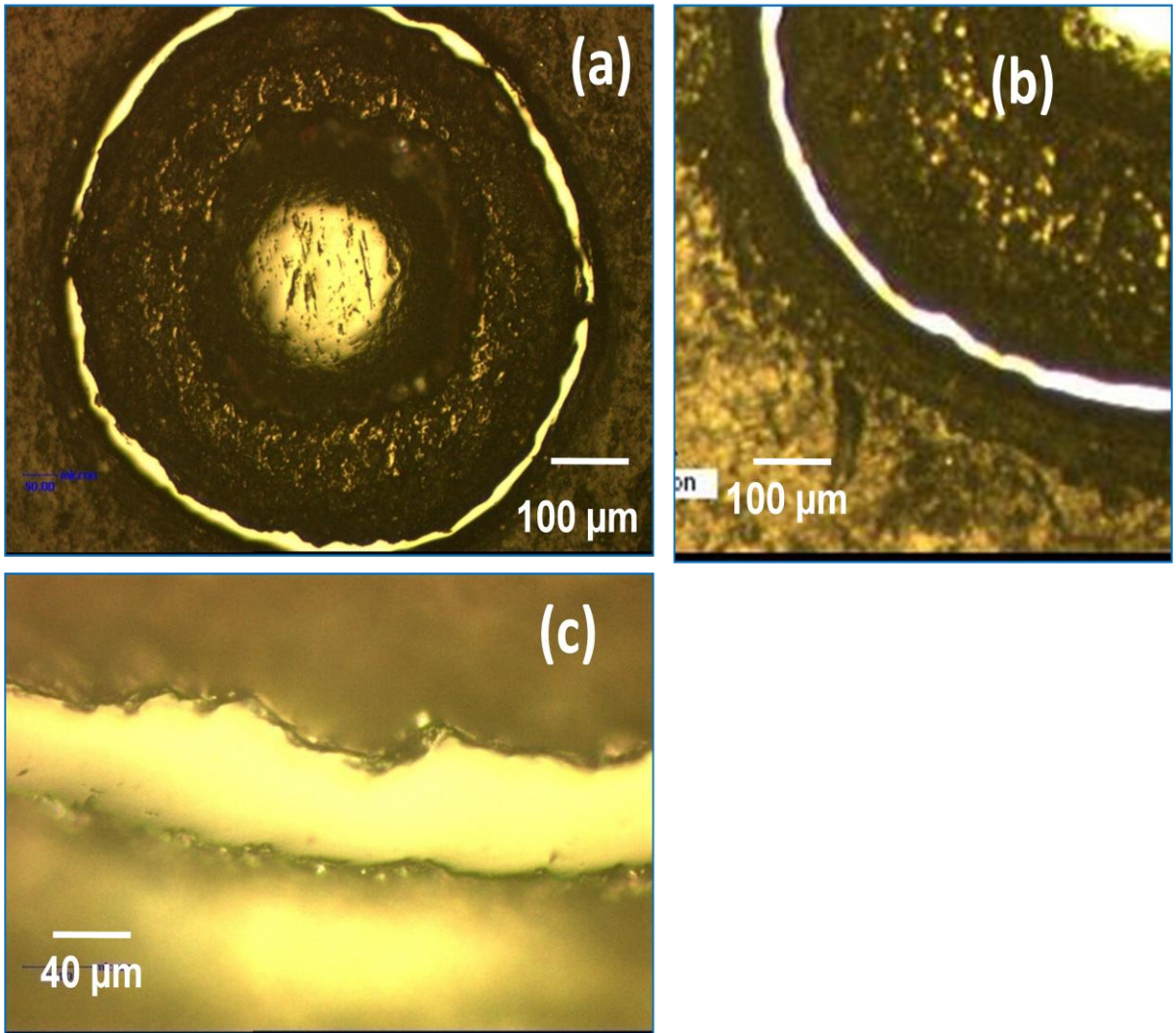


Fig. 3.14 The cross sectional microscopic images of the deposited SiC from HMDS at different magnification.

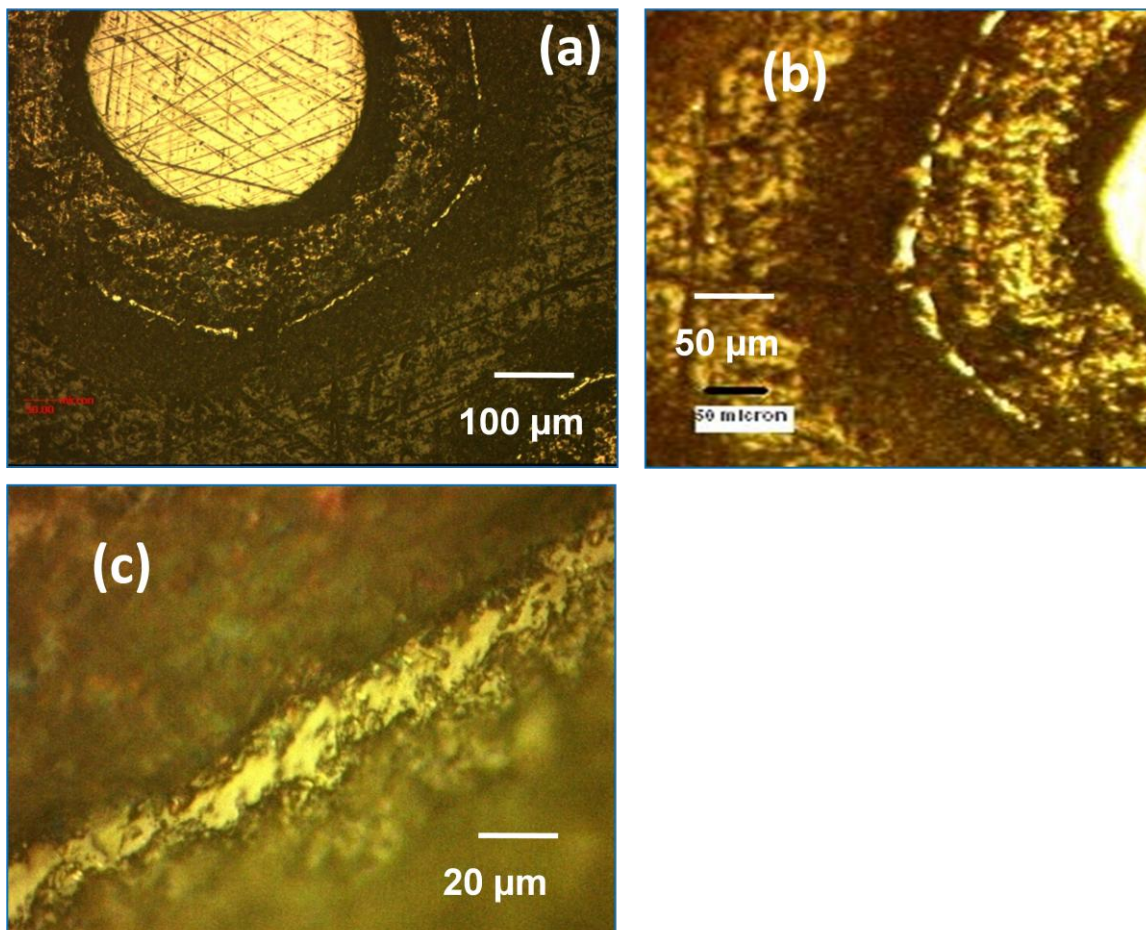


Fig. 3.15 The cross sectional microscopic images of the deposited SiC from TMS at different magnification.

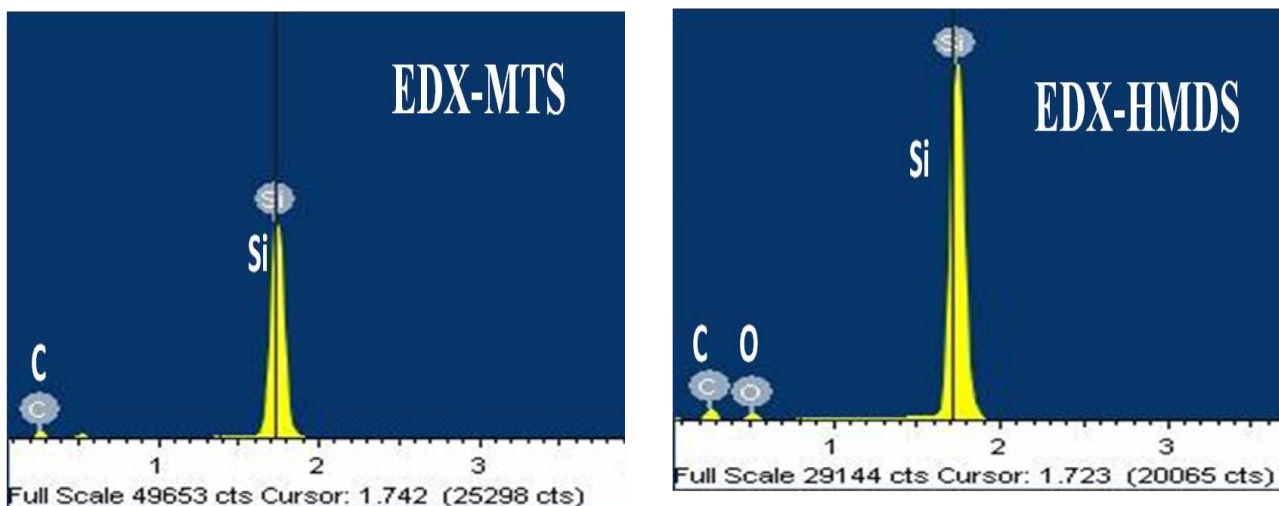


Fig. 3.16 EDX spectrum of SiC deposits using MTS and HMDS.

Table 3.1

Concentration of different Elementals in different SiC coatings.

| Element | SiC deposition using MTS | | SiC deposition using HMDS | |
|---------|--------------------------|-------|---------------------------|-------|
| | Wt% | At% | Wt% | At% |
| C | 30.43 | 48.28 | 35.85 | 55.47 |
| Si | 60.79 | 41.25 | 60.0 | 39.71 |
| O | 8.79 | 10.47 | 4.15 | 4.83 |

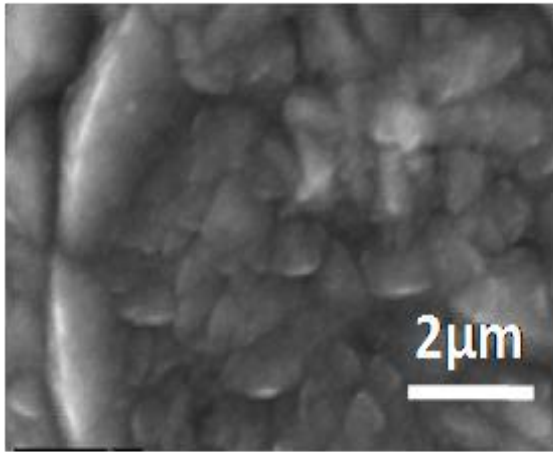


Fig. 3.17 SEM image of the SiC surface coated by MTS.

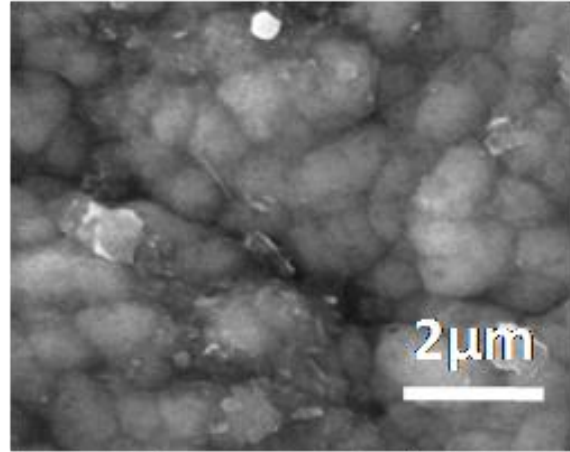


Fig. 3.18 SEM image of the SiC surface coated by HMDS.

The density of coating was found to be around 2.5-3.0 gm/cc in MTS and HMDS cases. The EDX data (Fig. 3.16, Table 3.1) showed that there was more deposition of free carbon with SiC in case of HMDS as precursor. The free carbon may have come from HMDS due to stoichiometric excess of carbon present in HMDS case. The co-deposition of oxygen occurs due to the presence of oxygen in the reactor at the time of coating. It can be avoided by taking proper vacuum in the reactor. Fig. 3.17 & 3.18 show the SEM images of the SiC surfaces obtained by

different precursors. It has been observed that columnar grains with the grain size: $1\text{w} \times 2\text{l} \mu\text{m}$ were present on the SiC layer surface coated by MTS precursor. Larger columnar grains were observed thru-wall of the SiC and Pyrolytic Carbon interface. Whereas in case of SiC layer coated by HMDS small equiaxed grains with the grain size: $1 \times 1 \mu\text{m}$ were present. The larger grain boundary surface area per unit thickness of the smaller grained SiC should in principle retain metallic fission products better than the large columnar grain. So smaller grain size of SiC was desired in the SiC layer. It has been observed that the grain size of SiC grains were not reduced upto desired level even by decreasing deposition temperature below $1500 \text{ }^\circ\text{C}$. Whereas in case of SiC layer from HMDS stoichiometric SiC coating with grain sizes around $1 \mu\text{m}$ were obtained. Silicon co-deposition can occur at low deposition temperatures for MTS due to the fact that the silicon bearing molecules, resulting from the decomposition of MTS, have a higher sticking coefficient than carbon species. This would mean that Si-Si bonds are formed due to the lack of reactive carbon molecules that could form Si-C bonds. This problem can be easily avoided in case of HMDS as in HMDS molecule has excess carbon. The decomposition of HMDS not only results in the formation of small reactive radicals but also its decomposition in a hydrogen environment reduces the possibility of gas saturation and the formation of larger and more complex molecules with lower sticking coefficients. Fracture toughness and hardness were measured using a micro-indenter. Micro-indentation was made using a Vickers indenter at a maximum load of 0.5Kg . For MTS and HMDS SiC coatings the hardness obtained were 30GPa and 29GPa respectively. From the theoretical hardness of SiC coating it can be concluded that the density of MTS SiC coating was about 98% and HMDS SiC coating was about 95% of the theoretical density.

The Fracture Toughness was measured by using indentation technique based on the measurement of the lengths of median-radial cracks produced by Vickers Indenter (a four-sided diamond pyramid). The method was used to calculate fracture toughness (K_{IC}) is as follows.

$$K_{IC} = \alpha \cdot \left(\frac{E}{H} \right)^{\frac{1}{2}} \cdot \left(\frac{P}{C} \right)^{\frac{3}{2}} \quad (3.1)$$

Where, α is empirical constant depending on geometry of indenter (0.016)E=(480 GPa) & H is hardness and E is elastic moduli, P is the peak indentation load (0.5 Kg).

The fracture toughness obtained for MTS SiC coating was 2.5-2.8 MPa√m and for HMDS SiC coating was 1.9-2.1 MPa√m. It has been observed that there was no significant difference in the hardness and fracture toughness of the different coatings obtained by MTS and HMDS.

The microstructure and mechanical properties of SiC coatings obtained from different precursors using spouted bed CVD process have been studied. Dense and uniform coatings of SiC were obtained for MTS and HMDS in our spouted bed system. Higher deposition of free carbon with SiC occurs in case of HMDS as precursor which may be due to the nonstoichiometric ratio of Si and C in HMDS. SiC coatings with a sub-micrometer grain size were deposited on simulated TRISO fuel particles by spouted bed CVD at a low temperature 1300 °C using HMDS as precursor. The mechanical properties were studied using microindentation. The microstructures were analyzed using SEM. SiC coatings using HMDS and MTS have shown almost similar hardness and fracture toughness. The hardness and fracture toughness values of the coated SiC layers show that the coating has good strength. HMDS liquid precursor has a potential to replace corrosive and toxic precursor MTS for SiC layer coating in TRISO particle.

3.3: Dense and nanowire morphology coating: Taguchi method study

SiC coating of different morphology using MTS and hydrogen by chemical vapor deposition under ambient pressure are presented in the current section. Taguchi method has been used to design experiments to get the optimum parameters for growing SiC wires of diameter in nanometer range. Chemical vapor deposition hydrogen reduction of MTS is most prominent method for production of SiC nanowires with controlled morphology. In a typical SiC nanowire synthesis process the cracking of MTS has been carried out in reducing atmosphere of hydrogen using chemical vapor deposition technique at high temperature and normal atmospheric pressure. Taguchi method is very useful to design experiments especially in the cases where large numbers of variables are to be considered. This statistical method has been used to design experiments for obtaining optimum parameters for bulk production of SiC wires of uniform diameter in nanometer range. Further, the effect of different parameters on the morphology of SiC deposit has been discussed.

3.3.1 Brief Introduction of Taguchi Method

Taguchi method ¹³¹ of experimental design provides a systematic and efficient approach for conducting experiments to determine near optimum settings of process parameters for optimal performance, e. g. nanodimensional growth of SiC wires in present case. Taguchi's method for experimental design is straightforward and easy to apply to many engineering situations, making it a powerful yet simple tool. It can be used to quickly narrow the scope of a research project or to identify problems in a process from data already in existence. The Taguchi method utilizes orthogonal arrays ¹³² to study a large number of variables with a small number of experiments. Using orthogonal arrays significantly reduces the number of experimental configurations to be

studied. The conclusions drawn from small scale experiments are valid over the entire experimental region spanned by the control factors and their settings. This method can reduce research and development costs by simultaneously studying a large number of parameters.

There are three types of objective function i.e. larger-the-better, smaller-the-better and nominal-the-best. The influences are commonly referred in terms of S/N (signal to noise) ratio as shown in Eq. 3.2 where η is the objective function to be optimized, μ is the measured signal (e.g. diameter of SiC wires) and σ is the standard deviation of the signal to noise ratio.

$$\eta \propto \frac{\mu^2}{\sigma^2} \quad (3.2)$$

For optimization of deposition rate and growth diameter of SiC wires, smaller-the-better type of objective function was used. In this case, the exact relation between S/N ratio and the signal is given by Eq. 3.3 where y_i is the signal (deposition rate or diameter of SiC wires) measured in each experiment averaged over “n” repetitions.

$$S/N (dB) = -10 \log \left(\frac{1}{n} \sum_i^n y_i^2 \right) \quad (3.3)$$

The effect of a parameter level on the S/N ratio, i.e., the deviation it causes from the overall mean of signal, is obtained by analysis of mean (ANOM). The relative effect of process parameters can be obtained from analysis of variance (ANOVA) of S/N ratios. Computation of ANOM and ANOVA are carried out using relations in Equations. 3.4 and 3.5.

$$m_i = \left(\frac{1}{N_i} \right) \sum S/N \quad (3.4)$$

$$Sum\ of\ squares(SoS) = \sum_{i=i}^{i=j} N_i (m_i - \langle m_i \rangle)^2 \quad (3.5)$$

Where m_i represents the contribution of each parameter level to S/N ratio, $\langle m_i \rangle$ is the average of m_i 's for a given parameter and the coefficient and N_i represents the number of times the experiment is conducted with the same factor level in the entire experimental region. *SoS* is obtained by using ANOVA. This term is divided by corresponding degrees of freedom (DoF = number of parameter level minus 1) to derive relative importance of various experimental parameters by utilizing Equation. 3.6.

$$Factor\ effect = \frac{SoS}{\{DoF \times \sum(SoS/DoF)\}} \quad (3.6)$$

Several research groups ¹³³⁻¹³⁴ have extensively used this technique in optimization of parameters. To the best of our knowledge, this was the first use of this technique for the optimization of the parameters to get nano-dimensional SiC wires by CVD method.

Using the Taguchi method for parameter design, the predicted optimum setting need not correspond to one of the rows of the matrix experiment. Therefore, an experimental confirmation is run using the predicted optimum levels for the control parameter is required. The purpose is to verify that the optimum conditions suggested by the matrix experiments do indeed give the projected improvement. If the observed and the projected improvements match, the suggested optimum conditions will be adopted. If not, it will be concluded that the additive model underlying the matrix experiment has failed, and ways need to be found to correct that problem. The corrective actions include finding better quality characteristics, or S/N ratios, or different control factors and levels, or studying a few specific interactions among the control factors.

3.3.2 Experimental methods and materials

3.3.2.1 Parameter Selection for Taguchi Optimization

The objective of the present studies was to synthesize SiC wires of nanometer (nm) diameter range from MTS. Based on the concept of smaller-the-better function in Taguchi method; the parameters for lowest deposition rate and growth of minimum diameter of SiC wires have been optimized. Four parameters at three different levels have been identified for optimization. These are: (i) temperature of the synthesis (1100/1300/1500 °C), (ii) MTS flow rate (0.5/1.0/ 2.0 ml/min), (iii) hydrogen flow rate (0.8/ 1.2/2.0 lpm) and (iv) total flow rate (2/4/6 lpm). Table 3.2 shows the parameters and their levels. This is a four-factor-three-level design. Therefore, L-9 orthogonal array has been chosen as per design and is presented in Table 3.3.

Table 3.2

Selection of parameters and their levels for Taguchi method.

| Parameter | Level 1 | Level 2 | Level 3 |
|--|----------------|----------------|----------------|
| Temperature (°C) | 1500 | 1300 | 1100 |
| MTS flow rate (ml/min) | 1.0 | 0.5 | 2.0 |
| Hydrogen flow rate (lpm) | 2.0 | 0.8 | 1.2 |
| Total flow rate (Ar+H₂)(lpm) | 2 | 4 | 6 |

Table 3.3

Design of L-9 orthogonal array for experiments.

| Exp. No. | Total flow (lpm) | Hydrogen flow (lpm) | MTS flow (ml/min) | Temperature (°C) |
|-----------------|-------------------------|----------------------------|--------------------------|-------------------------|
| T1 | 2 | 2 | 1.0 | 1500 |
| T2 | 2 | 0.8 | 0.5 | 1300 |
| T3 | 2 | 1.2 | 2.0 | 1100 |
| T4 | 4 | 2 | 0.5 | 1100 |
| T5 | 4 | 0.8 | 2.0 | 1500 |
| T6 | 4 | 1.2 | 1.0 | 1300 |
| T7 | 6 | 2 | 2.0 | 1300 |
| T8 | 6 | 0.8 | 1.0 | 1100 |
| T9 | 6 | 1.2 | 0.5 | 1500 |

3.3.2.2 Experimental Set up and synthesis of SiC wires

The SiC wires were grown on C/C composite (3.5 cm × 3.5 cm × 0.5 cm) using CVD technique. A high temperature vertical cylindrical graphite reactor of dimension ($l \times d$) 40 cm × 6 cm was used for the coating studies. Schematic diagram of the coating system is shown in Fig. 3.19. SiC coating has been carried out using MTS as the source for SiC and hydrogen-argon mixture as carrier gas. The MTS feed flow rate was varied using a peristaltic pump and was pumped at particular rate to the feed line that was connected to the vertical furnace (heated at 200 °C) (Fig. 3.19). Hydrogen-argon mixture was used as carrier gas to sweep the MTS vapors into the reactor. Initially, a set of nine experiments were carried out as per the L-9 array (Table 3.3). Later on the experiments have been performed using optimized parameters and varying hydrogen to MTS

ratio. The deposition temperature was kept constant at 1300 °C. The total amount of MTS (30 ml) used in each experiment was kept constant. The effect of hydrogen to MTS ratio on the morphology of grown SiC wires is presented in Table 3.4. The as grown SiC wires have been

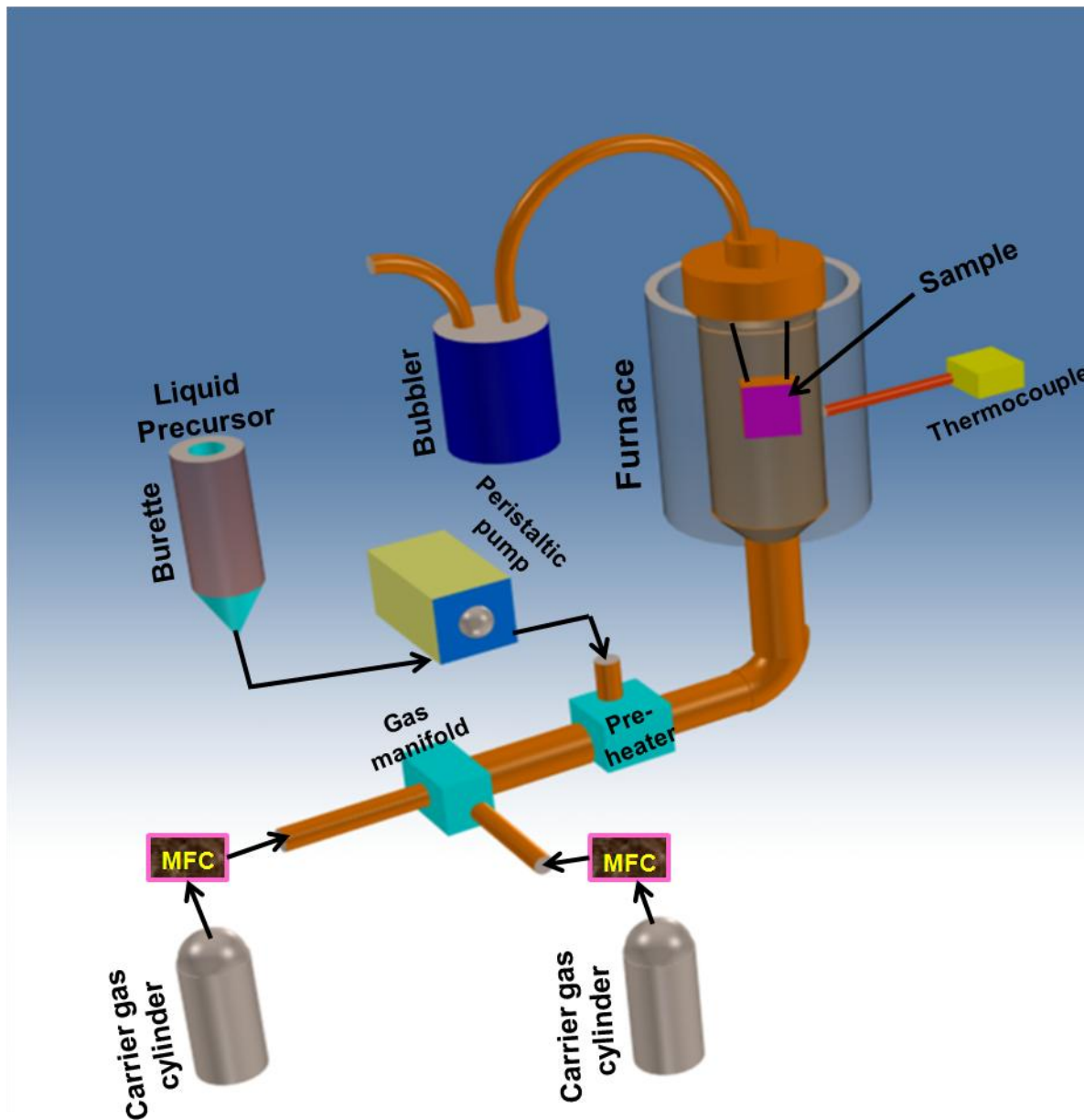


Fig. 3.19 Schematic diagram of experimental setup for growing SiC coating.

characterized by XRD and Raman spectroscopy for phase identification. SEM analysis was carried out for the micro structural and morphology details.

3.3.3 Results and discussion

3.3.3.1 Taguchi optimization calculations

Lee ¹³⁵ proposed that lower deposition rates and lower temperature for fcc crystals result in development of lowest surface energy plane i.e. {111} plane while higher temperature and higher deposition rates causes development of higher surface energy, i.e. the {110} plane.

The lower deposition rate at lower temperature limits the saturated precursor vapor concentration in the gaseous mixture. Therefore effective precursor vapor concentration near to the deposit surface must be lowest leading to deposit of [111] texture (Fig. 3.20 & 3.21).

Keeping the above facts in mind, the aim

was to minimize the deposition rate of SiC and increase the amount of deposits having [111] texture. Further, our aim was to reduce the diameter of the SiC wires from micron to nanometer range. The Taguchi calculation has been used for minimizing the deposition rate as well as reducing the diameter of grown SiC.

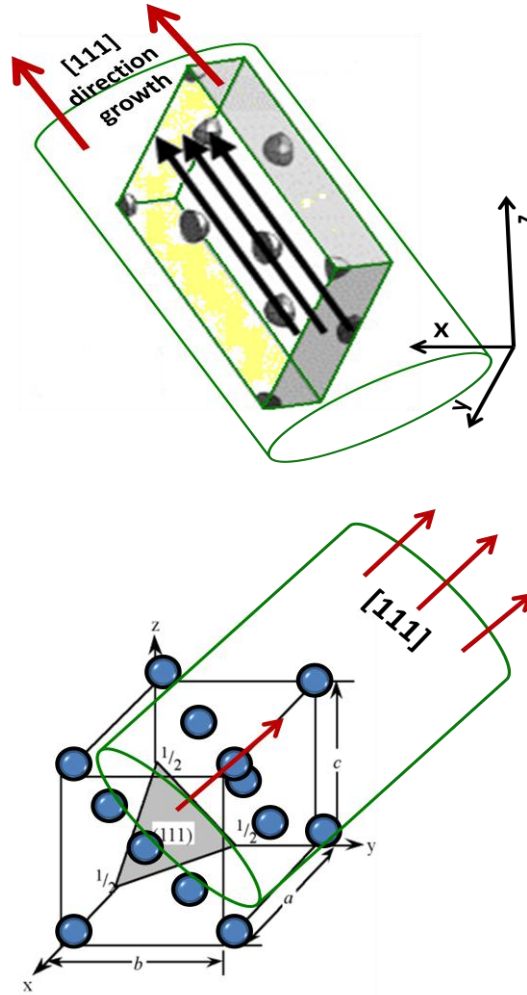


Fig. 3.20 Schematic representation of lowest surface energy growth direction in fcc crystal.

Table 3.4

Experiments performed by varying H₂/MTS ratio at 1300 °C.

| Exp. No. | Total gas flow rate of mixture (lpm) | Ar Flow rate (lpm) | H ₂ Flow rate (lpm) | MTS Flow rate (ml/min) | H ₂ /MTS ratio | Deposition Rate (g/min) | Average diameter of SiC wires |
|------------|--------------------------------------|--------------------|--------------------------------|------------------------|---------------------------|-------------------------|-------------------------------|
| 1. | 2 | 1.6 | 0.4 | 2.0 | 1.16 | 0.0223 | 1.5 μm |
| 2. | 2 | 1.2 | 0.8 | 2.0 | 2.32 | 0.0229 | 1.79 μm |
| 3. | 2 | 1.6 | 0.4 | 1.0 | 2.33 | 0.0195 | 900 nm |
| 4. | 2 | 0.8 | 1.2 | 2.0 | 3.5 | 0.025 | 2 μm |
| 5. | 2 | 1.2 | 0.8 | 1.0 | 4.65 | 0.013 | 700 nm |
| 6. | 2 | 1.2 | 0.8 | 0.5 | 9.3 | 0.00679 | 5 μm |
| 7. | 2 | 0.8 | 1.2 | 0.5 | 14.0 | 0.00644 | 3 μm |
| 8. | 6 | 4.8 | 1.2 | 0.5 | 14.0 | 0.0045 | Dense |
| 9. | 2 | 0 | 2.0 | 0.5 | 23.28 | 0.016 | 1.69 μm |
| 10. | 5 | 1.5 | 3.5 | 0.5 | 40.7 | 0.012 | 350 nm |
| 11. | 2 | 2 | 0 | 0.5 | 0 | 0.0089 | Dense |
| 12. | 8 | 2 | 6 | 0.5 | 70 | 0.0062 | 50 nm |

The results of the experiments as per the L-9 array and the corresponding S/N ratios are given in Table 3.5. The effects of each parameter on the deposition rate and the diameter of SiC were calculated by Equations. 2-5 and are presented in Tables 3.6-3.7. From the XRD pattern (Fig. 3.22), it could be inferred that the SiC deposit obtained through the experiments as shown in the Table II corresponds to the β -SiC phase. The XRD pattern showed the reflections from (111) and (220), corresponding to β -SiC phase. From SEM images (Fig. 3.23), it has been observed that there is no growth of SiC wires (dense SiC

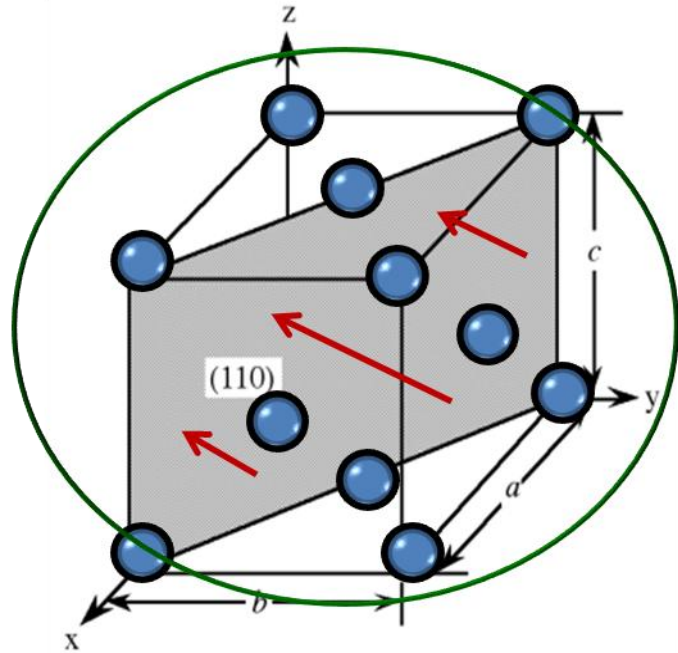


Fig. 3.21 Schematic representation of higher surface energy growth direction in fcc crystal.

deposition) at deposition temperature of 1500 °C. In addition, it was observed that the effect of MTS flow rate was maximum (56%) and the total flow rate has minimum effect (1.97%) on the deposition rate of SiC produced by CVD technique. The effect of deposition temperature and hydrogen flow rate was 18.6% and 23.2%, respectively.

Table 3.5

Results from deposition, micro structural analysis of SiC and corresponding S/N ratio.

| Exp. No. | Ave. Deposition rate (DR) (gm/min) | 10×DR[#] | S/N (dB) | Ave. Diameter (nm) | Modified ave. diameter[*] | S/N (dB) |
|-----------------|---|--------------------------|-----------------|---------------------------|---|-----------------|
| T1 | 0.0007 | 0.007 | 43.1 | dense | 2000 | -66.0 |
| T2 | 0.0184 | 0.184 | 14.7 | 265 | 265 | -48.5 |
| T3 | 0.091 | 0.91 | 0.82 | 1000 | 1000 | -60 |
| T4 | 0.0035 | 0.035 | 29.1 | 250 | 250 | -47.9 |
| T5 | 0.029 | 0.29 | 10.7 | dense | 2000 | -66.0 |
| T6 | 0.023 | 0.23 | 12.8 | 350 | 350 | -50.9 |
| T7 | 0.035 | 0.35 | 9.1 | 497 | 497 | -54 |
| T8 | 0.00193 | 0.0193 | 34.3 | 559 | 559 | -55 |
| T9 | 0.0076 | 0.076 | 22.4 | dense | 2000 | -66.0 |

[#]Since some of the average deposition values were too low, all deposition values have been multiplied by 10 to facilitate in calculations.

^{*}In case of dense deposition the average diameter was assumed to be 2000 nm to get the effects of different parameters on the growth diameter of SiC wires)

Table 3.6

Effect of different parameters on the deposition rate of SiC.

| Factor | Level | Ave. Deposition rate (gm/min) | m_i | $\langle m_i \rangle$ | SoS | % effect |
|---------------------------------|--------------|--|-------------------------|---|------------|-----------------|
| Total flow rate (lpm) | 2 | 0.367 | 19.5 | 19.6 | 9.7 | 1.96 |
| | 4 | 0.185 | 17.5 | | | |
| | 6 | 0.148 | 21.9 | | | |
| Hydrogen flow rate (lpm) | 2 | 0.13 | 27.1 | 19.7 | 114.09 | 23.2 |
| | 0.8 | 0.164 | 19.9 | | | |
| | 1.2 | 0.405 | 12.0 | | | |
| MTS flow rate (ml/min) | 1.0 | 0.085 | 30.0 | 19.7 | 275.69 | 56.1 |
| | 0.5 | 0.097 | 22.1 | | | |
| | 2.0 | 0.52 | 6.9 | | | |
| Temperature (°C) | 1500 | 0.12 | 25.4 | 19.7 | 91.63 | 18.6 |
| | 1300 | 0.25 | 12.2 | | | |
| | 1100 | 0.32 | 21.4 | | | |

Table 3.7

Effect of different parameters on the growth diameter of SiC.

| Factor | Level | Ave. diameter (nm) | m_i | $\langle m_i \rangle$ | SoS | % effect |
|------------------------------|--------------|---------------------------|-------------------------|---|------------|-----------------|
| Total flow rate (lpm) | 2 | 1088.3 | -58.2 | -57.1 | 7.49 | 4.89 |
| | 4 | 866.7 | -54.9 | | | |
| | 6 | 1018.7 | -58.3 | | | |
| Hydrogen flow (lpm) | 2 | 915.7 | -56.0 | -57.1 | 5.17 | 3.38 |
| | 0.8 | 941.3 | -56.5 | | | |
| | 1.2 | 1116.7 | -59.0 | | | |
| MTS flow (ml/min) | 1.0 | 969.7 | -57.3 | -57.1 | 17.45 | 11.39 |
| | 0.5 | 838.3 | -54.1 | | | |
| | 2.0 | 1165.7 | -60.0 | | | |
| Temperature (°C) | 1500 | 2000 | -66.0 | -57.1 | 123 | 80.34 |
| | 1300 | 370.7 | -51.1 | | | |
| | 1100 | 603.0 | -54.3 | | | |

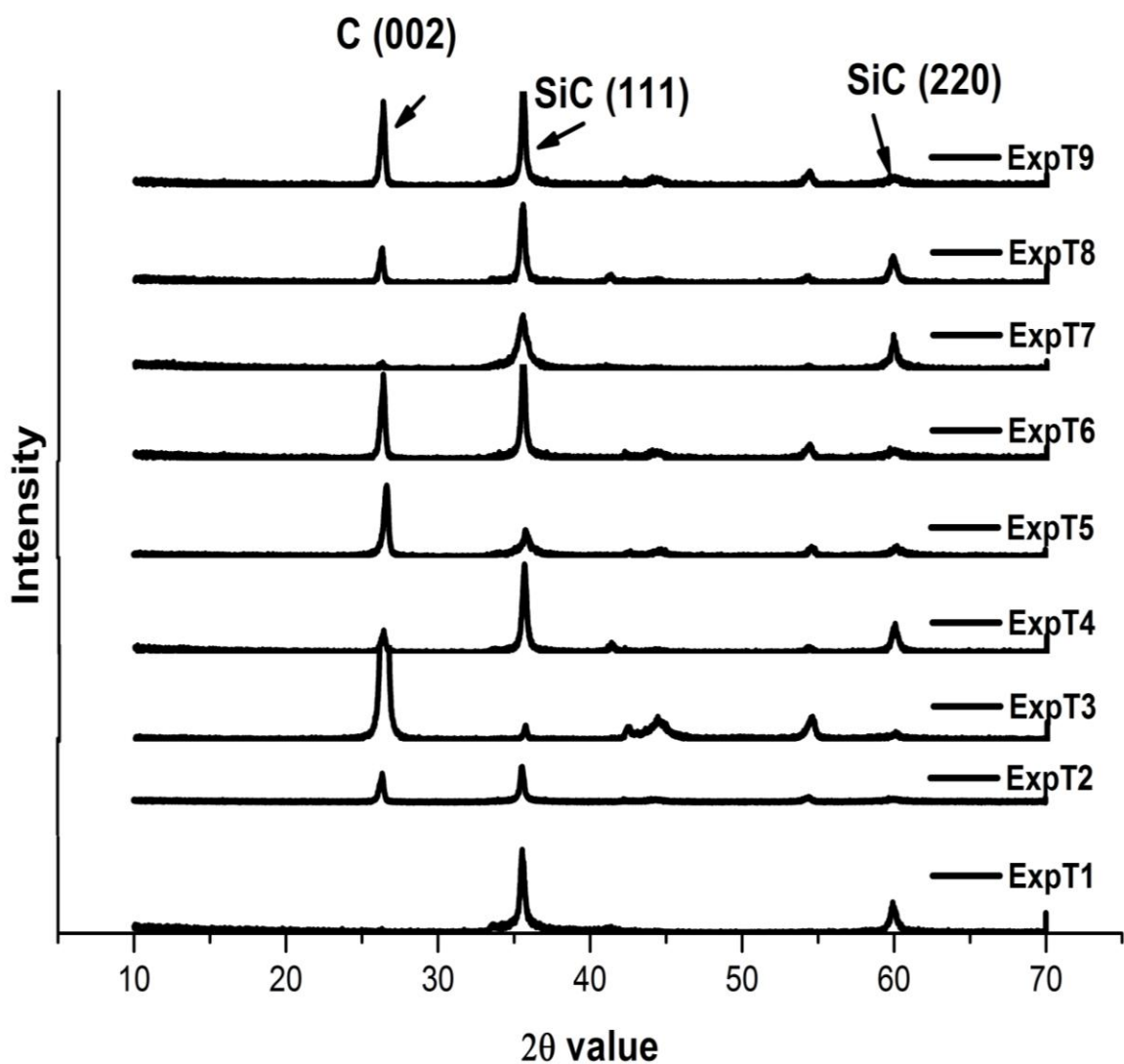


Fig. 3.22 XRD spectrum of the Different SiC deposits obtained through different experiments as presented in Table II.

In case of optimization of diameter of SiC wires, the temperature has the maximum effect (80%) and the hydrogen flow rate has the minimum effect (3.4%) on the growth diameter of SiC produced by CVD technique. The effect of total flow rate and MTS flow rate was 4.9% and 11.4% respectively. From the above studies it was inferred that temperature is the crucial parameter that decides the morphology of the grown SiC crystals.

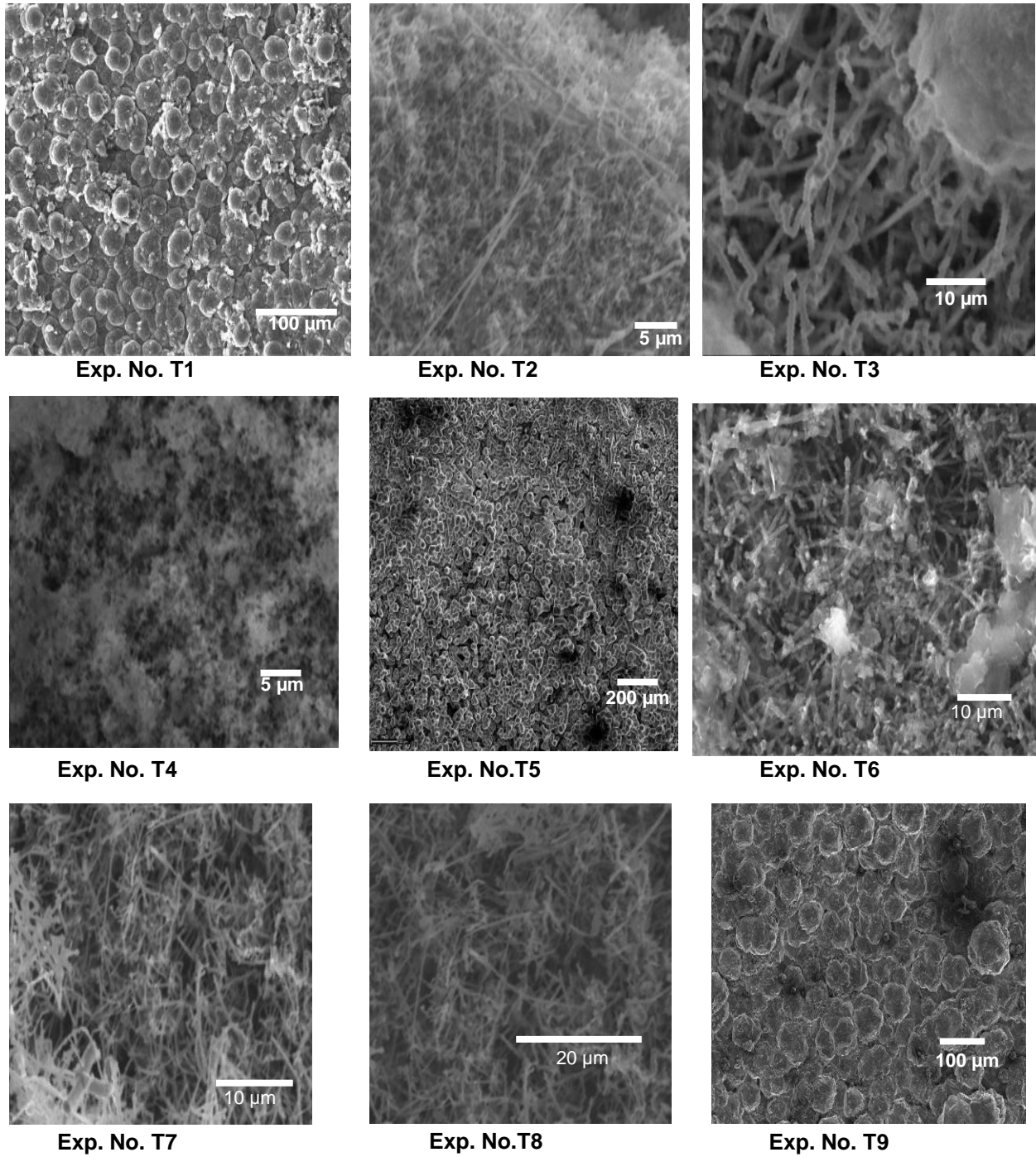


Fig. 3.23 SEM images of the SiC deposits grown by experiments designed by Taguchi method.

Figs. 3.24 and 3.25 show the graphical representation of the average effect of the parameters on the desired result. It shows that the minimum deposition rate would be obtained at

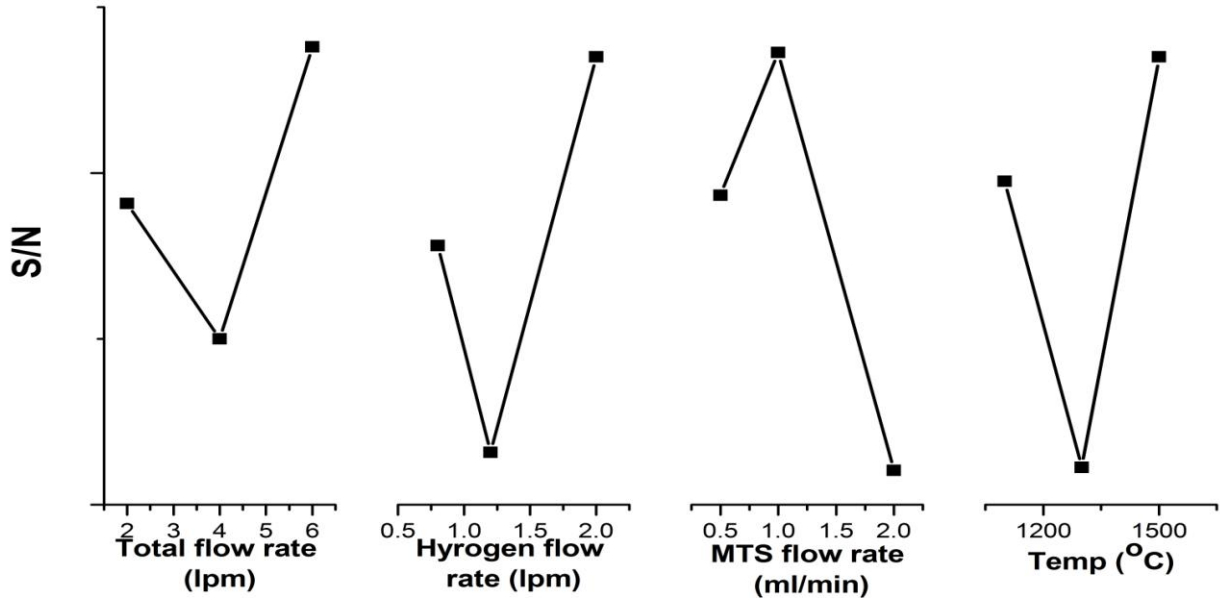


Fig. 3.24 Graphical representation of the average effect of different factors on the deposition rate of SiC.

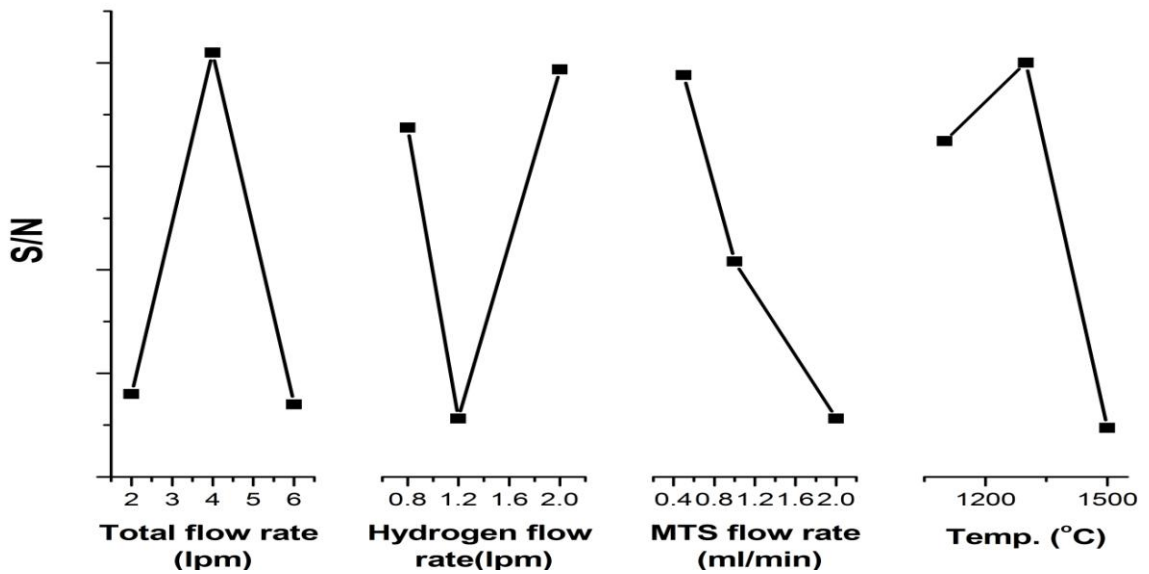
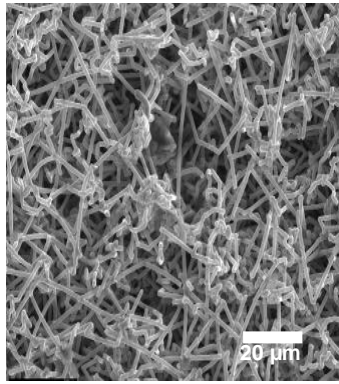


Fig.3.25 Graphical representation of the average effect of different factors on the growth diameter of SiC.

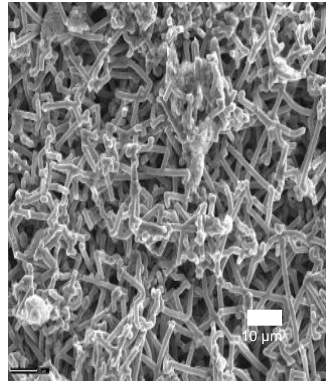
total flow rate 6 lpm, hydrogen flow rate 2 lpm, MTS flow rate 1 ml/min and deposition temperature of 1500 °C. The minimum growth diameter of SiC wires would be obtained at total flow rate 4 lpm, hydrogen flow rate 2 lpm, MTS flow rate 0.5 ml/min and 1300 °C deposition temperature.

3.3.3.2 Morphological study by changing Hydrogen to MTS ratio

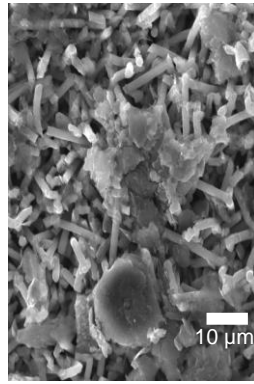
The result of the Taguchi optimization method showed that for minimum deposition rate, the total flow rate of 6 lpm and temperature 1500 °C were the optimum parameters. But under such conditions, the chances of grain growth are very high. Therefore, for the growth of SiC wires in nanometer dimension, the optimized parameters obtained by minimum growth diameter of SiC are suitable. The deposition temperature as optimized for diameter of grown SiC wire i.e. 1300 °C was kept constant and total flow rate and hydrogen to MTS ratio has been varied to observe its effect on the morphology of SiC wires. The experiments as designed and tabulated in Table 3.4 were performed to observe the effect of hydrogen to MTS ratio on the morphology of grown SiC. SEM images (Fig. 3.26) shows the growth of SiC wires of different diameter depending on the different growth parameters. The effect of hydrogen to MTS ratio on the diameter of grown SiC has been shown in Fig. 3.27. It has been observed that there were three different regions depending on the variation of diameter of SiC with H₂/MTS ratio, smoothness of surface and homogeneous growth of SiC on the substrate.



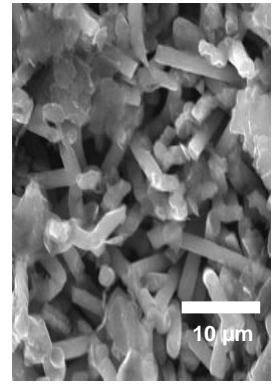
Exp. No.1.- $H_2/MTS = 1.16$
Avg. Diameter = 1.5 μm



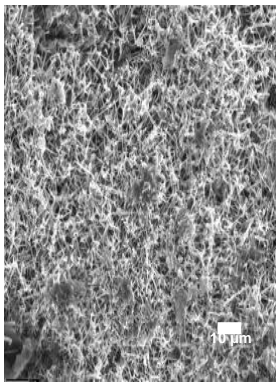
Exp. No.2.- $H_2/MTS = 2.32$
Avg. Diameter = 1.79 μm



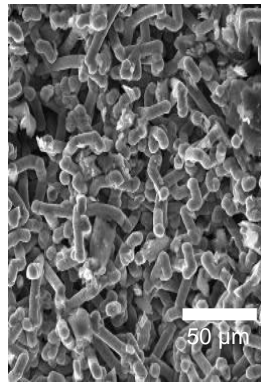
Exp. No.3.- $H_2/MTS = 2.33$
Avg. Diameter = 900 nm



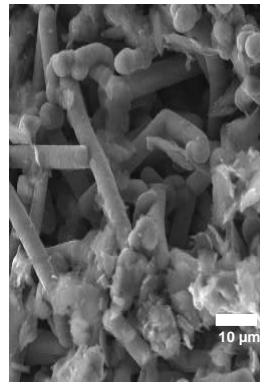
Exp. No.4.- $H_2/MTS = 3.5$
Avg. Diameter = 2.0 μm



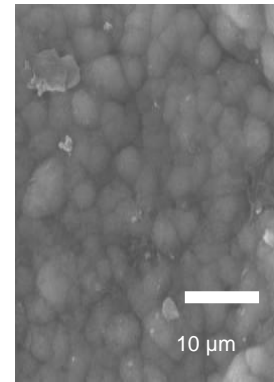
Exp. No.5.- $H_2/MTS = 4.65$
Avg. Diameter = 700 nm



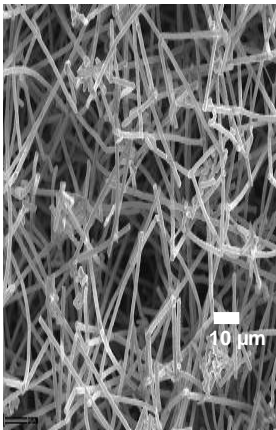
Exp. No.6.- $H_2/MTS = 9.3$
Avg. Diameter = 5 μm



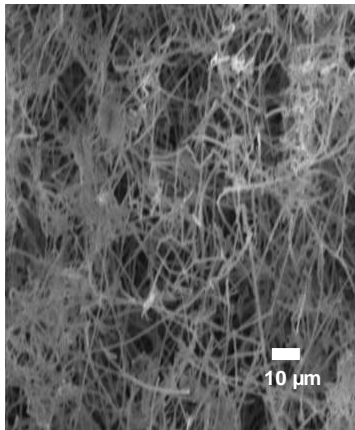
Exp. No.7.- $H_2/MTS = 14$
Avg. Diameter = 3 μm



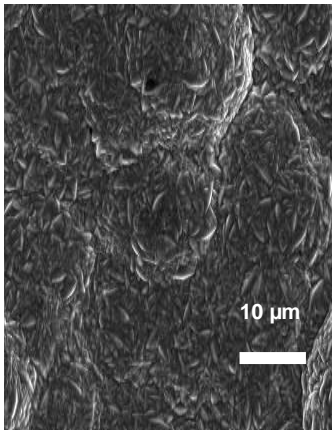
Exp. No.8.- $H_2/MTS = 14$
Dense deposition



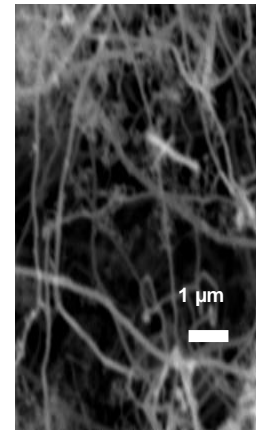
Exp. No.9.- $H_2/MTS = 23.3$
Avg. Diameter = 1.69 μm



Exp. No.10.- $H_2/MTS = 40.3$
Avg. Diameter = 350 nm



Exp. No.11.- $H_2/MTS = 0$
Dense deposition



Exp. No.12.- $H_2/MTS = 70$
Avg. Diameter = 50 nm

Fig. 3.26 SEM images of the SiC deposits grown by varying H_2/MTS ratio.

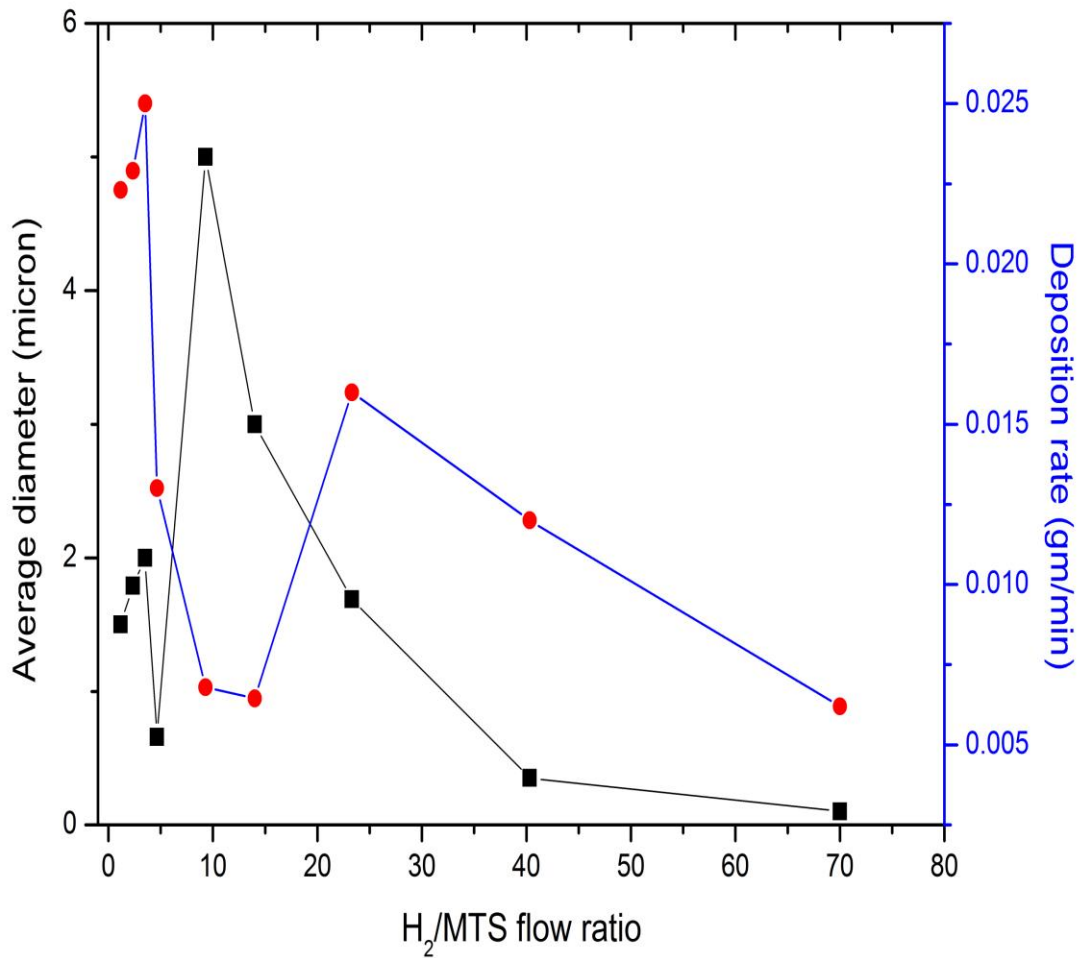


Fig. 3.27 Effect of H₂/MTS ratio on the growth morphology of SiC and deposition rate of SiC.

In the Ist region i.e. where the H₂/MTS ratio < 4, it has been observed that with decrease in H₂/MTS ratio the diameter of grown SiC wires also decreases but there is a critical ratio of H₂/MTS ratio below which there is no formation of SiC wires. At this point there was multi dimensional growth of SiC crystals resulting in growth of SiC grains. The observation (Exp. no. 11 of Fig. 3.27) that when H₂/MTS ratio was 0, there was no growth of SiC wires. It has been observed that in this region that the deposition rate also decreases with decreasing H₂/MTS ratio.

The average diameter of grown SiC wires in this region was ranging several microns. As the deposition rate decreases there was decrease in the diameter of SiC wires and formation of smoother surface with equal diameter distribution of SiC.

In the IInd region i.e. H_2/MTS ratio between 4 and 20, it has been observed that there was random variation in the diameter of the SiC wires. The SiC wires were randomly grown with unequal deposition.

In the IIIrd region, where H_2/MTS ratio > 20 , it was observed that the diameter of the grown SiC wires decreases from micron to nanometer range with increasing H_2/MTS ratio. Also, with increasing H_2/MTS ratio, the purity of SiC wires gradually increased. When H_2/MTS ratio reached to about 70, SiC wires without other SiC crystallites were deposited on the C/C composite. The SiC wires grown at this H_2/MTS ratio value were equally distributed on the surface with almost equal distribution of diameter.

These experiments have proved that for uniform diameter growth of SiC, smoothness of surface and homogeneous growth of SiC on the substrate, the hydrogen to MTS ratio must be high. For nanometer size diameter growth, the H_2/MTS ratio should be greater than 20. At a particular H_2/MTS ratio the MTS flow rate should not be too high. As it has been shown in the Exp. nos. 2 & 3 (Table 3.4) that at a particular H_2/MTS ratio, as the MTS flow rate increases the diameter of SiC wires also increases. The temperature of deposition should be around 1000-1300 °C for crystalline SiC wires and the total flow rate should be moderate for a particular H_2/MTS ratio. It has been observed in Exp. nos. 7 & 8 (Table 3.4) that at particular H_2/MTS ratio 14, as the total gas flow rate increases from 2 to 6 lpm the wire morphology of SiC disappears and

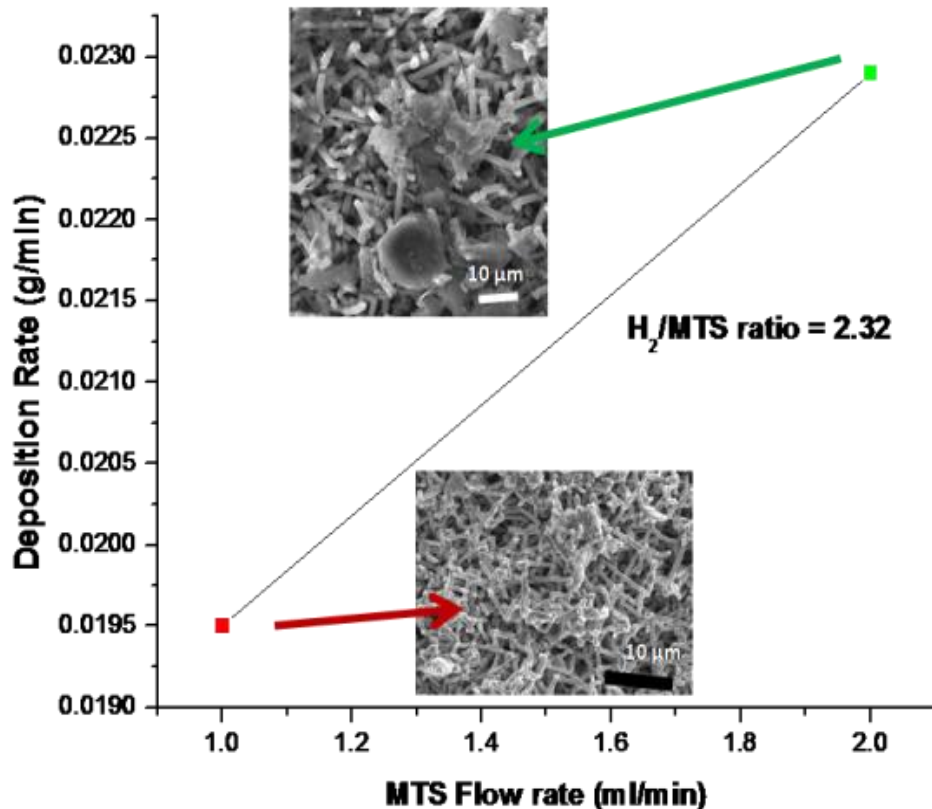


Fig. 3.28 Variation of deposition rate and morphology of SiC deposits with MTS flow rate at constant hydrogen to MTS ratio.

formation of grain occurs.

These findings verified the optimized parameters obtained by Taguchi method for growth of SiC wires of diameter in nanometer range. These experiments have proved that for uniform diameter growth of SiC, smoothness of surface and homogeneous growth of SiC on the substrate, the hydrogen to MTS ratio must be high (for nano dimensional diameter growth H₂/MTS ratio

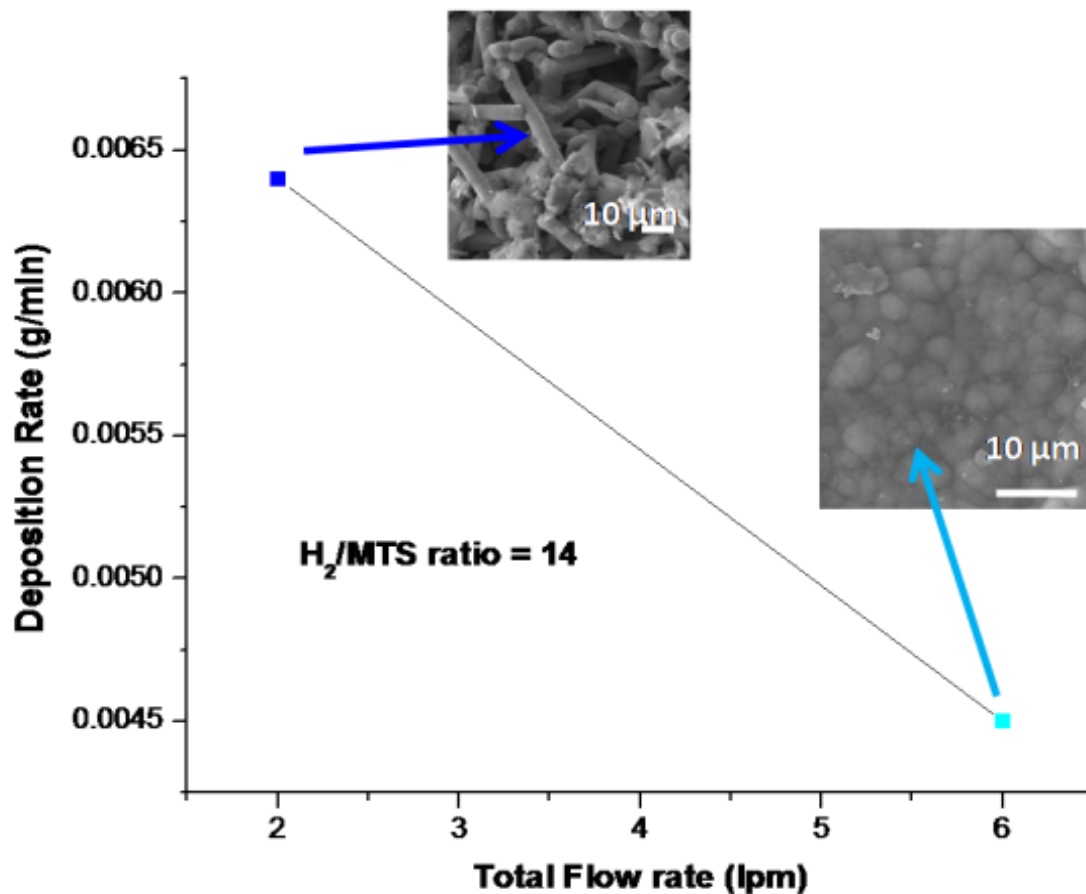


Fig. 3.29 Variation of deposition rate and morphology of SiC deposits with Total flow rate at constant hydrogen to MTS ratio.

should be greater than 20). At particular H₂/MTS ratio the MTS flow rate should not be too high. As it has been observed from the Fig. 3.28, that at particular H₂/MTS ratio as the MTS flow rate increases, the diameter of SiC wires increases. The results indicate that the reaction is very fast at

higher concentration of MTS i.e. the decomposition of MTS was fast. It means enough reaction intermediates were generated at high MTS flow. This high concentration of intermediates leads to the increase of diameter of SiC wires. In this situation still the intermediate concentration does not reach the saturation point. As discussed earlier at hydrogen to MTS ratio zero there was grain growth in the SiC deposits. It means at this point the MTS concentration was very high leading to drastic increase in the intermediate concentration. It means enough intermediates were generated which reached the saturation level and this intermediate concentration was enough for grain growth.

Further it was concluded from above observation that the temperature of deposition should be around 1000-1300 °C for crystalline SiC wires and total flow rate should be on moderate side for particular H₂/MTS ratio. It has been observed in Fig. 3.29, that at particular H₂/MTS ratio 14 as the total gas flow rate increases from 2 to 6 lpm the morphology of SiC changes from wire to grain. It can be attributed from above result that at lower total gas flow rate the intermediate reactant concentration was below saturation leading to wire morphology growth. According to the mass transfer mechanism there was less transport of reactive intermediates on the substrate surface. But when the total gas flow rate increases there was efficient transport of intermediates on the surface leading to the drastic increase in the intermediate concentration. This concentration reaches to the saturation level leading to the grain growth.

Further, the best obtained SiC nano wires in Exp. 12 (Table 3.4) were characterized by XRD and the patterns are depicted in Fig. 3.30. The peaks at (111), (200) and (220) confirm that the SiC nano wires are β -SiC. Beta SiC has zinc blend structure and shows two strong Raman peaks (Fig. 3.31) at 796 cm⁻¹ (transverse optical mode, TO mode) and 972 cm⁻¹ (longitudinal optic mode), respectively. SEM image (Fig. 7, H₂/MTS = 70) of SiC wires shows the growth of

homogeneous nanometer dimensional wires having diameter around 50 nm. EDX (Fig. 3.32) have been done to determine chemical composition of the SiC wires.

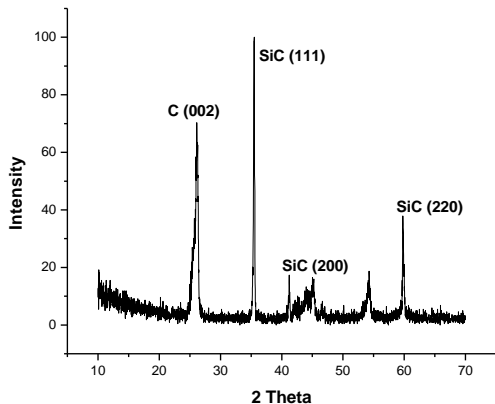


Fig. 3.30 XRD spectrum of the SiC wires grown at $H_2/MTS = 70$ and $T = 1300$ °C. It shows the characteristic peaks of SiC and graphite.

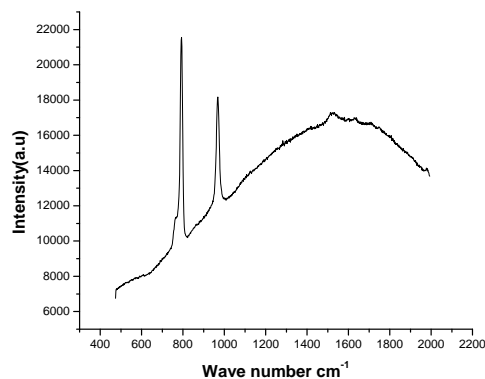


Fig. 3.31 Raman spectrum of the SiC wires grown at $H_2/MTS = 70$ and $T = 1300$ °C. It shows the TO (796 cm^{-1}) and LO (972 cm^{-1}) mode of β -SiC.

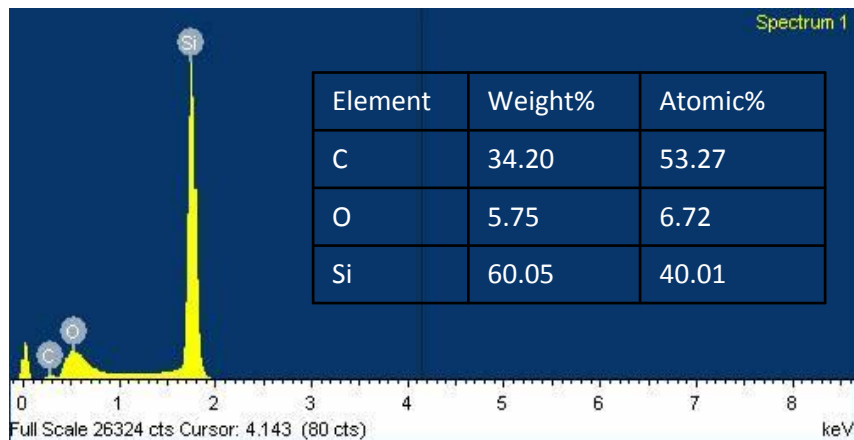


Fig. 3.32 EDX spectrum of the SiC wires grown at $H_2/MTS = 70$ and $T = 1300$ °C. It shows the characteristic peaks of Si, C, O and corresponding table indicates the elemental concentration.

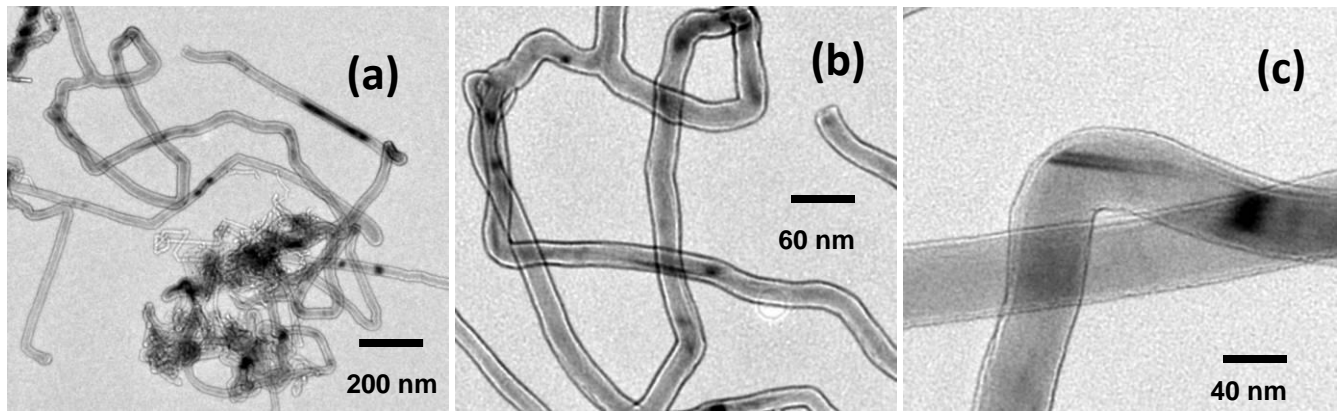


Fig. 3.33 TEM images of the SiC nanowires grown at $H_2/MTS = 70$ and $T = 1300\text{ }^\circ\text{C}$.

The elemental composition of the SiC wires were C- 53.27 At%, Si- 40.01 At% and O- 6.72 At%. The co deposition of oxygen occurs due to the presence of oxygen in the reactor at the time of coating. It can be avoided by carrying experiments in vacuum. Transmission electron microscopy (TEM) was performed to characterize the morphology and structure of the SiC nanowires grown by the Exp. 12 (Table 3.4). The TEM image (Fig. 3.33a,b and c) reveals that the nanowires possess a core-sheath structure. Fig. 3.33c shows the typical core-sheath nanowires with a dark inner core surrounded by a sheath layer. The core region of the uniform-core nanowires looks smooth. The uniform core nanowires have core diameters ranging from 35 to 45 nm. The core of nanowires is made of SiC surrounded by a SiO_2 sheath layer. EDX data confirms the presence of Si and O in the deposition. The thickness of the sheath layer for the uniform-core nanowires is 2-10 nm.

3.3.3.3 Growth Mechanism of SiC nanowires:

In the growth process of SiC micron and nano wires, the whole reaction involves the solid and vapor phase. So the SiC wires grown in the present process follow the Vapor Solid (VS) mechanism.

In a typical VS mechanism (Fig. 3.34) when the gaseous reactants come close in contact with the substrate, the absorption of gaseous reactants on the surface occurs. When the concentration of absorbed gaseous reactants reach to a particular value nucleation phenomena starts. In the present case when the concentration of silicon and carbon intermediates reach to a particular value on the surface nucleation of SiC occur. With the continuous supply of feed intermediate

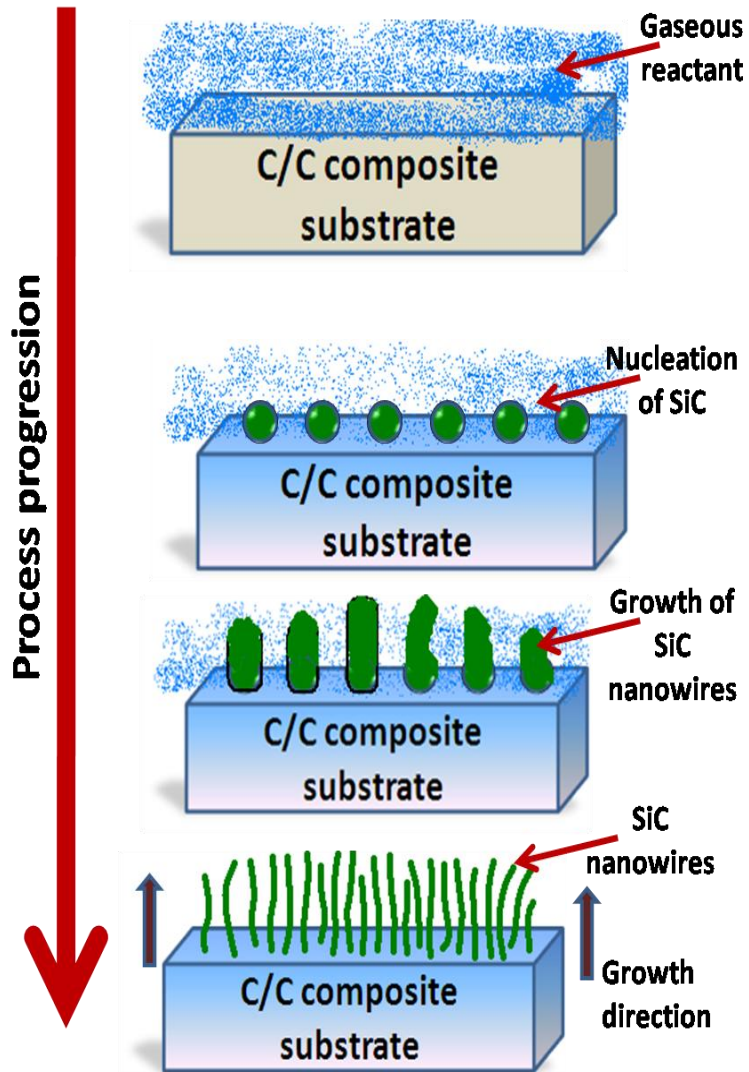


Fig. 3.34 Schematic representation growth mechanism of SiC nanowires.

reactants on the surface growth of SiC crystals through these nuclei

occur. The morphologies of as deposited SiC crystals are affected primary by the supersaturating degree of gaseous reactant, which was depended on the deposition temperature and the concentration of MTS in the process. As it has been seen in taguchi experiments, at higher deposition temperature, the SiC crystal dimensions increased and the morphologies of the as

grown SiC crystal change from nanowires to grains. The concentration of MTS plays a vital role

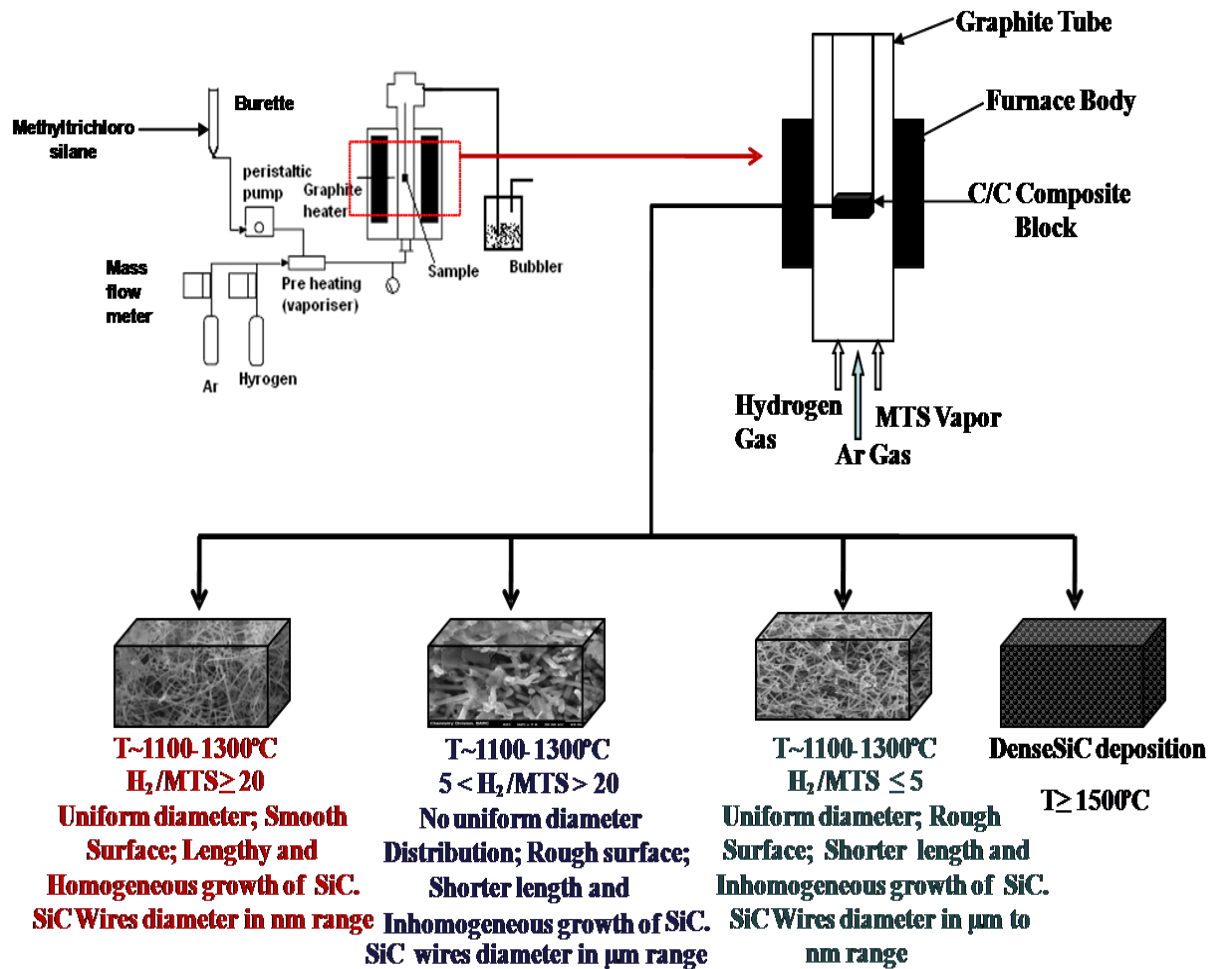


Fig. 3.35 The optimum deposition conditions for uniform diameter growth of SiC nano wires, smoothness of the surface and homogeneous growth of SiC.

in deciding the morphology and nature of the grown SiC. Fig. 3.35 shows the summary of different deposition conditions for different morphological growth of SiC. The SiC crystal nuclei apt to grow along the least energy direction i.e. along $\langle 111 \rangle$ direction, until the chemical reaction driving force are less than a certain value. As it has been seen in the 1st region (Fig. 3.27) that the SiC wires have diameter in micron range and with increasing the MTS concentration the wire

shape changes to grain shape. It means in this region the supersaturating degree of the gaseous reactant and the driving force of chemical reaction crosses the limit after a certain concentration of MTS and results in the growth of SiC crystal in several directions.

It was observed in the IIIrd region (Fig. 3.27) that the SiC wires have diameter in nano meter range and with decreasing the MTS concentration the wire diameter decreases. It was also observed in this region that the deposition rate of SiC decrease with increase in H_2 /MTS ratio. The decrease in the concentration of decomposition products at the growth site occur for higher H_2 /MTS ratio. This low concentration of reactive intermediates restrains the multi directional growth of SiC. Then the radial directional growth rate of the SiC wires becomes slow and the SiC wires grow along a certain direction and the purity of SiC whiskers is relatively high.

3.4 Conclusion

Different morphological SiC coating were carried out using different organosilicon compounds. Dense SiC coatings were carried out on graphite / zircaloy substrate using synthesized CVDP precursor and commercial available HMDS precursor. Uniform layer coating of SiC was achieved using CVDP precursor and fluidized bed coating process on zircaloy and graphite substrate. Uniform layer SiC coatings were also achieved using commercially available precursor HMDS on graphite and zirconia microsphere substrate. The CVDP precursor and HMDS precursor has shown that SiC can be deposited at low temperature.

Further SiC layer coating studies were carried out on TRISO particles using MTS, HMDS and TMS precursors via spouted bed chemical vapor deposition process and their properties were measured. Dense and uniform coatings of SiC were obtained for MTS and HMDS in our spouted bed system. Higher deposition of free carbon with SiC occurs in case of HMDS as precursor

which may be due to the nonstoichiometric ratio of Si and C in HMDS. SiC coatings with a sub-micrometer grain size were deposited on simulated TRISO fuel particles by spouted bed CVD at a low temperature 1300 °C using HMDS as precursor. The mechanical properties were studied using microindentation. The microstructures were analyzed using SEM. SiC coatings using HMDS and MTS have shown almost similar hardness and fracture toughness. The hardness and fracture toughness values of the coated SiC layers show that the coating has good strength. HMDS liquid precursor has a potential to replace corrosive and toxic precursor MTS for SiC layer coating in TRISO particle.

A comprehensive study on synthesis of SiC nanowires of high purity and homogeneous diameter by hydrogen reduction of MTS by a simple atmospheric pressure CVD method without using a metallic catalyst has been carried out. Taguchi method has been used to design experiments to get the optimum parameters for growing SiC wires of diameter in nanometer range. The optimum deposition conditions for uniform diameter growth of SiC nano wires, smoothness of the surface and homogeneous growth of SiC on the surface have been obtained as shown in Fig. 3.35. The hydrogen to MTS flow rate ratio should be above 20 for the growth of SiC wires of nanometer diameter. The deposition temperature for the growth of crystalline SiC wires should be 1100-1300 °C. The total flow rate of carrier gas comprising of argon and hydrogen for a particular H₂/MTS flow rate ratio is critical for morphological outcome of SiC. In the present study it was 2 lpm for H₂/MTS flow rate ratio 14 to obtain wire morphology. When the total gas flow rate was increased to 6 lpm for the same H₂/MTS flow rate ratio 14, the wire morphology of SiC disappeared and the formation of grains occurred. The optimum deposition temperature i.e. 1300 °C was kept constant and further experiments have been conducted by changing H₂/MTS mole ratio to verify morphological outcome of SiC.

Still there are many research opportunities to explore the application of these synthesized SiC nanowires. In coming years it is expected that many research laboratories across the world will take this synthesis method and application of these SiC nanowires to the higher level.

CHAPTER 4

STUDIES ON SOL-GEL ROUTE PREPARATION OF SiC AND SiC/CARBON COMPOSITE

4. Studies on sol gel route preparation of SiC and SiC/carbon composite

This chapter describes two step sol gel process for generating SiC material using tetraethylorthosilicate as silicon source and phenol formaldehyde as carbon source. A fabrication process has been developed for prepare SiC impregnated carbon fiber matrix composite. Further the feasibility of deriving SiC in carbon matrix using Polymethylhydrosiloxane (PMHS) as silicon source and Glycerine as carbon source by sol gel method was also studied.

Extensive research and development in the past decade have resulted in increasing awareness of the importance of chemical synthesis, particularly using organic precursors, in the processing and fabrication of ceramics such as SiC. The sol gel technique offers an easy route to synthesize SiC by employing alkoxides and a suitable carbon source¹³⁶⁻¹³⁸. Synthesis of SiC through the sol-gel process without using an external carbon source has also been reported¹³⁹⁻¹⁴¹. The sol-gel process is used commercially in many applications. The process gives excellent control of product purity and composition for the simple reason that the process starts with pure materials. The three basic steps in the sol-gel process are summarized in Fig. 4.1. The conversion of sol to a gel occurs by hydrolysis and condensation reactions. The gel is converted into oxides/carbide by drying and firing.

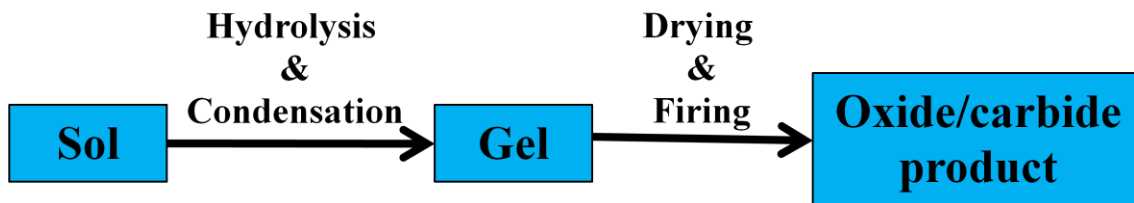
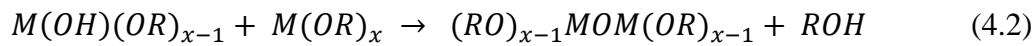


Fig. 4.1 The basic steps in sol-gel process using metal alkoxides.

Preparation of sol is the first requirement for sol-gel reaction. Of many available silicon alkoxide, Tetraethoxyorthosilicate (TEOS) is the most commonly used compound. It is insoluble in water, but water is necessary for hydrolysis reaction. Hence one needs to select a solvent for both the alkoxide and water. Ethanol is suitable solvent, and a typical formulation contains three main components: 43 vol% $\text{Si}(\text{OC}_2\text{H}_5)_4$, 43 vol% $\text{C}_2\text{H}_5\text{OH}$ and 14 vol% H_2O . This sol generates silica so for generating carbide equivalent amount of carbon source is also needed. Generally carbon source should be liquid so that it could be totally miscible in sol and makes homogeneous solution. The most frequently used silicon and carbon source are shown in Table 4.1.

Metal alkoxide undergo hydrolysis very easily. In many cases they are so sensitive to moisture that special precaution must be taken in handling and storage. During the initial stage of hydrolysis an alcohol molecule, ROH, is expelled (Equation 4.1). This is an example of a condensation reaction involving the elimination of an alcohol. The hydroxyl metal alkoxide product can react by a further condensation reaction to form polymerizable species (Equation 4.2 & 4.3).



Hydrolysis can be carried out either under basic or acidic conditions. In the context of sol-gel processing, acid catalyzed conditions are defined as $\text{pH} < 2.5$; base catalyzed conditions are defined as $\text{pH} > 2.5$. Of course, this is not usual definition of acid and base, where a neutral pH is 7, but corresponds to the point of zero charge (PZC) at which the surface is electrically neutral. The experimental variables used in the first stage of the sol-gel process determine the kinetics of

the hydrolysis of the sol to form a gel and have a major influence on gel structure. The relevant variables are:

- Alkoxide concentration
- Reaction medium
- Concentration of catalyst (The rates of hydrolysis and condensation can be affected by the addition of small amounts of acid (e.g. HCl) or base (e.g. NH₄OH), respectively.)
- Temperature

The second stage involves the transition from sol to gel. At the transition there is an abrupt increase in viscosity. After gelation the gel usually consists of a weak skeleton of amorphous material containing an interconnected network of small liquid filled pores. The liquid is usually mixture of alcohol and water, which must be removed by drying and firing step. Shrinkage during this step is usually large. After firing final compounds were obtained. There are several methods used for drying gels. Each method produces a dried gel with specific microstructure. In most cases, either an aerogel or a xerogel were obtained, but other microstructures were also possible as shown in Table 4.1.

Table 4.1

List of frequently used silicon and carbon precursors in sol-gel method and the various type of dried gel formation during drying and firing.

| Commonly used silicon and carbon precursors | | The various type of dried gel formation | | |
|--|-------------------------------|---|--|--|
| Name of the silicon alkoxide precursors | Name of the carbon precursors | Type | Drying conditions | Microstructure |
| Silicon tetraheptoxide (Si(OC ₇ H ₁₅) ₄ , Yellow liquid) | phenolic resin | Aerogels | In and autoclave, The fluid is removed by hypercritical evacuation | A network consisting of ~ 95% porosity |
| Silicon tetrahexoxide (Si(OC ₆ H ₁₃) ₄ , colorless liquid) | ethylcellulose | Xerogels | Natural evacuation | Dried gel has about 40-60% of the fired density and contains small pores |
| Silicon tetramethoxide (Si(OCH ₃) ₄ , colorless liquid) | polyacrylonitrile (PAN) | Sonogels | Gel exposed to ultrasound in the 20-kHz range prior to autoclave treatment | Assists in the formation of multicomponents gels |
| monomethyl triethoxysilane (MTES) | starch | Cryogels | Freeze dried | Finely divided powder, not suitable for producing monolithic ceramics |
| | | Vepogels | A fluid stream of SiCl ₄ is injected into acidified water; this allows rapid gelation; the gel is then dried to a xerogel | Allows incorporation of additives into the gel |

The present investigation employs the sol-gel process by preparing silica gel containing commercially available carbonaceous materials such as phenolic resin and glycerin by hydrolysis condensation of easily available TEOS and Polymethylhydroxysilane (PMHS). The gel obtained when carbonized at 1000 °C in argon and later heated to 1550 °C in argon yielded SiC. The effect of heating the gel at different temperatures has been investigated and shown that the formation of crystalline SiC takes place as low as 1200 °C. Further using sol gel impregnation approach, the fabrication of composite structure of carbon fibers and high density SiC nanowires with dense SiC matrix was reported. Here, sol containing silicon and carbon were generated using different silicon and carbon source and later on in-situ impregnation in carbon fabric and gel formation has been carried out at atmospheric condition.

4.1 Deriving silicon carbide carbon composite by sol-gel route using tetraethylorthosilicate as silicon source and phenol formaldehyde as carbon source

4.1.1 Experimental methods and materials

Small specimens ($10 \times 5 \times 5 \text{ mm}^3$) were cut from layered 2-D carbon fabric as preform. The carbon fibers used in the preform were PANEX35, 50K Tow, Zoltek make. The carbon fiber preforms were carbonized from room temperature to 1000 °C at a very slow heating rate (0.2 °C/min) in inert gas atmosphere before impregnation. These carbonized carbon fiber preforms were impregnated by sol gel technique. The modified sol gel process was used for preparing SiC nanowire/SiC matrix on C/C specimen surface different from reported in the literature¹⁴². The process includes the preparation of a carbonaceous silica xerogel, its impregnation in carbon fiber matrix and subsequent carbothermal reduction of the xerogel with carbon fiber matrix. The method is described in Fig. 4.2.

Firstly, 16 g of phenolic resin (Novolac type phenol formaldehyde (PF) condensation resin; para-toluene sulphonic acid (PTSA) is used as the cross-linking agent) was dissolved in 60 ml of ethanol and then mixed with 50 ml of tetraethoxysilane (TEOS) under stirring. The amount of TEOS corresponding to particular amount of PF resin was decided based on the silica yield from silica gel after heating gel to 1000 °C at 1.5 °C/min heating rate and carbon yield from PF resin after its carbonization to 1000 °C at 1.5 °C/min heating rate. Then, 8 ml of oxalic acid (3.4 wt %) was added into the mixture under stirring. After addition, final solution was sonicated for 2 h under stirring condition to enhance the hydrolysis of TEOS. The sonication step drastically increased the hydrolysis rate and reduced the sol formation time. After sonication the solution was stirred at 80 °C for 10 h to form the carbonaceous silica sol. Carbon fiber preform was dipped in this solution for one h so that it could soak the solution and then the sol was cooled in ice bath for rapid gelation. Enough time was given for soaking to completely wet the carbon fiber preform. The gel formation occurred after rapid cooling in the ice bath. The carbonaceous silica gel impregnated carbon fiber preform was separated from rest of the gel and cured for 3 days. The curing of PF resin occurred during 3 days and after curing sample was dried at 100 °C for 20 h. The gel impregnated carbon fiber samples were heat treated in argon atmosphere (100 sccm) to 1000 °C at rate of 1.5 °C/min and maintained for 120 min. Further these heat treated samples were heated to 1200 and 1500 °C at the rate of 2 °C/min and maintained for 120 min. Before high temperature heat treatment, the furnace was kept under high vacuum and then inert gas was inserted in the furnace to avoid any trace of oxygen in the furnace. The heat treated samples were further characterized for phase and microstructure analysis.

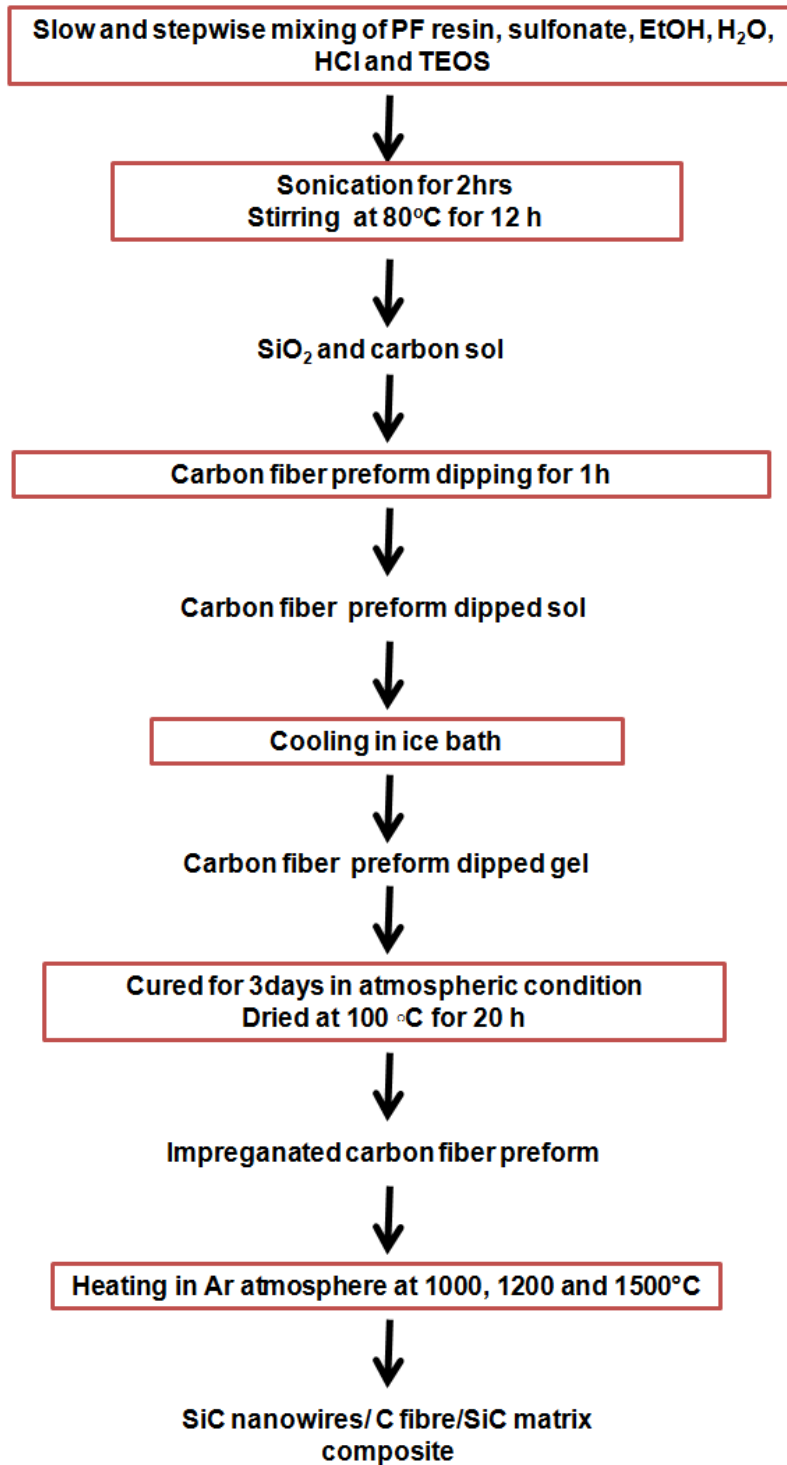


Fig. 4.2 Flow sheet for preparation of SiC impregnated carbon composite by sol gel method. The surface morphology of different SiC impregnated carbon composites and SiC powder were characterized by SEM. The microstructure of SiC nanowires were analyzed by a transmission

electron microscope (TEM, 2000FX JEOL). The crystalline structures of the different SiC impregnated carbon composites were characterized by XRD. Small angle x-ray scattering (SAXS) was further used to characterize the nanostructured SiC and SiC matrix with carbon fiber preform. Measurements were performed using a laboratory based SAXS facility using CuK_α source. The size of the incident photon beam on the sample was 0.4 mm diameter. The SAXS detector was mounted at a sample-to-detector distance of 1.07 m, corresponding to a q-range of 0.1 – 2.5 nm^{-1} . The magnitude of the scattering wave vector \mathbf{q} , is represented as $q = 4\pi\sin(\theta)/\lambda$, where 2θ is the scattering angle and $\lambda=0.154$ nm the used wavelength. SAXS arises from the fluctuations of electron density in a mesoscopic length scale (1-100 nm) in a specimen and hence scattering profile contains the information about the size/size distribution, shape etc. of the inhomogeneities. It is worthy to mention here that microscopy and SAXS are two complementary techniques to study such system. The carbon fabrics before and after impregnation were studied by X-ray tomography. They were scanned using a high resolution computer tomography (CT) system comprising of FXE160.50 Fein-Focus micro-focus X-ray source and Fiber-optically bonded charge-coupled device (CCD) camera. The source was operated at constant power (60 kV and 450 lA) for stable flux during the entire scanning operation. 400 radiographs, each with 15 s exposure, were recorded. Image reconstruction and two dimensional (2D) and three dimensional (3D) analyses were carried out using dedicated software supplied with instrument. The reconstruction grid was $787 \times 787 \times 256$ pixels.

4.1.2 Result and Discussion

4.1.2.1 Morphology studies

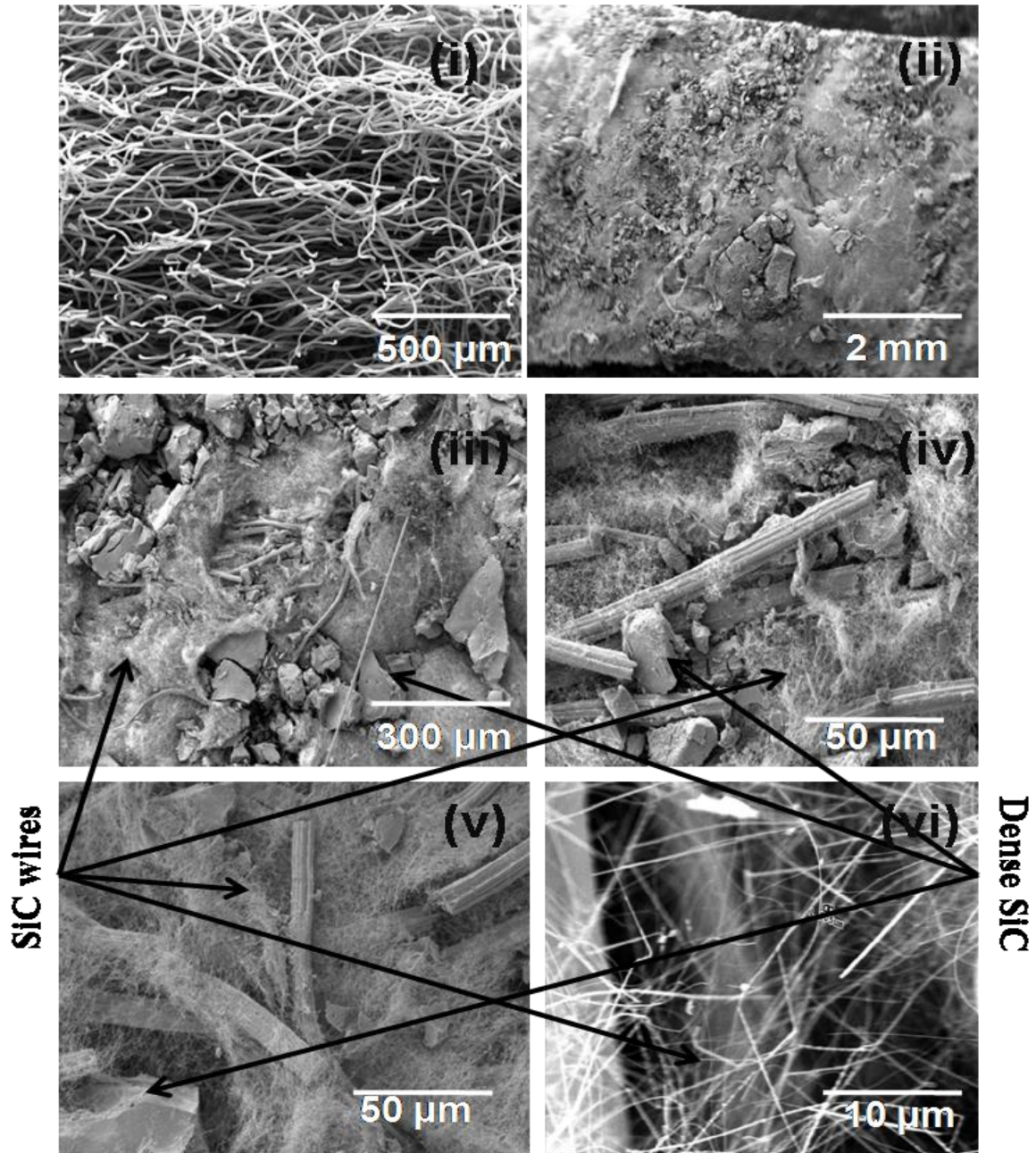


Fig. 4.3 SEM images of (i) Bare carbon fabric (ii),(iii),(iv),(v) &(vi) Surface of the SiC impregnated carbon composite at different magnification.

Fig. 4.3 (i-vi) shows the typical microstructures of carbon fabrics before and after impregnation.

It can be seen that the impregnated SiC deposit was composed of dense SiC and SiC nanowire.

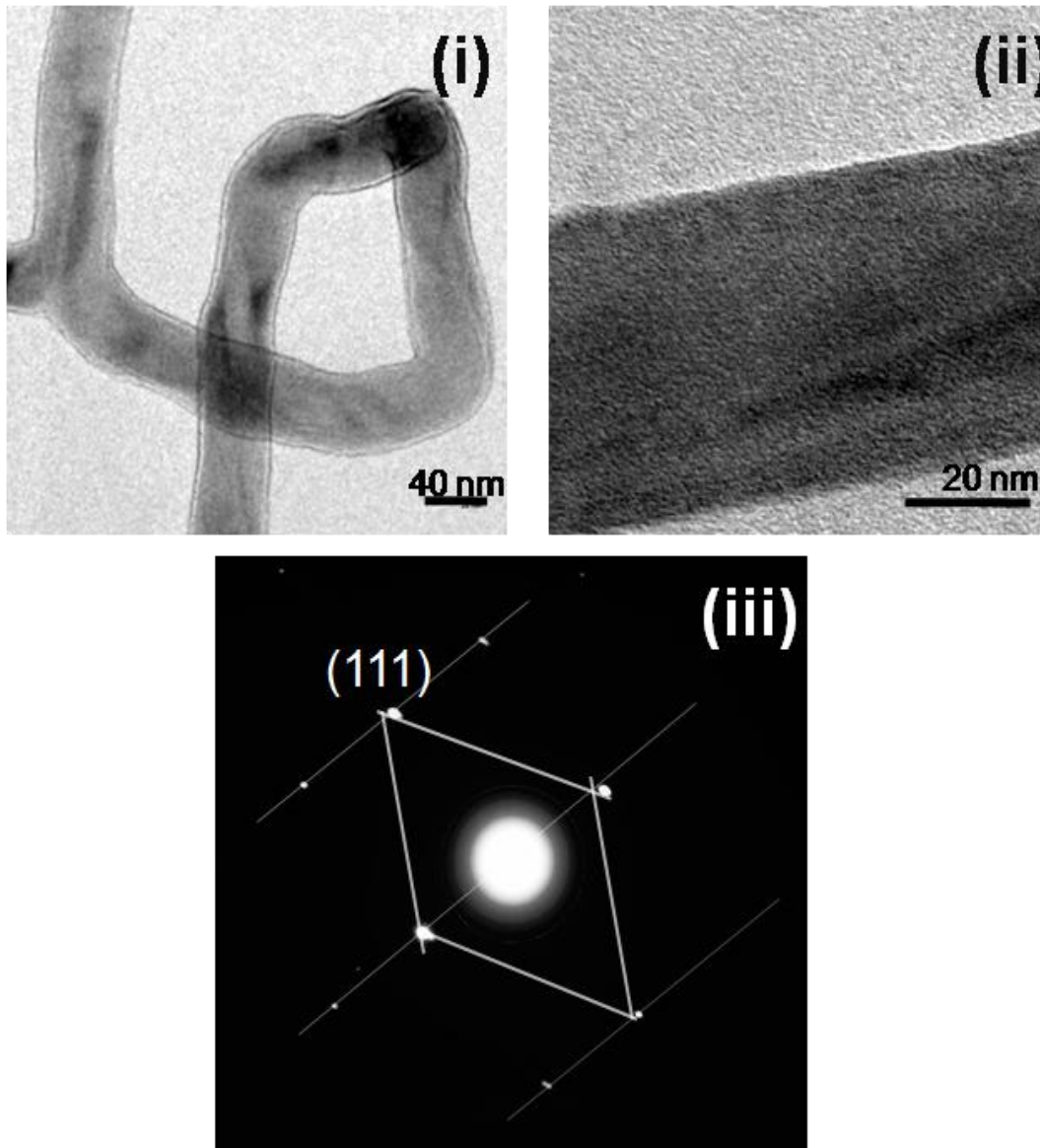


Fig. 4.4 TEM images of (i) SiC nanowires (ii) middle portion of a SiC nanowire (iii) SAD pattern of a SiC nanowire.

The SiC nanowires were uniformly distributed all over the SiC matrix. The nanowires were randomly oriented with the length of hundreds of micrometers. There were strong interaction between SiC matrix and carbon fibers at the interface of SiC matrix and carbon fiber. Fig. 4.4 shows TEM images of the SiC nanowire grown with dense SiC matrix. The TEM image reveals that the nanowire posses a core-sheath structure. TEM images show the typical core-sheath

nanowire with a dark inner core surrounded by a sheath layer. The core region of the uniform-core nanowire looks smooth. The uniform core nanowire has core diameters ranging from 35 to 50 nm. The core of nanowire was made of SiC surrounded by a wrapping layer. The reflection at (111) in selected area diffraction (SAD) spectra (Fig. 4.4) confirms the formation of SiC nanowire. The thickness of the sheath layer for the uniform-core nanowire was 3 nm to 6 nm. It was observed from Fig. 4.3 & 4.4 that the diameters of the SiC wires range from 50 to 300 nm.

4.1.2.2 X-ray micro-tomography studies: SiC matrix distribution and Matrix–core interaction

X-ray micro-tomography provides a non-destructive method for investigating distribution of different phases in sample and macroscopic pores (both open and closed) in a sample which were greater than or equal to the resolution of the tomography scans¹⁴³. The 3D reconstructed image provides an insightful view of the amount of porosity and cracks in the sample along its three dimensions while the phase contrast stretched 3D image shows the individual phases in the same sample. Uniformity of contrast indicates lesser number of cracks, uniform impregnation of second phase i.e. SiC phase in carbon fabric and better SiC matrix–carbon bonding in the sample. Different phase contrast images (Fig. 4.5) shows that before impregnation there were 50-55% pores in the carbon fabric and after impregnation 10-15% pores remain in the sample. The phase contrast images show that the SiC matrix was uniformly distributed in the carbon fabric after impregnation. Fig. 4.6(i) & (ii) show XY and YZ slices along the Z direction and X direction respectively of a bare carbon fabric. Similarly XY and YZ slices along the Z direction and X direction respectively of SiC carbon composite were shown in Fig. 4.6(iii) & (iv). These slices show that after impregnation there was lesser number of pores in carbon fabric.

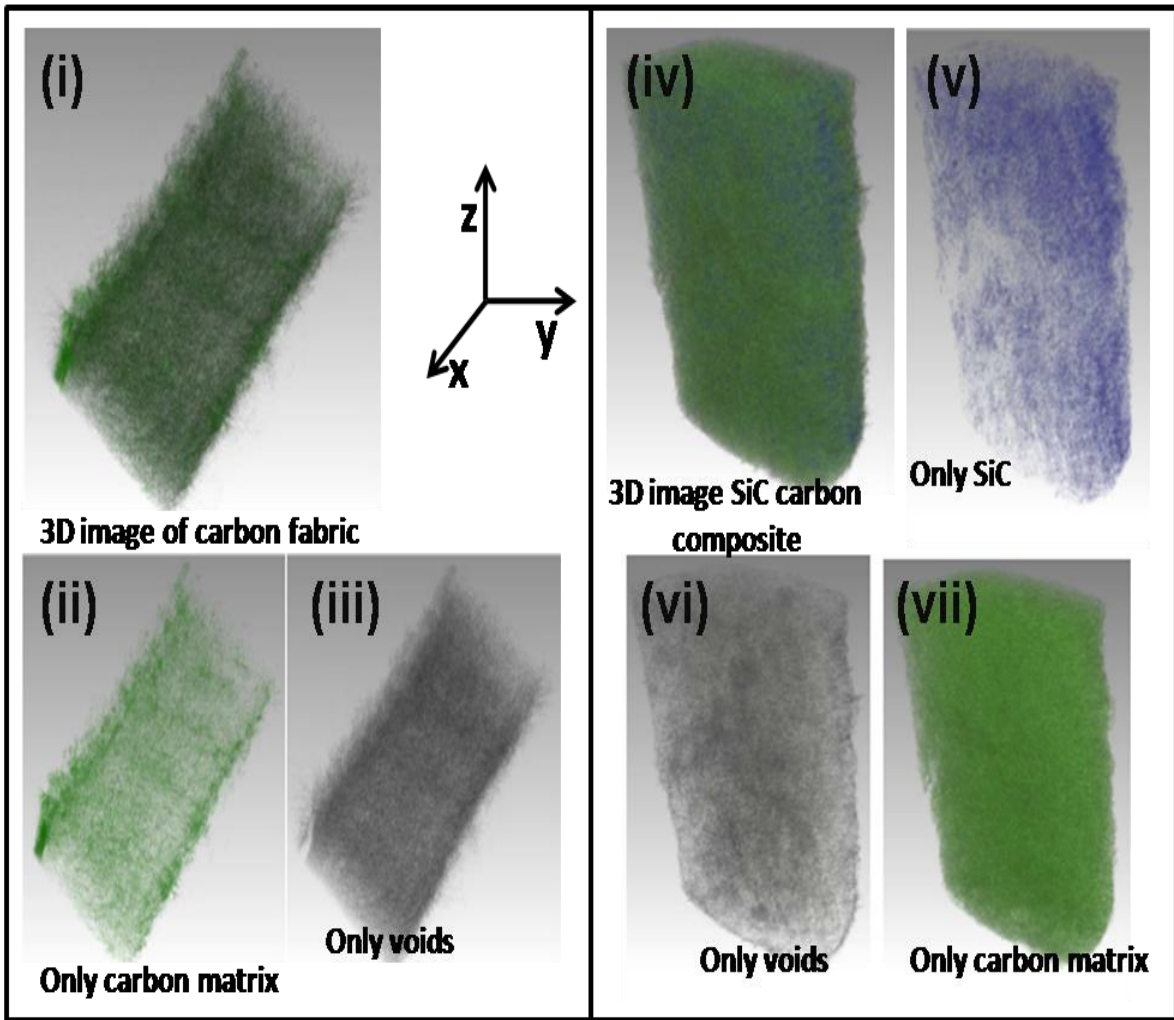


Fig. 4.5 3D phase contrast images of (i) bare carbon fabric (ii) only carbon matrix (iii) only voids in carbon fabric (iv) SiC carbon composite (v) Only SiC (vi) only voids (vii) only carbon matrix in SiC carbon composite.

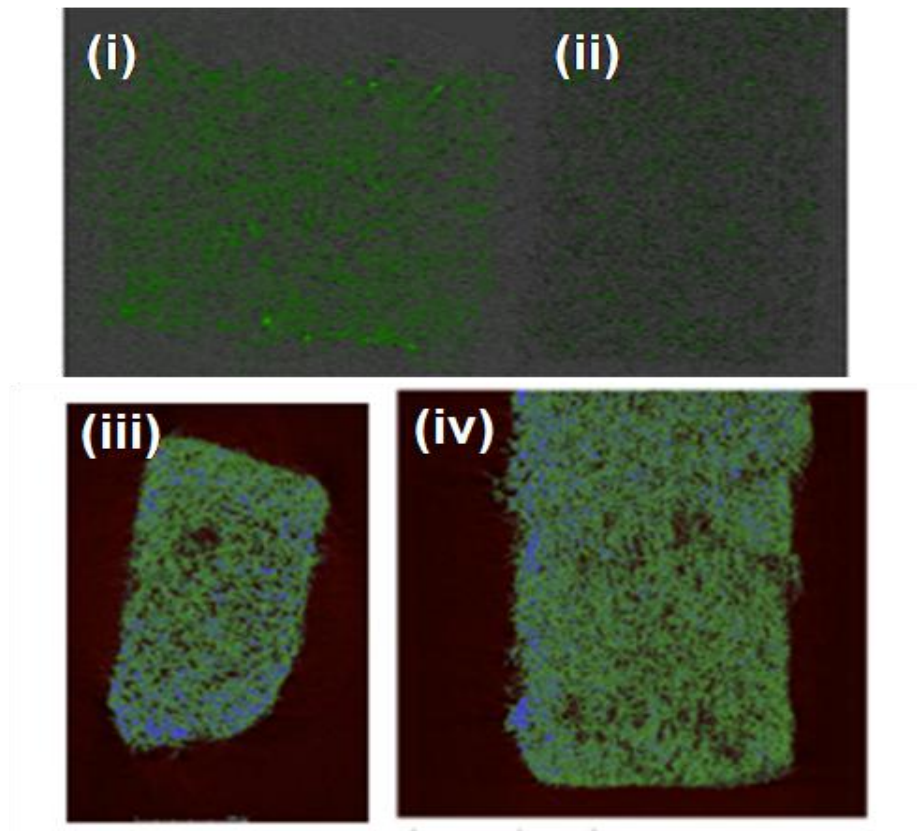


Fig. 4.6 2D X-ray tomography slices along XY and YZ directions of (i)&(ii) bare carbon fabric (iii)&(iv) SiC carbon composite.

4.1.2.3 Phase analysis by XRD

To ensure the crystal structure and crystal type of the impregnated materials and graphitization behavior of carbon fabrics after heat treatment the SiC impregnated carbon composites were analyzed by XRD at room temperature. The XRD patterns of the composites after heat treatment at three different temperatures are shown in Fig. 4.7(i), from which the diffracting peaks of the graphite and the cubical β -SiC were detected corresponding to the carbon

substrate and SiC substrate, respectively. The evolution of β phase of SiC was observed after heating at 1200 °C. There were several reports on alteration in properties of carbon fabric during heat treatment if oxygen is present in the system¹⁴⁴⁻¹⁴⁵. XRD technique was further used to study the graphitization behavior of impregnated carbon fabric after heat treatment at different temperatures. The calculation for degree of graphitization was based on the turbostratic model proposed by Warren et al.¹⁴⁶ for non-graphitic carbon materials. Using this model, percentage graphitization (g) in a mixed phase may be calculated in terms of deviation of the interlayer spacing from that of pure turbostratic structure ($d_{002} = 0.344$ nm) as per the equation 4.4.

$$g(\%) = (0.344 - d_{(022)}) / (0.344 - 0.3354) \times 100 \quad (4.4)$$

Table 4.2

Peak maximum 2θ (°) and width β (°) of the (022) XRD peaks under Gaussian approximation for SiC carbon composites heat treated at different temperature.

| Sample | $2\theta(^{\circ})$ | $d_{002}(\text{nm})$ | $\beta(^{\circ})$ | $L_c(\text{nm})$ |
|---------------|---------------------------------------|--|-------------------------------------|------------------------------------|
| S1000 | 21.53 | 0.4124 | 6.65 | 0.02098 |
| S1200 | 21.71 | 0.4090 | 6.39 | 0.02184 |
| S1500 | 22.047 | 0.4028 | 4.3477 | 0.03209 |

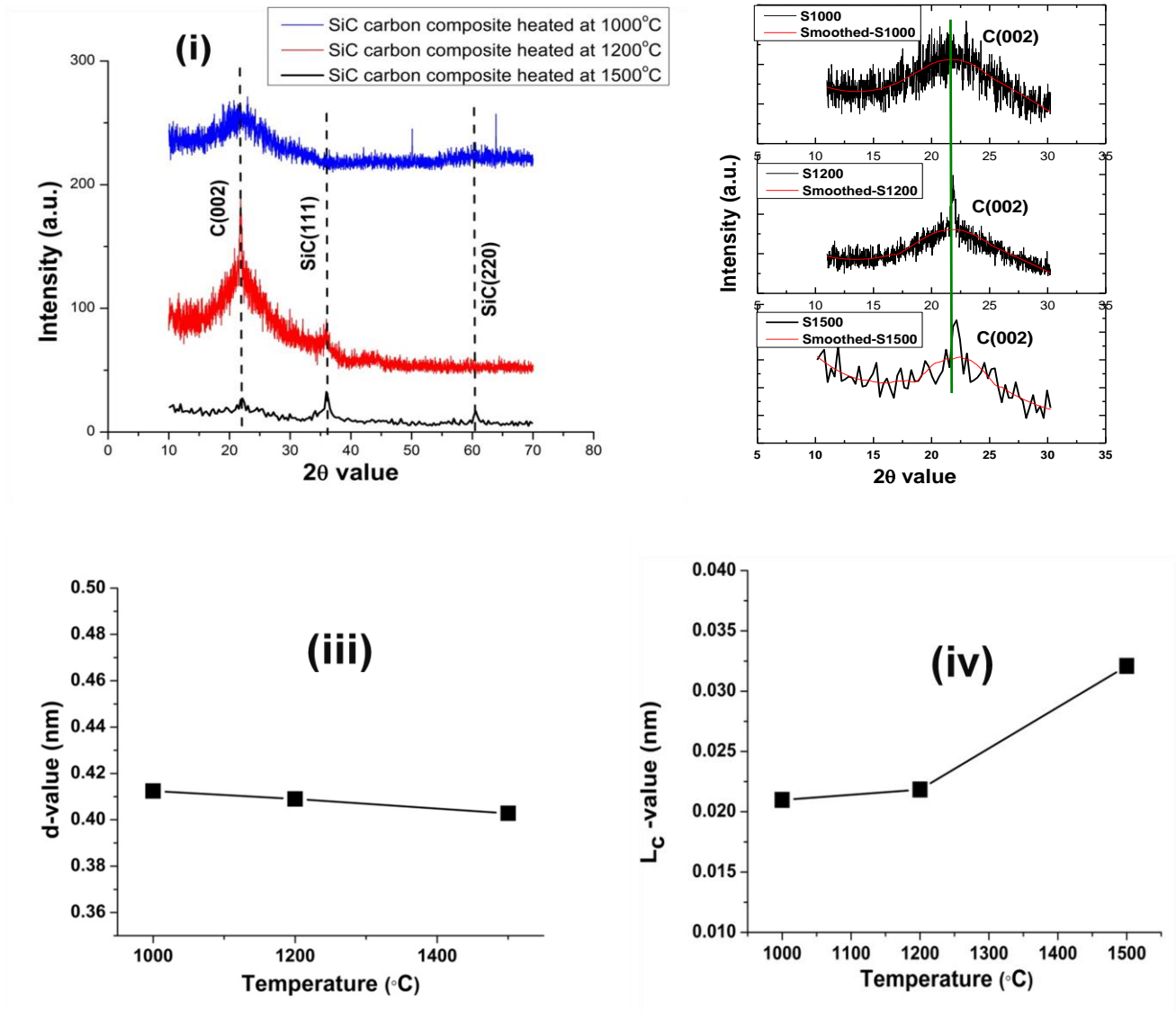


Fig. 4.7 (i) XRD pattern of the SiC carbon composites after different heat treatment. (ii) XRD patterns of a series of representative samples heat treated at different temperature specially d_{002} peak (iii) variation in d_{002} values (iv) variation of L_c .

All the composites after different heat treatment were found to be amorphous in nature with no induced graphitization in them. Interlayer spacing (d_{002}) was calculated from the (002) peak maximum (under approximation of Gaussian line profile with a linear background) (Fig. 4.7(ii)) using Bragg's law and given in Table 4.2 along with the corresponding 2θ values and full-width at half maximum (FWHM). Partial ordering in different heat treated composites was further reflected in the concomitant grain growth along c-axis. Grain size (L_c) (Fig. 4.7(iv)) along c-axis was approximately calculated from the (002) XRD peak broadening using a Scherrer equation 4.5¹⁴⁷.

$$L_c = K\lambda / \beta \cos\theta \quad (4.5)$$

where β and θ corresponds to the FWHM and Bragg's angle of the 002 peak respectively (see Table 4.2). K is a geometrical constant and is taken as 0.89 for the (002) plane. The variations of L_c for different heat treated samples are tabulated in Table 4.2 Fig. 4.7(ii) & (iii) show the XRD patterns of series of different heat treated samples. Throughout the series, peak positions remained almost unchanged as was manifested by the nearly comparable d_{002} values. L_c has shown slight increasing trend with increase in heat treatment temperature indicating that the extent of ordering (along c-axis) and hence grain growth was more at higher temperature heat treatment. This implies that the effect of different heat treatment does not have much significant effect on the properties of carbon fabric.

4.1.2.4 SAXS studies

SAXS arises from the fluctuations of electron density in a mesoscopic length scale (1-100 nm) in a specimen and hence scattering profile contains the information about the size/size distribution,

shape etc. of the inhomogeneities¹⁴⁸⁻¹⁴⁹. In the scattering experiments, the scattered intensity $I(q)$ was plotted against the magnitude of the wave vector transfer q which is defined as $4\pi\sin(\theta)/\lambda$ where 2θ is the scattering angle. SAXS experiments were performed on the carbon fabric and different heat treated SiC carbon composites using a microfocus SAXS instruments in the q -range of 0.1 to 2.3 nm^{-1} . The experimental SAXS profiles were corrected for transmission and background and are depicted in Fig. 4.8(i). It was evident that the scattering profiles get modified significantly for the composite specimens as compared to that for the only carbon fabric. It is interesting to mention that the scattering from carbon fabric was due to presence of the pores. In fact, the pore size in the carbon fabric varies in wide length scale. However, SAXS in present experimental range indicate the presence of two types of pores. The scattered intensity from carbon fabric was modeled as ensemble of bi-modal pores and may be written as,

$$I(q) = C \left[\int (D_s(r) + D_B(r)) V^2(r) P_s(q, r) dr \right] \quad (4.6)$$

where $P_s(q, r)$ is the spherical form factor for the pores, $V(r)$ is volume of the pore of radius r . $D_s(r)$ and $D_B(r)$ represents the pore size distribution of smaller and bigger pores, respectively. In present case, a normalized log-normal distribution¹⁵⁰

$$D(r) = \frac{1}{\sqrt{2\pi\sigma^2 r^2}} \exp \left[-\frac{[\ln(r/r_0)]^2}{2\sigma^2} \right] \quad (4.7)$$

is assumed as pore radius distribution, where r_0 and σ are the two parameters of the distribution and related to mean radius, $r_{av} = r_0 \exp(\sigma^2/2)$. From Fig. 4.8(i), it was evident that the above discussed model fits the data for the carbon fabric quite satisfactorily. The pores size distribution

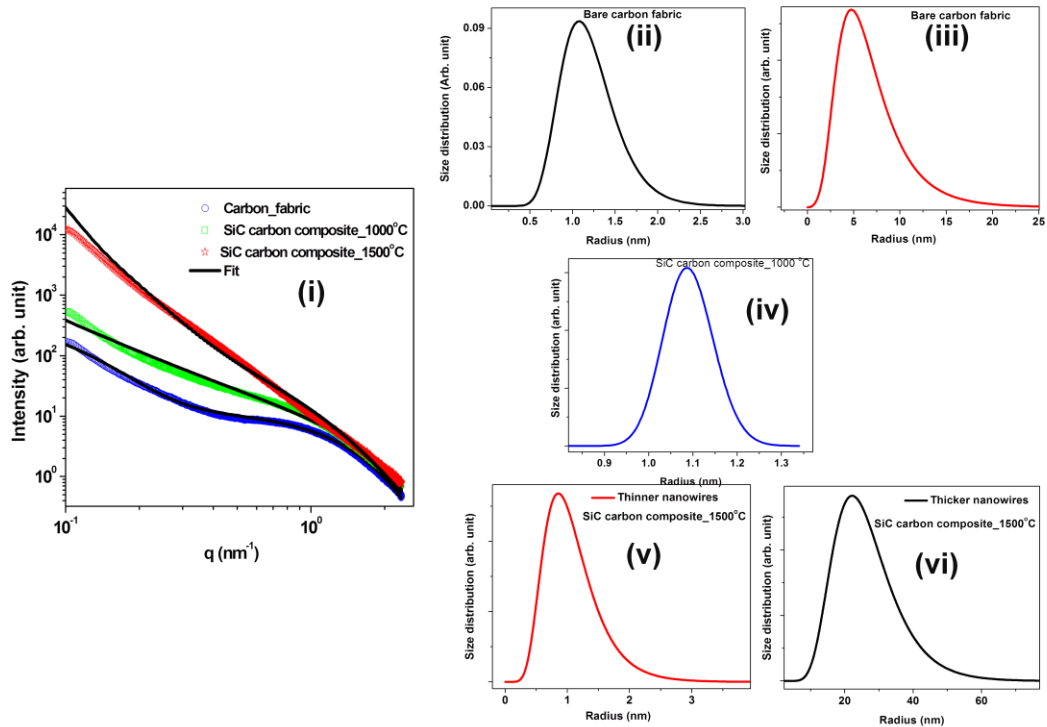


Fig. 4.8 (i) The SAXS profiles of the carbon fabric and SiC-carbon composites(ii),(iii) The pore size distribution as estimated by the SAXS data analysis for bare carbon fabric (iv) The nanowire radius distribution as estimated by the SAXS data analysis for SiC carbon composite heat treated at 1000°C. (v) & (vi) The nanowire radius distribution as estimated by the SAXS data analysis for SiC carbon composite heat treated at 1500°C.

estimated from SAXS analysis for the carbon fabric is shown in the Fig. 4.8(ii) & (iii). It was observed that average radius of the smaller pores was approximately 1.0 nm where as the average pore size of the bigger pores was approximately 5 nm.

It is evident from Fig. 4.8(i) that the scattering intensity in the lower q -range increases for the composite grains. The scattering intensity enhances further for the specimens treated at 1500 °C.

The scattering from the composites gives information about the morphology of the SiC

nanowires. It is to be noted that the scattering experiment in the present q-window could not give information about the length of the nanowires. However, SAXS can give information about the radius of the nanowires. In present case, the scattering profiles for the composite grains were modeled using the ensemble of cylindrical nanowires.

$$I(q) = C \left[\int D(r) V^2(r) P_{cl}(q, r, L) dr \right] \quad (4.8)$$

where $P_{cl}(r)$ is the form factor for the cylinder having cross section radius of r and length L . $D(r)$ is the size distribution of the cross section radius of nanowires. The average diameter for the nanowire was approximately 2.2 nm for the 1000°C specimens. It seems that the nanowire grows in the smaller pores of the carbon felt for the 1000°C samples (Fig. 4.8(iv)). For the 1500°C specimens, the single size distribution of the cross section could not fit the data. The bi-model cross section radius distribution of the nanowires was assumed to fit experimental profiles for the 1500°C. The estimated size distribution is shown in Fig. 4.8(v)&(vi). The appearance of the bigger pores were evident from the analysis which was also supported by electron microscopy results.

4.1.2.5 SiC nanowire growth mechanism

Owing to the absence of metal droplet, which is a critical feature based on the vapor liquid solid (VLS) growth mechanism¹⁵¹, the vapor solid (VS) growth mechanism¹⁵² may be plausible in growth of SiC wires. The whole growth process has been described in detail below. In the

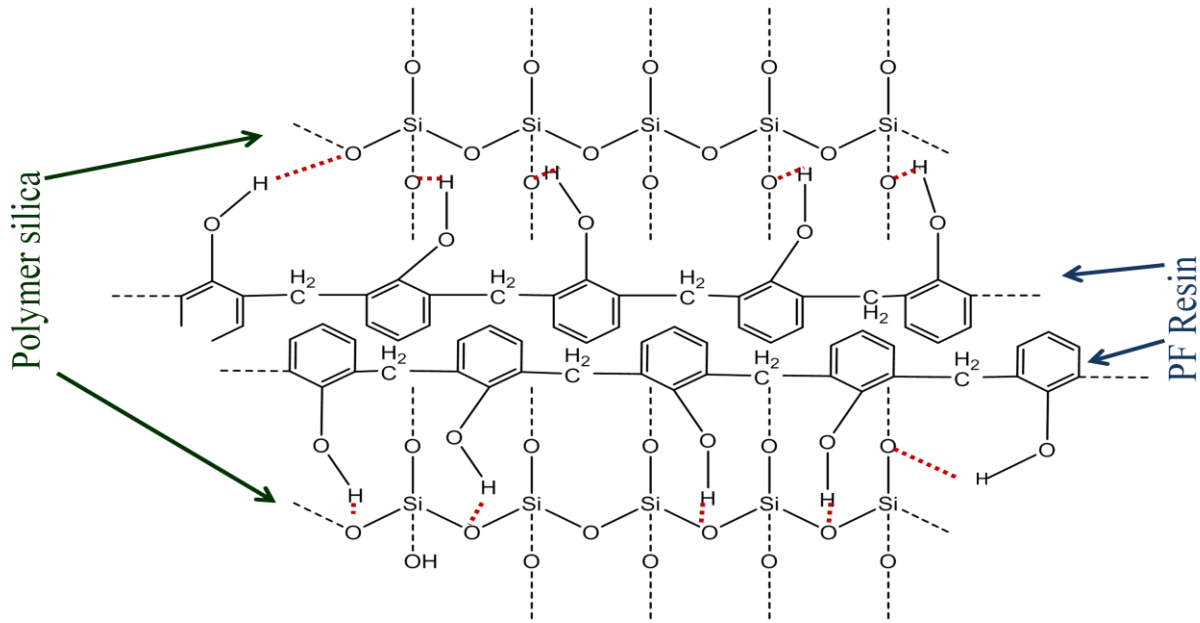


Fig. 4.9 Networking of polymer silica and PF resin to form uniform carbonaceous silica xerosol.

experiment, there was homogeneous xerosol formation with networking of polymer silica and PF resin as shown in Fig. 4.9. The networking between silica polymer and PF resin occur due to hydrogen bonding between phenolic hydrogen present in PF resin and oxygen present in silica polymer (marked as red dotted lines in Fig. 4.9). The carbothermic reduction reaction between SiO_2 and carbon (C/SiO_2 xerogel) could produce the reductive vapor (CO , SiO) by the following reaction:



Then, the following reactions take place at high temperature:



Generally, the production of the SiC nanostructures consists of two basic steps, the nucleation and growth. In the nucleation stage, the carbon atoms on the surface of carbonaceous silica xerogel react with SiO vapor to form SiC embryos heterogeneously by reaction 4.10¹⁵³. However, once the SiC embryos were produced, the reaction 4.10 could be hindered due to the solid diffusion of carbon or the diffusion of SiO vapor molecules through SiC¹⁵⁴. Therefore, the main process of growth of the nanowire was determined by the gas–gas reaction 4.11. A continuous generation of the SiO and CO at the high temperature could induce the growth of the nanowire. The first stage was the rapid growth of the core stem, as a result of the high temperature. A large amount of reductive gas (CO, SiO) was continuously produced by reaction 4.9. It has an important effect on the supersaturation in the local space. Consequently, the core nanowires were formed on the surface of the xerogel with uniform diameter. The amorphous SiO₂ layer can be obtained during the cooling stage by the following reaction 4.12:



Overall, the VS mechanism was proposed for SiC nanowire growth as discussed above and for exact growth process further study needed.

Dense and nanowire morphological SiC phases were impregnated simultaneously in carbon preform using simple, economical and environment friendly sol gel approach. The micrographical images and X-ray tomography images confirms that there was uniform

impregnation of SiC inside and on the surface of carbon fabric. XRD confirms the formation of β SiC. It also revealed that there was no degradation of the carbon composite during impregnation and heat treatment process. SAXS studies revealed that there was reduction in number of pores after impregnation and only one kind of nanowire grown after heat treatment at 1000 °C and bimodal distribution was observed after heat treatment at 1500 °C of SiC gel impregnated carbon composite. The VS mechanism has been proposed for the growth of SiC nanowires.

4.2 Deriving silicon carbide- carbon composite by sol-gel route using Polymethylhydrosiloxane (PMHS), tetraethylorthosilicate (TEOS) as silicon source and glycerin as carbon source

4.2.1 Experimental methods and materials

In this sol gel process TEOS and PMHS were used as the silicon source and glycerine was used as the carbon source. Small specimens (10×5×5 mm) were cut from layered 2-D carbon fabric as preform. The carbon fibers used in the preform were PANEX35, 50K Tow, Zoltek make. The carbon fiber preforms were carbonized from room temperature to 1000 °C at a very slow heating rate (0.2 °C/min) in inert gas atmosphere before impregnation. These carbonized carbon fiber preforms were impregnated by sol gel technique to prepare SiC-C/C composite samples. The process includes the preparation of a carbonaceous silica xerogel, its impregnation in carbon fiber matrix and subsequent carbothermal reduction of the xerogel with carbon fiber matrix. The detail method is described in Fig. 4.10.

The synthesis process includes the preparation of a carbonaceous silica xerogel and subsequent carbothermal reduction of the xerogel. Two routes have been adopted for preparing carbonaceous xerogel. In the first route, PMHS and TEOS were used as the silicon source whereas in the second route only PMHS was used as the silicon source. The carbon source glycerine was same in both cases.

- (a) The first route synthesis involved, mixing of 10 ml of PMHS, 10 ml glycerin and 60 ml of ethanol under stirring. The resultant solution was sonicated for 2h and further stirred for 5 h at room temperature in order to ensure complete reaction of PMHS with ethanol and release hydrogen under the catalysis of ethyldiamine.

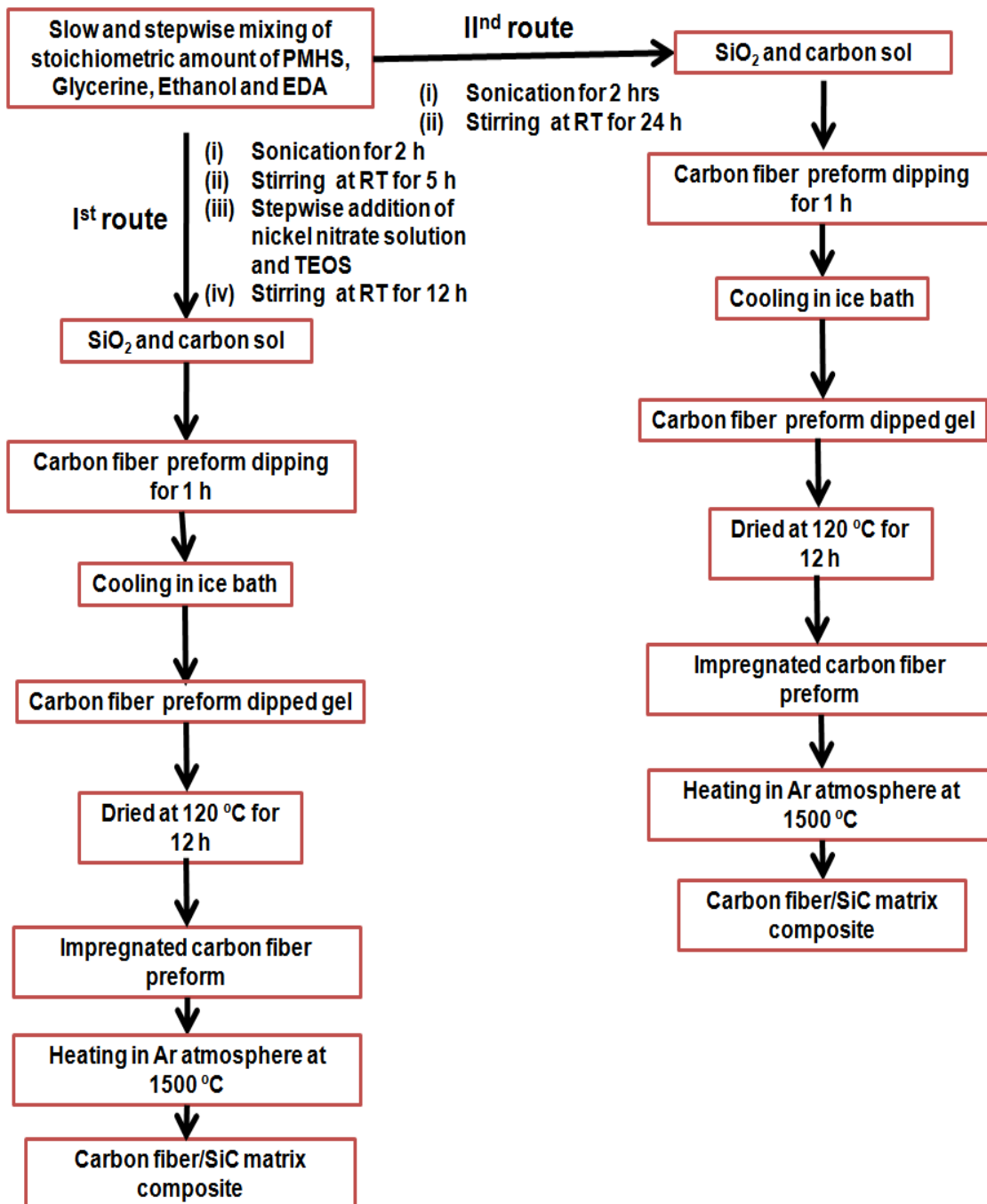


Fig. 4.10 Flow sheet for preparation of SiC impregnated carbon composite by sol gel method using glycerin as carbon source and TEOS & PMHS as silicon source.

The sonication step drastically increased the hydrolysis rate and reduced the sol formation time. Secondly, 6 ml of deionised water and 0.30 g of nickel nitrate were added in the mixture under vigorous stirring. Afterward 15 ml of TEOS was added into above mixture to form a sol. Carbon fiber preform was dipped in this solution for one h so that it could soak the solution and then the sol was cooled in ice bath for rapid gelation. Enough time was given for soaking to completely wet the carbon fiber preform. The gel formation occurred after rapid cooling in the ice bath. The carbonaceous silica gel impregnated carbon fiber preform was separated from rest of the gel. The impregnated carbon preform sample was dried at 120 °C for 12 h. The gel impregnated carbon fiber samples were heat treated in argon atmosphere (100 sccm) to 1000 °C at rate of 1.5 °C/min and maintained for 120 min. Further these heat treated samples were heated to 1500 °C at the rate of 2 °C/min and maintained for 120 min. Before high temperature heat treatment the furnace was kept under high vacuum and then inert gas was inserted in the furnace to avoid any trace of oxygen in the furnace. The heat treated samples were further characterized for phase and microstructure analysis.

- (b) The second route synthesis involved, mixing of 10 ml of PMHS, 10ml glycerin and 60 ml of ethanol under stirring. The resultant solution was sonicated for 2h and further stirred for 24 h at room temperature in order to ensure complete reaction of PMHS with ethanol and release hydrogen under the catalysis of ethyldiamine. After 24 h stirring sol formation occurred. Carbon fiber preform was dipped in this solution for one h so that it could soak the solution and then the sol was cooled in ice bath for rapid gelation. Enough time was given for soaking to completely wet the carbon fiber preform. The gel formation occurred after rapid cooling in the ice bath. The carbonaceous silica gel

impregnated carbon fiber preform was separated from rest of the gel. The impregnated carbon preform sample was dried at 120 °C for 12 h. The gel impregnated carbon fiber samples were heat treated in argon atmosphere (flow rate: 100 sccm) to 1000 °C at rate of 1.5 °C/min and maintained for 120 min. Further these heat treated samples were heated to 1500 °C at the rate of 2 °C/min and maintained for 120 min. Before high temperature heat treatment the furnace was kept under high vacuum and then inert gas was inserted in the furnace to avoid any trace of oxygen in the furnace. The heat treated samples were further characterized for phase and microstructure analysis.

4.2.2 Result and Discussion

4.2.2.1 Morphology studies

Fig. 4.11 (i-vii) shows the typical microstructures of carbon fabrics before and after impregnation. Fig. 4.11(ii-iv) and Fig. 4.11(v-vii) show the microstructure of SiC impregnated carbon fabric prepared by first and second routes respectively. In the first case, it can be seen that the impregnated SiC deposit composed of dense SiC. The dense SiC deposit was uniformly distributed all over the carbon fiber matrix. In the second case, the yield of dense SiC deposit was very low.

4.2.2.2 Phase analysis by XRD

To ensure the crystal structure and crystal type of the impregnated materials after heat treatment the SiC impregnated carbon composites were analyzed by XRD at room temperature. The XRD patterns of the composites after heat treatment at 1500°C is shown in Fig. 4.12, from which the

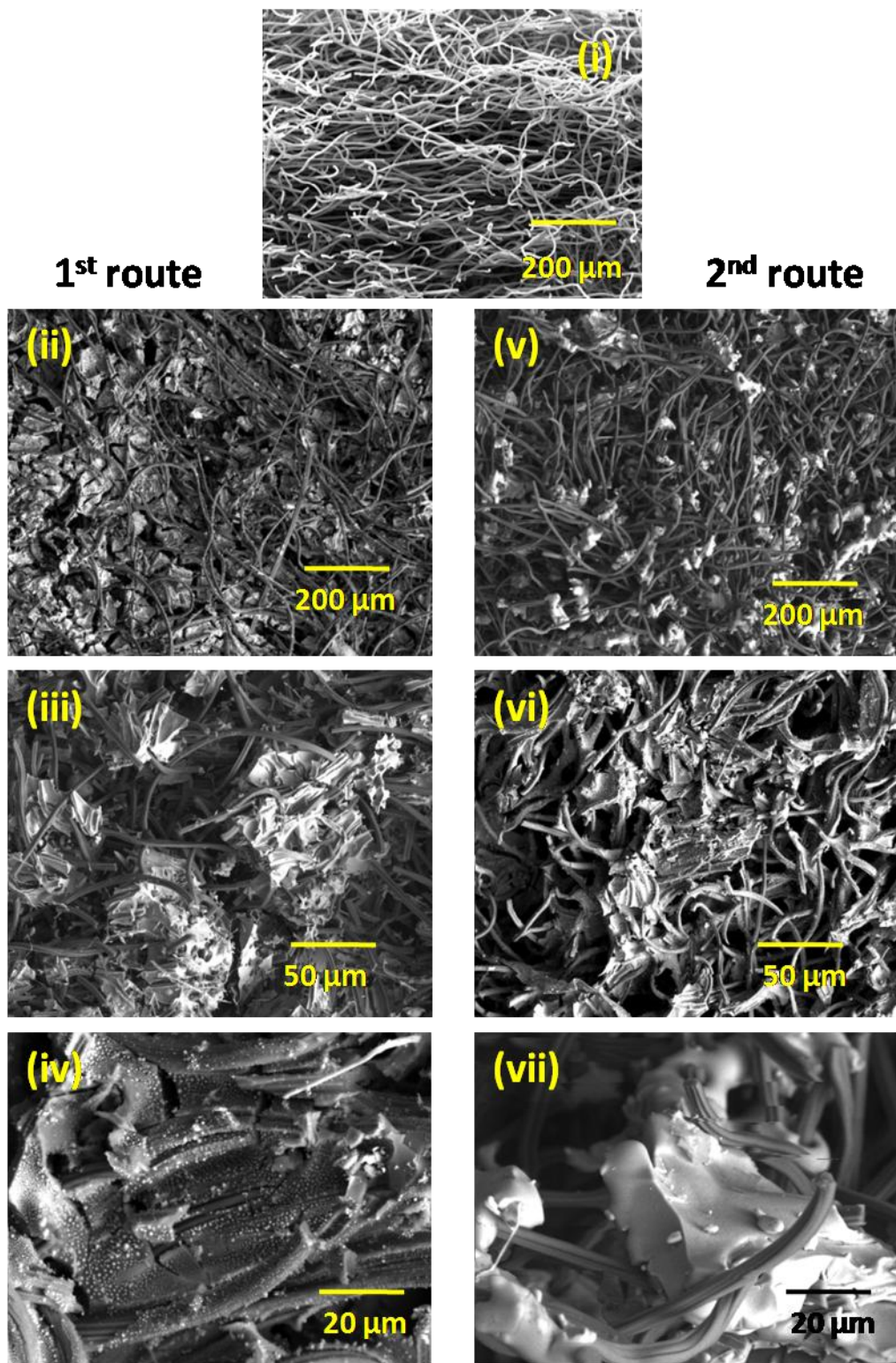


Fig. 4.11 SEM images of (i) Bare carbon fabric (ii),(iii),(iv) the microstructure of SiC impregnated carbon fabric prepared by first routes, and (v) (vi) &(vii) by second route at different magnification.

diffracting peaks of the graphite and the cubical β -SiC were detected corresponding to the carbon substrate and SiC substrate, respectively. The evolution of β phase of SiC was observed after heating at 1500 °C.

Dense morphological SiC phases were impregnated in carbon preform using simple, economical and environment friendly sol gel approach. In the first approach, using PMHS and TEOS silicon source, there was enough deposition of SiC in carbon preform, whereas in second approach there was low deposition of SiC in carbon preform.

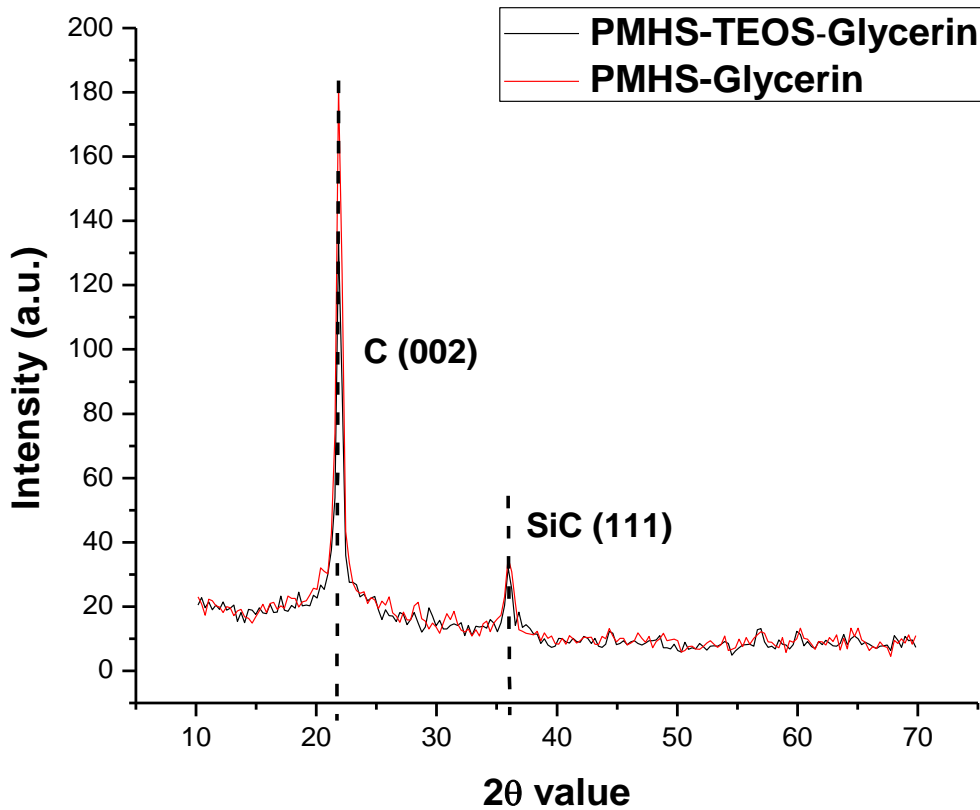


Fig. 4.12 XRD patterns of the SiC carbon composites after heat treatment prepared by first route (PMHS-TEOS-Glycerin) and second route (PMHS-Glycerin).

4.3 Conclusion

In the current chapter a novel and simple sol gel route for synthesis of SiC using organosilicon compounds were studied. The development of fabrication process for SiC impregnated carbon fiber matrix composite using tetraethylorthosilicate as silicon source and phenol formaldehyde as carbon source was carried out. Two step sol gel process was used for generating SiC material. Dense and nanowire morphological SiC phases were impregnated simultaneously in carbon preform using simple, economical and environment friendly sol gel approach. The micrographical images and X-ray tomography images confirms that there was uniform impregnation of SiC inside and on the surface of carbon fabric. XRD confirms the formation of β SiC. It also revealed that there was no degradation of the carbon composite during impregnation and heat treatment process. SAXS studies revealed that there was reduction in number of pores after impregnation and only one kind of nanowire grown after heat treatment at 1000 °C and bimodal distribution was observed after heat treatment at 1500 °C of SiC gel impregnated carbon composite. The VS mechanism was proposed for the growth of SiC nanowires.

Further the feasibility of impregnating SiC in carbon matrix using Polymethylhydrosiloxane (PMHS) as silicon source and Glycerine as carbon source by sol gel method was also studied. Dense morphological SiC phases were impregnated in carbon preform using PMHS and Glycerine in sol gel process. Two routes have been adopted for preparing carbonaceous xerogel. In the first route, PMHS and TEOS were used as the silicon source whereas in the second route only PMHS was used as the silicon source. The carbon source glycerine was same in both cases. In the first approach, using PMHS and TEOS silicon source, there was enough deposition of SiC in carbon preform, whereas in second approach there was low deposition of SiC in carbon preform.

CHAPTER 5

STUDY OF THERMAL DEGRADATION BEHAVIOR AND KINETIC OF DIFFERENT COATED AND IMPREGNATED CARBON SAMPLES IN OXIDATIVE ENVIRONMENTS

5. Study of thermal degradation behavior and kinetic of different coated and impregnated carbon samples in oxidative environments

The current chapter describes thermal degradation behavior and kinetic of thermal decomposition of dense and nanowires morphology coated carbon samples and SiC impregnated carbon composites.

Anti-oxidation property is the key requirement for carbon fibers and carbon fibers reinforced composites to be used in high temperature structural materials in oxygen containing environment^{18-19, 155}. SiC ceramic is widely used as a coating/reinforcement to provide protection against oxidation at high temperature, because of its compatibility with carbon surface. For dense SiC coated carbon fibers, at high temperature there are degradation in the properties of carbon composites due to the mismatch of coefficient of thermal expansion of carbon and SiC. Still it's a challenge to find an effective coating to protect the carbon fibers and composites which can avoid crack generation at high temperature. The recent development in SiC nanowires reinforced SiC matrix coating could overcome the above problem^{24, 62, 74, 156-158}. There has been numerous mechanism proposed by researchers to explain the oxidation behavior of these different SiC coated carbon fibers^{62, 159-161}. The word mechanism is used rather ambiguously in the literature concerned with the kinetics of these solid state oxidation reactions. Fitting of a suitable kinetic model for a particular system is required to get exact mechanism. There have been several kinetic models based on the isothermal and nonisothermal kinetic data obtained by thermal analysis (TG/DTG/DTA and DSC)¹⁶²⁻¹⁶⁸. Non isothermal methods are becoming more widely used because they are more convenient than the classical isothermal methods. A major problem of the isothermal experiment is that a sample requires some time to reach the experimental temperature. During this period of nonisothermal heating, the sample undergoes some

transformations that were likely to affect the results of the following kinetic analysis. The situation is especially aggravated by the fact that under isothermal conditions, a typical solid state process has its maximum reaction rate at the beginning of the transformation. This especially restricts the use of high temperatures. Nonisothermal heating (e.g. following a linear temperature program) resolves these problems and has therefore become more popular in the field of solid state kinetics than the classic isothermal experiment. The nonisothermal methods are mostly based on the multiple heat rate data and Ozawa¹⁶¹ and Kissinger¹⁶⁹ equations were widely used in the literature. There were several other reports to find the kinetic model, based on using various equations of kinetic analysis such as Achar-Brindley-Sharp-Wendworth (Differential method)¹⁶⁸, Satava-Sestak (Integral method)¹⁶⁴⁻¹⁶⁵, Coat-Redfern (Integral method)¹⁶⁰ and Madhusudan Krishanan (Integral method)¹⁷⁰ by setting the assumptions that the parameters of model were identical for differential and at least for two integral methods. Therefore, in current study these methods have been selected to study the kinetics of thermal oxidation decomposition of the SiC coated carbon fibers and SiC impregnated carbon composites.

5.1. Study of thermal degradation behavior of dense and nanostructured Silicon Carbide coated carbon fibers in oxidative environments

5.1.1 Materials and methods

The oxidation resistive properties of bare, dense SiC and nanostructured SiC coated carbon fibers were examined in different oxidative environments from room temperature to 1350 °C. Chemical vapor deposition process was used for the preparation of dense and nanostructured SiC coating

on carbon fiber using MTS as described in Chapter 3. A bundle of carbon fibers (Panex35, 50K Tow, Zoltek make) were used for coating purpose. For the dense deposition of SiC the flow rates of the carrier gases argon, hydrogen and MTS were 4.8 lpm, 1.2 lpm and 0.5 ml/min. The MTS flow rate was controlled using a peristaltic pump. During the SiC growth, the furnace was operated at 1450 °C under normal atmospheric pressure. For the nanostructured SiC growth the furnace was operated at 1300 °C and argon, hydrogen and MTS flow were kept at 2 lpm, 6 lpm and 0.5 ml/min respectively. The total MTS used for the present studies was 30 ml.

The surface morphology of different SiC coated carbon fiber and elemental distribution of coating before and after oxidation were characterized by SEM equipped with energy dispersive spectroscopy (EDS).

Oxidation behavior of the coated specimens was conducted using a thermo gravimetric (Setsys Evolution, Setaram, France) equipment in oxygen environment and in atmospheric environment (static air environment). Non-isothermal oxidation tests were carried out at the heating rate of 5 °C/min up to 1000 °C for carbon fibers and different SiC coated carbon fiber. The non isothermal oxidation test for different SiC coated carbon fibers was extended up to 1350 °C in oxygen environment. The oxygen flow rate of 200 ml/min was kept constant during the whole oxidation study in oxygen environment. The weight changes of the specimens corresponding to oxidation were recorded continuously in TG mode.

5.1.2 Results and discussion

5.1.2.1 Morphology analysis of the SiC coating

The coated carbon fibers were collected which were coated using process parameters for dense and nanowires SiC deposition in the CVD process. The carbon fibers were covered with a light gray color dense layer after the CVD coating using the process parameters for dense SiC coating.

SEM micrographs of the coated carbon fiber at different magnifications were shown in Fig. 5.1. The SiC deposition on the carbon fiber surface was homogeneous with dense grain deposition. Some microcracks were present on the SiC coating surface. The thickness of the SiC

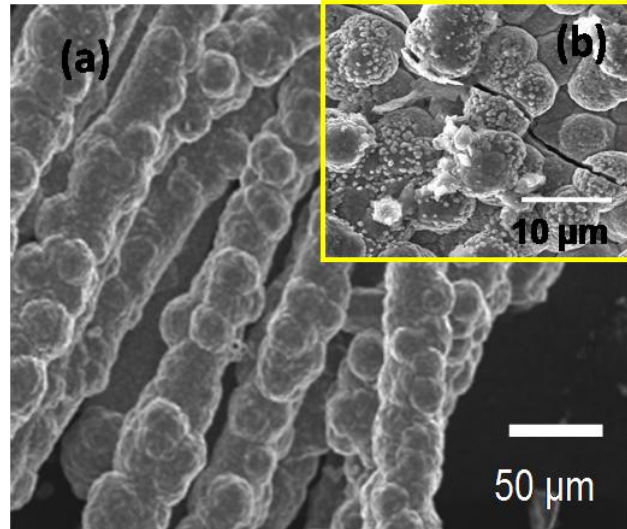


Fig.5.1 SEM image of the dense SiC coated carbon fibers (a) lower and (b) higher magnification.

layer was around 12-15 μm . EDX analysis (Fig. 5.2a, Table 5.1) showed that Si and C were the major elements present in the coating. There was little amount of oxygen present in the coating which may have come during the coating from the environment.

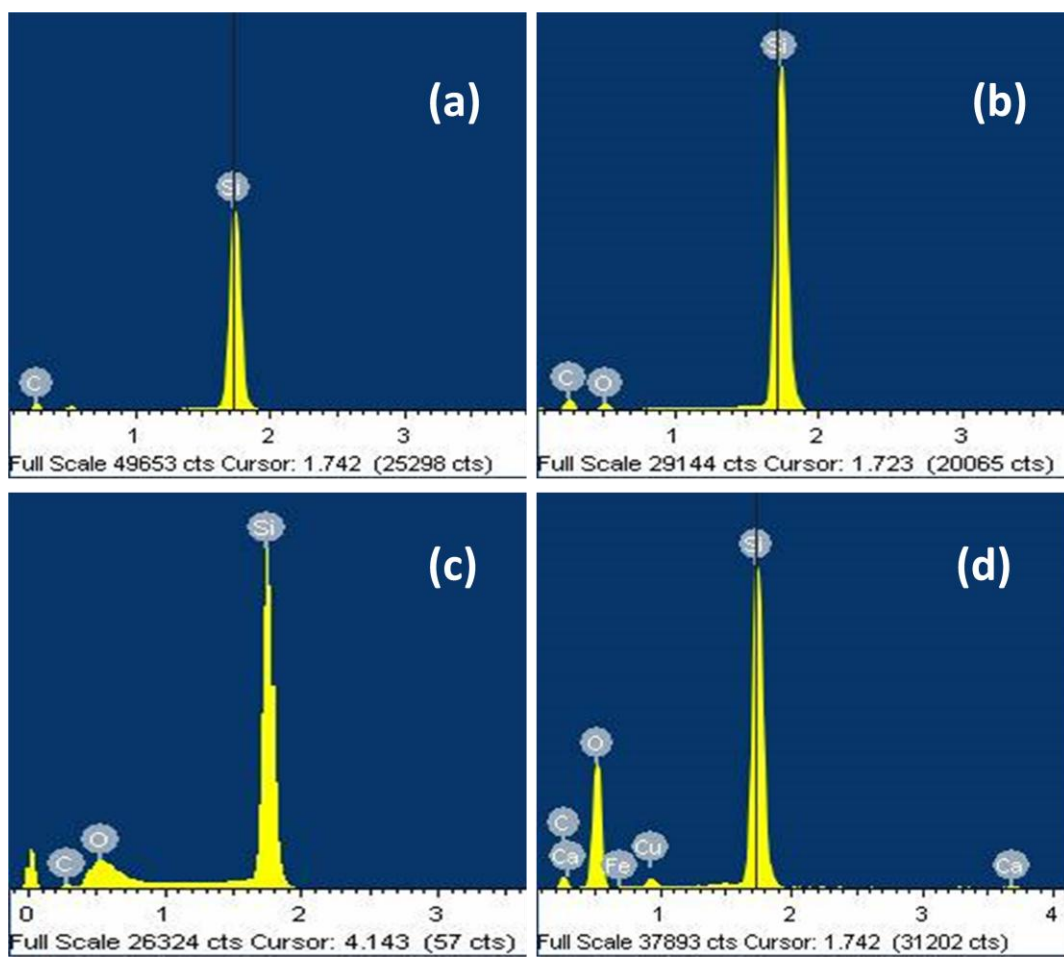


Fig. 5.2 EDX data of the elements in Dense SiC coated carbon fiber (a) before (b) after oxidation; SiC nanowires coated carbon fiber (c) before and (d) after oxidation in oxygen environment.

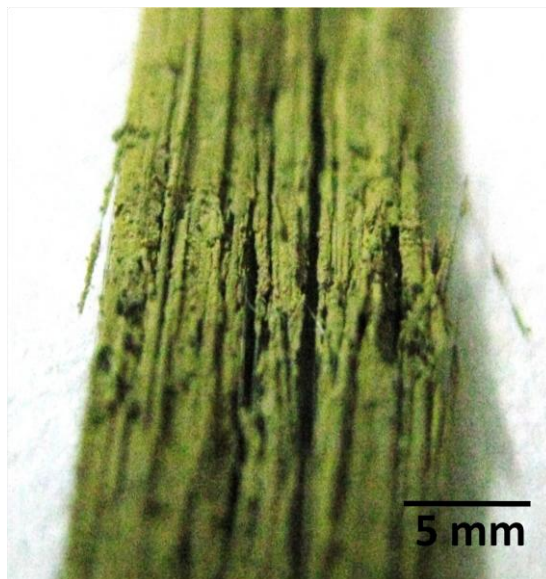


Fig. 5.3 Optical micrograph of the SiC nanowires coated carbon fibers.

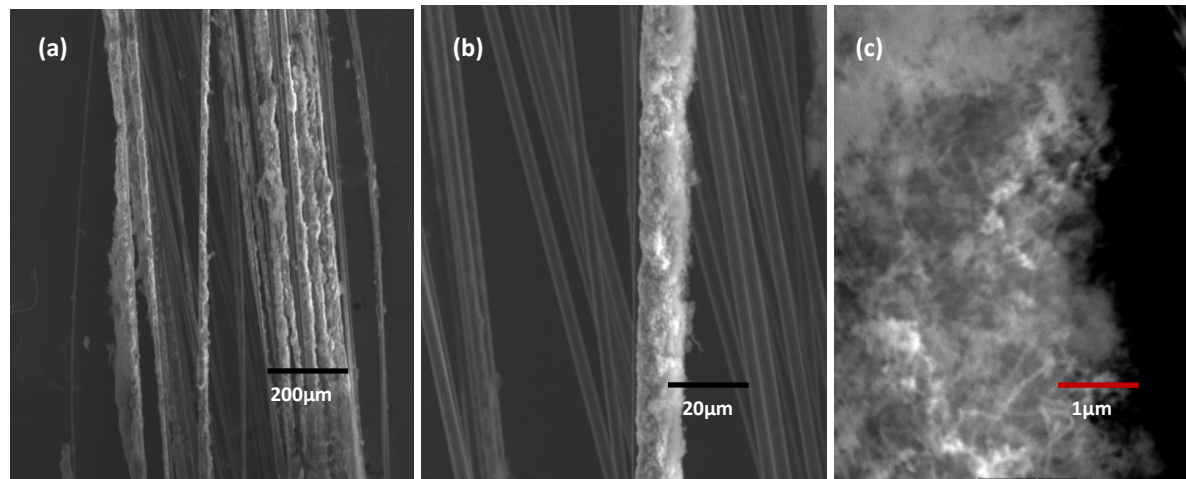


Fig. 5.4 SEM images of (a) Bundle of SiC nanowires coated carbon fibers (b) One SiC nanowires coated carbon fiber (c) Surface of the SiC nanowires coating.

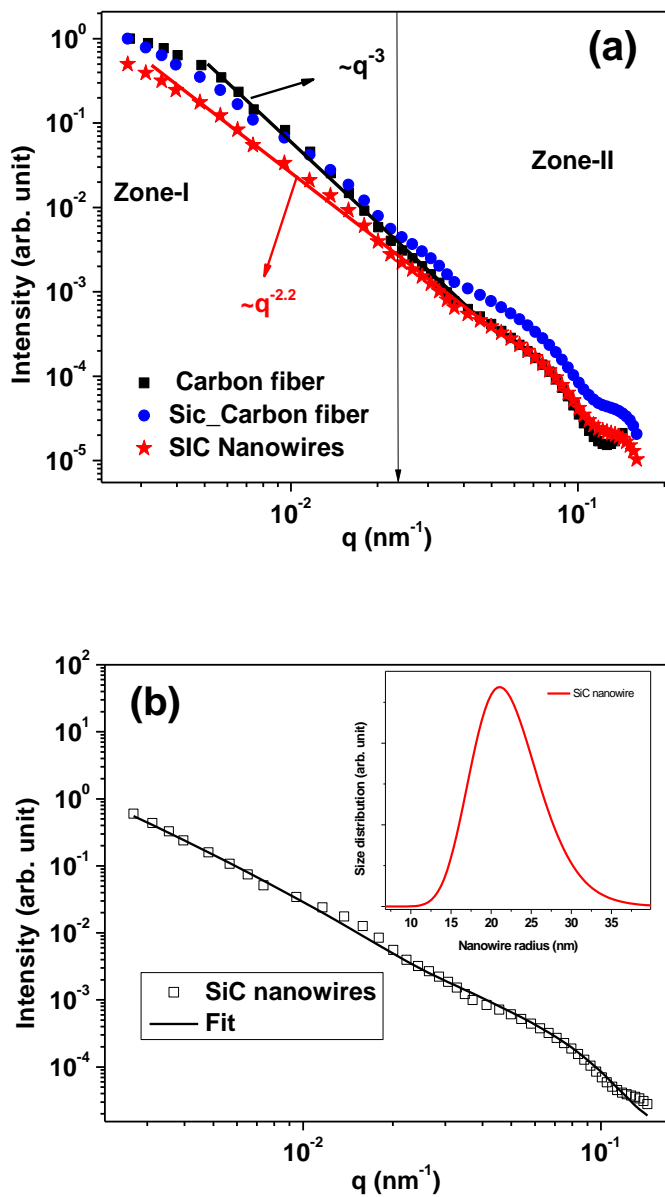


Fig. 5.5 (a) Scattering profiles for SiC nano wires coated and uncoated carbon fiber (b) The Fitted SANS profile of the SiC nanowires. The inset shows the nanowire radius distribution.

The optical micrograph image (Fig. 5.3) shows that the carbon fibers were covered with a light yellow color layer after the CVD coating using the process parameters for nanostructural SiC coating. SEM images (Fig. 5.4) shows the growth of uniform layer of SiC on the carbon fibers.

The thickness of the SiC layer was around 5-10 μm . The uniform layer of SiC was composed of SiC nanowires. It was observed that there was uniform diameter growth of SiC nanowires and smoothness of SiC coated surface on the substrate.

The chemical compositions of the SiC nanowire coated carbon fiber surface were characterized using EDX (Fig. 5.2c, Table 5.1). It was observed that Si and C were the major elements present in the coating while oxygen was present in small amount. The oxygen pick up may have come in the coating from environment during coating process. It can be avoided by creating proper vacuum in the chamber before coating.

Table 5.1

Elemental analysis of different SiC coated carbon fibers using EDX before and after oxidation.

| Environment | Sample | carbon | | Silicon | | Oxygen | |
|-------------------|---------------------|----------------------------------|---------------------------------|----------------------------------|---------------------------------|----------------------------------|---------------------------------|
| | | Before oxidation wt% (at%) | After Oxidation wt% (at%) | Before oxidation wt% (at%) | After Oxidation wt% (at%) | Before oxidation wt% (at%) | After Oxidation wt% (at%) |
| Oxygen atmosphere | Dense SiC coated cf | 44.26 (63.84) | 42.92 (61.10) | 51.94 (32.04) | 48.04 (29.24) | 3.80 (4.12) | 9.04 (9.66) |
| | SiC wires coated cf | 35.45 (54.82) | 19.22 (25.04) | 59.55 (39.38) | 39.04 (28.18) | 5.00 (5.8) | 41.74 (46.88) |

Small angle neutron scattering (SANS) experiments were carried out to probe the morphology of the SiC nanowire coated and uncoated carbon fibers. The SANS experiments were carried out at

double crystal based medium resolution instrument at guide tube laboratory of Dhurva reactor, Mumbai, India. The experimental profiles were corrected for transmission and background. Further, the profiles were also desmeasured for instrumental resolution. The corrected SANS profile is plotted in Fig. 5.5a. It is interesting to note that SANS gives statistically averaged information of the specimens while SEM and TEM are the local probe of the specimens. It was evident from the Fig. 5.5a that the scattering profiles can be divided in two zones. The zone-I of the profile gives the correlation of the constituent particles within the fibers. It is clear from Fig. 5.5a that the correlation of the constituent particles of the fiber gets modified after coating. In the present case, a fractal type correlation of the constituent particles was assumed. The fractal correlation was described by a power law with a characteristic exponent (D) and is called fractal dimension and it lies in range of 1 to 3. If the fractal dimension is closer to 3 then the morphology of the system will be more compact and the compactness of the morphology decreases with decreasing fractal dimension. The fractal dimension can be directly estimated by the SANS experiments as scattered intensity for fractal systems follow a power law with exponent as D . The fractal dimension in case of fibers was found to be 3 which indicate that carbon fiber is quite dense. However, the fractal dimension estimated from the SANS profiles of the SiC nanowires was found to be approximately 2.2. This indicates that the SiC nanowires were not arranged in a compact way but they were grown in cloud like morphology. This observation was also corroborated with the SEM results. Zone-II of the profiles gives the information about the SiC coated particles on fibers. In order to get information of the SiC nanowires coated on the fiber, scattering profile of carbon fiber was subtracted from the scattering profile of SiC coated carbon fiber. The estimated scattering profile of the SiC nanowires is shown in Fig. 5.5b. The calculated scattering profile of the nanowires was analyzed

to get the nanowire radius. The estimated nanowire radius distribution is depicted in the inset of Fig. 5.5b. The average nanowire radius was found to be about 22 nm and this observation was also supported by TEM results. In short, the SANS measurements could give the radius size distribution and the compactness of the nanowires on the carbon fiber.

5.1.2.2 Oxidation study of bare carbon fibers and different SiC coated carbon fibers in presence of oxygen environment

From the weight-loss curve for the oxidation carried out in oxygen environment (Fig. 5.6, curves i, ii and iii) it is obvious that the oxidation process of carbon fibers starts at 420 °C and the weight loss reached a maximum at about 644 °C; at this temperature there was 100% weight loss (Table 5.2). Whereas in case of dense SiC coated carbon fiber and SiC nanowires coated carbon fiber the oxidation process starts at 550 °C and 430 °C respectively. The weight loss reached a maximum value of 6-8% at about 1000 °C and 80-86% at 780 °C, for the dense SiC coated carbon fiber and SiC nanowires coated carbon fiber respectively. After certain period of oxidation of the sample there was weight gain in the deposit as seen in the TG curve. The weight gain was observed in dense SiC coated carbon fiber and SiC nanowires coated carbon fiber after 1000 °C and 800 °C respectively. During oxidation the carbon fiber and SiC coating react with oxygen as follows ¹⁷¹⁻¹⁷².



According to reactions 5.1-5.2 the oxidation of carbon fiber was a weight loss process and according to reaction 5.3-5.4 the oxidation of SiC was a weight gain process. It can be inferred that the oxidation of carbon fiber was the main factor due to which weight loss occur during oxidation process. At temperatures greater than 1000 °C (for dense SiC coated carbon fiber) and 800 °C (for SiC nanowires coated carbon fiber) the oxidation of SiC was the dominating factor due to which weight gain occur.

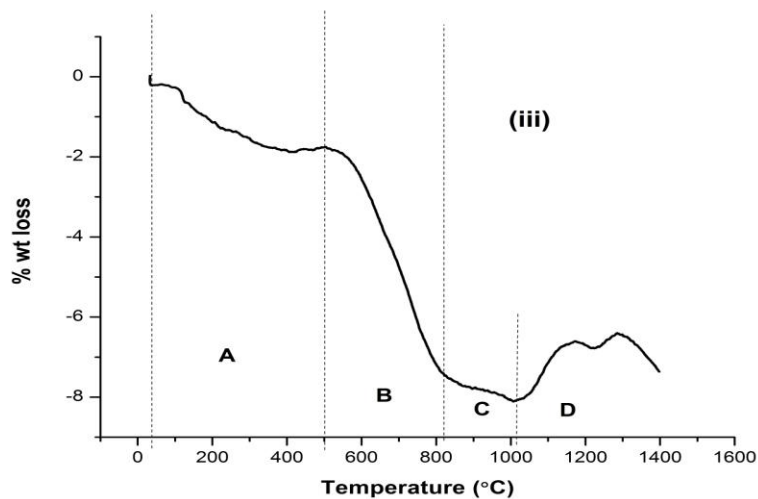
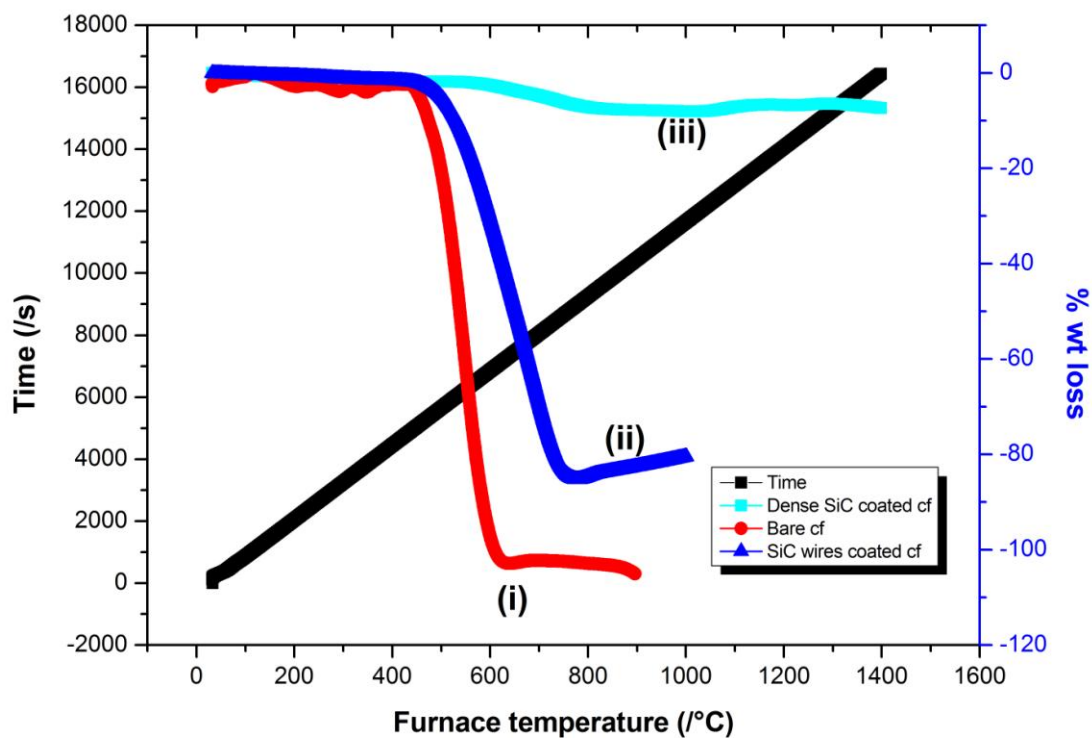


Fig. 5.6 Thermogravimetric analysis of (i) bare carbon fiber (ii) SiC nanowires coated carbon fiber (iii) Dense SiC coated carbon fiber in oxygen environment.

Once the SiO₂ layer was formed there was no further weight gain of deposit, it means SiO₂ layer also acts as the protective layer towards further oxidation of the SiC¹⁷³.

Table 5.2

Thermal Oxidation behavior of carbon fiber and different SiC coated carbon fibers in different oxidation environment.

| Environment | Sample | Temperature at which 10 wt% loss occurred (°C) | Onset temperature (°C) | Residue yield (%) (particular temperature) |
|------------------------------|---------------------|---|-------------------------------|---|
| Oxygen atmosphere | Carbon fiber- | 475 | 420 | 0% (630 °C) |
| | Dense SiC coated cf | 1000 (max. 8% wt loss) | 550 | 92-94 (1000°C) |
| | SiC wires coated cf | 530 | 430 | 20-24 (780°C) |
| Atmospheric condition | Carbon fiber | 562 | 450 | 0 (820°C) |
| | Dense SiC coated cf | 750 | 570 | 90-92 (818°C) |
| | SiC wires coated cf | 645 | 565 | 18- 24 (800°C) |

Figs. 5.7 and 5.8 shows the SEM images of the dense and SiC nanowire coated carbon fibers after oxidation. From Figs. 5.7a and b it was observed that there was no significant microcrack or pore generation on the surface of dense SiC coated carbon fiber after oxidation. It was noted that the surface of the coating was still dense and homogeneous and there was no significance change in diameter of coated carbon fibers. The thickness of coating remains almost unchanged after oxidation at 1350 °C. In case of SiC nanowire coated carbon fiber (Fig. 5.8) the carbon fibers

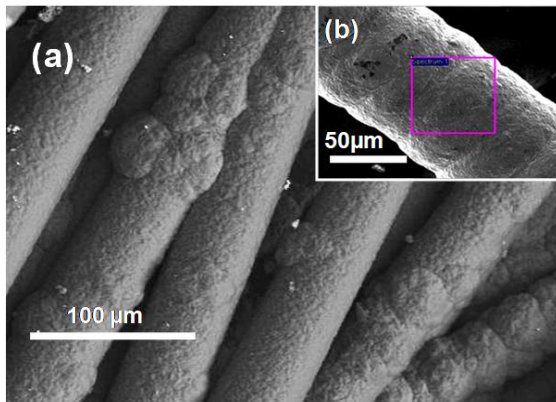


Fig. 5.7 SEM images of the Dense SiC coated carbon fibers after oxidation in oxygen environment (a) bunch of coated carbon fibers (b) surface of single coated carbon fiber.

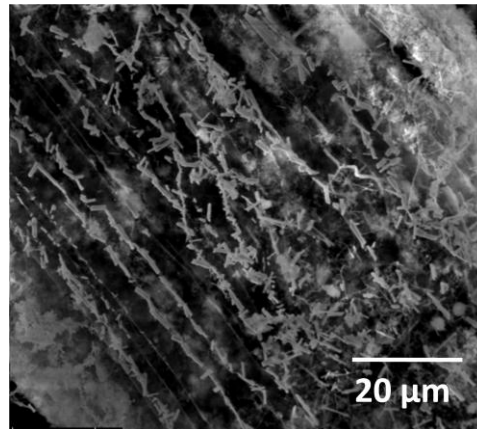


Fig. 5.8 SEM images of the SiC nanowires coated carbon fiber after oxidation in oxygen environment.

were oxidized and the residue containing SiC and SiO₂ remained. EDX (Table 5.1) shows that there was significant increase in the oxygen percentage in the residue after oxidation. It can be inferred that the formation of SiO₂ occurred due to oxidation of SiC. By considering that the oxygen percentage as estimated by EDX was present in the form of SiO₂, It was observed that the SiO₂ percentage increases from 2 to 5 % in case of dense SiC coated carbon fiber after oxidation. Whereas in case of SiC nanowire coated carbon fiber the increase was from 3 to 23%. It clearly indicates that in case of SiC nanowire coated carbon fiber most of the SiC nanowires also get oxidized. It was also confirmed from the TG data (Fig.5.6(ii) & (iii)). There were 2% and 10 % weight increase in case of dense and nanowire SiC coated carbon fibers respectively. It was observed that there was significant shrinkage in the diameter of SiC nanowire coated carbon fibers due to large weight loss i.e. due to exhaustive oxidation of carbon fibers.

5.1.2.3 TG-DTG analysis of coated non coated carbon fibers in oxygen environment

The DTG (Fig. 5.9, curves i, ii and iii) was the differential of the TG curve and hence gives the rate of weight loss. From the DTG curve it was obvious that the oxidation reaction rate (da/dT) of carbon fiber and SiC coated samples reached maximum when 62% (Bare carbon fibers), 64%

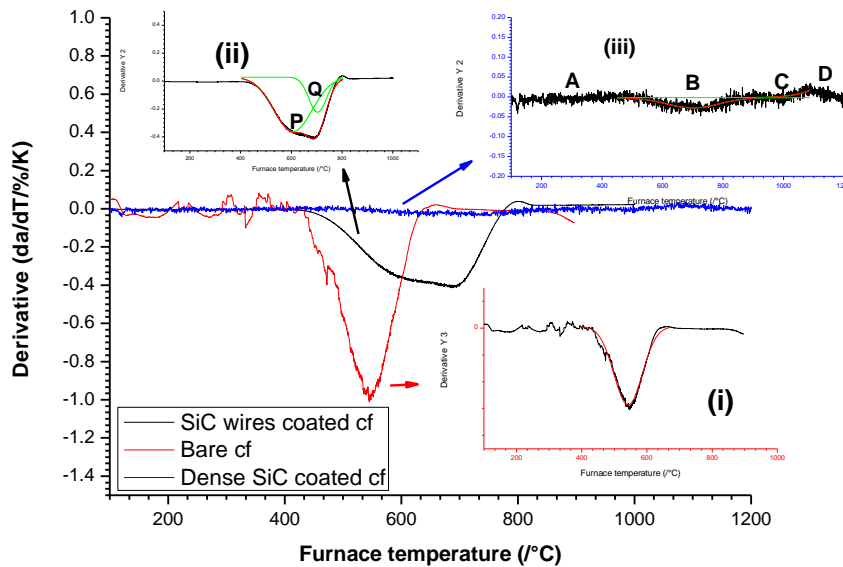


Fig. 5.9 DTG curves of (i) bare carbon fiber (ii) SiC nanowires coated carbon fiber (iii) Dense SiC coated carbon fiber in oxygen environment.

(SiC nanowire coated carbon fiber) and 7% (dense SiC coated carbon fiber) was burnt out. LR Zhao et al ¹⁷⁴ have explained the self catalytic oxidation behavior of carbon fiber. In case of oxidation of bare carbon fibers and SiC nanowire coated carbon fiber samples, self catalytic characteristic were observed.

For bare carbon fiber, initially the number of active carbon atom (ACA) on the fiber surface was few and the fiber had the lowest oxidation rate. The extended 2-D chain structure of fiber should be broken off by oxidation to form several smaller species thereby increasing the ACA ¹⁷⁴. Thus

with increasing oxidation-weight loss the amount of ACA increased and the reaction rate also increased. So the self catalytic characteristic was displayed and there arose a critical point (62% wt loss, At temperature: 550 °C). At this critical point the ACAs generated and consumed through oxidation were in equilibrium. When the value of weight loss was bigger than 62%, the consumption rate of ACAs increase with the increase of weight loss and the oxidation rate decreased.

In case of the SiC nanowire coated carbon fiber, the oxidation began at higher temperature at about 430 °C in comparison to bare carbon fiber because there was SiC on the carbon fiber surface and the SiC was well bonded with the carbon fiber. At this stage the number of ACAs on the surface was small, and the diffusion rate of oxygen was low, so the oxidation rate was low. With increasing temperature, there were generation of microcracks and pits on the surface. The diffusion of oxygen atoms through these micro pores, microcracks and pits to the carbon fiber surface get increased. Due to increase in oxygen concentration on carbon surface the rate of reaction with oxygen increased. For this reason, the reaction interface moved toward the center of the fiber gradually, and the number of ACA increased. However, there is a critical temperature (700 °C). When the temperature was higher than 700 °C, the oxidation rate of fibers reached the maximum and 64.0% carbon fiber was burnt off. After this maximum weight loss point again there was decrease in oxidation rate due to the higher consumption rate of ACAs. There were two troughs (P & Q in Fig. 5.9, curve ii) in the DTG curve of SiC nanowire coated carbon fiber. It indicates two different rates of weight loss corresponding to two different oxidation reactions. In order to find the individual curves for the two oxidation reactions, whose resultant was the present DTG curve, Gaussian fitting was performed on the DTG curve as shown in Fig. 5.9, curve ii. The first trough (P in Fig. 5.9, curve ii) represents the oxidation of the carbon fiber. It

was confirmed from the trough position of the carbon fiber from DTG curve of bare carbon fiber. The second trough (Q in Fig. 5.9, curve ii) may represent the competitive oxidation of carbon fiber as well as SiC. Since oxygen can penetrate through the micropores between SiC nanowires, the whole SiC coating was also exposed to oxidation. The oxidation rate of SiC increases with increase in temperature. At this point there may be competition between oxidation of carbon fiber and oxidation of SiC to dominate the overall reaction. The resultant of overall reaction was weight loss at this point. At temperature above 800 °C, there was weight gain in the residue indicating dominance of oxidation of SiC on overall reaction.

In case of dense SiC coated carbon fiber there was continuous layer of SiC which prevents the diffusion of oxygen to the carbon fiber center. According to TG curve (Fig. 5.6, curve iii), the oxidation behavior of the dense SiC coated carbon fiber could be divided into four processes, marked as A, B C and D in Figs. 5.6 and Fig. 5.9 (“curve iii” in each). The weight change in TG curve (Fig. 5.6, curve iii) can be estimated using straight line during different processes. A schematic of oxidation of dense SiC coated carbon fiber was shown in Fig. 5.11. The slopes of lines in three different processes A, B and C were different, indicating three different oxidation rates. The DTG curve (Fig. 5.9, curve iii) has also shown the three different troughs in the curve. From room temperature to 500 °C (process A), there was little weight loss in the sample weight. It indicates that due to presence of small microcracks on the coating, the oxygen can diffuse through them and oxidation occurs. Since the temperature was low in this range, the oxidation rate was low leading to low mass loss. From 500 to 800 °C (process B), the sample weight loss was maximum due to the oxidation through microcracks already present and due to formation of new small microcracks in the coating from the mismatch of CTE between the coating and carbon substrate. These microcracks serve as a channel for oxygen to penetrate into carbon fiber and

lead to the oxidation of carbon fiber. The slope of straight line in TG curve for process B was larger than the Process A and Process C. The area under curve for process B in DTG curve was larger than process A and process C. The weight change in TG curve decreases in the temperature range 800 to 1000 °C (process C). There might be quick self healing of some microcracks over the SiC surface during process C, which results in the decrease in oxidation rate . At temperature above 1000 °C (process D) there was weight gain in the sample and after 1200 °C there was no further weight gain. It means the small microcracks will be decreased or eliminated quickly at the oxidation temperature above 1000 °C for the formation of SiO₂ on the surface of coating. This oxidation of SiC and Si to SiO₂ dominate the overall oxidation reaction and leads to the weight gain of sample. There was no significant diffusion of oxygen through the dense SiC and SiO₂ layer above 1200 °C. The SiO₂ layer formed over the surface improves the anti oxidation property. The formation of SiO₂ system and its further reaction with coating at temperature above 1200 °C was a complex system¹⁷⁵. It leads to the constant weight of sample after oxidation temperature 1200 °C. It was confirmed from the SEM pictures (Figs. 5.7a and b) of the oxidized dense coated SiC carbon fiber that there was no significant number of cracks over the SiC surface after oxidation upto 1350 °C. The above reasons result in an obvious improvement of the oxidation protection ability of dense and nanostructured SiC coated carbon fibers.

5.1.2.4 Oxidation study of bare carbon fibers and different SiC coated carbon fibers in presence of atmospheric environment

From the oxidation weight-loss curve (Fig. 5.10, curves i, ii and iii) it was obvious that the oxidation process of fibers began from 450 °C the weight loss reached a maximum at about 820

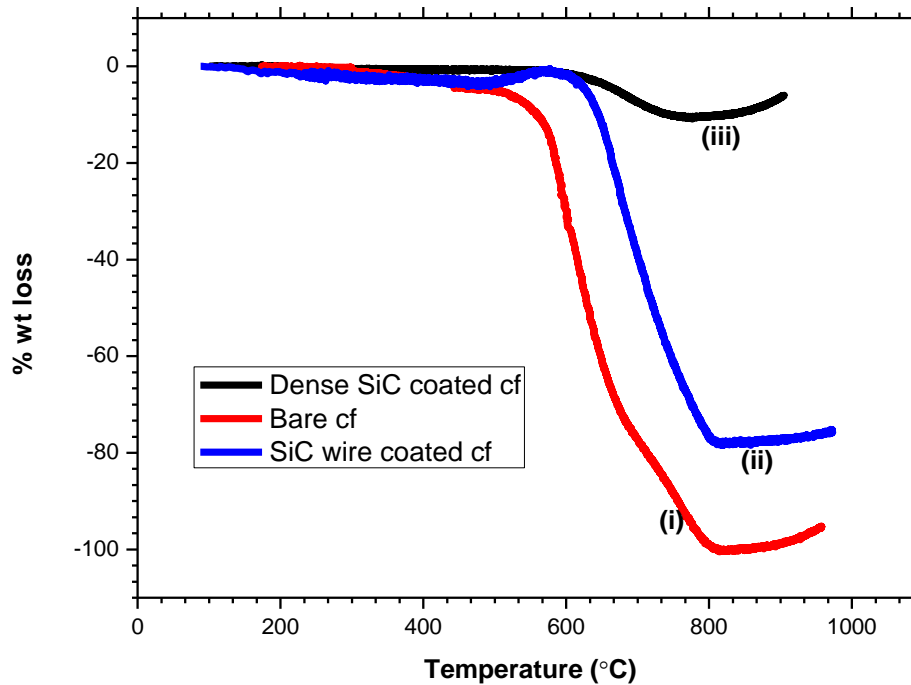


Fig. 5.10 Thermogravimetric analysis of (i) bare carbon fiber (ii) SiC nanowires coated carbon fiber (iii) Dense SiC coated carbon fiber in atmospheric environment.

°C; at this temperature there was 100% weight loss (Table 5.2). Whereas in case of dense SiC coated carbon fiber and SiC nanowires coated carbon fiber the oxidation process starts from 570 °C and 565 °C respectively. The weight loss reached a maximum value of about 8-10% at 818 °C and 76-82% at 800 °C for dense SiC coated carbon fiber and SiC nanowires coated carbon fiber respectively. After that with increase in temperature the weight increased which may be caused by oxidation of the SiC layer.

Figs. 5.11 and 5.12 show the SEM images of the dense and SiC nanowire coated carbon fibers after oxidation. From Figs. 5.11a and b it was observed that there was microcrack generation on the surface of dense SiC coated carbon fiber after oxidation. It was noted that the microcracks propagate through the grains. These microcracks were responsible for oxidation of carbon at high temperature. In case of oxidation in oxygen environment it was observed that there was self healing of microcracks. But in atmospheric environment there might be no quick self healing of some microcracks over the SiC surface ¹⁷⁶. The formation of silica was decelerated due to low percentage of oxygen in environment. The slow healing of microcracks was responsible for the retaining of microcracks on the surface of atmospheric environment oxidized dense coated carbon fibers. In case of SiC nanowire coated carbon fiber (Figs. 5.12a, b and c), It was observed that there were formation of microcracks and pits on the oxidized surfaces. The carbon fibers were oxidized due to channeling of oxygen through these microcracks, pits and micropores present on the surface at high temperature. The residue containing Carbon, SiC and SiO₂ remained after oxidation. The chemical compositions of the SiC nanowire coated carbon fiber surface before and after oxidation were characterized using EDX (Table 5.3). It was observed that Si and C were the major elements present in the coating while oxygen was present in small amount before oxidation. The oxygen pick up may have come in the coating from environment during coating process. EDX (Table 5.3) shows that there was significant increase in the oxygen percentage in the residue after oxidation. It can be inferred that the formation of SiO₂ occurred due to oxidation of SiC. By considering that the oxygen percentage as estimated by EDX was present in the form of SiO₂, it was observed that the SiO₂ percentage increases from 2 to 4 % in case of dense SiC coated carbon fiber after oxidation; whereas in case of SiC nanowire coated carbon fiber the increase was from 3 to 16%. It clearly indicates that in case of SiC nanowire

coated carbon fiber most of the SiC nanowires also got oxidized. Due to the channeling of oxygen through microcracks, pits and micropores most of the SiC nanowires were also exposed to the oxygen with carbon at high temperature. It was observed that the weight gain in TG was more in case of SiC nanowire coated carbon fiber than the dense coated one. Comparatively large exposure of carbon and SiC nanowires to oxygen at high temperature in case of SiC nanowire coated carbon fiber was the reason for large weight loss and comparative more weight gain.

Table 5.3

Elemental analysis of different SiC coated carbon fibers using EDX before and after oxidation.

| Environment | Sample | carbon | | Silicon | | Oxygen | |
|-------------------------|---------------------|----------------------------|---------------------------|----------------------------|---------------------------|----------------------------|---------------------------|
| | | Before oxidation wt% (at%) | After Oxidation wt% (at%) | Before oxidation wt% (at%) | After Oxidation wt% (at%) | Before oxidation wt% (at%) | After Oxidation wt% (at%) |
| Atmospheric environment | Dense SiC coated cf | 44.26 (63.84) | 43.32 (62.15) | 51.94 (32.04) | 48.58 (29.69) | 3.80 (4.12) | 8.10 (8.16) |
| | SiC wires coated cf | 35.45 (54.82) | 35.31 (37.15) | 59.55 (39.38) | 34.33 (31.40) | 5.00 (5.8) | 30.36 (31.45) |

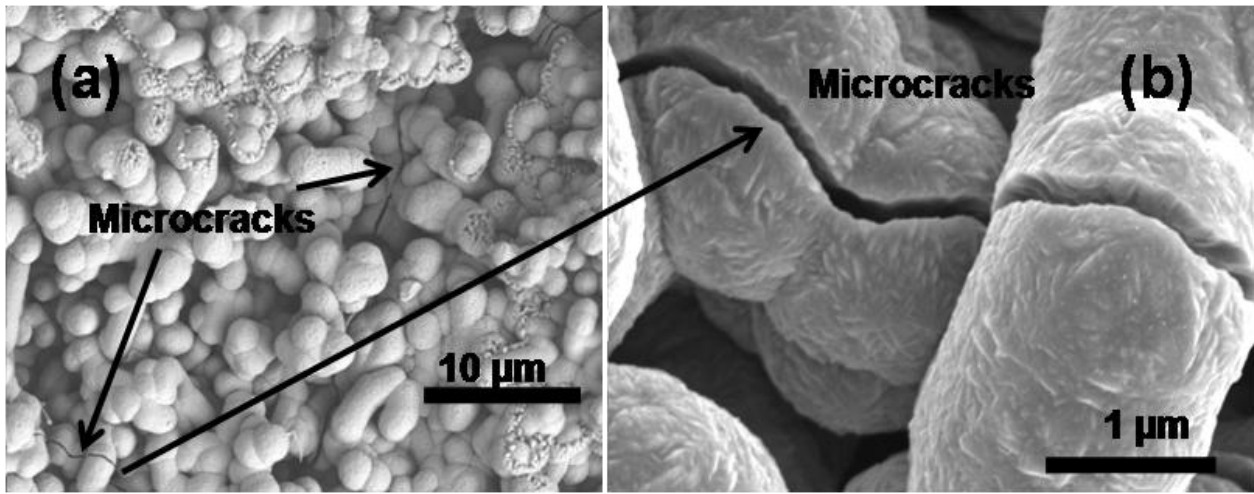


Fig. 5.11 SEM images of the Dense SiC coated carbon fibers after oxidation in atmospheric environment (a) surface of coated carbon fiber (b) Crack propagation through grain.

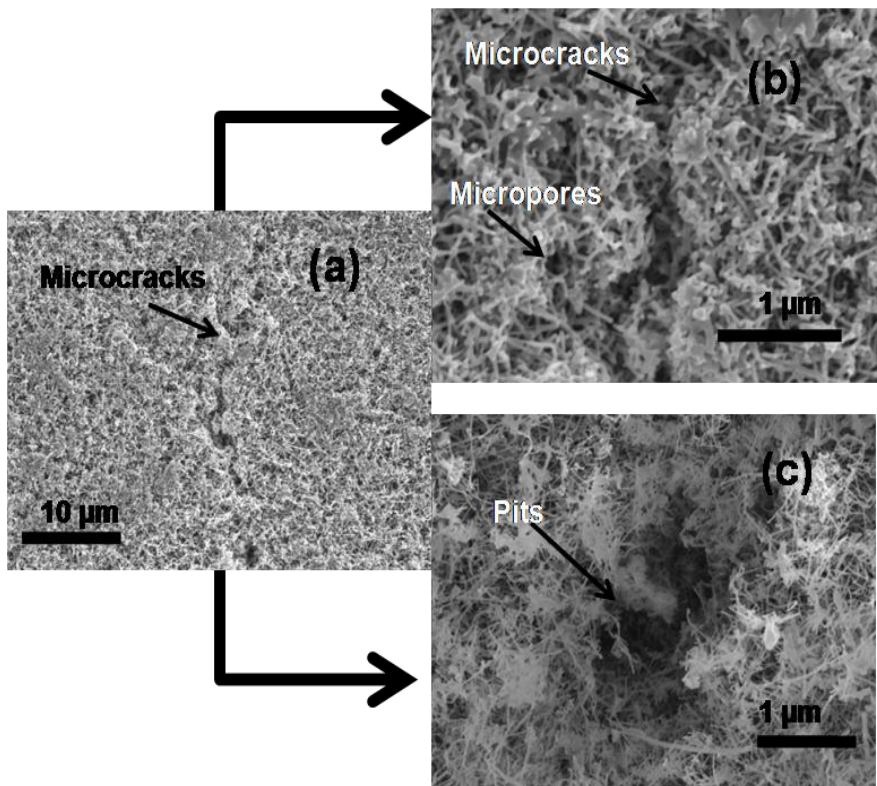


Fig. 5.12 SEM images of the SiC nanowires coated carbon fiber after oxidation in atmospheric environment (a) surface of a coated carbon fiber (b) & (c) microcracks, micropores and pits on the surface.

5.1.2.5 Mechanism of oxidation of different SiC coated carbon fibers in different oxidative environment

The SiC coatings of different morphology under different oxidation conditions have exhibited different oxidation behaviors. There were different oxidation mechanism reported in the literature¹⁷⁷⁻¹⁸¹ for oxidation of SiC in different environment and temperature. In a typical oxidation process, the chemical reaction in the coating and the oxygen diffusion inside the coating will occur simultaneously, and thus the oxidation process was controlled by both oxygen diffusion and reaction kinetics at high temperature. This means that the oxidation rate was mainly determined by the competition process between the chemical reaction and oxygen diffusion. Much specifically, when the chemical reaction rate was lower than the diffusion rate, the rate of oxygen diffused inward is higher than that of reaction, and in this case, the oxidation process is controlled by chemical reaction. On the other hand, if the chemical reaction rate is higher than the diffusion rate, the oxygen diffused inside the coating is insufficient for reaction consumed, thus the oxidation process is controlled by oxygen diffusion.

For oxidation of dense SiC coated carbon fiber in oxygen environment, the coating was dense and the oxygen permeability of the formed SiO₂ glass was very low. So, when the cracks on the coating surface were sealed, oxygen can hardly diffuse into the substrate. In this case, the oxidation can only occur in the superficial of the coating and consequently the oxidation process was controlled by oxygen diffusion. However in case of dense SiC oxidation in atmospheric environment, the microcracks does not get healed quickly. The diffusion of oxygen through these defects was much easy. As the carbon surface was covered with SiC coating the amount of active carbon atom exposed to air was small, thus the reaction rate was very low and then the oxidation was determined by chemical reaction. In case of SiC nanowire coated carbon fibers, the

micropores, microcracks and pits were present on the surface through which oxygen can diffuse easily. In different oxidative environment there was no significant change in surface morphology of SiC nanowire coated carbon fibers. Since the amount of active carbon atom exposed to oxygen was low due to SiC layer, resulting in low reaction rate. So the oxidation was determined by chemical reaction.

Dense SiC coating and SiC nanowires composed SiC coating was achieved on the carbon fiber surface. The dense SiC coated carbon fibers and SiC nanowires coated carbon fibers have shown much improved oxidation property than the bare carbon fibers in oxygen as well as in static air environment. In non-isothermal oxidation condition in oxygen environment, the oxidation process of carbon fiber and SiC nanowire coated carbon fiber exhibited a self catalytic characteristic. In case of SiC nanowires coated carbon fiber the micropores present in between the SiC nanowires over carbon fiber substrate serve as a channel for oxygen to penetrate into carbon fiber and lead to the oxidation of carbon fiber. The whole oxidation process consists of the oxidation of the carbon fiber and competitive oxidation of carbon fiber as well as SiC. In case of dense SiC coated carbon fiber the small microcracks formed in the coating due to the mismatch of CTE between the coating and carbon substrate act as the channel for oxygen diffusion and leads to the oxidation of carbon fiber. The SiO₂ layer formed over the SiC coating plays an important role in improving the anti oxidant property of the coating. The oxidation of SiC nanostructured coating which starts from around 700 °C forms SiO₂ layer over the SiC nanostructure and it contributes as a weight gain in the oxidation process. The layer of SiO₂ was formed at lower temperature in nanostructured SiC in comparison with the dense SiC coating (starts at around 900 °C). This phenomenon may be useful for healing pre existing micropores at lower temperature and improving oxidation resistive property of dense SiC/SiC nanowire matrix

carbon composites. In such composites it is observed that at high temperature there were formation of small microcracks/ holes. The SiC nanowires which were present with dense SiC matrix at the microspores will get oxidized first and form SiO₂/SiC nanowires. These SiO₂/SiC nanowires will heal the micropores/holes.

5.2. Kinetics model study for oxidation of carbon fiber and SiC nanowires coated carbon fibers

5.2.1 Isothermal Oxidation properties of carbon fiber and SiC nanowire coated carbon fiber

The isothermal oxidation weight loss and Arrhenius curve of carbon fiber and SiC nanowires coated carbon fiber were shown in Figs. 5.13 & 5.14. From the oxidation weight-loss curve in oxygen environment (Fig. 5.13), it was observed that the oxidation process of carbon fibers began from 400 °C and the weight loss reached a maximum at about 600 °C. At that temperature there was 100% weight loss. Whereas in case of SiC nanowires coated carbon fiber the oxidation process

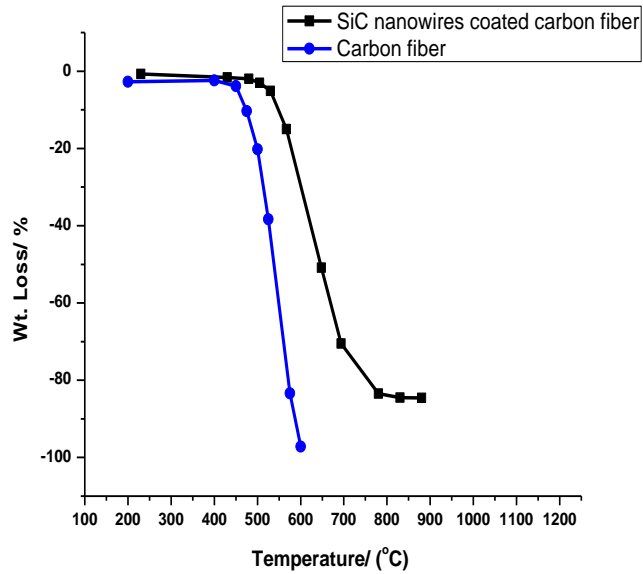


Fig. 5.13 The isothermal oxidation weight loss curve of bare carbon fiber and coated carbon fiber samples.

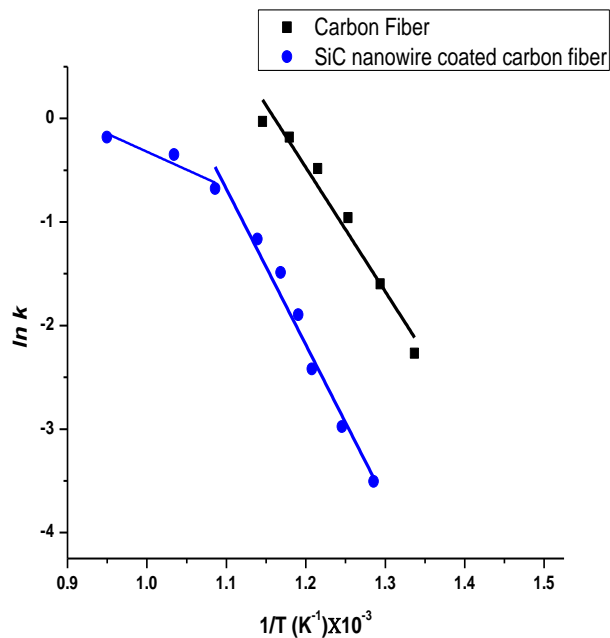


Fig. 5.14 Arrhenius curve of bare carbon fiber and coated carbon fiber samples.

starts from 480 °C. The weight loss reached a maximum value at about 780 °C and at that temperature there was 84% weight loss. The results showed that the oxidation resistance property of carbon fiber was improved due to uniform layer of SiC nanowire coating.

It is well established¹⁸² that for coating/carbon materials, the oxidation-weight loss was proportional to time when weight-loss was below 70% and correlation equation 5.5 to calculate activation energy and pre-exponential factor was derived as shown below.

$$\ln\left(\frac{m_o - m}{m_o}\right) = (C) - \left(\frac{E_a}{RT}\right) \quad (5.5)$$

where m_o was the initial quantity of sample, m the quantity of sample at time t , C is a constant represented as $(\ln A + \ln t)$, A was pre-exponential factor, E_a the apparent activation energy of fiber oxidation reaction in kJ mol^{-1} , T the absolute temperature in K , R the gas constant in $\text{J mol}^{-1} \text{K}^{-1}$. In the experimental conditions, the value of $(\ln A + \ln t)$ was constant. The Arrhenius curve was obtained through plotting $\ln((m_o - m)/m_o)$ versus $1/T$ (the data of m_o , m , and T were obtained from Fig.5.13 (weight loss curves). And the value of E_a could be obtained from the slope of Arrhenius curve (Fig. 5.14).

The Arrhenius curve of carbon fiber and SiC nanowire coated carbon fiber were shown in Fig 5.14. The activation energy value calculated from Arrhenius curve of carbon fiber was $99.01 \text{ kJ mol}^{-1}$. It was observed that The Arrhenius curve of SiC nanowire coated carbon fiber consisted of two different slope lines, thus there was two different E_a values (125.04 and 28.89 kJ/mol). Two E_a values mean that there were two different reaction mechanisms with the increase of temperature, with a transition region around 650 °C .

In the first oxidation step, the temperature was low and the amount of active carbon atom (ACA) in carbon fiber surface was small because of the SiC coating existing, thus the reaction rate was low. And the rate that gas diffused through coating was higher than that of reaction. The oxidation process was controlled by chemical reaction. Even through gas diffusion made some contribution to the overall reaction rate (for E_a , 125.04 kJ mol⁻¹). In the second oxidation step, the oxidation reaction rate increased with the increase of temperature. It was in the vicinity or even exceeding the gas diffusion rate, i.e., the oxidation process of SiC nanowire coated carbon fiber was controlled by chemical reaction and gas diffusion together.

5.2.2 Kinetic Studies

The kinetic results reported in literature showed that the kinetic parameters depend strongly on the selection of a proper mechanism function for the process. Therefore, the determination of the most probable function is highly essential.

In the present work, the equations of Achar-Brindley-Sharp-Wendworth¹⁶⁸, Satava-Sestak^{164, 183}, Coat-Redfern¹⁶⁰ and Madhusudanan-Krishnan-Ninan¹⁷⁰ were used to study the oxidation kinetics and to estimate most probable mechanism function of carbon fiber and SiC nanowire coated carbon fiber in non isothermal condition.

Achar-Brindley-Sharp-Wendworth equation:

$$\ln\left[\frac{1}{F(a)}\frac{da}{dT}\right] = \ln\left(\frac{A}{\beta}\right) - \frac{E_a}{R} \frac{1}{T} \quad (5.6)$$

Satava-Sestak equation:

$$\ln[G(a)] = \ln\left(\frac{AE_a}{\beta R}\right) - 2.135 - 0.4567 \frac{E_a}{R T} \quad (5.7)$$

Coats-Redfern equation:

$$\ln\left[\frac{G(a)}{T^2}\right] = \ln\left(\frac{AR}{\beta E_a}\right) - \frac{E_a}{R T} \quad (5.8)$$

Madhusudanan-Krishnan-Ninan equation

$$\ln\left[\frac{G(a)}{T^{1.921503}}\right] = \left[\ln\left(\frac{AE_a}{\beta R}\right) + 3.772050 - 1.921503 \ln E\right] - 0.120394 E_a \frac{1}{T} \quad (5.9)$$

where β was the heating rate, a the reaction fraction, $F(a)$ and $G(a)$ the differential and integral mechanism function, respectively.

The TG–DTG curve of carbon fiber and SiC nanowire coated carbon fiber is shown in Fig. 5.15 & 5.16a, b. The basic data of a , T and da/dT obtained by the TG–DTG curves were listed in Table 5.4 and Table 5.5 for carbon fiber and SiC nanowire coated carbon fiber respectively.

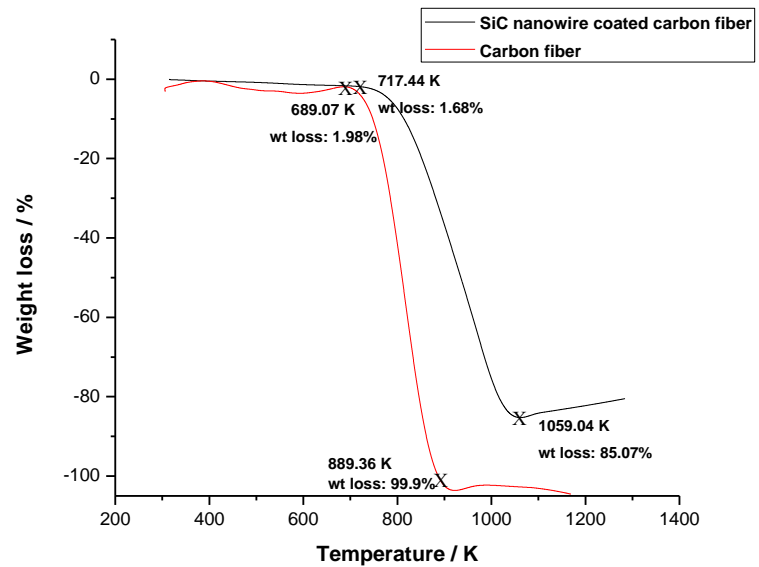


Fig. 5.15 The nonisothermal TG curve of bare carbon fiber and coated carbon fiber samples.

The integral ($G(a)$) and

differential ($F(a)$) functions for the most common mechanism used in kinetic study of solid-state decomposition in this work were listed in Table 5.6^{161, 164, 169-170, 183-186}.

Table 5.4

Oxidation decomposition data of a , T and da/dT obtained from the TG–DTG curves for oxidation of carbon fiber.

| Temperature (T,K) | Weight loss (a) | Differential weight loss ($da/dT, K^{-1}$) |
|-------------------|---------------------|--|
| 739.33 | 0.09163 | 0.154 |
| 743 | 0.09429 | 0.203 |
| 746.11 | 0.10124 | 0.279 |
| 751.18 | 0.12291 | 0.325 |
| 755.98 | 0.12773 | 0.476 |
| 761.91 | 0.13122 | 0.504 |
| 766.41 | 0.16991 | 0.535 |
| 771.19 | 0.17316 | 0.569 |
| 776.25 | 0.19935 | 0.611 |
| 781.04 | 0.23093 | 0.644 |
| 786.09 | 0.26235 | 0.66 |
| 792.84 | 0.33828 | 0.71 |
| 794.53 | 0.3452 | 0.76 |
| 799.61 | 0.39254 | 0.801 |
| 803.82 | 0.4361 | 0.868 |
| 809.7 | 0.4889 | 0.881 |
| 814.46 | 0.5237 | 0.895 |
| 818.1 | 0.5485 | 0.959 |
| 824.55 | 0.6172 | 1.126 |
| 829.02 | 0.66566 | 1.182 |
| 832.93 | 0.7107 | 1.102 |
| 838.24 | 0.7648 | 1.016 |
| 844.13 | 0.8263 | 0.954 |

| | | |
|--------|---------|-------|
| 848.91 | 0.8683 | 0.804 |
| 853.42 | 0.8924 | 0.452 |
| 859.32 | 0.92671 | 0.283 |
| 863.53 | 0.947 | 0.217 |
| 869.97 | 0.9729 | 0.209 |
| 875.36 | 0.9892 | 0.18 |
| 877.05 | 0.9944 | 0.146 |

Table 5.5

Oxidation decomposition data of a , T and da/dT obtained from the TG–DTG curves for oxidation of SiC nanowire coated carbon fiber.

| Temperature (T,K) | Weight loss (a) | Differential weight loss ($da/dT, K^{-1}$) |
|--------------------------|-------------------------------------|--|
| 855.464 | 0.24286 | 0.34166 |
| 860.79 | 0.261189 | 0.34737 |
| 865.8328 | 0.278787 | 0.3546 |
| 869.79 | 0.29306 | 0.35989 |
| 874.85 | 0.31165 | 0.36508 |
| 879.87 | 0.32995 | 0.36837 |
| 885.5 | 0.3507 | 0.37143 |
| 889.44 | 0.365275 | 0.37224 |
| 895.63 | 0.388432 | 0.37448 |
| 900.13 | 0.405355 | 0.37586 |
| 904.9 | 0.4233 | 0.3769 |
| 909.98 | 0.4424 | 0.37775 |
| 915.59 | 0.4637 | 0.37751 |
| 920.95 | 0.4839 | 0.38089 |
| 924.87 | 0.49899 | 0.38393 |
| 930.47 | 0.52055 | 0.38689 |
| 934.96 | 0.53804 | 0.38891 |

| | | |
|----------|----------|---------|
| 940.02 | 0.557699 | 0.39005 |
| 945.91 | 0.5808 | 0.39356 |
| 950.41 | 0.59846 | 0.39456 |
| 955.75 | 0.61955 | 0.39459 |
| 960.25 | 0.6372 | 0.3952 |
| 966.7271 | 0.66277 | 0.39409 |
| 970.06 | 0.6761 | 0.39274 |
| 976.29 | 0.7003 | 0.38784 |
| 980.8 | 0.71775 | 0.38461 |
| 985.56 | 0.73607 | 0.38102 |
| 991.15 | 0.757 | 0.37164 |
| 996.19 | 0.7753 | 0.35767 |
| 1000.69 | 0.7909 | 0.33917 |
| 1005.72 | 0.8074 | 0.31175 |
| 1010.76 | 0.82216 | 0.2721 |
| 1015.73 | 0.83455 | 0.21359 |
| 1020.177 | 0.842588 | 0.14783 |
| 1025.241 | 0.848275 | 0.07229 |

The kinetic analyses were completed using a linear regression of the least square method on a computer using MATLAB

programming software. The plots of $\ln[(da/dT)/F(a)]$ versus $\log[G(a)]$,

$\ln[G(a)/T^2]$ and $\ln[G(a)/T^{1.921503}]$

versus $1/T$ lines were carried out using linear least square fitting

according to Equations (5.6)–

(5.9). The values of linear

correlation coefficient r and

standard deviation were obtained

from $\ln[(da/dT)/F(a)]$, $\log[G(a)]$,

$\ln[G(a)/T^2]$ and $\ln[G(a)/T^{1.921503}]$

versus $1/T$ lines directly, the

values of activation energy E_a

and pre-exponential function A

can be calculated from the slope

and intercept of above lines,

respectively. The results (E_a , A , r

and Standard Deviation) of

$\ln[(da/dT)/F(a)]$, $\log[G(a)]$,

$\ln[G(a)/T^2]$ and $\ln[G(a)/T^{1.921503}]$

versus $1/T$ for all possible

mechanisms ($F(a)$ and $G(a)$) were listed in Table 5.7-5.14 for carbon fiber and SiC nanowire coated carbon fiber.

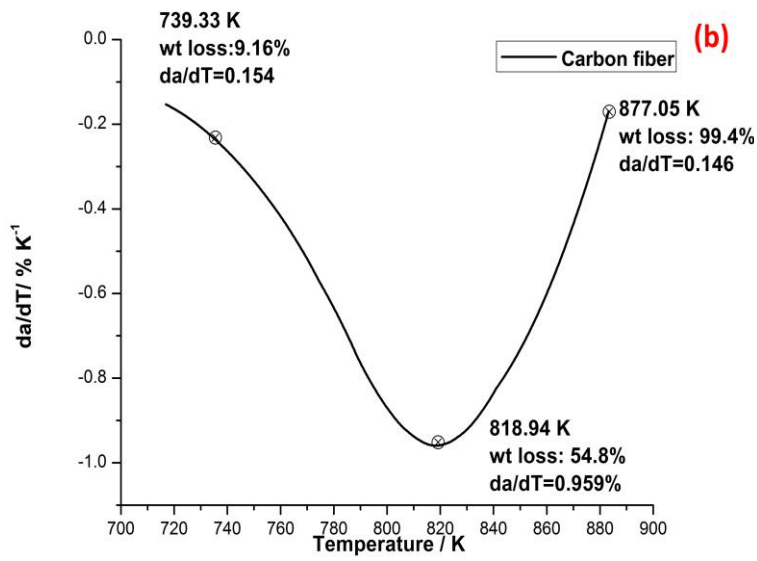
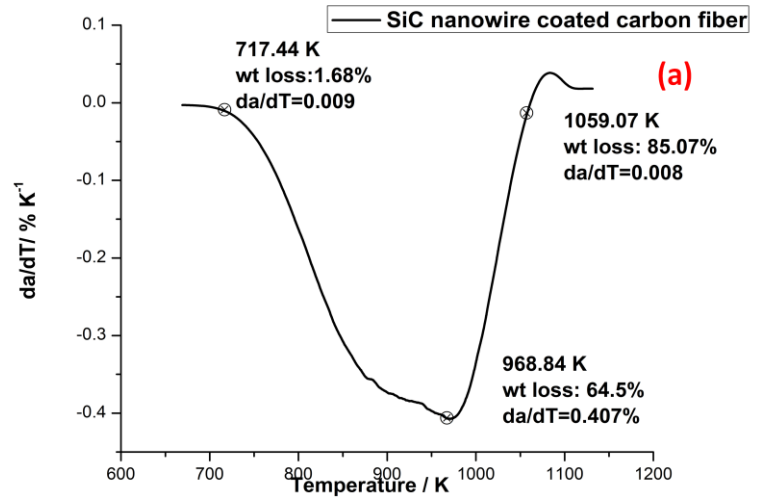


Fig. 5.16 The DTG curve of (a) SiC nanowire coated carbon fiber samples (b) bare carbon fibers samples.

To determine the most probable mechanism the following conditions should be satisfied at the same time:

- (1) The values of E_a were between 80 and 250 kJ mol⁻¹ and the values of log A were between 7 and 15 min⁻¹, which were obtained by the different methods were approximately equal;
- (2) The linear relevant coefficient r was better (<-0.98);
- (3) The standard deviation was small (<0.3).

The relevant function which satisfies all above conditions will be considered as the probable mechanism of oxidation reaction.

5.2.3 Determination of most probable mechanism function and calculation of Activation energy, Pre-exponential factor for oxidation of carbon fiber

The result of most probable mechanism functions during oxidation process is tabulated in Tables 5.7-5.10. From the data in these tables, it can be seen clearly that only function A1 (A1 stood for Avrami-Erofeev equation, Random Nucleation¹⁸⁶) satisfied the above-mentioned conditions in case of Achar-Brindley-Sharp-Wendworth equation, Satava-Sestak equation and Madhusudanan-Krishnan-Ninan equation. Thus the possible mechanism function was function A1 as it has been satisfying one differential and two integral equations. Therefore it can be stated that the mechanism function with differential form $f(a) = (1 - a)$ and integral form $g(a) = -\ln(1 - a)$ belongs to the mechanism of random nucleation. It is concluded that the kinetic equation for the thermal decomposition of fiber was: $da/dT = (A/\beta)\exp(-E_a/RT)(1 - a)$. The kinetic parameters were $\log A = 8.343 \text{ min}^{-1}$, $E_a = 143.57 \text{ kJ mol}^{-1}$. We conclude that the kinetic equation for the thermal decomposition of fiber was: $f(a) = (1 - a)$.

The oxidation mechanism of fiber in oxygen environment was random nucleation; only one active nucleus on each species. There was some reaction active point (RAP), which could react with oxygen, existed random and symmetrically in carbon fiber surface. When the carbon atom in RAP reacted with oxygen, one RAP would be consumed. But the extended 2-D chain structure of fiber should be broken off by the oxidation to form several smaller species. Every species has become a new RAP. Namely with the increased of oxidation, more and more new RAP were produced, the oxidation rate of fiber increased. The self-catalytic characteristic was observed. As we knew, the amount of new produced RAP was determined by the length of 2-D molecular chain and fiber surface were, which all decreased with the increase of oxidation rate. But with the increase of oxidation rate, more and more RAPs were consumed. Namely, with the increase of oxidation rate, the amount of new produced RAP decreased and more RAPs were consumed. Thus, when the amount of consumed was equal to that of produced RAP. The reaction rate was up to maximum (weight loss = 54.8%). When the weight loss was bigger than 54.8%, the amount of consumed RAP by oxidation was bigger than that of new produced. The oxidation rate decreased with the increase of weight loss. In other words, the self-catalytic characteristic of fiber oxidation reaction could be explained through the oxidation decomposition mechanism.

Table 5.6

Kinetic model mechanism functions used for the kinetic analysis.

| Sr. No. | Name of function | Mechanism | | Common form of Function | | No. |
|---------|-------------------------|--|---------|--|--------------------------|-------|
| | | | | $F(a)$ | $G(a)$ | |
| 1. | Avrami-Erofeev equation | Random nucleation | $n = 1$ | $(1-a)$ | $-\ln(1-a)$ | A1 |
| 2. | | | $n=3/2$ | $1.5(1-a)(-\log(1-a))^{(1/3)}$ | $(-\log(1-a))^{(2/3)}$ | A3/2 |
| 3. | | | $n = 2$ | $2(1-a) [-\ln(1-a)]^{1/2}$ | $[-\ln(1-a)]^{1/2}$ | A2 |
| 4. | | | $n = 3$ | $3(1-a) [-\ln(1-a)]^{2/3}$ | $[-\ln(1-a)]^{1/3}$ | A3 |
| 5. | | | $n=4$ | $4(1-a)(-\log(1-a))^{(3/4)}$ | $(-\log(1-a))^{(1/4)}$ | A4 |
| 6. | Parabola law | D diffusion, decelerator $a-t$ curve | | $1/(2a)$ | a^2 | D1 |
| 7. | Valensi equation | 2D diffusion, decelerator $a-t$ curve | | $[-\ln(1-a)]^{-1}$ | $a + (1-a)\ln(1-a)$ | D2 |
| 8. | Jander equation | 3D diffusion, decelerator $a-t$ curve | | $1.5(1-a)^{2/3}[1-(1-a)1/3]^{-1}$ | $[1-(1-a)^{1/3}]^2$ | D3 |
| 9. | G-B equation | 3D diffusion, spherical symmetry | | $1.5 [(1-a)^{-1/3}-1]^{-1}$ | $[1-2a/3]-(1-a)^{2/3}$ | D4 |
| 10. | Z-L-T equation | 3D diffusion | | $1.5(1-a)^{4/3}[(1-a)^{-1/3}-1]^{-1}$ | $[(1-a)^{-1/3}-1]^2$ | D5 |
| 11. | Anti-Jander equation | 3D diffusion, decelerator $a-t$ curve | | $1.5(1+a)^{2/3}[(1+a)^{1/3}-1]^{-1}$ | $[(1+a)^{1/3}-1]^2$ | D6 |
| 12. | Anti G-B eqn | (3D diffusion) | | $1.5(1-(1+a)^{(-1/3)})^{-1}$ | $(1+2a/3)-(1+a)^{(2/3)}$ | D7 |
| 13. | Anti ZLT eqn | (3D diffusion) | | $1.5((1+a)^{(4/3)}(1-(1+a)^{(-1/3)})^{-1})^{-1}$ | $((1+a)^{(-1/3)}-1)^2$ | D8 |
| 14. | Reaction order | $n = 1/3$ | | $1.5(1-a)^{(1/3)}$ | $1-(1-a)^{(2/3)}$ | F1/3 |
| 15. | | $n = 3/4$ | | $4(1-a)^{(3/4)}$ | $1-(1-a)^{(1/4)}$ | F3/4 |
| 16. | | $n = 1/2$ | | $2(1-a)^{(3/2)}$ | $((1-a)^{(-1/2)}-1)$ | F1/2 |
| 17. | | $n = 2$ | | $0.5(1-a)^{-1}$ | $1-(1-a)^2$ | F2 |
| 18. | | $n = 3$ | | $1/3(1-a)^{-2}$ | $1-(1-a)^3$ | F3 |
| 19. | | $n=4$ | | $1/4(1-a)^{-3}$ | $1-(1-a)^4$ | F4 |
| 20. | Mampl power | $n = 3/2$ | | $(2/3)(a^{(-1/2)})$ | $a^{(3/2)}$ | M 3/2 |
| 21. | | $n = 2$ | | $2 a^{1/2}$ | $a^{1/2}$ | M2 |
| 22. | | $n = 3$ | | $3a^{2/3}$ | $a^{1/3}$ | M3 |
| 23. | | $n = 4$ | | $4a^{3/4}$ | $a^{1/4}$ | M4 |
| 24. | Phase boundary reaction | Decelerator $a-t$ curve (Cylindrical symmetry) | | $(1-a)^{1/2}$ | $2[1-(1-a)^{1/2}]$ | P2 |
| 25. | | (Spherical symmetry) | | $(1-a)^{2/3}$ | $3[1-(1-a)^{1/3}]$ | P3 |
| 26. | Power Law | | | $(1-a)$ | A | R1 |
| 27. | | | | $2(1-a)^{(1/2)}$ | $1-((1-a)^{(1/2)})$ | R2 |
| 28. | | | | $3(1-a)^{(2/3)}$ | $1-((1-a)^{(1/3)})$ | R3 |

Table 5.7

Kinetic parameters (E_a , A , r and Standard Deviation) obtained from Achar-Brindly-Sharp Method for oxidation of carbon fiber.

| Achar-Brindly-Sharp Method | | | | |
|---|---------------------------------|-----------------------|---------------------------|----------------------------|
| E_a (kJ mol⁻¹) | log A (min⁻¹) | r | Standard Deviation | Mechanism model no. |
| 149.0587 | 9.9741 | -0.9102 | 0.6119 | D1 |
| 190.6377 | 12.5785 | -0.971 | 0.4239 | D2 |
| 246.8179 | 15.8327 | -0.9974 | 0.1621 | D3 |
| 210.4156 | 13.2998 | -0.9867 | 0.3129 | D4 |
| 356.0249 | 23.4312 | -0.983 | 0.5996 | D5 |
| 123.7097 | 7.2034 | -0.8701 | 0.6323 | D6 |
| 131.9458 | 7.794 | -0.8852 | 0.6259 | D7 |
| 99.0016 | 5.4317 | -0.8077 | 0.6521 | D8 |
| 145.7963 | 10.4153 | -0.9826 | 0.2484 | A1 |
| 94.4468 | 6.9853 | -0.9631 | 0.2383 | A3/2 |
| 68.7721 | 5.2334 | -0.9359 | 0.2337 | A2 |
| 43.0974 | 3.4303 | -0.8615 | 0.2292 | A3 |
| 30.26 | 2.4919 | -0.7688 | 0.2271 | A4 |
| 92.824 | 6.421 | -0.8494 | 0.5204 | M3/2 |
| -19.6453 | -0.9125 | 0.4619 | 0.3404 | M1/2 |
| -38.3902 | -2.2313 | 0.7439 | 0.3112 | M1/3 |
| -47.7626 | -2.9276 | 0.8237 | 0.2967 | M1/4 |
| 72.9917 | 5.1735 | -0.9447 | 0.2287 | F1/3 |
| 118.4946 | 7.9136 | -0.9934 | 0.1239 | F3/4 |
| 200.3998 | 13.9135 | -0.9559 | 0.5555 | F1/2 |
| 255.0032 | 18.0138 | -0.9351 | 0.8723 | F2 |
| 364.2101 | 25.9134 | -0.9086 | 1.5107 | F3 |
| -72.6176 | -4.4808 | 0.5248 | 1.0628 | F4 |
| -181.825 | -11.903 | 0.6941 | 1.702 | P2 |
| -291.031 | -19.376 | 0.7463 | 2.3423 | P3 |
| 91.1928 | 6.616 | -0.9853 | 0.1428 | R1 |
| 109.394 | 7.8824 | -0.9942 | 0.1064 | R2 |
| 145.7963 | 10.4153 | -0.9826 | 0.2484 | R3 |

Table 5.8

Kinetic parameters (E_a , A , r and Standard Deviation) obtained from Satava-Sestak Method for oxidation of carbon fiber.

| Satava-Sestak Method | | | | |
|---|---------------------------------|----------------|---------------------------|----------------------------|
| E_a (kJ mol⁻¹) | log A (min⁻¹) | r | Standard Deviation | Mechanism model no. |
| 213.9032 | 13.0013 | -0.9835 | 0.1624 | D1 |
| 233.7145 | 14.1256 | -0.9906 | 0.1328 | D2 |
| 261.364 | 15.4543 | -0.9974 | 0.0781 | D3 |
| 242.632 | 14.1114 | -0.9934 | 0.1154 | D4 |
| 330.5968 | 20.4179 | -0.9953 | 0.1321 | D5 |
| 197.0206 | 10.8121 | -0.9787 | 0.1705 | D6 |
| 202.4407 | 11.2086 | -0.9803 | 0.168 | D7 |
| 181.3566 | 9.6669 | -0.973 | 0.1773 | D8 |
| 146.4908 | 9.2147 | -0.9993 | 0.0232 | A1 |
| 97.6606 | 6.1369 | -0.9993 | 0.0155 | A3/2 |
| 73.2454 | 4.6349 | -0.9993 | 0.0116 | A2 |
| 48.8303 | 3.1846 | -0.9993 | 0.0077 | A3 |
| 36.6227 | 2.4984 | -0.9993 | 0.0058 | A4 |
| 160.4274 | 9.6981 | -0.9835 | 0.1218 | M3/2 |
| 53.4758 | 3.3193 | -0.9835 | 0.0406 | M1/2 |
| 35.6505 | 2.3563 | -0.9835 | 0.0271 | M1/3 |
| 26.7379 | 1.9171 | -0.9835 | 0.0203 | M1/4 |
| 117.6615 | 7.0185 | -0.9915 | 0.0638 | F1/3 |
| 134.3579 | 7.7616 | -0.9983 | 0.0322 | F3/4 |
| 175.7747 | 10.9738 | -0.9911 | 0.0971 | F1/2 |
| 210.8009 | 13.7498 | -0.9726 | 0.2078 | F2 |
| 291.8222 | 19.8117 | -0.9321 | 0.4672 | F3 |
| 84.1236 | 5.1548 | -0.9566 | 0.1056 | F4 |
| 69.3598 | 4.3048 | -0.9315 | 0.1117 | P2 |
| 58.887 | 3.7048 | -0.909 | 0.1113 | P3 |
| 123.8501 | 7.6276 | -0.9948 | 0.0523 | R1 |
| 130.682 | 8.1061 | -0.9974 | 0.0391 | R2 |

Table 5.9

Kinetic parameters (E_a , A , r and Standard Deviation) obtained from Coats-Redfern Method for oxidation of carbon fiber.

| Coats-Redfern Method | | | | |
|---|---------------------------------|----------------|---------------------------|----------------------------|
| E_a (kJ mol⁻¹) | log A (min⁻¹) | r | Standard Deviation | Mechanism model no. |
| 211.7287 | 9.1475 | -0.9811 | 0.377 | D1 |
| 232.5621 | 10.3509 | -0.9893 | 0.3088 | D2 |
| 261.638 | 11.7793 | -0.997 | 0.183 | D3 |
| 241.9396 | 10.3702 | -0.9925 | 0.2688 | D4 |
| 334.4426 | 16.9516 | -0.995 | 0.302 | D5 |
| 193.9751 | 6.8845 | -0.9754 | 0.3956 | D6 |
| 199.6749 | 7.3054 | -0.9774 | 0.39 | D7 |
| 177.503 | 5.6648 | -0.9686 | 0.4113 | D8 |
| 140.8385 | 5.0194 | -0.9991 | 0.0538 | A1 |
| 89.489 | 1.5685 | -0.999 | 0.0361 | A3/2 |
| 63.8143 | -0.2053 | -0.9989 | 0.0272 | A2 |
| 38.1396 | -2.0558 | -0.9986 | 0.0184 | A3 |
| 25.3022 | -3.0475 | -0.9981 | 0.014 | A4 |
| 155.494 | 5.5852 | -0.9802 | 0.2835 | M3/2 |
| 43.0247 | -1.8292 | -0.9704 | 0.0966 | M1/2 |
| 24.2799 | -3.2204 | -0.9582 | 0.0655 | M1/3 |
| 14.9074 | -4.0036 | -0.9376 | 0.0499 | M1/4 |
| 110.5219 | 2.6227 | -0.9889 | 0.15 | F1/3 |
| 128.0796 | 3.4875 | -0.9978 | 0.0771 | F3/4 |
| 171.6332 | 6.9435 | -0.9899 | 0.2213 | F1/2 |
| 208.4663 | 9.8829 | -0.9694 | 0.476 | F2 |
| 293.6675 | 16.2348 | -0.9269 | 1.0733 | F3 |
| 75.2537 | 0.4464 | -0.9401 | 0.2463 | F4 |
| 59.7282 | -0.5878 | -0.9005 | 0.2603 | P2 |
| 48.7151 | -1.3475 | -0.8613 | 0.2593 | P3 |
| 117.0297 | 3.279 | -0.9932 | 0.1236 | R1 |
| 124.214 | 3.8066 | -0.9966 | 0.093 | R2 |
| 99.2594 | 1.9621 | -0.9782 | 0.1901 | R3 |

Table 5.10

Kinetic parameters (E_a , A , r and Standard Deviation) obtained from Madhusudanan-Krishnan-Ninan Method for oxidation of carbon fiber.

| Madhusudanan-Krishnan-Ninan Method | | | | |
|---|---------------------------------|----------------|---------------------------|----------------------------|
| E_a (kJ mol⁻¹) | log A (min⁻¹) | r | Standard Deviation | Mechanism model no. |
| 212.0327 | 11.9883 | -0.9812 | 0.3769 | D1 |
| 232.8451 | 13.27 | -0.9894 | 0.3087 | D2 |
| 261.8916 | 14.7965 | -0.997 | 0.1829 | D3 |
| 242.2131 | 13.3222 | -0.9925 | 0.2686 | D4 |
| 334.6227 | 20.1735 | -0.995 | 0.3021 | D5 |
| 194.2971 | 9.6524 | -0.9755 | 0.3955 | D6 |
| 199.9911 | 10.0974 | -0.9775 | 0.3898 | D7 |
| 177.8416 | 8.3588 | -0.9688 | 0.4112 | D8 |
| 141.2141 | 7.5209 | -0.9991 | 0.0538 | A1 |
| 89.9165 | 3.6936 | -0.999 | 0.036 | A3/2 |
| 64.2678 | 1.6401 | -0.9989 | 0.0272 | A2 |
| 38.619 | -0.6339 | -0.9986 | 0.0184 | A3 |
| 25.7946 | -1.9601 | -0.9982 | 0.014 | A4 |
| 155.8549 | 8.1691 | -0.9803 | 0.2834 | M3/2 |
| 43.4992 | -0.3085 | -0.9711 | 0.0965 | M1/2 |
| 24.7733 | -2.1663 | -0.9599 | 0.0653 | M1/3 |
| 15.4103 | -3.3408 | -0.9416 | 0.0498 | M1/4 |
| 110.9281 | 4.9229 | -0.989 | 0.1499 | F1/3 |
| 128.4681 | 5.9101 | -0.9978 | 0.077 | F3/4 |
| 171.9777 | 9.6096 | -0.99 | 0.2214 | F1/2 |
| 208.7736 | 12.7108 | -0.9696 | 0.4761 | F2 |
| 293.8888 | 19.3483 | -0.9271 | 1.0734 | F3 |
| 75.6956 | 2.428 | -0.9409 | 0.2462 | F4 |
| 60.1858 | 1.2029 | -0.902 | 0.2602 | P2 |
| 49.1839 | 0.2753 | -0.8637 | 0.2592 | P3 |
| 117.4294 | 5.6266 | -0.9933 | 0.1235 | R1 |
| 124.6065 | 6.2037 | -0.9966 | 0.0929 | R2 |
| 99.677 | 4.1731 | -0.9785 | 0.19 | R3 |

5.2.4 Determination of most probable mechanism function and calculation of Activation energy, Pre-exponential factor for oxidation of SiC nanowire coated carbon fibers

The result of most probable mechanism functions during oxidation process is tabulated in Tables 5.11-5.14. From the data in these tables, it can be seen clearly that only function D5 (D5 stood for 3D diffusion, Zhuravlev–Lesokhin–Tempel’man (ZLT) equation ¹⁸⁶) satisfied the above-mentioned conditions in case of Achar-Brindley-Sharp-Wendworth equation, Satava-Sestak equation and Madhusudanan-Krishnan-Ninan equation. Thus the possible mechanism function

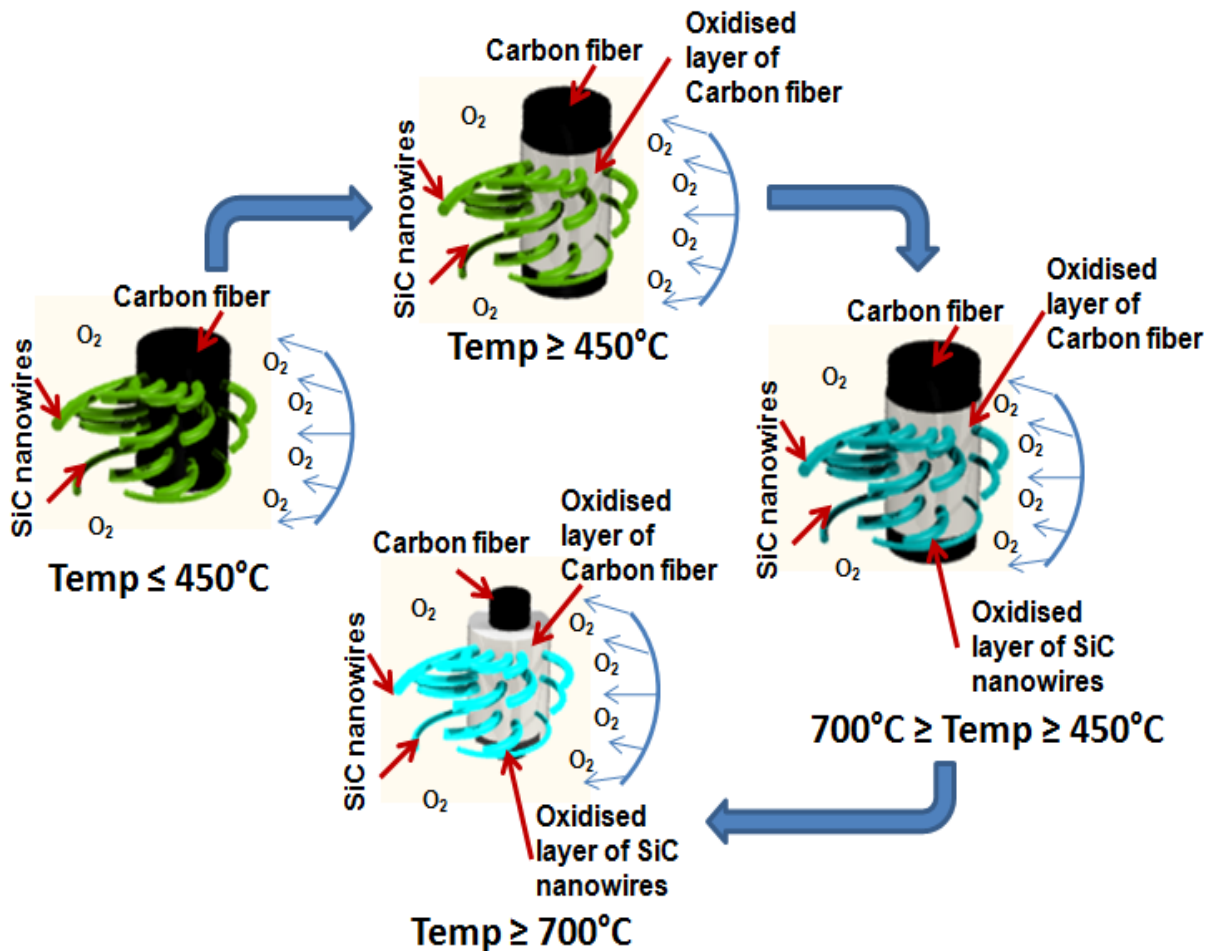


Fig. 5.17 Pictorial depiction of oxidation of SiC nanowires coated carbon fibers at different temperature region (For representation purpose only few SiC nanowires were shown over the surface of carbon fibers, actually they were densely grown over carbon fiber).

was function D5 as it is satisfying one differential and two integral equations. Therefore it can be stated that the mechanism function with differential form $f(a) = 1.5(1-a)^{4/3}[(1-a)^{-1/3}-1]^1$ and integral form $g(a) = [(1-a)^{-1/3}-1]^2$ belongs to the mechanism of 3D diffusion reaction following ZLT equation. It was concluded that the kinetic equation for the thermal decomposition of SiC nanowire coated carbon fiber was $da/dT = (A/\beta)\exp(-E_a/RT)(1.5(1-a)^{4/3}[(1-a)^{-1/3}-1]^{-1})$. The kinetic parameters were: $\log A = 8.577 \text{ min}^{-1}$ and $E_a = 190.41 \text{ kJmol}^{-1}$.

The oxidation mechanism of SiC nanowire coated carbon fiber was 3D diffusion, ZLT model. The 3D diffusion reaction mechanism assumes that the reaction process was diffusion-controlled mechanism. The 3D diffusion obeys the ZLT model. The whole oxidation mechanism is shown in Fig 5.17. In the ZLT model it is assumed that reaction zone is not only localized on the outer boundaries of particles but also penetrates in to particles and thus it is localized both on outer and inner surfaces of particles. The oxidative gas has the accessibility at outer and inner layer of coating due to porous nature of SiC coating. The SEM images confirm that there were several pores present on the SiC nanowire coating surface which acts as a channel for oxygen diffusion. Due to exposure of inner and outer surface to the oxidative gas the reaction zone moves from outer surface to inner surfaces. There was some ACA, which could react with oxygen, existed in coating/fiber interface. When the oxygen diffused through coating and reacted with ACA, one ACA would be consumed. But the extended 2D chain structure of fiber should be broken off by the oxidation to form several smaller species. Every species has become a new ACA. Namely with the increase of oxidation, more and more new ACA were produced, the oxidation rate of fiber increased and it leads to the self-catalytic characteristic of oxidation as discussed in previous section. Two peaks were observed in the DTG curve as discussed in the previous section. Oxidation process at second peak was attributed to the oxidation of carbon fiber and

oxidation of SiC nanowires. The ZLT 3D diffusion model for oxidation supports the statement. When oxidative gases diffuse through SiC nanowires, the surface of SiC nanowires were also prone to oxidation at higher temperature. At around 700 °C the oxidation SiC nanowires contributes with the oxidation of carbon fibers to the overall oxidation process. Thus the reaction process was diffusion-controlled mechanism. In a word, the self-catalytic characteristic of SiC nanowire coated carbon fiber oxidation reaction could be explained through the ZLT model 3D diffusion oxidation mechanism.

Table 5.11

Kinetic parameters (E_a , A , r and Standard Deviation) obtained from Achar-Brindly-Sharp Method for oxidation of SiC nanowire coated carbon fiber.

| Achar-Brindly-Sharp Method | | | | |
|---|---------------------------------|----------------|---------------------------|----------------------------|
| E_a (kJ mol⁻¹) | log A (min⁻¹) | r | Standard Deviation | Mechanism model no. |
| 109.8601 | 6.346 | -0.9182 | 0.6364 | D1 |
| 126.8744 | 7.1797 | -0.9512 | 0.5528 | D2 |
| 146.5358 | 7.8325 | -0.9751 | 0.4474 | D3 |
| 133.6075 | 6.9734 | -0.9611 | 0.5155 | D4 |
| 185.3208 | 10.4099 | -0.9943 | 0.2676 | D5 |
| 94.8219 | 4.3615 | -0.8865 | 0.6645 | D6 |
| 99.7253 | 4.6977 | -0.8981 | 0.6556 | D7 |
| 80.1116 | 3.3529 | -0.8412 | 0.6915 | D8 |
| 69.9056 | 4.5263 | -0.9592 | 0.2766 | A1 |
| 37.9877 | 2.6067 | -0.8946 | 0.2548 | A3/2 |
| 22.0287 | 1.6099 | -0.7702 | 0.2449 | A2 |
| 6.0697 | 0.5621 | -0.3267 | 0.2357 | A3 |
| -1.9098 | 0.0012 | 0.1101 | 0.2315 | A4 |
| 70.4904 | 4.1731 | -0.8647 | 0.5498 | M3/2 |
| -8.2491 | -0.4001 | 0.2764 | 0.3851 | M1/2 |
| -21.3724 | -1.2588 | 0.6237 | 0.3596 | M1/3 |
| -27.934 | -1.7251 | 0.7339 | 0.3472 | M1/4 |
| 44.0489 | 2.632 | -0.8294 | 0.3983 | F1/3 |
| 60.2093 | 3.2799 | -0.9301 | 0.3194 | F3/4 |
| 89.2981 | 5.514 | -0.9848 | 0.2117 | F1/2 |
| 108.6905 | 7.1037 | -0.991 | 0.1967 | F2 |
| 147.4755 | 9.9821 | -0.9871 | 0.3213 | F3 |
| -85.2343 | -5.181 | 0.715 | 1.1189 | F4 |
| 50.5131 | 3.2376 | -0.8801 | 0.3659 | P2 |
| 56.9773 | 3.6672 | -0.9162 | 0.3345 | P3 |
| 69.9056 | 4.5263 | -0.9592 | 0.2766 | R1 |
| 50.5131 | 2.9366 | -0.8801 | 0.3659 | R2 |
| 56.9773 | 3.1901 | -0.9162 | 0.3345 | R3 |

Table 5.12

Kinetic parameters (E_a , A , r and Standard Deviation) obtained from Satava-Sestak Method for oxidation of SiC nanowire coated carbon fiber.

| Satava-Sestak Method | | | | |
|---|---------------------------------|----------------|---------------------------|----------------------------|
| E_a (kJ mol⁻¹) | log A (min⁻¹) | r | Standard Deviation | Mechanism model no. |
| 149.7531 | 7.6355 | -0.985 | 0.1607 | D1 |
| 159.1528 | 7.97 | -0.9897 | 0.1414 | D2 |
| 170.3296 | 8.0704 | -0.994 | 0.115 | D3 |
| 162.8497 | 7.5659 | -0.9913 | 0.1327 | D4 |
| 194.9178 | 9.7301 | -0.9988 | 0.0575 | D5 |
| 139.8036 | 5.9954 | -0.9809 | 0.1702 | D6 |
| 143.0142 | 6.2167 | -0.9823 | 0.1672 | D7 |
| 130.4779 | 5.353 | -0.9761 | 0.1783 | D8 |
| 91.0561 | 4.8902 | -0.997 | 0.0434 | A1 |
| 60.7041 | 3.3232 | -0.997 | 0.0289 | A3/2 |
| 45.5281 | 2.5783 | -0.997 | 0.0217 | A2 |
| 30.352 | 1.8922 | -0.997 | 0.0145 | A3 |
| 22.764 | 1.5935 | -0.997 | 0.0109 | A4 |
| 112.3148 | 5.7124 | -0.985 | 0.1205 | M3/2 |
| 37.4383 | 2.1009 | -0.985 | 0.0402 | M1/2 |
| 24.9589 | 1.6103 | -0.985 | 0.0268 | M1/3 |
| 18.7191 | 1.4083 | -0.985 | 0.0201 | M1/4 |
| 79.7781 | 3.9817 | -0.9899 | 0.0699 | F1/3 |
| 86.5899 | 3.9977 | -0.9948 | 0.0541 | F3/4 |
| 100.8504 | 5.2282 | -0.9993 | 0.0227 | F1/2 |
| 111.7587 | 6.2439 | -0.9991 | 0.0293 | F2 |
| 136.5215 | 8.1774 | -0.9927 | 0.1019 | F3 |
| 46.7996 | 2.6423 | -0.9294 | 0.114 | F4 |
| 82.4093 | 4.3283 | -0.9921 | 0.0639 | P2 |
| 85.1648 | 4.5071 | -0.994 | 0.0575 | P3 |
| 74.8766 | 3.8406 | -0.985 | 0.0803 | R1 |
| 82.4093 | 4.0273 | -0.9921 | 0.0639 | R2 |
| 85.1648 | 4.0301 | -0.994 | 0.0575 | R3 |

Table 5.13

Kinetic parameters (E_a , A , r and Standard Deviation) obtained from Coats-Redfern Method for oxidation of SiC nanowire coated carbon fiber.

| Coats-Redfern Method | | | | |
|---|---------------------------------|----------------|---------------------------|----------------------------|
| E_a (kJ mol⁻¹) | log A (min⁻¹) | r | Standard Deviation | Mechanism model no. |
| 143.0088 | 3.3747 | -0.9812 | 0.3782 | D1 |
| 152.8934 | 3.7647 | -0.987 | 0.3338 | D2 |
| 164.6469 | 3.9268 | -0.9925 | 0.273 | D3 |
| 156.7811 | 3.3815 | -0.9891 | 0.3138 | D4 |
| 190.5035 | 5.7083 | -0.9985 | 0.1394 | D5 |
| 132.546 | 1.6718 | -0.9756 | 0.4001 | D6 |
| 135.9222 | 1.9139 | -0.9776 | 0.3933 | D7 |
| 122.7392 | 0.966 | -0.9692 | 0.4188 | D8 |
| 81.2836 | 0.168 | -0.9951 | 0.1079 | A1 |
| 49.3657 | -1.7921 | -0.9937 | 0.0746 | A3/2 |
| 33.4067 | -2.8335 | -0.9918 | 0.0579 | A2 |
| 17.4478 | -3.9874 | -0.9848 | 0.0413 | A3 |
| 9.4683 | -4.6887 | -0.9679 | 0.033 | A4 |
| 103.6391 | 1.1869 | -0.9796 | 0.2857 | M3/2 |
| 24.8996 | -3.5285 | -0.9575 | 0.1007 | M1/2 |
| 11.7763 | -4.5363 | -0.9146 | 0.0699 | M1/3 |
| 5.2147 | -5.2314 | -0.7892 | 0.0545 | M1/4 |
| 69.4237 | -0.8665 | -0.9839 | 0.1691 | F1/3 |
| 76.5869 | -0.7722 | -0.9918 | 0.1328 | F3/4 |
| 91.5832 | 0.6022 | -0.9989 | 0.0579 | F1/2 |
| 103.0543 | 1.7138 | -0.999 | 0.0631 | F2 |
| 129.0946 | 3.8321 | -0.9915 | 0.2272 | F3 |
| 34.7439 | -2.7402 | -0.8649 | 0.2707 | F4 |
| 72.1907 | -0.4888 | -0.9874 | 0.1554 | P2 |
| 75.0884 | -0.2785 | -0.9904 | 0.1406 | P3 |
| 64.2693 | -1.0686 | -0.9758 | 0.1932 | R1 |
| 72.1907 | -0.7898 | -0.9874 | 0.1554 | R2 |
| 75.0884 | -0.7557 | -0.9904 | 0.1406 | R3 |

Table 5.14

Kinetic parameters (E_a , A , r and Standard Deviation) obtained from Madhusudanan-Krishnan-Ninan Method for oxidation of SiC nanowire coated carbon fiber.

| Madhusudanan-Krishnan-Ninan Method | | | | |
|---|---------------------------------|----------------|---------------------------|----------------------------|
| E_a (kJ mol⁻¹) | log A (min⁻¹) | r | Standard Deviation | Mechanism model no. |
| 143.4317 | 5.8894 | -0.9813 | 0.3778 | D1 |
| 153.3063 | 6.335 | -0.9872 | 0.3335 | D2 |
| 165.0479 | 6.5586 | -0.9925 | 0.2727 | D3 |
| 157.19 | 5.9726 | -0.9892 | 0.3135 | D4 |
| 190.8784 | 8.4615 | -0.9985 | 0.1391 | D5 |
| 132.9794 | 4.1234 | -0.9759 | 0.3998 | D6 |
| 136.3523 | 4.3864 | -0.9778 | 0.393 | D7 |
| 123.1825 | 3.3538 | -0.9695 | 0.4185 | D8 |
| 81.7689 | 2.2142 | -0.9952 | 0.1076 | A1 |
| 49.8832 | -0.1571 | -0.9939 | 0.0743 | A3/2 |
| 33.9403 | -1.5181 | -0.9921 | 0.0576 | A2 |
| 17.9975 | -3.1957 | -0.9859 | 0.041 | A3 |
| 10.0261 | -4.3748 | -0.9718 | 0.0327 | A4 |
| 104.1017 | 3.4343 | -0.9798 | 0.2854 | M3/2 |
| 25.4418 | -2.4516 | -0.9595 | 0.1004 | M1/2 |
| 12.3318 | -4.0542 | -0.9221 | 0.0696 | M1/3 |
| 5.7768 | -5.3589 | -0.8202 | 0.0542 | M1/4 |
| 69.921 | 1.0494 | -0.9842 | 0.1688 | F1/3 |
| 77.0769 | 1.2247 | -0.9919 | 0.1324 | F3/4 |
| 92.058 | 2.7472 | -0.9989 | 0.0577 | F1/2 |
| 103.5175 | 3.9565 | -0.999 | 0.0632 | F2 |
| 129.5315 | 6.2618 | -0.9916 | 0.2275 | F3 |
| 35.2761 | -1.3928 | -0.8687 | 0.2704 | F4 |
| 72.6851 | 1.4594 | -0.9876 | 0.1551 | P2 |
| 75.5799 | 1.7021 | -0.9906 | 0.1403 | P3 |
| 64.7717 | 0.7835 | -0.9763 | 0.1929 | R1 |
| 72.6851 | 1.1583 | -0.9876 | 0.1551 | R2 |
| 75.5799 | 1.225 | -0.9906 | 0.1403 | R3 |

5.3. Oxidation study of bare carbon fabric and SiC impregnated carbon fabric in presence of atmospheric environment:

5.3.1 Materials and methods

The oxidation resistive properties of bare carbon fabric and SiC impregnated carbon fabric were examined in atmospheric oxidative environment from room temperature to 1400 °C using a thermo gravimetric (Setsys Evolution, Setaram, France) equipment. The preparation of SiC impregnated carbon fabric is described in Chapter 4. The surface morphology of SiC impregnated carbon fabric and elemental distribution of SiC impregnated carbon fabric before and after oxidation were characterized by SEM.

Non-isothermal oxidation tests were carried out at the heating rate of 5 °C/min up to 1400 °C for bare carbon fabric and at the heating rate of 2.5, 5, 10, 15 °C/min up to 1400 °C for SiC impregnated carbon fabric. The weight changes of the specimens corresponding to oxidation were recorded continuously in TG mode.

5.3.1.1 Kinetic Study

The oxidation degradation of material is a solid-state process of the type: A(solid) + B(gas)¹⁸⁷.

The kinetics of such reactions is described by various equations taking into account the special features of their mechanisms. All kinetic studies were assumed to be based on the following equations:

$$\frac{d\alpha}{dt} = kf(\alpha) \quad (5.10)$$

$$k = Ae^{-\frac{E\alpha}{RT}} \quad (5.11)$$

where α is the extent of conversion and is equal to $(m_0 - m_t)/(m_0 - m_f)$; m_0 , m_t , and m_f were the initial mass of sample, current mass of sample at temperature t , and final mass at a temperature at which the mass loss is approximately unchanged, respectively. $f(\alpha)$ is a function depending on the particular decomposition mechanism and is referred to as the difficult form. The pre-exponential factor, A (min^{-1}) is assumed to be independent of temperature, E_a is the activation energy (kJ mol^{-1}), R is the gas constant ($8.314 \text{ J K}^{-1} \text{ mol}^{-1}$), and k is the rate constant.

Various scientists suggested different ways to use these equations to find out the kinetics and mechanism of particular process. The kinetics of solid-state oxidation reactions can be described by various equations taking into account the special features of their mechanism. In kinetic study of oxidation of SiC nanowire/carbon fiber/ SiC matrix composite Ozawa and KAS equations were used to determine the activation energy (E_a) of the oxidation reaction. These methods were well described and widely used in the literatures, which provides reliable results. Therefore, these methods were selected for kinetic analysis of the oxidation of the SiC carbon composites. The equations used for E_a calculation were

Ozawa equation (Ozawa, 1965):

$$\ln \beta = \ln\left(\frac{0.0048AE_\alpha}{g(\alpha)R}\right) - 1.0516 (E_\alpha/RT) \quad (5.12)$$

KAS equation (Kissinger, 1957; Akahira & Sunose, 1971):

$$\ln(\beta|T^2) = \ln\left(\frac{AR}{g(a)R}\right) - \frac{E_a}{RT} \quad (5.13)$$

All other parameters were the same as given in equations (5.10) and (5.11). The Arrhenius parameters, together with the reaction model, were sometimes called the kinetic triplet. $g(a)$ is the integral form of $f(a)$, which is the reaction model that depends on the reaction mechanism. According to the above-mentioned equations, the plots of $\ln\beta$ versus $1000/T$ (eq. (5.12)) and $\ln(\beta/T^2)$ versus $1000/T$ (eq. (5.13)) corresponding to different extents of conversion “ a ” can be obtained by a linear regression of the least-square method. The activation energy E_a can be evaluated from the slopes of the straight lines with better linear correlation coefficients (r^2), respectively. The determination of most probable mechanism function has been discussed in next section. The activation energy values were calculated at the heating rates of 5, 10, 15, and 20 °C min^{-1} via the mentioned methods in the α range of 0.2–0.8.

5.3.1.2 Determination of the Most Probable Mechanism Function

In this present work, the most probable mechanism function can be determined by using the equations as stated in Table 5.6.

$$\ln g(a) = \left[\ln \frac{AE_a}{R} + \ln \frac{e^{-x}}{x^2} + \ln h(x) \right] - \ln \beta \quad (5.14)$$

where, x is E_a/RT and

$$h(x) = \frac{x^4 + 18x^3 + 88x^2 + 96x}{x^4 + 20x^3 + 120x^2 + 240x + 120} \quad (5.15)$$

which is expressed by the fourth Senum and Yang approximation¹⁸⁸. The plots of $\ln g(a)$ versus $\ln\beta$ were carried out by using a linear regression of the least-square method. To determine the

most probable mechanism function, the degrees of conversion α corresponding to four heating rates taken at the same temperature (Temperatures at 1000 and 1010 °C were selected for oxidation of SiC carbon composite) were substituted into the left side of eq. (5.14) for all 26 types of mechanism functions as presented in Table 5.6. If the mechanism functions according to equation (5.15) exhibits the slope and the linear correlation coefficient r^2 close to -1.0000 and unity, respectively, then the function $g(a)$ is the most probable mechanism function. The results of the most probable mechanism functions during the oxidation process were tabulated in Table 5.19.

5.3.2 Results and discussion

5.3.2.1 Thermo gravimetric analysis and morphological studies

From the oxidation weight-loss curve (Fig. 5.18) it is obvious that the oxidation process of bare carbon fabrics began from 600 °C and the weight loss reached a maximum at about 825 °C; at this temperature there was 100% weight loss (Table 5.15). Whereas in case of SiC impregnated carbon fabric the oxidation process starts from 490 °C. The oxidation occurred in two steps, first it was oxidized 17% at 660 °C and the weight loss reached a maximum value of about 40-42% at 800 °C in next step. After that with increase in temperature the weight increased which may be caused by oxidation of the SiC layer.

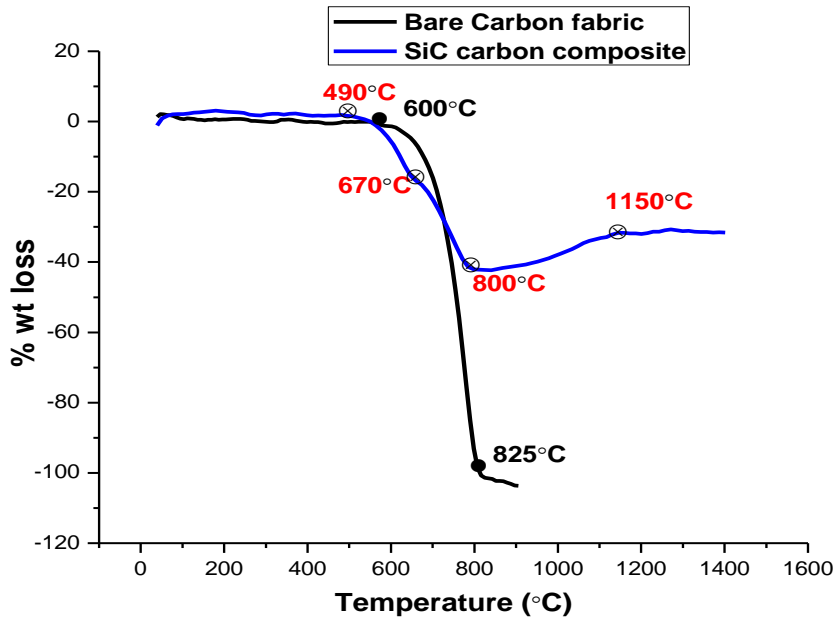


Fig. 5.18 Thermogravimetric analysis of bare carbon fabric and SiC carbon composites in atmospheric environment.

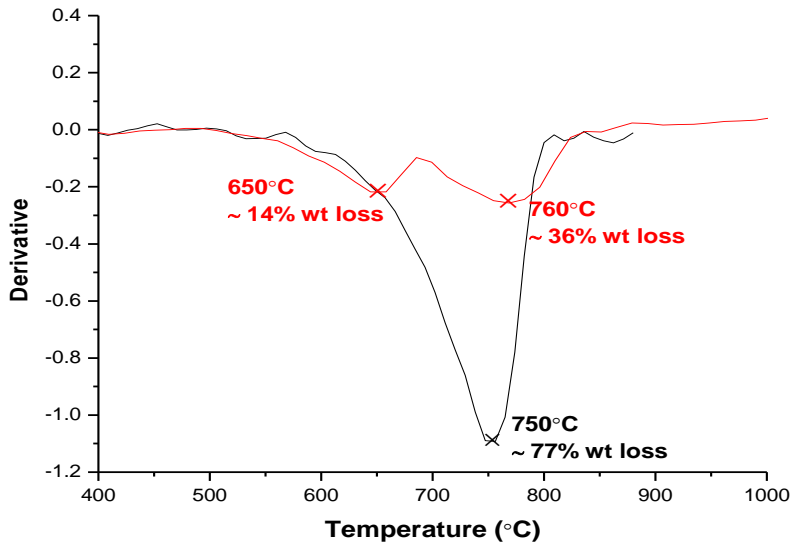


Fig. 5.19 The DTG curve of bare carbon fabric and SiC carbon composites in atmospheric environment.

Table 5.15

Thermal Oxidation behaviors of carbon fabric and SiC impregnated carbon composite in atmospheric oxidation environment.

| Environment | Sample | Onset temperature (°C) | Temperature at which different wt% loss occurred (°C) | Residue yield (%) (particular temperature) |
|------------------------------|----------------------------------|-------------------------------|--|---|
| Atmospheric condition | Carbon fabric | 600 | 680 (10%) | 0 (825°C) |
| | SiC impregnated carbon composite | 490 | 660 (17%) | 40-42 (800°C) |
| | | | 800 (42%) | |
| | | | 1150 (32%) | |

The DTG curve (Fig. 5.19) also supports the two step oxidation phenomena. There were two troughs in the DTG curve at 650 °C and 760 °C corresponding to 14% and 36% weight loss respectively. The second peak position was almost at the same peak position of carbon fiber (750 °C). It indicates that in second step oxidation of carbon fibers occurred.

The oxidation of SiC impregnated carbon fabric starts much before the oxidation of carbon fiber that may be due to free carbon present in the impregnated SiC. The elemental analysis by EDX spectra (Fig. 5.20, Table 5.16) show that there was around 15-20 % free carbon was present with SiC matrix in composite before oxidation.

In the first step from 490 to 670 °C the oxidation of these free carbon present with SiC occurred and it corresponds to the about 17 % weight loss of the composite. This weight loss agrees well with the free carbon concentration calculated from the EDX spectra. In the second step (670-800

°C) the oxidation of carbon fibers occurred. After 800 °C, the weight gain was observed due to the oxidation of SiC.

Table 5.16

Elemental analysis of SiC carbon composites before oxidation.

| Element | Wt % | At % |
|---------|-------|-------|
| C | 37.84 | 52.66 |
| O | 11.56 | 10.91 |
| Si | 50.60 | 36.44 |

The SEM micrograph of oxidized surfaces of composite at different stage of oxidation is shown in Fig. 5.21. There were microcracks and micropores present on the surface through which oxidation phenomena starts. Through cracks and pores oxygen penetrates to the matrix and oxidises first the free carbon present with the SiC matrix. These free carbon present with SiC matrix were more prone to oxidation.

It was observed from the micrograph after oxidation at 700 °C that the microcracks and micropores got widen

due to oxidation of carbon and there were generation of more microcracks, pits and micropores on the surface of SiC carbon composite during oxidation. The microcracks/pores propagate through the SiC matrix. These microcracks/pores were responsible for oxidation of carbon which are inside the matrix. The carbon fibers present on the surface also got partially oxidized. The

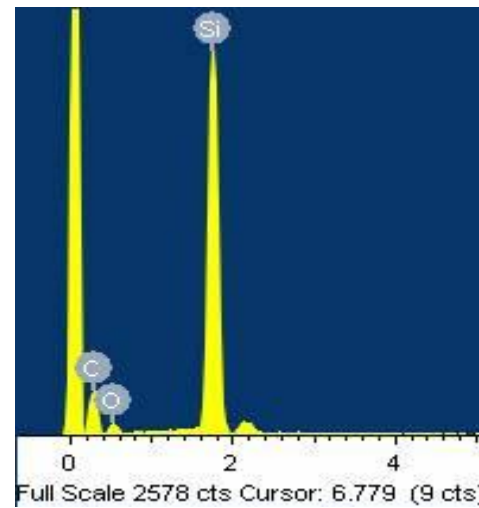


Fig. 5.20 EDX data of the elements in SiC carbon composites before oxidation.

micrograph at 800 °C shows that the carbon fibers which were inside the matrix also got oxidized due to the widening of pores and cracks.

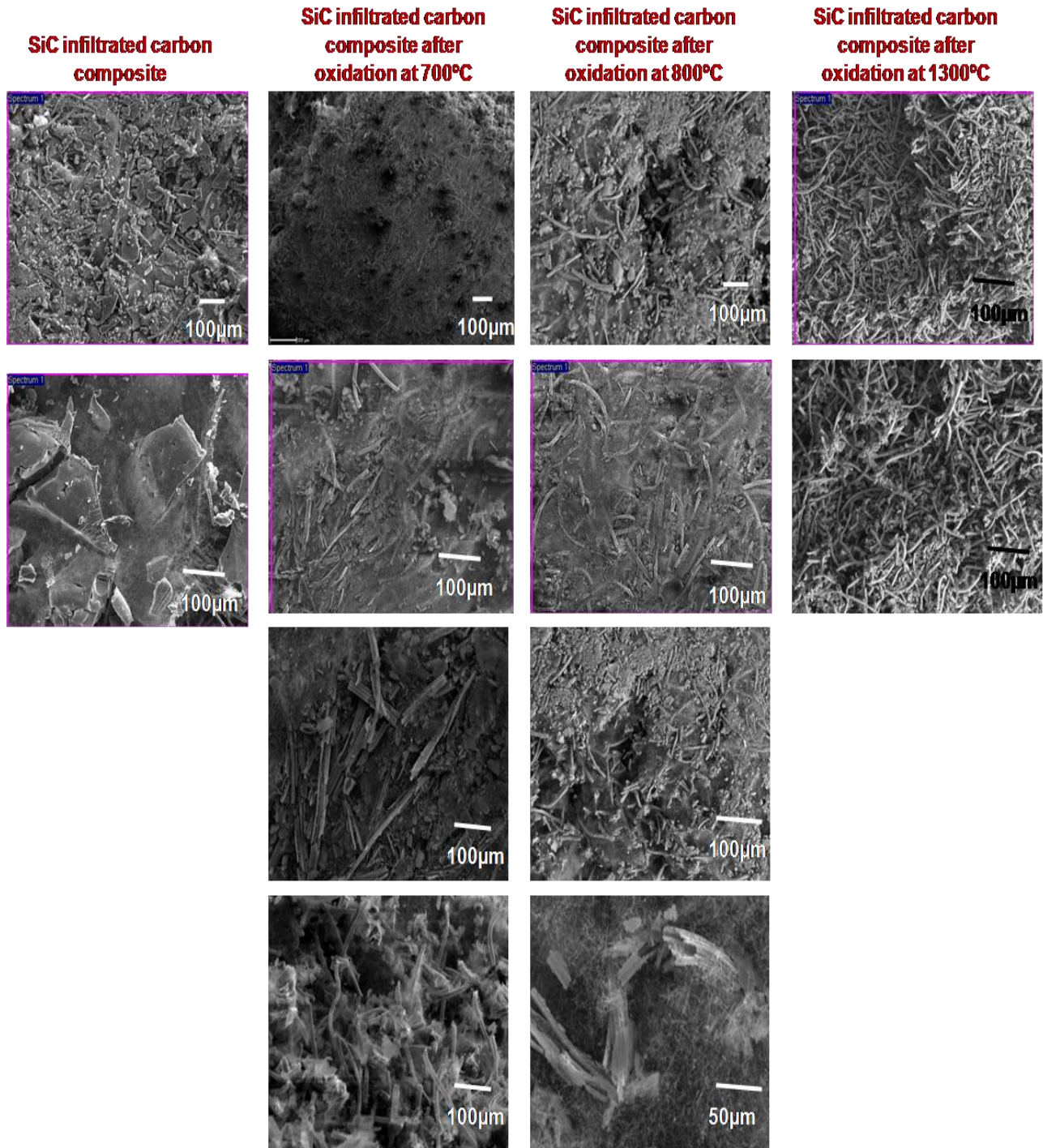


Fig. 5.21 The SEM micrograph of oxidized surfaces of composite at different stage of oxidation.

Due to widening of pores and cracks the carbon fibers which were deep in matrix were also accessible for oxidation. The second stage of oxidation arises due to channeling of oxygen through these widen microcracks, pits and micropores present on the surface at high temperature. In case of oxidation in oxidative environment it was observed that there was self healing of microcracks due to oxidation of SiC^{178, 189}. The oxidation of SiC was observed as the weight gain in the TG curve. The formation of silica occurred due to oxidation of SiC. It can be inferred that the formation of SiO₂ over the surface of composite, reduces the oxidation of carbon fiber and SiC by forming an inert layer. This phenomenon was observed as weight gain in the TG curve after 800 °C. After reaching to oxidation temperature 1150 °C there was no further weight gain. It means after that the silica layer formed over the composite surface stops the oxidation of SiC as well as carbon fiber. The micrograph at 1300 °C shows that there was no oxidized carbon present on the surface and its EDX spectra (Fig. 5.22, Table 5.17) shows that there was formation of silica layer over the surface.

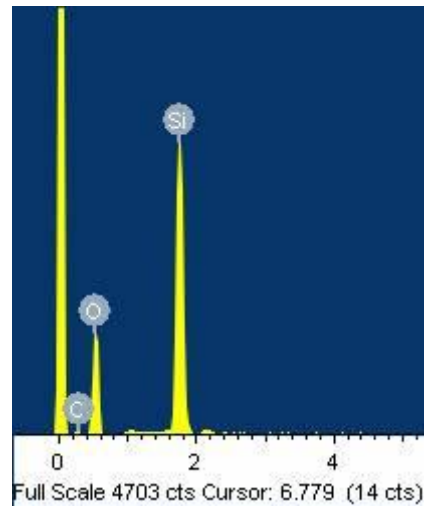


Fig. 5.22 EDX data of the elements in SiC carbon composites after oxidation at 1300°C.

Table 5.17

Elemental analysis of SiC carbon composites after oxidation at 1300°C.

| Element | Wt % | At % |
|---------|-------|-------|
| C | 6.22 | 9.68 |
| O | 55.46 | 64.81 |
| Si | 38.31 | 25.50 |

5.3.2.2 Calculation of Activation Energy Values and determination of the Most Probable Mechanism Function

The TG and DTG curves of the oxidation of SiC nanowire/carbon fiber/ SiC matrix composite for all four heating rates were illustrated in Fig. 5.23 (a) & (b). All curves were approximately in same shape and indicate that the maximum temperature and the mass loss increase when increasing the heating rate. The calculated results from Ozawa and KAS methods according to four TG measurements were presented in Fig. 5.24– 5.25. The activation energy values E_a for the whole oxidation process is tabulated in Table 5.18, respectively. The average activation energy values from the conversion factor from 0.1 to 0.35 of Ozawa and KAS methods were 82.87 and 62.80 kJ mol⁻¹, respectively. The activation energy of the oxidation is reliable via the small difference of the calculated values from two methods (~20 kJ mol⁻¹).

According to Table 5.19, only the slopes determined from the function no. 21 were close to - 0.1000 for two selected temperatures (1000 and 1010 °C) and the correlation coefficients were very close to each other. Hence, the most probable mechanism function for oxidation step is in the integral form $g(a) = a^{1/2}$ and the differential form $f(a) = 2 a^{-1/2}$, which is the Mampl power. This is a special case of Mampl Power model or the second order reaction.

The TG/DTG behavior of SiC carbon composite has been discussed. The kinetics of oxidation was calculated using Ozawa and KAS equations. The activation energy values from both methods were close to each other. The mechanism of oxidation of SiC carbon composite was found to be Mampl second order reaction. The SiC carbon composite has the improved oxidation resistance property than carbon composite.

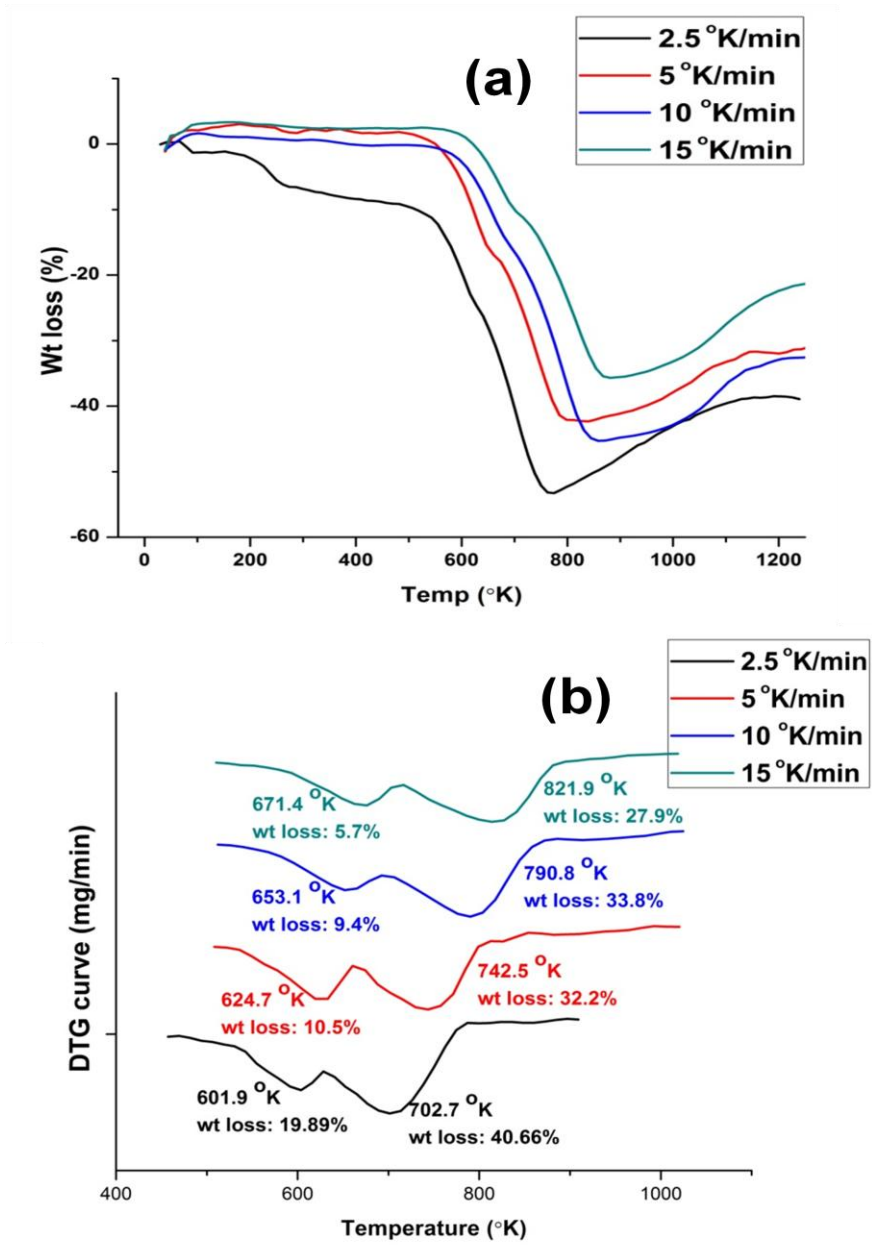


Fig. 5.23 (a) & (b) TG/DTG curve of oxidation of SiC carbon composite at different rates of 2.5, 5, 10 and 15 °C/min.

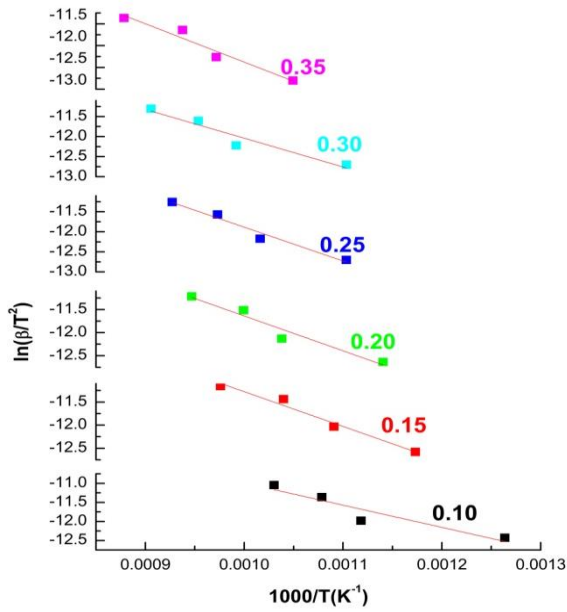


Fig. 5.24 KAS plot for the oxidation of SiC carbon composite.

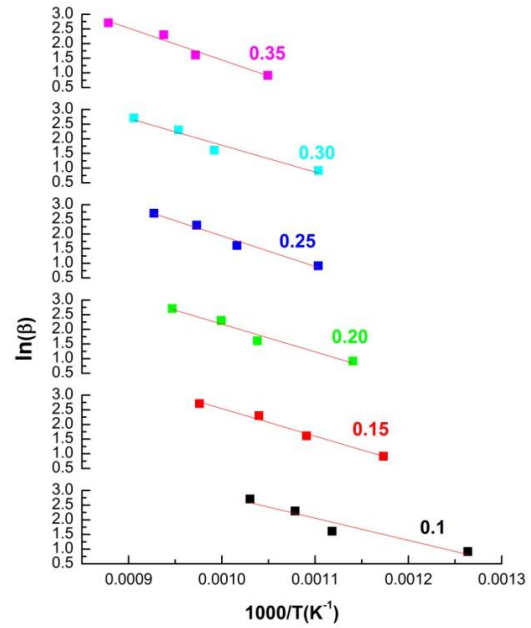


Fig. 5.25 Ozawa plot for the oxidation of SiC carbon composite.

Table 5.18

Activation Energy values and correlation coefficients (r^2) calculated using KAS and Ozawa method for oxidation of SiC carbon composite.

| α | KAS method | | Ozawa Method | |
|----------|-------------------------|---------|-------------------------|---------|
| | E_a/kJmol^{-1} | r^2 | E_a/kJmol^{-1} | r^2 |
| 0.1 | 48.42±5.89 | 0.8939 | 66.12±6.32 | 0.9318 |
| 0.15 | 62.59±3.45 | 0.97627 | 82.11±3.15 | 0.98506 |
| 0.2 | 62.81±5.09 | 0.94991 | 82.78±5.44 | 0.96653 |
| 0.25 | 70.18±4.21 | 0.97196 | 91.01±4.50 | 0.9807 |
| 0.30 | 59.59±5.59 | 0.93411 | 80.04±6.01 | 0.95689 |
| 0.35 | 73.22±5.66 | 0.95425 | 95.16±5.43 | 0.96985 |
| Average | 62.80±4.98 | 0.8939 | 82.87±5.29 | 0.9318 |

Table 5.19

Most probable mechanism function $g(a)$, slopes, and correlation coefficients of linear regression (r^2) at 1000 and 1010 °C.

| Temperature (°C) | Mechanism No. | Slopes | r^2 |
|------------------|----------------|------------------|----------------|
| 1000 °C | 14 (F1/3) | -1.084303517 | 0.973998724 |
| | 20 (M3/2) | -0.924651645 | 0.979472606 |
| | 21 (M2) | -1.00087 | 0.97963 |
| 1010 °C | 14 (F1/3) | -1.049345575 | 0.974091652 |
| | 20 (M3/2) | -0.913821941 | 0.982156392 |
| | 21 (M2) | -0.995496 | 0.98291 |

5.4 Conclusion

In the current chapter thermal degradation behavior and kinetic of thermal decomposition of dense and nanowires morphology coated carbon samples and SiC impregnated carbon composites were studied.

Dense SiC coating and SiC nanowires composed SiC coating was achieved on the carbon fiber surface. The dense SiC coated carbon fibers and SiC nanowires coated carbon fibers have shown much improved oxidation property than the bare carbon fibers in oxygen as well as in static air environment. In non-isothermal oxidation condition in oxygen environment, the oxidation process of carbon fiber and SiC nanowire coated carbon fiber exhibited a self catalytic characteristic. In case of SiC nanowires coated carbon fiber the micropores present in between the SiC nanowires over carbon fiber substrate serve as a channel for oxygen to penetrate into carbon fiber and lead to the oxidation of carbon fiber. The whole oxidation process consists of

the oxidation of the carbon fiber and competitive oxidation of carbon fiber as well as SiC. In case of dense SiC coated carbon fiber the small microcracks formed in the coating due to the mismatch of CTE between the coating and carbon substrate act as the channel for oxygen diffusion and leads to the oxidation of carbon fiber. The SiO₂ layer formed over the SiC coating plays an important role in improving the anti oxidant property of the coating. The oxidation of SiC nanostructured coating which starts from around 700 °C forms SiO₂ layer over the SiC nanostructure and it contributes as a weight gain in the oxidation process. The layer of SiO₂ was formed at lower temperature in nanostructured SiC in comparison with the dense SiC coating (starts at around 900 °C). This phenomenon may be useful for healing pre existing micropores at lower temperature and improving oxidation resistive property of dense SiC/SiC nanowire matrix carbon composites. In such composites it is observed that at high temperature there were formation of small microcracks/ holes. The SiC nanowires which were present with dense SiC matrix at the micropores will get oxidized first and form SiO₂/SiC nanowires. These SiO₂/SiC nanowires will heal the micropores/holes.

Kinetics model for oxidation of carbon fiber and SiC nanowires coated carbon fibers was studied. The isothermal and nonisothermal weight loss curve showed that the SiC nanowires coated carbon fiber has improved the oxidation resistance property than bare carbon fibers. Kinetic analysis from isothermal TG curve shows that oxidation of SiC nanowires coated carbon fibers were two step processes with two different activation energy. It indicates that the oxidation process in isothermal process is reaction controlled below 650 °C and gas diffusion and reaction both controlled above 650 °C. The kinetic analysis of bare carbon fiber and SiC nanowires coated carbon fibers was carried out using nonisothermal TG curve and using different model. The kinetic analysis results from the nonisothermal TG curves applying the model fitting method

provide a single value of activation energy E and pre-exponential factor (A -Arrhenius constant). The possible mechanism function for bare carbon fiber was function A1 as it was satisfying one differential and two integral equations. The mechanism function A1 with differential form $f(a) = (1-a)$ and integral form $g(a) = -\ln(1-a)$ belongs to the mechanism of random nucleation. It is concluded that the kinetic equation for the thermal decomposition of fiber was: $da/dT = (A/\beta)\exp(-E_a/RT)(1-a)$. The kinetic parameters were $\log A = 8.343 \text{ min}^{-1}$, $E_a = 143.57 \text{ kJ mol}^{-1}$. The oxidation mechanism of fiber in oxygen environment was random nucleation; only one active nucleus on each species. The mechanism of oxidation process for SiC nanowires coated carbon fibers was the 3D diffusion reaction (ZLT model). The rate of this reaction is controlled by the resulting reaction interfaces progressed towards the centre through diffused faces. The kinetic equation for the thermal decomposition of SiC nanowire coated carbon fiber was $da/dT = (A/\beta)\exp(-E_a/RT)(1.5(1-a)^{4/3}[(1-a)^{-1/3}-1]^{-1})$. The kinetic parameters were: $\log A = 8.577 \text{ min}^{-1}$ and $E_a = 190.41 \text{ kJmol}^{-1}$.

The TG/DTG behavior of SiC carbon composite prepared by sol-gel method was studied. The kinetics of oxidation was calculated using Ozawa and KAS equations. The average activation energy values from the conversion factor from 0.1 to 0.35 of Ozawa and KAS methods were 82.87 and 62.80 kJ mol^{-1} respectively. The activation energy values from both methods were close to each other. The mechanism of oxidation of SiC carbon composite was found to be Mamp1 second order reaction. The SiC carbon composite has the improved oxidation resistance property than carbon composite.

CHAPTER 6

SUMMARY AND FUTURE SCOPE OF WORK

6. Summary and future scope of work

6.1 Summary

There is a lot of research going on to develop advanced composite materials such as carbon/carbon composites by introducing compatible coating or by introducing second phase in the parent matrix, which can withstand extreme environment. The performance of composites in many cases, depend upon the development of suitable coatings to protect against environmental degradation. For example, carbon composite exhibits very poor oxidation resistance property so the applications of reinforced carbon composites have been limited to inert atmosphere to prevent the oxidation of carbon composite. To widen the application area of carbon composites, it is necessary to improve their oxidation resistance property. Hence, intensive efforts are underway to deposit a protective coating or impregnate with second phase ceramic material in parent matrix, which would prevent the oxidation of carbon for continuous use at elevated temperatures of 1000–1500 °C in an oxygen containing environment.

During the present thesis, different SiC precursors were synthesized; further coating studies were carried out on different substrates using synthesized and other commercial available precursors. The high temperature oxidation properties of coated and impregnated carbon composite samples were studied.

In chapter 1, a thorough literature survey was carried out to screen out suitable SiC precursors. MTS is the most common and commercial precursor used for SiC deposition using CVD process. Since MTS is corrosive, toxic in nature and needs high temperature to deposit SiC, a lot of alternative precursors are proposed in literature to replace it. The halogen free single molecular organometallic precursors such as dimethylsilane, $[(\text{CH}_3)_2\text{SiH}_2]$, trimethylsilane, $[(\text{CH}_3)_3\text{SiH}]$, tetramethylsilane, $[(\text{CH}_3)_4\text{Si}]$, 1,3-disilabutane, $(\text{H}_3\text{SiCH}_2\text{SiH}_2\text{CH}_3)$, 1,2-

bis(silyl)ethane, $(\text{H}_3\text{SiCH}_2\text{CH}_2\text{SiH}_3)$, diethylsilane, $[(\text{C}_2\text{H}_5)_2\text{SiH}_2]$, tripropylsilane, $[(\text{C}_3\text{H}_7)_3\text{SiH}]$, silacyclobutane, $[\text{c-C}_3\text{H}_6\text{SiH}_2]$, 1,3-disilacyclobutane, $[\text{C}_2\text{H}_8\text{Si}_2]$, and hexamethyldisilane, $[(\text{CH}_3)_6\text{Si}_2]$ were reported as an alternate precursor to MTS. Deposition of SiC was reported using these precursors at relatively low temperature. The polymeric organometallic precursors such as polysilanes and polycarbosilanes were also reported for SiC deposition. To form SiC by CVD, the precursor composition must be cleanly and easily vaporizable. Many polymers are viscous oils or solids, which cannot be easily evaporated even under extreme vacuum. Except CVD process, sol gel process is also one of the viable options for deposition of SiC using harmless precursors. Keeping all aspects in mind the potential precursors of SiC were screened which are non corrosive, non toxic, easy to handle and commercial cheap.

Chapter 2 deals with the synthesis of potential precursors of SiC. The compounds 2,4,6-trimethyl-2,4,6-trisila-heptane (Trimethyltrisilaheptane), 2,4,6-trisilacyclohexane, mixture of organosilicon compounds (named as CVDP) and sol gel precursors comprising Tetraethylortho silicate (as silicon source) and Glycerine and Phenol formaldehyde resin (as carbon source) were selected as potential precursors for SiC. Three compounds, 2,4,6-trimethyl-2,4,6-trisila-heptane, 2,4,6-trisilacyclohexane and mixture of organosilicon compounds (CVDP) were identified as potential SiC precursor specially for CVD application and their synthesis was carried out. Among these precursors CVDP precursor found out to be the potential precursor of SiC which can be cheaply synthesized in bulk amount. The process parameters such as temperature of reaction, dichloromethane flow rate, argon flow rate and reaction time were optimized for bulk synthesis of CVDP precursor. It has been observed that for process parameters, temperature of reaction: 400 °C, dichloromethane flow rate: 0.25 ml/min, argon flow rate: 500 sccm and reaction time: 3 h maximum yield of CVDP precursor was obtained.

Chapter 3 comprises the coating studies carried out on important materials for nuclear reactor / industries such as graphite / zircaloy substrate using synthesized CVDP precursor and commercial available HMDS precursor. The metallorganic fluidized bed CVD (MOFBCVD) technique was used for coating purpose using CVDP precursor. The presently developed CVDP precursor and fluidized bed coating process to deposit SiC coatings proves that there exists no chlorine etching problem, and the uniform coating of SiC can be achieved. The microscopic and phase analysis revealed that the use of HMDS precursor yielded dense SiC coating on graphite substrates and zirconia microsphere at low deposition temperature.

TRISO coated particles are used as the fuel in High Temperature Reactors. A TRISO coated particle consists of a kernel, usually uranium oxide (UO_2) or mixed uranium oxide and uranium carbide (UCO) which is surrounded by four layers developed by chemical vapor deposition (CVD). The coated layers are: (i) buffer porous carbon layer, 90–100 μm thick; (ii) the inner pyrolytic carbon (IPyC) layer, 35–40 μm thick; (iii) the SiC layer with a thickness of ~ 35 μm ; and (iv) the outer pyrolytic carbon (OPyC) layer, 35–40 μm thick. The SiC coating in the TRISO fuel particles is of interest to the nuclear industry due to its small neutron-capture cross-section and strong covalent/ionic Si-C bond, one which give long term resistance to irradiation and excellent mechanical properties. SiC coating is the most important component for structural integrity of TRISO fuel particles as it sustains most of the internal pressure produced by the fission gases produced within the kernel. The SiC layer used for the formation of TRISO coated fuel particles is normally produced at high temperatures via fluidized bed chemical vapor deposition from MTS in a hydrogen environment. Only the cubic polymorph of SiC (β -SiC) is desired for nuclear applications due to its dimensional stability under irradiation. The high temperature coating process is not desired for bulk production of coated radioactive TRISO

coated particle. The drawbacks related to the use of MTS for SiC layer deposition are its toxicity, corrosive nature of MTS and the generation of gaseous corrosive reaction products. During CVD, corrosive gaseous products can attack the fuel kernel. The chlorine retained in the SiC layer can change to its radioisotope under irradiation and drift to the kernel. The mechanical properties of SiC can also degrade due to the presence of chlorine. Therefore an alternate precursor is required which is non-toxic, halogen free and contains both silicon and carbon atom as single molecule.

According to above requirement layers of SiC were deposited using different organosilicon precursors such as MTS and HMDS and TMS via spouted bed chemical vapor deposition. The microstructure and mechanical properties of SiC coatings obtained from different precursors using spouted bed CVD process were studied. Dense and uniform coatings of SiC were obtained for MTS and HMDS, whereas non uniform layer of SiC was obtained for TMS as precursor in our spouted bed system. Higher deposition of free carbon with SiC occurs in case of HMDS as precursor which may be due to the nonstoichiometric ratio of Si and C in HMDS. SiC coatings with a sub-micrometer grain size were deposited on simulated TRISO fuel particles by spouted bed CVD at a low temperature 1300 °C using HMDS as precursor. The mechanical properties were studied using microindentation. The microstructures were analyzed using SEM. SiC coatings using HMDS and MTS have shown almost similar hardness and fracture toughness. The hardness and fracture toughness values of the coated SiC layers show that the coating has good strength. HMDS liquid precursor has a potential to replace corrosive and toxic precursor MTS for SiC layer coating in TRISO particle.

SiC nanowires play an important role in high temperature oxidation resistance behavior of dense SiC coating. A comprehensive study on synthesis of SiC nanowires of high purity and

homogeneous diameter by hydrogen reduction of MTS by a simple atmospheric pressure CVD method without using a metallic catalyst has been carried out. SiC coating of different morphology using MTS and hydrogen by chemical vapor deposition under ambient pressure were studied. Taguchi method has been used to design experiments to get the optimum parameters for growing SiC wires of diameter in nanometer range. The optimum deposition conditions for uniform diameter growth of SiC nano wires, smoothness of the surface and homogeneous growth of SiC on the surface have been obtained. The hydrogen to MTS flow rate ratio should be above 20 for the growth of SiC wires of nanometer diameter. The deposition temperature for the growth of crystalline SiC wires should be 1100-1300 °C. The total flow rate of carrier gas comprising of argon and hydrogen for a particular H₂/MTS flow rate ratio is critical for morphological outcome of SiC. In the present study total flow rate of carrier gas comprising of argon and hydrogen was 2 lpm for H₂/MTS flow rate ratio 14 to obtain wire morphology. When the total gas flow rate was increased to 6 lpm for the same H₂/MTS flow rate ratio 14, the wire morphology of SiC disappeared and the formation of grains occurred. The optimum deposition temperature i.e. 1300 °C was kept constant and further experiments were conducted by changing H₂/MTS mole ratio to verify morphological outcome of SiC.

Chapter 4 deals with different sol-gel process for deriving SiC. The sol gel technique offers an easy route to synthesize SiC by employing alkoxides and a suitable carbon source. The sol-gel process is one method that is used commercially in many applications. The process gives excellent control of product purity and composition for the simple reason that the process starts with pure materials.

Two step sol gel process was used for generating SiC material using tetraethylorthosilicate as silicon source and phenol formaldehyde as carbon source. A fabrication

process has been developed for prepare SiC impregnated carbon fiber matrix composite. Further the feasibility of deriving SiC in carbon matrix using Polymethylhydrosiloxane (PMHS) as silicon source and Glycerine as carbon source by sol gel method was also studied.

Dense and nanowire morphological SiC phases were impregnated simultaneously in carbon preform using tetraethylorthosilicate as silicon source and phenol formaldehyde as carbon source. The micrographical images and X-ray tomography images confirms that there was uniform impregnation of SiC inside and on the surface of carbon fabric. XRD confirms the formation of β -SiC. It also revealed that there was no degradation of the carbon composite during impregnation and heat treatment process. SAXS studies revealed that there was reduction in number of pores after impregnation and only one kind of nanowire grown after heat treatment at 1000 °C and bimodal distribution was observed after heat treatment at 1500 °C of SiC gel impregnated carbon composite. The VS mechanism has been proposed for the growth of SiC nanowires.

In case of impregnated SiC carbon composite prepared using PMHS and TEOS as silicon source and Glycerine as carbon source by sol gel method, dense morphological SiC phases were impregnated in carbon preform. In the first approach, using PMHS and TEOS silicon source, there was enough deposition of SiC in carbon preform, whereas in second approach using only PMHS as silicon source, there was low deposition of SiC in carbon preform.

Chapter 5 comprises the thermal degradation behavior and kinetic of thermal decomposition study of dense and nanowires morphology coated carbon samples and SiC impregnated carbon composites.

Dense SiC coating and SiC nanowires composed SiC coating has been achieved on the carbon fiber surface. The oxidation resistive properties of bare, dense SiC and nanostructured SiC coated carbon fibers were examined in different oxidative environments from room temperature to 1350 °C. The dense SiC coated carbon fibers and SiC nanowires coated carbon fibers have shown much improved oxidation property than the bare carbon fibers in oxygen as well as in static air environment. In non-isothermal oxidation condition in oxygen environment, the oxidation process of carbon fiber and SiC nanowire coated carbon fiber exhibited a self catalytic characteristic. In case of SiC nanowires coated carbon fiber the micropores present in between the SiC nanowires over carbon fiber substrate serve as a channel for oxygen to penetrate into carbon fiber and lead to the oxidation of carbon fiber. The whole oxidation process consists of the oxidation of the carbon fiber and competitive oxidation of carbon fiber as well as SiC. In case of dense SiC coated carbon fiber the small microcracks formed in the coating due to the mismatch of CTE between the coating and carbon substrate act as the channel for oxygen diffusion and leads to the oxidation of carbon fiber. The SiO₂ layer formed over the SiC coating plays an important role in improving the anti oxidation property of the coating. The oxidation of SiC nanostructured coating which starts from around 700 °C forms SiO₂ layer over the SiC nanostructure and it contributes as a weight gain in the oxidation process. The layer of SiO₂ was formed at lower temperature in nanostructured SiC in comparison with the dense SiC coating (starts at around 900 °C). This phenomenon may be useful for healing pre existing micropores at lower temperature and improving oxidation resistive property of dense SiC/SiC nanowire matrix carbon composites. In such composites it has been observed that at high temperature there has been formation of small microcracks/ holes. The SiC nanowires which were present with dense

SiC matrix at the microspores will get oxidized first and form SiO₂/SiC nanowires. These SiO₂/SiC nanowires will heal the micropores/holes.

Further isothermal and nonisothermal oxidation decomposition kinetics model of bare carbon fibers and SiC nanowires coated carbon fibers were studied. The equations of Achar-Brindley-Sharp-Wendworth, Satava-Sestak, Coat-Redfern and Madhusudanan-Krishnan-Ninan were used to study the oxidation kinetics and to estimate most probable mechanism function of bare carbon fiber and coated carbon fiber in non isothermal condition.

The isothermal and nonisothermal weight loss curve shows that the SiC nanowires coated carbon fiber has improved the oxidation resistance property than bare carbon fibers. Kinetic analysis from isothermal TG curve shows that oxidation of SiC nanowires coated carbon fibers were two step processes with two different activation energies. It indicates that the oxidation process in isothermal process has been reaction controlled below 650 °C and gas diffusion and reaction both controlled above 650 °C. The kinetic analysis of bare carbon fiber and SiC nanowires coated carbon fibers was carried out using nonisothermal TG curve and using different model. The kinetic analysis results from the nonisothermal TG curves applying the model fitting method provide a single value of activation energy E and pre-exponential factor (A-Arrhenius constant). It was observed that only function A1 (A1 stood for Avrami-Erofeev equation, Random Nucleation) satisfied the conditions in case of Achar-Brindley-Sharp-Wendworth equation, Satava-Sestak equation and Madhusudanan-Krishnan-Ninan equation. Thus the possible mechanism function was function A1 as it has been satisfying one differential and two integral equations. Therefore it can be stated that the mechanism function with differential form $f(a) = (1-a)$ and integral form $g(a) = -\ln(1-a)$ belongs to the mechanism of random nucleation. It has been concluded that the kinetic equation for the thermal decomposition of fiber was: $da/dT =$

$(A/\beta)\exp(-E_a/RT)(1-a)$. The kinetic parameters were $\log A = 8.343 \text{ min}^{-1}$, $E_a = 143.57 \text{ kJ mol}^{-1}$. We conclude that the kinetic equation for the thermal decomposition of fiber was: $f(a) = 1.5 [(1-a)^{-1/3} - 1]^{-1}$. The mechanism of oxidation process of SiC nanowires coated carbon fiber has been the 3D diffusion reaction (ZLT model). Therefore it can be stated that the mechanism function with differential form $f(a) = 1.5(1-a)^{4/3}[(1-a)^{-1/3} - 1]^{-1}$ and integral form $g(a) = [(1-a)^{-1/3} - 1]^2$ belongs to the mechanism of 3D diffusion reaction following ZLT equation. We conclude that the kinetic equation for the thermal decomposition of SiC nanowire coated carbon fiber was $da/dT = (A/\beta)\exp(-E_a/RT)(1.5(1-a)^{4/3}[(1-a)^{-1/3} - 1]^{-1})$. The kinetic parameters were: $\log A = 8.577 \text{ min}^{-1}$ and $E_a = 190.41 \text{ kJmol}^{-1}$. The rate of this reaction has been controlled by the resulting reaction interfaces progressed towards the centre through diffused faces.

The oxidation resistive properties of bare carbon fabric and SiC impregnated carbon fabric prepared by sol-gel method were examined in atmospheric oxidative environment from room temperature to 1400 °C. In kinetic study of oxidation of SiC impregnated carbon fabric Ozawa and KAS equations were used to determine the activation energy (E_a) of the oxidation reaction. In non-isothermal oxidation condition in atmospheric environment, SiC carbon composite has shown improved oxidation resistance property and the oxidation process of SiC carbon composite occurred through microcracks, pits and micropores generated on the surface of composite. The average activation energy values from the conversion factor from 0.1 to 0.35 of Ozawa and KAS methods were 82.87 and 62.80 kJ mol^{-1} , respectively. The activation energy of the oxidation has been reliable via the small difference of the calculated values from two methods ($\sim 20 \text{ kJ mol}^{-1}$). The most probable mechanism function for oxidation step has been in the integral form $g(a) = a^{1/2}$ and the differential form $f(a) = 2 a^{-1/2}$, which has been the Mampfl power. This has been a special case of Mampfl Power model or the second order reaction.

In the present thesis an effort has been made to significantly contribute towards the development of halogen free & commercially cheap SiC precursors and developing advance coating and composites materials using such precursors. The economical synthesis routes of some of the technologically important organosilicon precursors and their growth mechanism has been discussed. The fundamental understanding of different morphological SiC coating and high temperature oxidation behavior has been studied. These findings will add in further understanding of oxidation behavior of dense, nanowires SiC matrix coated/impregnated carbon materials and developing a better advance composite material.

6.2 Future scope of work

In the last few years, ceramic coatings/ceramic composites have been receiving considerable attention for a variety of reasons including economics (substitution of expensive alloys by cheaper alternatives, extension of service life of alloys), material protection from wear, corrosion and erosion, and improvement and development of new material properties. In the present thesis, a significant contribution has been made towards development of different organosilicon compounds precursors of SiC, coating technique development for different morphological SiC deposition & SiC/carbon composites development. The study of economical route synthesis of some of the technologically important organosilicon precursors using cheap chemicals has given a scope for commercializing the production of such precursor.

Due to the serious concern over economy as well as environmental pollution, the economical and environmentally safer coating methods are gaining an ever increasing importance now-a-days over the conventional methods. The CVD and sol-gel techniques for SiC deposition based on organometallic compounds as precursor has potential to address economy

and pollution related issues to a great extent. In addition, the use of organometallic precursors in CVD process has the advantage of producing high quality protective coatings without degrading the substrates.

References

1. J. J. Berzelius, *Ann. Phys. Lpz.* **1**, 169 (1824).
2. A. H. Cowles and E. H. Cowles, U.S. Pat. 1885, 319945.
3. A. G. Acheson, *Engl. Pat.* 1892,17911.
4. H. J. Round, *Electrical World* 1907,19, 309.
5. Y. M. Tairov and V. F. Tsvetkov, *Journal of Crystal Growth* **43**, 209 (1978).
6. H. Matsunami, S. Nishino and H. Ono, *IEEE Trans. Electron. Devices* **28**, 1235 (1981).
7. W. F. Knippenberg, *Philips Research Reports* **18**, 161-274 (1963).
8. J. A. Powell, D. J. Larkin, L. G. Matus, W. J. Choyke, J. L. Bradshaw, L. Henderson, M. Yoganathan, J. Yang and P. Pirouz, *Applied Physics Letters* **56**, 1442 (1990).
9. J. A. Powell, J. B. Petit, J. H. Edgar, I. G. Jenkins, L. G. Matus and W. J. Choyke, *Applied Physics Letters* **59**, 183 (1991).
10. R. Forthmann, E. Gyarmati, J. Linke and E. Wallura, *High Temp- High Press* **14**, 477 (1982).
11. R. E. Bullock, *Journal of Nuclear materials* **125**, 304 (1984).
12. R. H. Jones, C. H. Kenager Jr and G. W. Hollenberg, *Journal of Nuclear Materials* **191-194**, 75 (1992).
13. R. H. Baney, J. S. Tulenko and D. Butt, University of Florida, NERI Research Project, DE-FG03-99SF21882, Gainesville, FL (2003).
14. Y. H. Chu, Q. G. Fu, C. W. Cao, H. J. Li, K. Z. Li and Q. Lei, *Surface Coating Technology* **205**, 413-418 (2010).
15. Y. Chu., Q. Fu., Z. Zhang., H. Li., K. Li. and Q. Le., *Journal of Alloys and Compounds* **508**, L36-L39 (2010).

16. Q. G. Fu, H. J. Li, K. Z. Li, X. H. Shi, M. Huang and G. D. Sun, *Material Science Engineering A* **445-446**, 335-338 (2007).
17. G. B. Zheng, M. Hironori, S. Hideaki and U. Yasuo, *Carbon* **46**, 1792-1828 (2008).
18. F. J. Buchanan and J. A. Little, *Corrosion Science* **35**, 1243-1250 (1993).
19. N. S. Jacobson and D. M. Curry, *Carbon* **44**, 1142-1150 (2006).
20. Akihiko Otsuka, Yoshikazu Matsumura, Kazuya Hosono and R. Tanaka, *Journal of the European Ceramic Society* **23**, 3125-3134 (2003).
21. H. Araki, W. Yang, Q. Hu, H. Suzuki and T. Noda, *Novel Materials Processing by Advanced Electromagnetic Energy Sources*, 369-372 (2005).
22. A. K. Chaddha, J. D. Parsons, J. Wu, H.-S. Chen, D. A. Roberts and H. Hockenhull, *Applied Physics Letters* **62**, 3097-3098 (1993).
23. J. Chen, R. Wu, G. Yang, P. Yi, J. Lin, L. Wu and R. Zhai, *Journal of Alloys and Compounds* **456** 320-323 (2008).
24. Y. Chu, H. Li, Q. Fu, X. Shi, L. Qi and B. Wei, *Corrosion Science* **58**, 315-320 (2012).
25. H. Fritze, J. Jojic, T. Witke, C. Ruscher, S. Weber, S. Scherrer, R. Web, B. Schultrich and G. Borchardth, *Journal of European Ceramic Society* **18**, 2351-2364 (1998).
26. Q. G. Fu, H. J. Li, Y. J. Wang, K. Z. Li and X. H. Shi, *Corrosion Science* **51**, 2450-2454 (2009).
27. H. Schmidt, S. Langenfeld and R. Nab, *Mater. Design* **18**, 309 (1997).
28. J.-C. Hierso, R. Feurer and P. Kalck, *Chemistry of Materials* **12**, 390 (2000).
29. I.V. Dulera and R. K. Sinha, *Journal of Nuclear Materials* **383**, 183-188 (2008).
30. J.E. Gray and B. Luan, *Journal of Alloys and Compounds* **336**, 88-113 (2002).

31. Laura Treccani, Tanja Yvonne Klein, Fabian Meder, Karoline Pardun and K. Rezwani, *Acta Biomaterialia* **9**, 7115-7150 (2013).
32. B.L. Mordike and T. Ebert, *Materials Science and Engineering A* **302**, 37-45 (2001).
33. C.Y. Wang, P. Yao, D.H. Bradhurst, H.K. Liu and S. X. Dou, *Journal of Alloys and Compounds* **285**, 267 (1999).
34. C. K. Mittal, *Transactions of the Metal Finishers Association of India Metal Finishing* **34**, 34 (1993).
35. J.L. Luo and N. Cui, *Journal of Alloys and Compounds* **264**, 299 (1998).
36. J. Mazia, *Metal Finishing* **88**, 466 (1990).
37. B. Luan and H. O. Pierson, *ASM Handbook: Corrosion* **13**, 456 (1987).
38. Ulf Helmersson, Martina Lattemann, Johan Bohlmark, Arutian P. Ehiasarian and J. T. Gudmundsson, *Thin Solid Films* **513**, 1-24 (2006).
39. K. L. Choy, *Progress in Materials Science* **48**, 57-170 (2003).
40. D.J. Varacalle Jr., L.B. Lundberg, H. Herman and G. Bancke, *Surface and Coatings Technology* **86-87**, 70-74 (1996).
41. Jin Zhang, Qi Xue and S. Li, *Applied Surface Science* **280**, 626-631 (2013).
42. Sanjay Mathur and P. Kuhn, *Surface and Coatings Technology* **201**, 807-814 (2006).
43. S. Vidal, F. Maury, A. Gleizes and C. Mijoule, *Applied Surface Science* **168**, 57-60 (2000).
44. L. Niinistö, *Current Opinion in Solid State and Materials Science* **3**, 147-152 (1998).
45. H.M. Yates, L.A. Brook, D.W. Sheel, I.B. Ditta, A. Steele and H. A. Foster, *Thin Solid Films* **517**, 517-521 (2008).
46. R. Luo, *Carbon* **40**, 1279-1285 (2002).

47. Andrew R. Teren, Reji Thomas, Jiaqing He and P. Ehrhart, *Thin Solid Films* **478**, 206-217 (2005).
48. H.B Wang, C.R Xia, G.Y Meng and D. K. Peng, *Materials Letters* **44**, 23-28 (2000).
49. S. B. Desu, *Materials Chemistry and Physics* **31**, 341-345 (1992).
50. S. B. S. Tamir, K. Rabinovitch, M. Gilo and R. Dahan, *Thin Solid Films*, **332**, 10-15 (1998).
51. Christopher J. Jensen and W. K. S. Chiu, *Surface and Coatings Technology* **201**, 2822-2828 (2006).
52. E. P. Marsh, US Patent **US 6204178 B1** (2001).
53. E. P. Marsh, US Patent Appl. **2006/0014367 A1** (2006).
54. M. S. Bell, *Applied Physics Letters* **85**, 1137-1139.
55. Catherine B. Labelle, K. K. S. Lau and K. K. Gleason, *MRS Proceedings* **511** (1998).
56. A. Botman, J.J.L. Mulders, R. Weemaes and S. Mentink, *Nanotechnology* **17**, 3779 (2006).
57. B.W. Kempshall, L.A. Giannuzzi, B.I. Prenzler, F.A. Stevie and S. X. Da, *Journal of Vacuum Science and Technology B* **20**, 286 (2002).
58. C. Vahlas, F. Juarez, R. Feurer, P. Serp and B. Caussat, *Chemical Vapor Deposition* **8**, 127 (2002).
59. J. Perez-Mariano, K.-H. Lau, A. Sanjurjo, J. Caro, J.M. Prado and C. Colominas, *Surface and Coatings Technology* **201**, 2174-2180 (2006).
60. Mikko Ritala and M. Leskelä, *Handbook of Thin Films* **1**, 103-159 (2002).
61. Walter S. Knodle and R. Chow, *Handbook of Thin Film Deposition Processes and Techniques (Second Edition)*, 381-461 (2001).

62. Q. G. Fu, H. J. Li, Z. Z. Zhang, X. R. Zeng and K. Z. Li, *Corrosion Science* **52**, 1879-1882 (2010).
63. K. Sato, H. Morozumi, O. Funayama, H. Kaya and T. Isoda, *Journal of the American Ceramic Society* **85** (7), 1815-1822 (2002).
64. Y. Zhang, X. Han, K. Zheng, Z. Zhang, X. Zhang, X. Fu, Y. Ji, Y. Hao, X. Guo and Z. Wang, *Advance Functional Materials* **17**, 3435-3440 (2007).
65. Y. Chu, Q. Fu, H. Li, K. Li, X. Zou and C. Gu, *Corrosion Science* **53**, 3048-3053 (2011).
66. X.-H. Sun, C.-P. Li, W.-K. Wong, N.-B. Wong, C.-S. Lee, S.-T. Lee and B.-K. Teo, *Journal of american chemical society* **124** (9), 14468 (2002).
67. B. K. Teo, S.-P. Huang, R. Q. Zhang and W.-K. Li, *Coordination Chemistry Reviews* **253**, 2935-2958 (2009).
68. J. C. Bokros, *Chemistry and Physics of Carbon*, P. L. Walker, Jr., Ed., Vol. 5, p. 1, Dekker, NY (1969).
69. W. V. Kotlensky, *Chemistry and Physics of Carbon*, F. L. Walker, Jr., Ed., Vol. 9, p. 173, Dekker, NY (1973).
70. J. D. Brooks and J. H. Taylor, *Nature* **206**, 697 (1965).
71. G. S. Rellick, *Carbon* **28**, 589 (1990).
72. J. L. White and F. M. Sheaffer, *Carbon* **27**, 697 (1989).
73. W. T. Barry, C. Gaulin and R. Kobayashi, *Review of Polyacetylene Matrices for Thin-Walled Composites*. Report No. TR-0089(4935-06)-1. The Aerospace Corporation. El Segundo. CA (25 September 1989).
74. W. Yang, H. Araki, A. Kohyama, S. Thaveethavorn, H. Suzuki and T. Nod, *Materials Letters* **58**, 3145-3148 (2004).

75. A. J. Steckl and J. P. Li, IEEE Trans. Electron Devices **ED-39**, 64 (1992).
76. S. Nishino, H. Suhara, H. Ono and H. Matsunami, Journal of Applied Physics **61**, 4889 (1987).
77. T. Ueda, H. Nishino and H. Matsunami, Journal of Crystal Growth **104**, 695 (1990).
78. P. Liaw and R. F. Davis, Journal of Electrochemical Society **132**, 642 (1985).
79. G. S. Fischman and W. T. Petuskey, Journal of American Ceramic Society **68**, 185 (1985).
80. C. D. Stinspring and J. C. Wourmhoudt, Journal of Crystal growth **87**, 481 (1988).
81. J. H. Koh and S. I. Woo, Journal of Electrochemical Society **137**, 2215 (1990).
82. I. Golecki, F. Reidinger and J. Marti, Applied Physics Letters **60**, 1703 (1992).
83. A. J. Steckl, C. Yuan, J. P. Li and M. J. Loboda, Applied Physics Letters **63**, 3347-3349 (1993).
84. M. Kaplan, D. L. Matthies and N. J. Princeton, U.S. Pat. No. 3,843,399.
85. K. Yasui, M. Hashiba, Y. Narita and T. Akahane, Materials Science Forum **367**, 367-370 (2002).
86. Y. Avigal, M. Schieber and R. Levin, Journal of Crystal Growth **24-25**, 188-192 (1974).
87. S. H. Jeong, D. C. Lim, H.-G. Jee, O. M. Moon, C.-K. Jung, J. S. Moon, S. K. Kim, S.-B. Lee and J.-H. Boo, Journal of Vacuum Science and Technology B **22**, 2216 (2004).
88. J.-H. Boo, K.-S. Yu, M. Lee and Y. Kim, Applied Physics Letters **66**, 3486 (1995).
89. C. Curran, R. M. Witucki and P. A. McCusker, Journal of American Chemical Society **72**, 4471 (1950).
90. A. E. Finholt, J. A. C. Bond, K. E. Wilzbach and H. I. Schlesinger, Journal of American Chemical Society **69**, 2692 (1947).

91. V. A. Ponomaranko and V. F. Mironov, Bull. Acad. Sci. USSR, Div. Chem. Sci. (Engl. Transl.) 423 (1954).
92. Beleg. Pat. 553496 [U.S. Prior. 19.12.1955].
93. N. C. Goodspeed and S. R.T., Journal of Inorganic Nuclear Chemistry **2**, 266 (1956).
94. German Appl. (West German) 1055511 [15.12.1956], Brit. Pat. 823483 (German prior.(west German) 3.11.,12.12. and 15.12.1956).
95. L. I. Zakharkin, Bull. Acad. Sci. USSR, Div. Chem. Sci. (Engl. Transl.), 2079 (1960).
96. W. Sundermeyer, European Research Associates S.A.German appl. (West German)1080077 (8.8.1957).
97. J. H. Boo, K. S. Yu and Y. Kim, Chemistry of Materials **7**, 694-698 (1995).
98. I. N. Jung, S. H. Yeon and Han.J.S., Organometallics : A Concise Introduction (2nd ed.). Weinheim: Wiley-VCH. ISBN 3-527-28165-7 **12**, 2360 (1993).
99. I. N. Jung, G. H. Lee and C. H. Song, Korean Patent appl. No. 1992, 92, 4705. (1992).
100. P. G. Cambell, Ph.D. Thesis, Pennsylvania State University (1957).
101. V. M. Vdovin, K. S. Nametkin and P. L. Grinberg, Dokl.Akad.Nauk SSSR **150**, 799 (1963).
102. D. J. larkin and L. V. Interrante, Chemistry of Materials **4**, 22 (1992).
103. J. Laane, Journal of American Chemical Society **89**, 1144 (1967).
104. N. S. Nametkin, V. M. Vdovin, V. I. Zavgalov and P. L. Grinberg, IZV, Akad. Nauk, SSSR, Ser.Khim. **929** (1965).
105. K. Takahashi, S. Nishino and J. Saraie, Journal of Electrochemical Society **139**, 3565-3571 (1992).
106. Pioneering Advanced Ceramics, www.starfiresystems.com.

107. W. C. Lacourse, S. Dahar and M. M. Akhtar, *Journal American Ceramic Society* **67**, C200 (1984).
108. I. Artaki, T. W. Zerda and J. Jonas, *Journal Non- Crystalline Solids* **81**, 381 (1986).
109. L. L. Hench, *Science of Ceramic Chemical Processing*: eds L. L. Hench & D. R. Ulrich, Wiley-Interscience, New York, 52 (1986).
110. G. Orcel and U. Hench, *Ceramic Engineering Science Proceedings*, 546 (1984).
111. S. S. Jada, *Journal of American Ceramic Society* **70**, C298 (1987).
112. D. C. Bradley, R. C. Mehrotra and D. P. Gaur, *Metal Alkoxides*. Academic Press, London, 149 (1978).
113. W. G. Klemperer, M. M. Mainz and D. M. Millar, *Better Ceramics Through Chemistry II*, eds C. J. Brinker, D. E. Clark & D. R. Ulrich, *MRS Symposia Proceedings*, MRS, Pittsburgh **73**, 3 (1986).
114. S. Madapura, A. J. Steckl and M. Lobada, *Journal of Electrochemical Society* **146**, 1197-1202 (1999).
115. J.-H. Boo, S.-B. Lee, K.-S. Yu, M. M. Sung and Y. Kim, *Surface Coating Technolgy* **131**, 147 (2000).
116. H. Q. Ly, R. Taylor, R. J. Day and H. F., *Journal of Materials Science* **36** (16), 4037-4043 (2001).
117. H. Q. Ly, R. Taylor and R. J. Day, *Journal of Materials Science* **36** (16), 4045-4057 (2001).
118. E. G. Rochow, *Journal of American Chemical Society* **67** (6), 963-965 (1945).
119. L. L. Snead, T. Nozawa, Y. Katoh, T.-S. Byun, S. Kondo and D. A. Petti, *Journal of Nuclear Materials* **371**, 329 (2007).

120. Y. Katoh, L. L. Snead, T. Nozawa, N. B. Morley and W. E. Windes, *Advance Science Technology* **45**, 1915 (2006).
121. V. D. Krstic, M. D. Vljajic and R. A. Verrall, *Key Engineering Materials* **122-124**, 387 (1996).
122. T. Nishitani, H. Tanigawa, T. Nozawa, S. Jitsukawa and M. Nakamidhi, *Journal of Nuclear Materials* **417**, 1331 (2011).
123. E. Lopez-Honorato, J. Tan, P. J. Meadows, G. Marsh and P. Xiao, *Journal of Nuclear Materials* **392**, 219 (2009).
124. D. Carpenter, K. Ahn, K. Kao, S. P. Kao, P. Heizlar and S. M. Kazimi, Assessment of silicon carbide cladding for high performance light water reactors. Nuclear Fuel Cycle Program (CANES Reports), MIT-NFC-TR-098 (2007).
125. R. A. Andrievski, *Reviews on advanced materials science* **22**, 1 (2009).
126. O. Kordina and S. E. Sadow, *Advances in Silicon Carbide Processing and Applications*, edited by S.E. Sadow and A. Aggarwal (ARTECH House, Inc., Norwood, MA, 2004); p. 1.
127. A. Acir and T. Altunok, *Journal of Fusion Energy* **29**, 436 (2010).
128. W. F. G. Van Rooijen, *Improving Fuel Cycle Design and safety Characteristics of a Gas Cooled Fast Reactor* (IOS Press, Amsterdam, Netherlands, 2006).
129. K. J. Krueger and G. P. Ivens, *Safety-Related Experiences With the AVR Reactor, Specialists' Meeting on Safety and Accident Analysis for Gas-Cooled Reactors* (IAEA-TECDOC-358, Oak Ridge, TN, 1985); p. 61.

130. S. Brandes, Core Physics Test of THTR Pebble Bed Core at Zero Power, Specialists' Meeting on Safety and Accident Analysis for Gas-Cooled Reactors (IAEA-TECDOC-358, Oak Ridge, TN, 1985); p. 285.
131. G. Taguchi, Introduction to quality Engineering, Asian Productivity Organization, 1986.
132. G. Taguchi and S. Konishi, Orthogonal Arrays and Linear Graphs, ASI press, Dearborn, MI 1987.
133. K. K. Chee, M. K. Wong and H. K. Lee, Journal of Chromatography A **723**, 259 (1996).
134. D. Monaghan and R. D. Arnell, Surface and Coating Technology **49**, 298 (1991).
135. D. N. Lee and . Journal of Material Science **24**, 4375-4378 (1989).
136. C. J. Brinker, G. W. Scherer and E. P. Roth, Journal of Non-Crystalline Solids **72**, 345 (1985).
137. L. L. Hench and J. K. WEST, Chemical Review **90**, 33 (1990).
138. D. W. Johnson Jr, American Ceramic Society Bulletin **64**, 1597 (1985).
139. E. M. Rabinovich, Journal of Material Science **20**, 4259 (1982).
140. C. J. Brinker and G. W. Scherer, Sol-gel science (Academic Press, New York, 1989).
141. T. Maki and S. Sakka, ibid **100**, 303 (1988).
142. X.-Y. Guo and G.-Q. Jin, Journal of Materials Science **40**, 1301-1303 (2005).
143. Y. S. Kashyap, P. S. Yadav, P. S. Sarkar, A. Agrawal, T. Roy, A. Sinha, K. Dasgupta and D. Sathiyamoorthy, NDT&E International **42**, 384-388 (2009).
144. P. Serf and J. L. Figueiredo, Carbon **35**, 675-683 (1997).
145. K. Miura, H. Nakagawa and K. Hashimoto, Carbon **33** (3), 275-282 (1995).
146. B. E. Warren, Physical Review **59**, 693-698 (1941).
147. P. Scherrer, Nachr Ges Wiss Gottingen **2**, 98. (1918).

148. A. Guinier, G. Fournet, B. C. Walker and L. K. Yudowith, Wiley, New York (1955).
149. G. Prorod, Small-Angle X-ray Scattering. O. Kratky and O. Glatter, editors. Academic Press London (1982).
150. J. Bahadur, D. Sen, S. Mazumder, R. Shukla and A. K. Tyagi, Journal of Physics: Condensed Matter **20**, 345201-345207 (2008).
151. Y. Y. Wu and P. D. Yang, Journal of American Chemical Society **123**, 3165-3166 (2001).
152. C. Liu, Z. Hu, Q. Wu, X. Z. Wang, Y. Chen and H. Sang, Journal of American Chemical Society **127**, 1318-1322 (2005).
153. C. V. Guterl and P. Ehrburger, Carbon **35**, 1587-1592 (1997).
154. W. Wang, Z. H. Jin, T. Xue, G. B. Yang and G. J. Qiao, Journal of Material Science **42**, 6439-6445 (2007).
155. N. S. Jacobson, T. A. Leonhardt, D. M. Curry and R. A. Rapp, Carbon **37**, 411-419 (1999).
156. Y. Chu, Q. Fu, H. Li, K. Li, X. Zou and C. Gu, Corrosion Science **53**, 3048-3053 (2011).
157. C. Yanhui, L. Hejun, F. Qiangang, W. Haipeng, H. Xianghui and Z. Xu, Carbon **50**, 1280-1288 (2012).
158. K. Zhao, K. Li and Y. Wang, Composites: Part B **45**, 1548-1586 (2013).
159. Y. Chu, Q. Fu, H. Li, K. Li, X. Zou and C. Gu, Corrosion Science **53**, 3048-3053 (2011).
160. A. W. Coats and J. P. Redfern, Nature **20**, 68 (1964).
161. T. A. Ozawa, Bulletin of the Chemical Society of Japan **38**, 1881 (1965).
162. T. Akahira and T. Sunose, Report of Research Institute. Chiba Institute of Technology (Sci. Technol.) **16**, 22 (1971).

163. H. E. Kissinger, *Anal. Chem.* **29**, 1702 (1957).
164. V. Satava and J. Sestak, *Journal of Thermal Analysis* **8** (3), 477-489 (1975).
165. J. Sestak, *Academia: Prague* (1984).
166. J. H. Sharp and S. A. Wendworth, *Anal. Chem.* **41** (14), 2060-2062 (1969).
167. D. W. Van Krevelens and P. J. Hoftijzer, *Transactions of the Institution of Chemical Engineers* **32**, 5360 (1954).
168. W. W. Wendland, *John Wiley & Sons Inc: New York* (1974).
169. H. E. Kissinger, *Analytical Chemistry* **29**, 1702 (1957).
170. P. Madhusudanan, K. Krishnan and K. Ninan, *Thermochemica Acta* **97**, 189-201 (1986).
171. G. Takashi, *Material Science Forum* **522-523**, 27-36 (2006).
172. X. R. Zeng , H. J. Li and Z. Yang, *Journal of Chinese Ceramic Society* **27** (1), 8-14 (1999).
173. G. Takashi, *Mater Sci Forum* **522-523**, 27-36 (2006).
174. L. R. Zhao and B. Z. Zang, *Journal of Material Science* **32**, 2811-2819 (1997).
175. J. W. Hinze and H. C. Graham, *Journal of Electrochemical Society* **123** (7), 751-754 (1976).
176. L. Li , X. R. Zeng, H. J. Li, X. B. Xiong, S. H. Xie and J. Z. Zou, *Rare Metal Materials and Engineering* **38** (2), 751-754 (2009).
177. J. J. Fritze H, Witke T, Ruscher C, Weber S, Scherrrer S, Web R, Schultrich B, Borchardth G, *Journal of European Ceramic Society* **18**, 2351-2364 (1998).
178. P. D. Gaudio, H. Behrens and J. Deubener, *Journal of Non-Crystalline Solids* **353**, 223-236 (2007).
179. X. H. Gao P, Wang H, Jin Z, *Materials Chemistry and Physics* **93**, 164-169 (2005).

180. T. A. Hiroshi H, Yasuo K, Toshio Y, Composites: Part A **30**, 515-520 (1999).
181. Z. X. Huang J, Li H, Xiong X, Fu Y, Carbon **42**, 1517-1521 (2004).
182. R. Luo, J. Cheng and T. Wang, Carbon **40**, 1965-1972 (2002).
183. J. Sestak, Thermodynamical Properties of Solids, Academia: Prague (1984).
184. J. H. Sharp and S. A. Wendworth, Analytical Chemistry **41** (14), 2060-2062 (1969).
185. W. W. Wendland, Thermal Methods of Analysis: John Wiley & Sons Inc: New York (1974).
186. V. F. Zhuravlav, I. G. Lesokhin and R. G. Tempelman, Journal of applied Chemistry USSR (English Translation) **21**, 887 (1948).
187. T. Vlase, G. Vlase, M. Doca and N. Doca, Journal of Thermal Analysis and Calorimetry **72**, 597-604 (2003).
188. G. I. Senum and R. T. Yang, Journal of Thermal Analalysis Calorimetry **11**, 445-447 (1977).
189. T.-M. Wu, W.-C. Wei and S.-E. Hsu, Journal of the European Ceramic Society **9**, 351-356 (1992).